POTENTIAL OF A COMPACT LOW ENERGY PROTON ACCELERTOR FOR MEDICAL APPLICATIONS

NAOMI RATCLIFFE

A thesis submitted to the University of Huddersfield in partial fulfilment of the requirements for the degree Doctor of Philosophy

The University of Huddersfield in collaboration with Siemens plc

May 2014

ABSTRACT

This thesis explores the potential of a compact low energy (<10MeV) proton accelerator for medical applications such as the production of neutrons for cancer neutron therapy and the production of SPECT (Single Photon Emission Computed Tomography) and PET (Positron Emission Tomography) radioisotopes.
During the course of this study the simulation code GEANT4 was used to study yields of these neutrons and isotopes from the typically low threshold high cross-section (p,n) reactions. Due to the limits of the current models within GEANT4 some development of a new data-driven model for low energy proton interactions was undertaken and has been tested here. This model was found to be suitably reliable for continued study into the low energy production of positron emitting, PET, isotopes of copper and gallium as replacements for the main SPECT isotope technetium-99m. While ^{99m}Tc is currently the most popular radioisotope being used in over 90% of the worlds nuclear medicine diagnostic procedures supply is under threat by the impending shut down of the current reactor based sources
Simulations of both thin and thick targets were carried out to study the potential of low energy production of these isotopes. The final activity of the radioisotopes after irradiation of these targets produced by the simulations has been shown here to be sufficient for multiple doses. The useable activity is dependent on the efficiency of the extraction process and the time between irradiation and administration.

Acknowledgements

Acknowledgment of the funding for this work from the EPSRC and Siemens plc and the use of the resources of the University of Huddersfield.

Firstly a special thank you to my supervisor Prof. Bob Cywinski for all of his time and support. I have grown both professionally and personally from his guidance and insights.

I have to thank Drs. A. & C. Bungau for all their work on GEANT4 without them there would still not be a working model. I would also like to thank P. Beasley and O. Heid of Siemens for their input into this work.

I have been privileged to be the first student through the IIAA at the University of Huddersfield. This has given me a special opportunity to have unlimited access to pick the brains of international reputations such as Prof. Roger Barlow, Prof. Becky Seviour(who put me in touch with this project in the first place), Prof. Sue Kilcoyne and Prof. Rob Edgecock. Each of these people have supported me throughout our time together and have brightened my day when I needed it most, even if they could not give me the answers that were eluding me.

And of course a special mention to all the other students in our group that joined me over the years, especially to my office mates Anna Kolano and Simon Albright. What a pair, thank for the laughs and making everyday so interesting.

Finally my family for supporting me through all the choices that led me here.

Copyright Statement

i. The author of this thesis (including any appendices and/or schedules to this thesis) owns any copyright in it (the "Copyright") and s/he has given The University of Huddersfield the right to use such Copyright for any administrative, promotional, educational and/or teaching purposes.

ii. Copies of this thesis, either in full or in extracts, may be made only in accordance with the regulations of the University Library. Details of these regulations may be obtained from the Librarian. This page must form part of any such copies made.

iii. The ownership of any patents, designs, trademarks and any and all other intellectual property rights except for the Copyright (the "Intellectual Property Rights") and any reproductions of copyright works, for example graphs and tables ("Reproductions"), which may be described in this thesis, may not be owned by the author and may be owned by third parties. Such Intellectual Property Rights and Reproductions cannot and must not be made available for use without the prior written permission of the owner(s) of the relevant Intellectual Property Rights and/or Reproductions.

Contents

Word Count: 25771

1. INTRODUCTION

For centuries physics has played a role in medicine. As early as the 1700s physics was used as a way of exploring and understanding the human body, from the mechanics of the skeletal and muscle structure to the use of fluid dynamics for the study of blood flow[1][2]. The primary role of the physicist in modern medicine often involves radiation, its production, uses, and protection, in both clinical and non-clinical situations.

The first instance of radiation use in medicine was that of the X-ray, discovered by Röntgen, which lead to a rapid development in medicine. This was encouraged by the discovery of radioactivity and radioisotopes by Becquerel and the Curies[2][3][4]. Another of the big developments brought about by physics was the invention of the particle accelerator: Both circular and linear[5][6] accelerators played a role in the birth of modern nuclear medicine, and the imaging and therapeutic techniques we use today have changed little since this time.

Cyclotron machines provided a method of producing new radioisotopes in sufficient commercial quantities for the birth of nuclear medicine and its development to the full clinical status it holds today. There are several complementary imaging techniques, including traditional X-ray imaging, X-ray Computed Tomography (CT), Single Photon Emission Tomography (SPECT), Positron Emission Tomography (PET), and Magnetic Resonance Imaging (MRI)[3], each with their own advantages and disadvantages for different applications. SPECT and PET both use a radioactive tracer isotope and will be discussed later in more detail as part of the focus of this work. They are often used as combination procedures either combined imaging and therapy with isotopes with multiple types of particle emission or as combined imaging techniques such as MR PET. One of the world's main supplies of such machines is the sponsor of this work, Siemens healthcare[5]. Linear accelerators, or "linacs", also have use, directly, in imaging and therapy.

Linacs have been adopted to provide the radiation source for X-ray therapy in oncology[5]. Both linear and circular types of accelerator have been used as a source of particles such as protons, carbon ions, and neutrons, for hadron and neutron capture therapy. The accelerated charged particles are fired into the patient towards the tumour with sufficient energy for the particles to reach the tumour and deposit their energy within the Bragg peak region. Here the traveling particles lose most energy due to ionization interactions within the tumour stopping the particles abruptly thus minimising the damage to the surrounding healthy tissue with dose behind and little dose leading up to the tumour. This gives protons (and other hadrons) an advantage over the use of photons, which have a longer range and are constantly loosing energy; consequently supplying a dose to the tissue they pass through as shown by the dose curves in fig1. Another advantage of hadrons is the ability to manipulate this Bragg peak region, altering the energy of the particle alters the depth position of the peak, to give the spread out Bragg peak (SOBP), as seen in fig.1, such that it covers the depth of the tumour and the main dose is delivered into the full depth of the tumour while sparing much of the healthy tissue in front and behind the tumour[6][7]. The use of neutrons is somewhat different and is explained in more detail later in the next section.

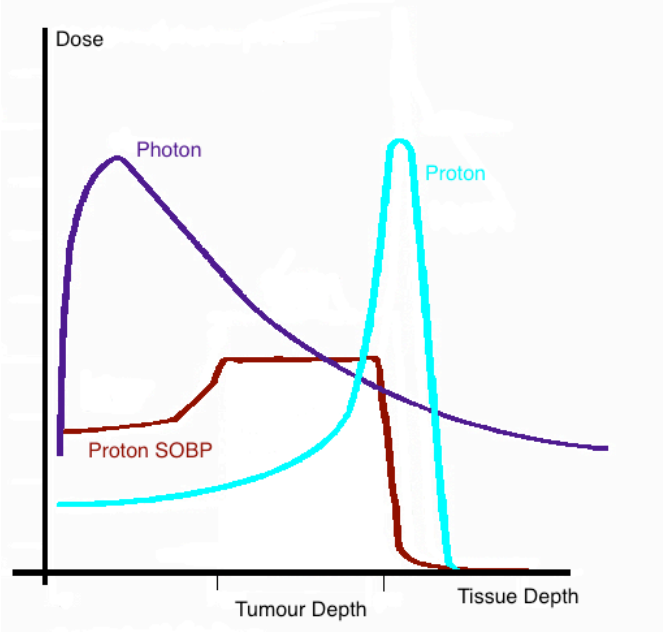

Figure 1. Effective relative dose demonstrating the Bragg peak and comparing doses from both photons and protons[6]

The accelerators mentioned above are typically heavy, complex machines that accelerate the particles to over 20MeV. This work is predominantly focused upon exploring whether some of these large and expensive accelerator systems can be replaced by a more compact, low energy accelerator system. There are two proposed types of accelerators:

(i) The ONIAC, currently being developed by Siemens[8], is an electrostatic accelerator based on the Cockcroft-Walton concept. A series of capacitors and diodes are used to multiply the voltage from an alternating current(AC) into a higher direct current(DC), in multiples of the original source voltage. The diodes control the AC source such that for the first polarity the current passes through the first diode and charges the first capacitor, when the source changes polarity the current passes through the second diode and charges the second capacitor. The second capacitor is also charged form the first capacitor and so doubling the charge at the second capacitor. A circuit schematic of the ONIAC voltage multiplier design can be seen in fig. 2. In this case concentric hemispherical shells are used as the electrodes, to keep the physical footprint of the machine as compact as possible. The 4 shell proof of principle machine can be seen in fig.3[8].

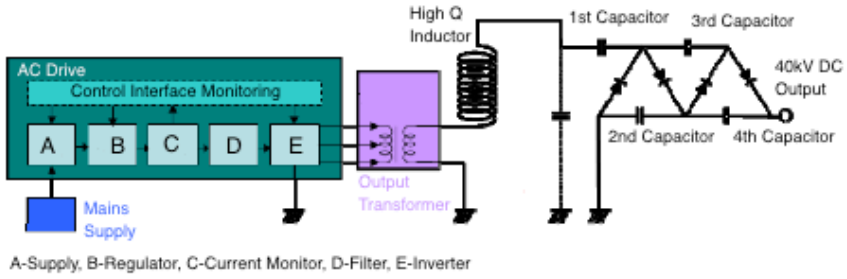

Figure 2. Circuit schematic of the ONIAC reproduced with permission from P.Beasley, courtesy of Siemens[8]

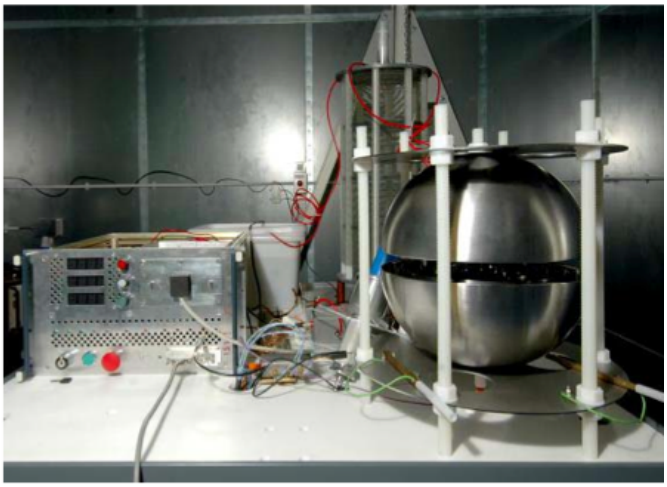

Figure 3. Proof of principle prototype for the ONIAC design reproduced with permission from P.Beasley, courtesy of Siemens[8]

(ii) A slightly higher energy Proton Isotope Production (PIP) accelerator (<14MeV)[9] is being developed by the International Institute for Accelerator Applications (IIAA), University of Huddersfield in collaboration with the Particle Accelerator Corporation (UK). PIP is a non-scaling Fixed Field Alternating Gradient accelerator, or ns-FFAG. The design schematic presented in fig.4 shows that this is a circular machine constructed of four sectors created by four normal conducting magnets with an increasing field (red to purple to blue) with increasing radius, strictly speaking, therefore not an alternating gradient just an increasing gradient accelerator. While not quite as compact as the ONIAC design this is still a small machine, radius of approximately 60cm, capable of fitting within the size restriction[9].

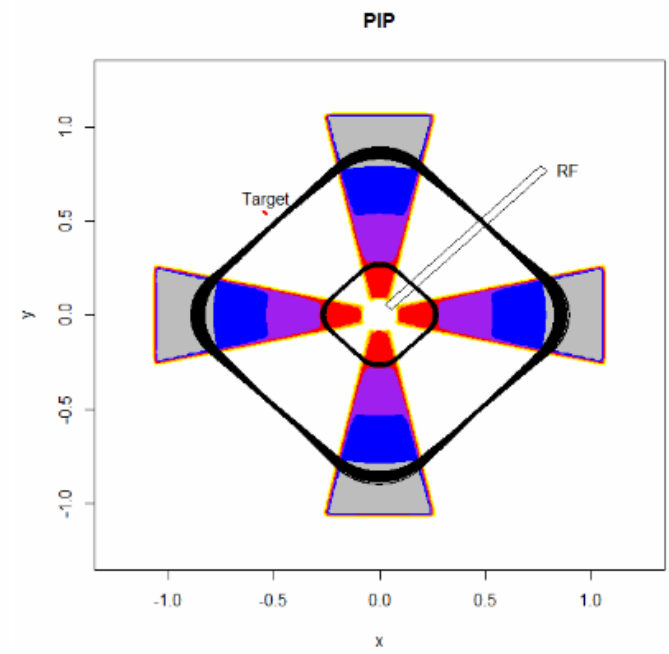

Figure 4. PIP design schematic reproduced with permission from R.Barlow[9]

The key applications of these accelerators focused on in this work are a specific type of neutron therapy, BNCT, and the production of radiotracer isotopes for SPECT and PET imaging.

1.1 Boron Neutron Capture Therapy

1.1.1 Introduction

Boron Neutron Capture Therapy, BNCT, is a still developing form of radiation therapy for the treatment of cancers such as advanced stage glioblastoma. Locher[10] first postulated the original concept of BNCT as early as 1936, not long after the discovery of the neutron itself[11]. The basic principle of neutron capture therapy, remaining relatively unchanged since Locher, involves injecting the patient with a drug designed specifically for uptake to be favoured by the tumour tissue over healthy tissue. Once the drug has had time to accumulate in the required area the patient is taken for irradiation by a neutron beam. The use of boron-enhanced pharmaceuticals for neutron capture therapy, BNCT, is favoured for two main reasons. Firstly it has been demonstrated that, although it is only a small difference, boron is taken up more readily by tumour tissue.

Boron also combines well with the pharmaceuticals used to target these tumours. Secondly boron has a high cross-section (barns) for neutron absorption, as shown in fig.5, compared to typically a few millibarns for other elements in the thermal neutron region (E_n < 1eV) where the cross-section has a 1/v dependence[12].

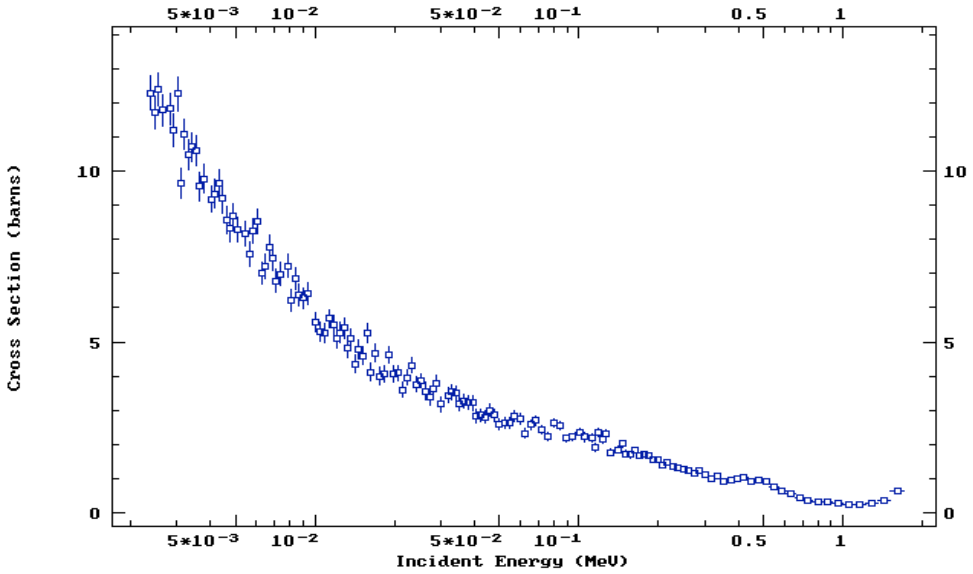

Figure 5. Neutron absorption cross-section for Boron-10 in the 1/v region. Data obtained and reproduced in accordance with EXFOR guidelines [12]

When the neutrons are absorbed by boron the following reaction (1) occurs within the tissue cell[13]:

$$^{10}B(n,a)^{7}Li \qquad (1)$$

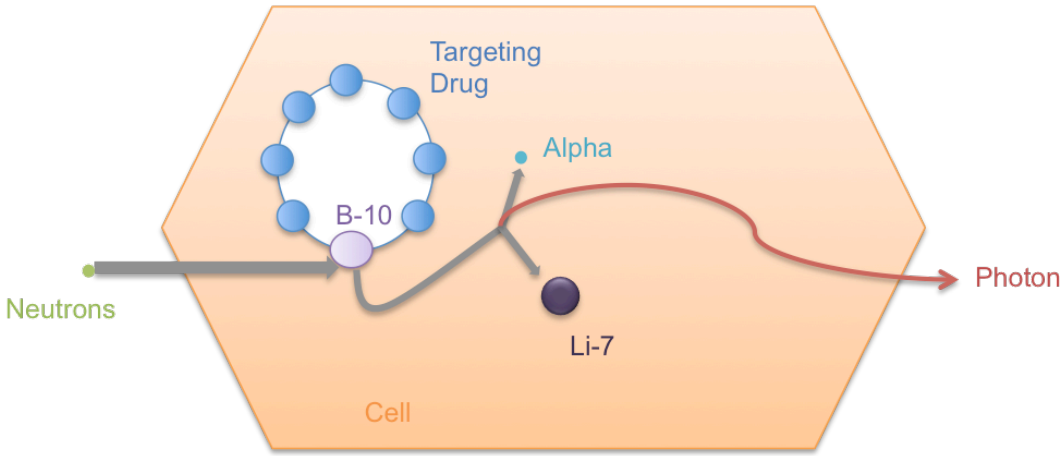

Figure 6. Pictorial representation of the reaction mechanism for BNCT within a cell[13]

The reaction mechanism depicted in fig.6 shows the result of the reaction of neutrons colliding with the boron, absorbed by the cell in the form of a targeting ligand, is the creation of two high-energy Linear Energy Transfer (LET)[14][15] particles: ^{7}Li and alpha radiation. Both of these LET particles are of short range, depositing all their energy within the cell in which they are created. Due to tumour cells being poor quality copies of healthy tissue that do not function properly this radiation is more damaging to tumour tissue and these cells are unable to repair themselves as quickly as healthy tissue[13]. Although healthy cells containing boron do not escape completely unscathed the damage is less and more easily repaired. Treatment plans are adjusted such that radiation is delivered in several short doses with the time between doses allowing for maximum regeneration of healthy tissue while still causing as much damage as possible to tumour tissue[13]. The short range of this radiation is also a factor contributing to minimizing the collateral damage to healthy tissue as it is contained within the cell in which it is produced.

1.1.2 Trials

There are two main contributions which determine the success of BNCT: (a) The ability to deliver adequately enough of the boron enhanced drug to the tumour tissue, minimizing the uptake in healthy tissue, and (b) the production and delivery of a suitable neutron beam to the patient.

The first instance of BNCT trials were carried out by Sweet[16] in the 1950/60s on patients with glioblastoma multiforme. These trials used the research reactor at Massachusetts Institute of Technology, USA, as a source of thermal neutrons. Unfortunately the results of these trials proved to be unsuccessful for reasons relating to both the contributions previously mentioned. It was found that, especially for deep-seated tumours using a thermal neutron source meant that there was not a sufficient neutron dose to the tumour site[15][16]. Part of the reason for this could be due to the high attenuation of thermal neutrons by the skull.

Independent studies simulating neutron transport through the body and the subsequent absorption by boron using GEANT4 came to the conclusion that an epithermal neutron source ($1eV < E_n < 10keV$)[17] would prove more suitable, allowing the neutrons to penetrate further into the patient. These results also show that the boron delivery agents that were used did not provide adequate targeting of the tumour tissue with the uptake being dispersed widely between both tumour and healthy tissue[15][16].

There has been continuous development in medicine to improve the targeting of these delivery drugs to increase localised uptake of the drug in tumour tissue. It was this development that lead to a renewal of BNCT trials in the 1970/80s, this time with the Japanese[18][19] at the forefront. Reactors were still used as the primary neutron source for these trials however this time both thermal and epithermal neutrons were used. A sample of over 100 patients with glioblastoma participated in this study. Typical survival rates for this type of tumour, even with an aggressive combination of conventional treatment, were 6 - 9 months with a long-term prognosis of 5year survival for less than 5% of patients. However over the course of this trial, with the use of BNCT, over 25% of patients survived for over 3 years from treatment[19].

Recent BNCT studies have been attempted by several groups, including some in the UK, with a focus upon the development of new neutron sources to replace the reactor-based technology. In particular accelerator-based approaches have been adopted in order to provide more flexible, accessible, cheap, and compact neutron sources and therefore a better quality of therapy in terms of availability, which can be tailored to the needs of each individual patient[13][20].

1.1.3 Neutron Production

As mentioned before, all previous trials have used nuclear reactors as a neutron source. There are several disadvantages associated with using such a facility for this type of medical procedure. The patients undergoing this therapy are seriously ill and require a properly equipped medical facility to provide

appropriate care for their situation. However the locational criteria of a nuclear reactor, typically a large unpopulated area, is often incompatible with those of a hospital, which is expected to be easily accessible and typically located within populated areas. This causes logistical difficulties in transporting the patients between the two facilities and could also have a detrimental effect on the health (and comfort) of the patient. Practically the reactor is an inflexible source of neutron beams for medical applications and is not a feasible option when considering the transition from trials into mainstream clinical operation[13][20].

The focus of new trials is now to develop an accelerator-based low energy neutron source capable of being located in a hospital environment. High-energy accelerator-based neutron sources are already widely used in research in the form of the spallation source. Spallation produces neutrons via the intra-nuclear cascade induced by firing high-energy protons at heavy nuclei.

However BNCT cannot rely upon the multimillion-pound proton accelerators required to produce spallation neutrons (typically with proton energies E_p>600MeV) and an alternative approach, using lower energy protons is required. For example it is possible to exploit specific high cross-section reactions of a light element target bombarded by low energy protons, E_p < 5MeV (just above the reaction threshold energy)[21]. Currently both linear accelerators and cyclotrons[22] are being used to provide protons of these energies and work is in progress to develop smaller and cheaper accelerator technology such as the non-scaling Fixed Field Alternating Gradient Accelerator (ns-FFAG)[9] or an electrostatic DC type machine such as the ONIAC[8].

The targetry for such a system comprises of a light element disc surrounded by blocks of hydrogenous moderator and absorbing shielding material to collimate a neutron beam such that the neutrons exit the target assembly and are directed to the patient at the most suitable energy for treatment.

1.1.4 Targetry

An extensive literature search into current work on accelerator-based neutron sources for BNCT reveals a divided community. Whilst the overall target assembly design is similar for each BNCT group there are several different neutron production targets that are currently considered, including those based upon lithium and beryllium discs[20][21].

There are advantages and disadvantages to each type of target, and correspondingly various compromises have to be made in designing a practical target:

Most notably lithium targets have excellent neutronic properties. Neutron yields from a lithium target are significantly higher (orders of magnitude) than those from an identical beryllium target at near threshold energies (< 3MeV)[13][23].

However lithium also has other less desirable properties that can favour the beryllium target. A principle concern for a practical target design is the melting point of the target material. During neutron producing reactions a significant proportion of the proton beam power is delivered into the target as heat. For a target material with low melting point and low heat conductivity, such as lithium (180°C)[13], this can cause severe structural damage, including melting, to the target even with the low beam power (5.6kW)[13][22] used by low proton energy systems. Various techniques have been explored to minimise the detrimental effects of beam delivery. After extensive studies the groups using both thick and thin lithium targets have implemented a copper substrate backing to the lithium target, to increase the target stability and aid in heat extraction. The copper backing also houses the cooling system[13][20][22].

This is not a straightforward solution, as solid and molten targets require different methods of affixing the lithium to the substrate to ensure maximum thermal conductivity between the layers. Some properties of lithium, such as thermal conductivity, and the target's structural integrity are changed when a

solid target liquefies. Some studies showed problems affixing a solid thin layer of lithium to the substrate and often if the lithium layer was too thin it would peel away from the copper during irradiation[13].

This all makes for a complex design and correspondingly complex manufacturing processes to obtain a suitable and practical lithium target. In comparison the beryllium target can be much simpler, for example the higher melting point of beryllium (1287°C)[13] allows for a much simpler cooling system.

The moderating materials surrounding the target disc are used to thermalize the neutron energy and thereby facilitate their absorption in the surrounding shielding, in order to reduce the risk of stray high-energy neutrons escaping from the target assembly into the treatment room and also to collimate the neutrons into a beam for delivery to the patient. The shielding and moderator designs appear to be standardised across the current BNCT facilities such as those of the Birmingham design[13] shown in fig.7.

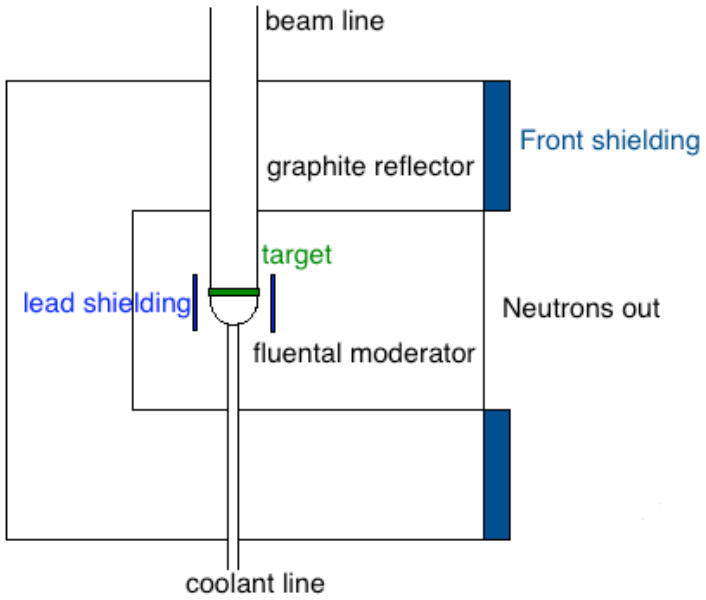

Figure 7. A schematic of a target design for a low-energy accelerator based neutron source[13[

The schematic in fig.7 shows that directly surrounding the target is a block of fluental of a suitable thickness to moderate the energy of the neutrons so that they are delivered to the patient in the epithermal energy range (1eV <E< 10keV)[17]. This is in turn surrounded by blocks of graphite reflector to contain

the higher energy neutrons within the target assembly and structured at one end to provide an outlet portal to the patient's position.

1.1.5 The Basis of the Current Study

The Medical Physics group at Birmingham University, University Hospitals Birmingham NHS Foundation Trust is currently attempting to optimise an accelerator-based BNCT treatment facility. This group favours the thick (0.7mm) lithium disc target and their full target assembly, fig.7, comprises of features mentioned previously but will be described in more detail later. The workhorse of their operation is currently an old 3MV Dynamitron accelerator, which produces a 1mA, 2.8MeV proton beam. This assembly utilises the following reactions (2)(3) to produce a therapy strength neutron flux[26]:

$$^{7}Li(p,n)^{7}Be \quad (2)$$

$$^{7}Li(p,n)^{7}Be^{*}(431keV) \quad (3)$$

Experimental neutron fluxes of $1.37X10^{12}$n/s have already been achieved[27]. Whilst this facility can boast a working accelerator-driven low energy neutron source, improvements are still necessary to develop a fully working trial facility.

Part of the research presented in this thesis focuses upon the optimization of the Birmingham BNCT target design using the particle physics simulation package GEANT4. Part of this study will also compare the performance of this target to that of the beryllium target reported in the literature.

There are two contributing channels to the neutron production from a beryllium target (4),(5):

$$^{9}Be(p,n)^{9}B \quad (4)$$

which dominates for incident proton energies up to 2.5MeV and

$$^{9}Be(p,p',n)^{8}B \quad (5)$$

which dominates above 3MeV[23-25].

However the neutron yield form a beryllium target is significantly lower at these energies than that from a similar lithium target and does not become comparable until proton energies close to 5MeV are reached. Presented in this thesis are the simulations of neutron yields from each of a lithium and beryllium target for a range of proton energies ($2MeV<E_p<5MeV$) and target thicknesses ($0.05mm<t<0.7mm$).

1.2 RADIOISOTOPES FOR IMAGING AND THERAPY

1.2.1 Introduction

Since the beginning of the 20th century, and within a few decades of their initial discovery, radioactive isotopes have been used in nuclear medicine as both a treatment and a diagnostic tool. The first studies of the medical uses and biological effects of radioactivity were carried out using naturally occurring radioactive materials such as radium salts and isotopes of lead, as used by George de Hevesy[28][29] in the first tracer experiments on both animals and humans.

Significant developments were made in nuclear medicine during the 1930s and 40s as new technologies allowed for the artificial production of new radioactive isotopes, and in much larger quantities than was currently available at the time from natural resources. The first of these advances was a consequence of the invention of the cyclotron by Lawrence[30]. His machine, a schematic of which can be seen in fig.8, is primarily comprised of a bras box containing a D shaped electrode (section A in fig.8). A second electrode is created using the box itself and a dividing wall (S) with slits positioned parallel to the straight section of electrode A. These two electrodes create an oscillating electric field, which causes the acceleration of charged particles as they circulate between the

electrodes on a path similar to that shown by the dashed line. These energetic particles are then fired into targets to create excited nuclei. A photograph of the first cyclotron built by Lawrence can be seen in fig.9.

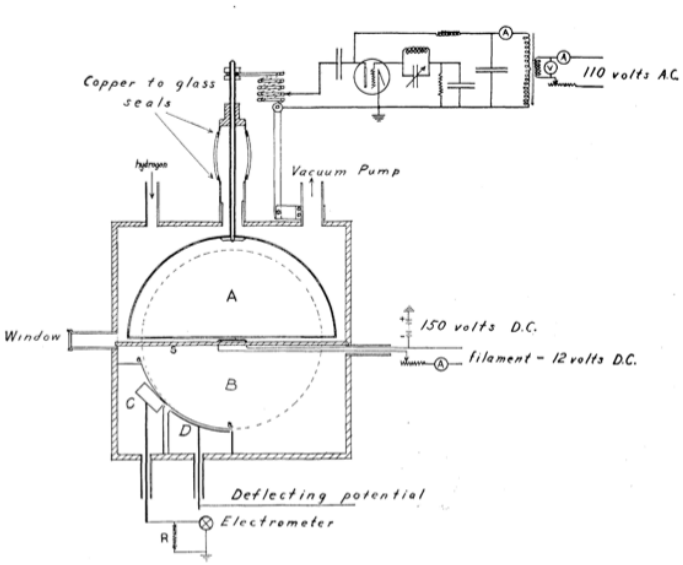

Figure 8. Schematic of the first cyclotron by Lawrence[30]. Reproduced with permission from E.O Lawrence and M.S. Livingston, Phys. Rev. 40, Pg.19-37, (1932). Copyright (1932) by the American Physical Society.

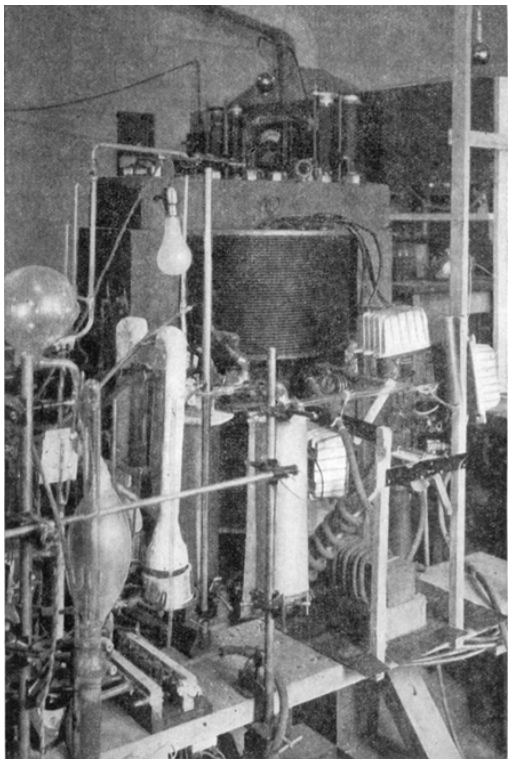

Figure 9. The first cyclotron used to discover new isotopes[30]. Reproduced with permission from E.O Lawrence and M.S. Livingston, Phys. Rev. 40, Pg.19-37, (1932). Copyright (1932) by the American Physical Society.

Many groups went on to carry out studies on the production of new elements and isotopes using machines identical to that shown in figs 8 & 9. One such group, led by Seaborg and Segre[1][2][31], discovered what has become the most popular and widely used gamma emitting tracer isotope ^{99m}Tc, a metastable isotope of the first artificially produced element technetium.

The second major advancement was provided by the work of Enrico Fermi[1], during the Manhattan Project, which resulted in the production of many new radioactive isotopes and the nuclear reactor[29].

1.2.2 Production of Radioisotopes Using Nuclear Reactors

It was found that the spent fuel of the nuclear reactor was not entirely comprised of waste material and that with suitable separation techniques it was possible to extract useable isotopes. One such isotope that is found in research fuel rods is molybdenum-99 a radioactive isotope that decays, via β- with a half-life of ~3 days, into ^{99m}Tc[32][33]. As a waste by-product it is very cheap to produce large quantities of ^{99}Mo. The supply chain for ^{99m}Tc is shown in fig.10, the only part of the chain that is extra to the cost already incurred in the waste disposal is that of the generator production and transportation to the hospital. As such production costs are typically less than 1% of the total cost for a single dose of ^{99m}Tc making it the cheapest radiotracer isotope available.

Figure 10. Tc-99m supply chain[36]

Because it was so readily produced ^{99m}Tc became the favoured isotope in further studies with the consequence that all later development of nuclear imaging techniques were based on the use of ^{99m}Tc. Indeed many of the delivery drugs and gamma cameras were developed specifically for optimal use with ^{99m}Tc.

Almost all other potential SPECT isotopes were ignored during this developmental period and ^{99m}Tc is still used in over 90% of all SPECT procedures[34]. There are currently over a dozen research reactors around the globe that contribute to the supply of ^{99}Mo although only about 5 of these play a major role[32][35]. A summary of current reactor based production of ^{99m}Tc can be seen in fig.11.

The supply chain in fig.10 shows that after the waste fuel is processed and the ^{99}Mo is removed, it is distributed to the regional hospitals in the form of a generator kit. The production of this generator kit is key to the availability of short lived radioisotopes.

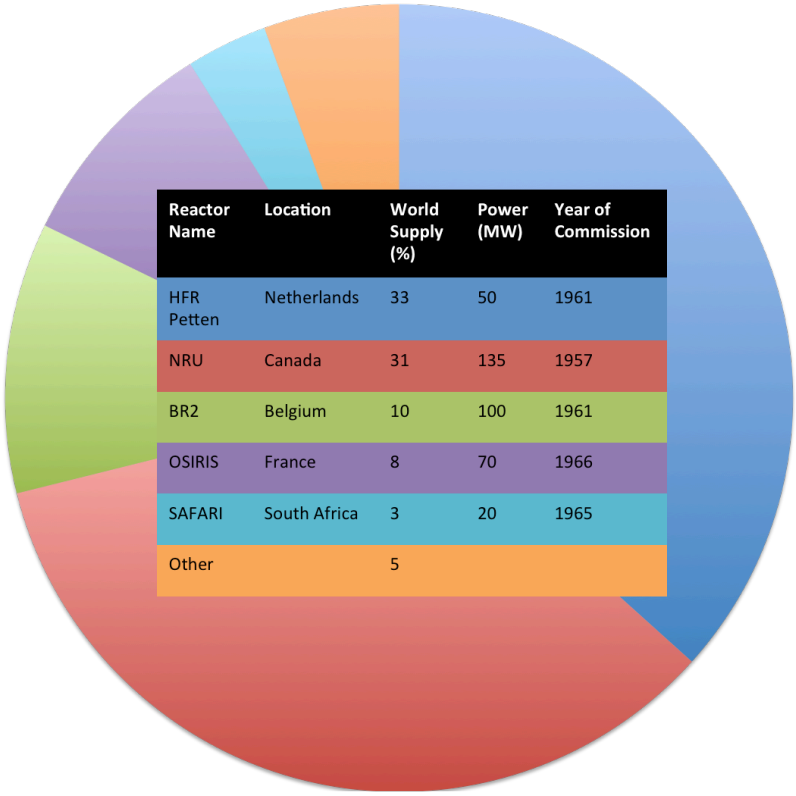

Reactor Name	Location	World Supply (%)	Power (MW)	Year of Commission
HFR Petten	Netherlands	33	50	1961
NRU	Canada	31	135	1957
BR2	Belgium	10	100	1961
OSIRIS	France	8	70	1966
SAFARI	South Africa	3	20	1965
Other		5		

Figure 11. Breakdown of current reactor production of ^{99}Mo, background pie chart corresponding to world supply of each reactor as shown in the table[36]

1.2.3 Generator Technology

The principle of the generator system is to produce short-lived daughter nuclei from the decay of longer-lived parent nuclei. Primarily this is to enable the

transportation of the daughter isotope over a long distance between production site and implementation site, without losing too much of the radioactivity.

It is imperative that the chemistry of the system, including separating the isotope and drug delivery, be as simple as possible[37]. For example the most common type of generator system described in fig.12 is a simple column system of parent isotope from which the daughter isotope can be easily extracted via elution with a standard solution, which separates the two elements, with the only contaminants being other isotopes of the daughter element. In most cases the elution is all that is needed for the radioisotope to be ready for labelling with the drug delivery compound and administration to the patient however other separation methods are also available, such as centrifuge and mass spectrometry [37][38].

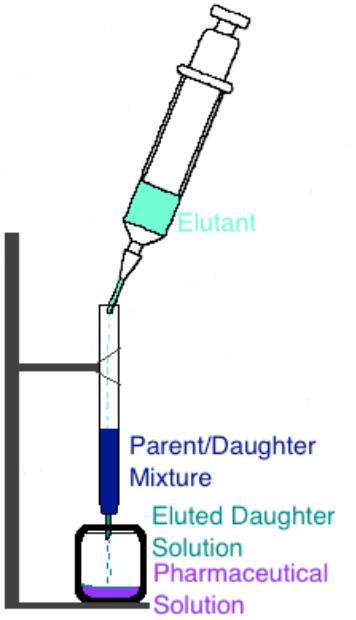

Figure 12. A generator 'cow' system for medical isotope production[38]

One of the first, and most common, generator systems in use is the $^{99}Mo/^{99m}Tc$ generator. When the ^{99}Mo decays in the column the ^{99m}Tc forms pertechnetate, TcO_4, which is a soluble anion. Therefore, the compound can be washed out easily by passing a sterile saline solution through the column. The eluted solution is then mixed with a pre-prepared drug assembly kit where the TcO_4 readily reacts into the ligand and is almost instantly ready for administration to the patient[34].

Such generator kits have many advantages. Given the current distribution system that relies upon a few regional production centres to service the entire world's supply, this system allows for the transportation and use of short-lived isotopes compatible with biological processes that would not be possible via direct production. For the use of short-lived isotopes direct production is only viable as a local source at the medical facility[29][32].

1.2.4 Modern Nuclear Medicine

There are two branches of nuclear medicine: treatment and diagnostics. The medical isotopes referred to in this work are predominantly diagnostic in nature and can be classed into two main procedures, SPECT (Single Photon Emission Computed Tomography) and PET (Positron Emission Tomography).
Even with massive advances in technology the basic principle of diagnostic nuclear imaging techniques has remained the same. The most notable of these advances is the invention of the gamma (or scintillator) camera, by Anger, which gave rise to the modern imaging technique SPECT in the 1950s[39-41].

1.2.4.1 SPECT

A SPECT procedure uses a radioactive, gamma emitting, isotope injected into the patient as either a soluble ion or, more commonly, in combination with a ligand designed for targeted uptake by a specific part of the body. The isotope must have a compatible half-life with the biological process to obtain suitable activity from the required area. Some specific processes require the use of an isotope with much shorter half-lives than normal. Most SPECT imaging procedures use ^{99m}Tc which has a half-life of ~6hours[33]. This is long enough to allow suitable up-take in the required region but short enough that the activity sufficiently diminishes to avoid long stays in hospital for the patient.

Scintillator cameras positioned at various angles around the patient detect the gammas emitted by the isotope from inside the body. While a SPECT scan only

requires one detector it is possible to reduce the time needed to take an image by using multiple cameras in order to cover the full 360degrees around the patient, for instance using two cameras each covering an opposite 180degree arc could halve the procedure time for the patient[39][40].

A scintillator camera, as depicted in fig.13, is comprised of several layers, the key elements being a collimator, scintillator crystal and photomultiplier tubes. The first layer, the collimator, is typically comprised of a thick lead sheet full of many small holes. Any gammas that enter the collimator at an angle are attenuated by the lead such that the majority of the gammas emitted by the source are not detected, only those gammas which enter the collimator in a trajectory that takes them straight up through one of the holes reaches the second layer of the camera. It is possible to then trace these trajectories back in a straight line through the holes to the source to pin point the location from which these gammas were emitted. Those gammas that reach the second layer interact with electrons as they pass through the crystal. This interaction excites the electrons out of their energy level. As the electrons return to their minimum energy level they emit a flash that is detected by the photomultipliers behind the crystal. The signal from the photomultipliers is in turn sent to a computer to be counted and the position of these detections can be used by the software to produce 2D and 3D maps of the source of the gammas and hence an image of the area of interest in which the radioactive isotope has been taken up[41].

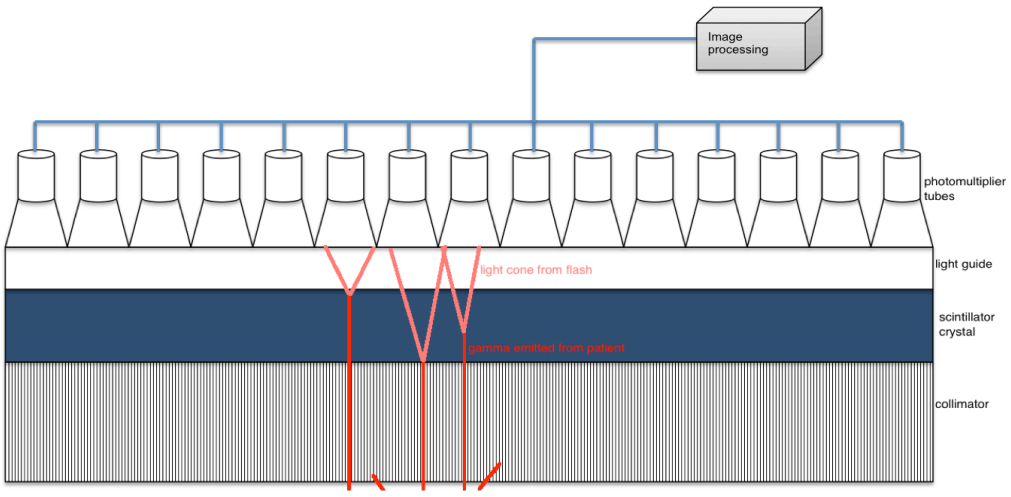

Figure 13. Working principle of a modern gamma camera for SPECT[41]

1.2.4.2 PET

The PET system is similar to SPECT, both use the same computer software to reconstruct 2D and 3D images of the inside of the body by the detection of gamma rays. However the main difference is that PET uses secondary gammas produced from the interactions of emitted positrons with electrons[40].

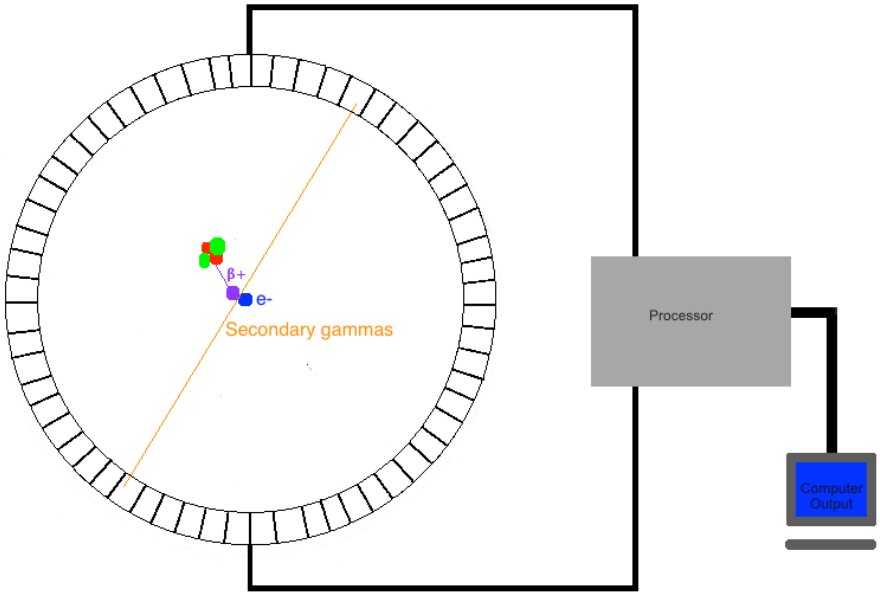

Figure 14. Working principle behind a PET procedure[42]

In a similar fashion to SPECT the patient is injected with a short-lived positron-emitting isotope, such as ^{18}F, as a combination with a targeting ligand for uptake in the required part of the body. When the positrons are emitted they quickly interact with an electron to produce a gamma pair that are then detected by the scintillator cameras. Figure 14 shows a typical PET set up, the positron/gamma source (the patient) in the centre of a ring of detectors connected to a processor and screen. Unlike SPECT, PET requires the use of two cameras in opposite positions in order to simultaneously detect the two gammas produced by each positron. This double signal improves the resolution of a PET image over that of SPECT[42]. The double signal can also be used to calculate the source of the gammas and so PET detectors do not require the collimator on SPECT gamma cameras. Unfortunately it is also more expensive than SPECT, because of this and

the requirement of shorter-lived isotopes. The majority of PET isotopes, including the most popular ^{18}F, are produced directly using medical cyclotrons[43][44] (15MeV < E < 20MeV). This means that PET facilities are large and expensive in order to cater for onsite production of the isotopes, which limits the availability of PET to the general population.

1.2.5 The ^{99m}Tc Crisis

In the current state of nuclear medicine SPECT, or more specifically ^{99m}Tc, is responsible for over 80% of the world's nuclear medical imaging procedures[45]. The global supply of ^{99m}Tc is provided by an aging fleet of over a dozen research reactors, however only 5 of these are major contributors, each covering a sizable region. Two of these reactors, namely the NRU(National Research Universal)-Canada, for the Americas, and HFR(High Flux Reactor)-Petten, for Europe, are jointly responsible for over 60% of the world's supply of $^{99}Mo/^{99m}Tc$[32][34][35]. As is the nature of reactors periodic planned and unplanned shutdowns are required to carry out necessary maintenance and repairs to extend the lifetime of the reactor until such a point that maintenance and refurbishment is no longer efficient and the reactor is permanently shutdown.

In 2009/2010 the two main reactors both underwent an extended period of overlapping shutdowns, both scheduled and unscheduled, not long after the reopening of several of the smaller reactors. This caused a significant depletion in the world wide supply of ^{99}Mo. Over 90% of SPECT procedures had to be cancelled or postponed during this time[45][46].

This situation highlighted nuclear medicine's dependence on ^{99m}Tc and upon reactors for its production, prompting a discussion on possible alternatives. It has also become apparent, in light of these shutdowns, that the current fleet of reactors are at a point where it is not possible to keep repairing them and they will soon, within the next decade, have to be permanently shutdown. Therefore it is now a pressing matter to find a suitable replacement system that can be

implemented within the short timeframe before decommissioning of these reactors begins.

1.2.6 The Role Of This Research Programme

In the wake of this crisis there has been a drive towards securing a new supply of $^{99}Mo/^{99m}Tc$ and re-evaluation of the current production system. As there is no wide scale strategy in place for replacing the world's ^{99m}Tc supply, new production routes that secure a more local supply network are favoured. In order to do this, and with time being of the essence, it is timely to consider technology which does not require the commissioning of new reactor sources and towards implementing cheaper and smaller accelerator based systems which could be realised in a shorter time frame[45-47]. As the NRU is one of the major current suppliers close to shut down, the Canadian government has started the exploration into new production routes in order to maintain their domestic supply by commissioning studies at two major national laboratories, TRIUMF[46] and CLS[47].

CLS, the Canadian Light Source, has developed a method of producing ^{99}Mo by using X-rays to irradiate ^{100}Mo targets[47]. The ^{99m}Tc can be separated from the $^{100}Mo/^{99}Mo$ mixed target after irradiation in a simple column similar to the generator separation and prepared for use in the same way[37][38].

The TRIUMF[32][35][40,41] facility has implemented a proton driven method for the direct production of ^{99m}Tc

$$^{100}Mo(p,2n)^{99m}Tc \qquad (6)$$

using their existing 20MeV cyclotron. During this study acceptable medical grade ^{99m}Tc has been produced and suitable target processing and recycling have been developed proving this route to be a feasible method for the production of ^{99m}Tc. This production method is planned for use in a smaller regional hub

supply system due to the larger dimensions of the cyclotron required at these proton energies.

However direct production of ^{99m}Tc is more suited to a local on-site type production system in order to minimize the activity lost during transport.
To achieve this goal a smaller low energy (< 10MeV) system is proposed and there are several types of accelerator under development with this in mind. At these energies the physical footprint of the accelerator/production system can be made much smaller so as to fit into a basement or current generator room at a local hospital facility. Within this thesis there are also discussions on the potential of replacement isotopes for ^{99m}Tc such as the PET isotopes^{60}Cu, ^{61}Cu, ^{62}Cu, ^{66}Ga and ^{68}Ga which were chosen for study here as they have all undergone previous use or trials as PET tracer isotopes, therefore much of the processing chemistry work has been previously determined. Due to the work that has already been carried out it should make introduction of this new production system to the market much smoother, quicker and simpler, compared to the introduction of previously unused isotopes. To assess the potential of this system GEANT4 simulations were carried out to replicate the possible production yields and obtainable activity of the isotopes mentioned above under a 10MeV, 1mA proton beam. This matches the beam parameters given for the ONIAC machine as the remit for this work given by the sponsors, Siemens, was to investigate medical applications of this machine. A GEANT4 benchmarking study was also undertaken for low energy proton interactions for neutron and isotope production , during this phase the production of current SPECT isotopes Cu, Zn, and I from low energy E_p< 20MeV (p,n) reactions was studied and simulated yields and cross-sections were compared to experimental data.

2. GEANT4

2.1 Introduction

GEANT4 was developed at CERN in the 1990s to fill the need for a complex and comprehensive simulation toolkit for the modelling of high-energy particle-matter interactions, primarily for the ATLAS(A Toroidal LHC Apparatus) detector components of the LHC(Large Hadron Collider)[49]. Since its initial conception GEANT4 has developed into a worldwide collaboration project and as such undergoes continual development and extension both from within and outside the high-energy physics (HEP) community. Over the years the applications of GEANT4 have broadened into many areas of physics and beyond[50] including astrophysics, modelling for the International Space Station[51], and medical physics, for example modelling biological and chemical interactions within the body[52].

Other medical based applications include the use of GEANT4 to model mixed accelerator and biological systems such as hadron therapy facilities. GEANT4 already has the capabilities to simulate all the accelerator components of the system and the material libraries have been updated by the medical community to incorporate biological materials such as bone and muscle, avoiding the need for the simulator to create them from their elemental composition, which simplifies the building of regular or complex simulations[52][53].

GEANT4 is an object-oriented code written in the C++ language[49][54]. The decision to use an object-oriented approach was made at the conception of the project and allowed for a modular structure that could split components into small working groups during development, for a more efficient design process. This has also allowed for an open and transparent design to be passed on to the user, providing considerable flexibility and control in creating their simulation.

The standard toolkit and libraries incorporated in even the most basic version of GEANT4 contain an immense collection of objects, materials and features at the

users disposal. Each of these can be called, defined, and implemented to the users specification to meet the requirements of the scenario. This approach also gives the user the flexibility to make developments to the toolkit as required, after suitable validation testing these developments may even be included in the standard release at a later update[49].

2.2 Structure

From the original design as a simulation package for the transport and interaction of particles through matter GEANT4 is split into the following domains, which determine the class structure and working groups[49]:

1. geometry and materials
2. particle interaction in matter
3. tracking management
4. digitation and hit management
5. event and track management
6. visualisation
7. user interface

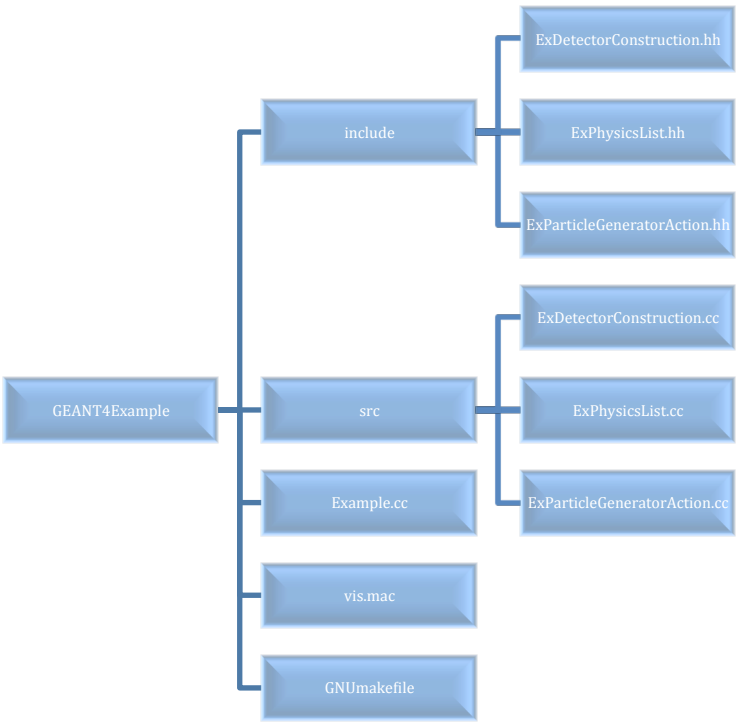

Figure 15. Example of implementation class structure

As the medium by which the user interacts with GEANT4 the user interface is the most significant of the domains, where features from each of the other six can be pulled together to build and run a simulation. The basic user interface provides eight classes, two user initialization and six user actions[54], for use in building a simulation. The file structure of a GEANT4 simulation is shown in fig.15 starting with the main simulation folder (GEANT4Example) that contains the executable file(example.cc), the make file (GNUmakefile) any macros to be used in the simulation(vis.mac), the header folder(include) and the source folder(src).
Each of the classes used in a GEANT4 simulation is comprised of a header (fig.15:GEANT4Eample/include/*.hh) and a source (fig.15:GEANT4Example/src/*.cc) file in which declarations and identifiers can be called and implemented from the libraries. An example of the code for each of the files in the GEANT4Example folder are given in appendix A. Three of the user interface classes are mandatory in order to create a working simulation and posses no default options as all components are to be specified by the users requirements[49].

i) Detector Construction
ii) Physics List
iii) Primary Generator Action

The other five classes are optional and can be used to improve the simulation, such as decrease the run time, or include advanced features as per the scenario requirements. For these classes default settings are in place but can easily be altered by the user[49].

iv) User Run Action
v) User Event Action
vi) User Stacking Action
vii) User Tracking Action
viii) User Stepping Action

For the purposes of this work only i, ii, iii, and viii were required and will be discussed in more detail.

2.3 Creating a GEANT4 Simulation

2.3.1 Detector Construction

As the first mandatory class, the detector construction, as the name would suggest, is where the geometries are created. The structure of GEANT4 geometry creation can be described as a stacking doll approach where an initial world volume is created within which all other volumes are placed. No volume can overlap another volume but must be completely contained within its mother volume, be that the world or another previously created volume in the geometry, and is positioned such that the coordinates of the volume's central point are given with respect to the central point of the mother volume. Any object that intersects two or more separate volumes e.g. a beam pipe that runs through multiple levels of shielding, must be created in sections where each section is contained within its mother volume and positioned so that the edges of the two sections are adjacent. An example of this using the Birmingham design (fig.7) is shown in fig.16 where the beam line and coolant pipe line have to be created in separate sections that run through two or more objects within the geometry.

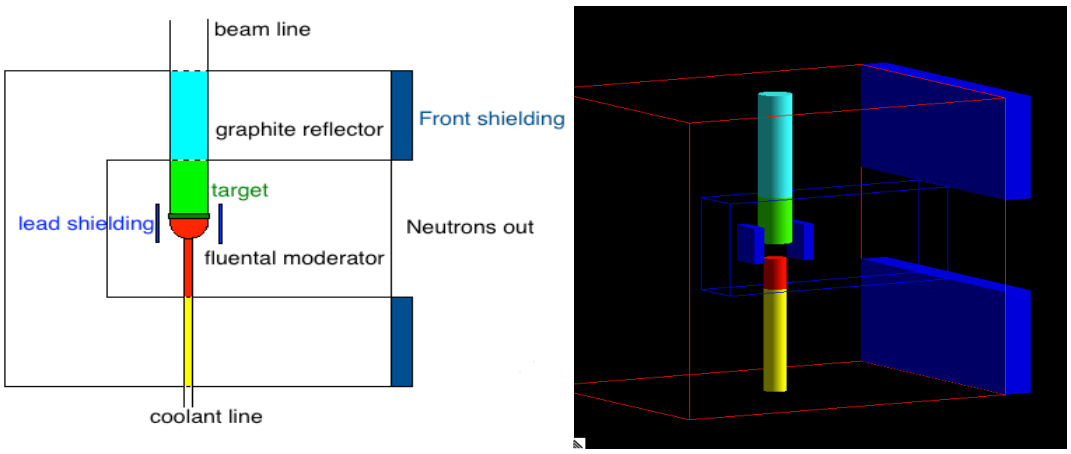

Figure 16. GEANT4 visualisation (right)of the Birmingham target assembly (left)[13]demonstrating two sections of adjoined beam pipe (green and aqua) and two sections of adjoined coolant line (red and yellow)

Objects can be created using the many shapes contained in the GEANT4 libraries, ranging from simple boxes and cylinders to the more complex, but typical accelerator and detector structures, such as the polycone shown in fig.17.

```
//Dimensions

G4double phiStart = 0.*deg;
G4double phiTotal = 360.*deg;
G4int numZPlane = 9;
const G4double zPlane[] = {5,7,9,11,25,27,29,31,35};
const G4double rInner[] = {0,0,0,0,0,0,0,0,0};
const G4double rOuter[] = {0,10,10,5,5,10,10,2,2};

//Polycone

G4Polycone* Object1 = new G4Polycone("ob1", phiStart, phitotal,numZPlane, zPlane, rInner, rOuter);
```

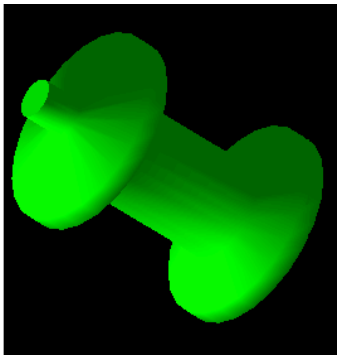

Figure 17. The polycone: an example of shapes available in the GEANT4 libraries and the code lines which create it.

Each volume of the geometry is created in three stages. Firstly the solid: at this stage the object is given a shape and dimensions. Secondly the logical volume is used to give the solid a material. Materials are defined at the beginning of the source file and can be either elements or compounds, which are called from the libraries as their natural composition or created from individual isotopic constituents, an example of the code required to create a material is shown in fig.18. Finally the physical volume places the logical volume within the geometry, defining the mother volume, central coordinates and rotation, among other properties[49][54]. An example of the code lines required to create an object are shown in fig.19.

```
//Air
G4Element* N = new G4Element("Nitrogen","N",z= 7., a= 14.01*g/mole);
G4Element* O = new G4Element("Oxygen","O",z=8., a= 16.00*g/mole);
G4Material* Air = new G4Material("Air", density= 0.0*mg/cm3, nel=2);
Air->AddElement(N, 70*perCent);
Air->AddElement(O, 30*perCent);
```

Figure 18. Example of material definition in GEANT4 (for full code see appendix A)

```
//world dimensions
G4double worldLength=1*m;

//target dimensions
G4double innerRadOfT = 0.*m;
G4double outerRadOfT = 0.02*m;
G4double hightOfT = 0.00035*m;
G4double startAngOfT = 0.*deg;
G4double spanningOfT = 360.*deg;

//world
solidWorld = new G4Box("world", worldLength,worldLength,worldLength);
logicWorld = new G4LogicalVolume(solidWorld,Air,"World",0,0,0);
physiWorld = new G4PVPlacement(0,G4ThreeVector(), logicWorld,"World",0,false,0);

//target
    //rotation
G4RotationMatrix* xRot = new G4RotationMatrix;
xRot->rotateX(90.*deg);
    //solid disc
 G4Tubs* target = new G4Tubs("target",innerRadOfT, outerRadOfT, hightOfT, startAngOfT,spanningOfT);
    //logical volume
logicTarget = new G4LogicalVolume(target,Li,"Target",0,0,0);
    //phyical volume
 physiTarget = new G4PVPlacement(xRot,G4ThreeVector(),logicTarget,"Target",logicDet,false,0);
```

Figure 19. Example of geometry definition in GEANT4 (for full code see appendix A)

Also in this class visualisation properties, such as colour, can be set for each individual object.

2.3.2 Physics List

As the second mandatory initialisation class the physics list is the place to specify the physical processes required by, or of interest in, the simulation. The standard GEANT4 libraries contain the majority of the most commonly occurring and relevant physical processes and up to date reaction cross-section data. There are several additional libraries catering to more specialised processes and restricted data which can be obtained from the relevant development team. Within the physics list it is possible for the user to implement specific physical processes of interest. For example, an initial test physics list used in this work for low energy proton interactions contained only hadronic processes and excluded all optical and electromagnetic processes as they were of no interest or had no bearing on the desired results of the simulation.

For broader, more detailed overview of results or if the user is uncertain as to the specific processes relevant it is possible to implement all physical processes

in this class, however it is not recommended as, among other reasons, this can increase the runtime of the simulation.

Also contained in the libraries are several pre-designed physical models that can be used in place of the physics list. These models can be entirely theoretical, data-driven or semi-empirical[50].

2.3.3 Primary Generator Action

The final mandatory class, and first of the user actions, the primary generator action is used to set up the parameters of the incident particles. GEANT4 has two methods of incident particle generation, the general particle source and the particle gun.

The particle gun is a simpler and the most commonly used method of particle generation, as it is more suitable for typical GEANT4 applications. In this case the source is analogous to an accelerator based model, a number of incident particles, specified by the user, are fired uniformly from a point like source to create a beam with momentum specified by the user[49][54].

The general particle source, the more complex of the two methods to implement, has more sophisticated settings that can be applied to the incident particles, such as spectrum and angular distribution. Each of these features has several pre-defined options as well as the option to be arbitrarily described by the user. The general source also allows for the use of multiple sources within the same geometry[49][54].

The coordinates of the incident source are defined by the user with respect to the centre of the world volume.

2.3.4 User Run Action

The first optional user action, the user run action deals with run processes, where the run is defined as the length of a simulation. The beginning of a run is denoted by the `beamOn` command and lasts until all the secondaries from the specified incident particles have been tracked through the simulation. Three virtual methods `GenerateRun`, `BeginOfRunAction` and `EndOfRunAction` can be implemented at various points during the run in order to obtain specific information about, and analysis of, the run[54].

2.3.5 User Event Action

A user action dealing with events, a stack of particle tracks, contains two virtual methods: `beginOfEventAction` and `endOfEventAction`. These are used to obtain and process information about a single or series of events[54].

2.3.6 User Stacking Action

A user action to prioritise and process the stack, the ordering of track importance, by three virtual methods: `ClassifyNewTrack`, `NewStage` and `PrepareNewEvent`. This allows the user to prioritise specific particle tracks, for instance highlighting attention of proton and neutron tracks and interactions and disregarding lepton tracks in order to speed up the run time of a simulation[54].

2.3.7 User Tracking Action

A user action to manage and detail the particle track. A particle track is the trajectory of each particle updated by each step from the particles creation until it reaches one of three conclusions, its path exits the world, the particle interacts in a manner that causes it to cease to exist or its kinetic energy reaches zero[54].

2.3.8 User Stepping Action

The only optional user action implemented in this work the stepping action relates to the step, a section of the particle trajectory. A step is bounded by two step points, the `PrePoint` and `PostPoint`, and while its length can be specified by the user a step point must occur whenever a particle reaches a volume boundary, fig.20.

The stepping action can be used to acquire output of specific information about a particle during a particular step at any point within the geometry. For example in this class the user can ask GEANT4 to output the kinetic energy of a particle type as it reaches the boundary and exits a specified volume[54].

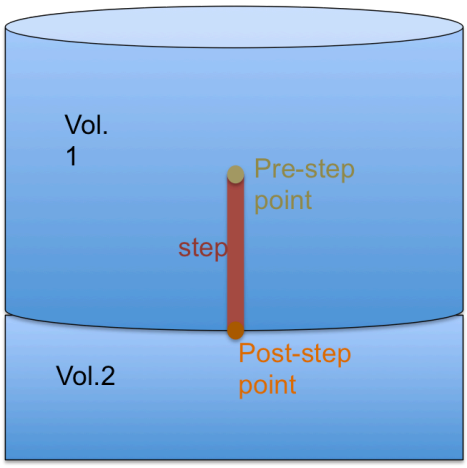

Figure 20. Illustration of the definition of a step between two volumes bounded by the step points

2.3.9 Other Files

2.3.9.1 Macros

Macros can be used in GEANT4 where sections of code such as a series of command lines can be written and then called for use in a run. Within this work the common macro vis.mac was used in order to set up and run commands for the visualisation software used with GEANT4 during a run. An example of a vis.mac feature is the ability to specify which tracks to include in the visualisation such as only showing the neutron tracks for a given run.

2.3.9.2 Executable

The executable file is where all the other files and macros are pulled together and compiled under the various managers in order to run a complete simulation. The executable file is also where the run mode is set up, either batch or interactive. Interactive mode allows the terminal command prompt to be used to make some modifications to the simulation between runs, for example the energy of the incident particles can be changed without having to alter the code and recompile. The number of incident particles can be changed between runs using the `run/beamOn` command.

GEANT4 can also be run non-interactively in batch mode. To do this the same terminal commands can be given in the executable or called here from a macro to run the simulation.

A simulation example to run a proton beam through the full BNCT geometry using a modified example physics list to obtain the neutron spectrum produced can be seen in appendix A.

2.4 Physics Models

A key feature of GEANT4 is the physics models available within its libraries and the ability to tailor the exact processes to include for any given simulation at the users discretion. The models and processes are split into either electromagnetic or hadronic in nature. As well as all the individual processes there are also many of the standard physical models, made up of various processes, which are currently thought to be the best approximations to explain the physics of various interactions. These models can be theoretical, data-driven or semi-empirical. Theoretical models rely on mathematical calculations to explain processes and determine the outcome of interactions where there is very poor, or no, experimental data available. Data-driven models base the processes and outcomes on experimental cross-section data from the accepted libraries ENDF and TENDL, which are downloaded within the GEANT4 libraries during

installation. Semi-empirical models use mathematical calculations to derive and extrapolate outcomes and processes from the available experimental data when a comprehensive data set is not available for the scenario, for example when modelling interactions of protons with higher energies than have currently been reached in the lab for design of a new facility.

At the conception of this work, while GEANT4 had an exceptional reputation for its capabilities of data-driven neutron transport models for a range of energies available in the standard release libraries, there were only theoretical models available for the interactions and transport of low energy protons[55]. An important part of this work was to benchmark the two most suitable theoretical models, the high precision neutron transport version of both the Bertini cascade model, QGSP_BERT_HP, and the binary cascade model, QGSP_BIC_HP, with experimental data and the newly developed low energy proton data-driven model QGSP_BIC_PHP.

2.4.1 QGSP_BERT_HP

The Bertini cascade model is based on the intra nuclear cascade (INC). The INC takes the particle-nucleus collision to the approximation of particle-nucleon collision. The justification for this comes from the observation that the incident particle's de Broglie wavelength is shorter than the average spacing between nucleons, so that the incident particle only sees the effect of or interacts with one nucleon at a time[56][57]. The suitability for using this model is therefore determined by the following condition:

$$\frac{\lambda_B}{v} \ll \tau_c \ll \Delta t \tag{7}$$

where λ_B is the de Broglie wavelength of the nucleon, v the relative velocity of two nucleons, τ_c is the distance between collisions, and Δt the time between

collisions[57]. At incident particle energies below 200MeV this condition does not hold true and the pre-equilibrium model must be implemented.

In the standard INC model an incident particle enters a nucleus at a uniformly selected point on the surface and traverses a path whose length is determined by the total free particle-particle cross-section and nucleon density ending in an inelastic collision. The speed of the collision determines the outcome of the collision and how the products are handled. For fast, near-instantaneous collisions, such as spallation, an excited nucleus is created which is solved by the pre-equilibrium emission. Slow collisions result in a compound nucleus decaying by evaporation. The reactions that occur, and their resulting products, are governed by the Pauli exclusion principle. Any interaction that results in products being formed in an already occupied state and thus break the Pauli exclusion principle are not permitted[56][57].

In the Bertini cascade the nucleus is treated as a 2-dimensional smooth medium. The nuclear radius and momentum are defined according to the Fermi gas model. For the targets of interest, A = 7,9 and A > 50, the nucleus is modelled as three concentric spheres, i = {1,2,3}, with a radius defined by[56]

$4 < A < 11$

$$r_i(\alpha_i) = \sqrt{C_1^2\left(1-\frac{1}{A}\right) + 6.4\sqrt{-\log(\alpha_i)}} \tag{8}$$

where $C_1 = 3.3836A^{1/3}$ and α_i = {0.01,0.3,0.7}

$A > 11$

$$r_i(\alpha_i) = C_2 \log\left(\frac{1+e^{-\frac{C_1}{C_2}}}{\alpha_i} - 1\right) + C_1 \tag{9}$$

where C_2 = 1.7234.

Each collision is represented within the nucleus as particle-hole states. At the end of the cascade, defined as the point at which all particles that are able to leave the nucleus have done so, the total particle-hole states are summed to give an excited nucleus which decays via either pre-equilibrium or evaporation to determine the final states[56].

The pre-equilibrium model is based on the exciton model where the nuclear states are determined by the number of particles and holes. The particle-hole state configuration during the cascade is determined by the following selection rules:

$$\Delta p = 0^{+}_{-}1\,,\ \Delta h = 0^{+}_{-}1\,,\ \Delta n = 0^{+}_{-}2 \tag{10}$$

Where p is the number of particles, h is the number of holes and n is the sum of particles and holes. The nucleus is treated as a pre-compound state until it reaches a number of excitons (holes) and particle emissions that give rise to an equilibrium state[58]. This state is fixed by

$$\lambda_{+2}\left(n_{eq}, E^{*}\right) = \lambda_{-2}(n_{eq}, E^{*}) \tag{11}$$

where $n_{eq}$is the number of exciton states at equilibrium:

$$n_{eq} = \sqrt{2gE^{*}} \tag{12}$$

g is the particle density, $\lambda_{\pm 2}$ is the transition rate of the state by ±2 and E^{*} is the exciton energy[58]. At this point all transitions, changes in state possible for each collision, are equally probable. In the pre-equilibrium model the nucleus does not reach this state, but instead undergoes de-excitation via non-equilibrium evaporation. The angular distribution of the emitted particles is isotropic in the exciton frame of reference. In some cases light nuclei with high exciton energy undergo Fermi breakup where the whole nucleus breaks up into its constituent protons and neutrons[58].

The evaporation model requires the nucleus to be in the equilibrium state before evaporation occurs and to be re-established after the particle is emitted. This gives rise to an isotropic distribution of particles from the nucleus[58].

After the final states are determined energy conservation laws are applied to the secondary particles. To do this GEANT4 creates virtual gamma particles with appropriate energies to balance initial and final state particle energies. Without this feature the secondary particles created are seen to be more energetic than would be expected by approximately +/- 0.5MeV. At the higher energies (> 100MeV) typically used in GEANT4 this discrepancy can go almost unnoticed and has very little bearing on the accuracy of the results, however at lower energies (<10MeV) in which this work is interested in this becomes a significant discrepancy in the energy spectrum of the secondaries, although is preferential for accurate cross-section and particle yield counts[56][57].

This model has been well tested and implemented for the incident proton energy region 100MeV < E_p < 5GeV[56].

2.4.2 QGSP_BIC_HP

The binary cascade is also based on the INC. However in this case the nucleus is described as a 3-dimensional collection of nucleons. The propagation of the incident particle through the nucleus is broken down into sections of straight trajectories governed by a given time stamp[56]. The time stamp is defined as the time taken for the incident particle to reach the distance of closest approach, d_i^{min}, to the first nucleon with which a collision could occur, when $d_i^{min} < \sqrt{\frac{\sigma_i}{\pi}}$. σ_i is the interaction cross-section for the particles involved, calculated using the total inclusive cross-section[56], which is derived from experimental data whenever possible. The collisions themselves, and the creation of secondary particles, are modelled as the decay of resonances within the nucleus and obey Pauli exclusion principles. For a secondary to be created the particle's momentum must be greater than that of the Fermi momentum, at which point the primary particle is discarded and the secondary is tracked in its place. The cascade ends when all secondaries, with mean energy above the cut off threshold (15MeV) have decayed, reacted or left the nucleus[56][59].

The nucleus decays according to the pre-compound model as in the Bertini cascade. The state of the nucleus at the time when the particle's kinetic energy drops below the threshold for which the cascade holds is used as the initial state of the nucleus for the pre-compound model. The number of holes is determined by the difference in the number of nucleons at this time and the initial number of nucleons before any collisions occurred. At this point the decay is treated the same as the Bertini model via evaporation or pre-equilibrium decay[56][59].

2.4.3 QGSP_BIC_PHP

Originally based on the standard binary cascade model the PHP (Proton High Precision) model incorporates new data-driven features to model the interactions of low energy protons. Unlike the previous two models, here experimental data libraries are used to determine the occurrence and outcome of a collision between an incident proton and target nucleus. This model has been used with two different accepted data libraries, either ENDF or TENDL, depending on the environmental settings implemented for each run. The environmental settings for these simulations are chosen depending on the suitability of the data contained within each library for the materials used in the simulation. In this work the ENDF libraries were used for simulating interactions of protons with light lithium and beryllium targets, as the data in the TENDL libraries was known to be less reliable for elements with low atomic mass. However for the isotope production simulations the TENDL libraries were used as data for some heavier elements, most notably for this case molybdenum, was not available in the ENDF libraries.

2.5 Validation

The use of GEANT4 and its reputation is built on the accuracy and reliability of the results obtained by using the code. In order to safeguard this reputation every official update released through the GEANT4 site undergoes a stringent and vigorous validation process before it can be implemented.

This process consists of two stages, testing the microscopic and macroscopic levels of a GEANT4 model. The microscopic level includes process features such as cross-sections, angular and energy distributions, and stopping power, which are just a few examples. For each quantity in each model a systematic testing over a range of energies and materials is carried out where simulation results are compared to experimental data. The same tests are carried out on macroscopic properties where simulations of entire experimental set ups are carried out to test the ability of all the GEANT4 processes to work together and the results are compared to experimental results taken at the corresponding real life facility[60].

This is an on going process as data libraries and process models are continuously updated to fill gaps in the code's capabilities and to improve results. One such gap identified in GEANT4's applications is the models available for the simulation of low energy (E < 10MeV) proton interactions. At the conception of this project the only available method for simulating low energy protons were the theoretical models QGSP_BERT_HP and QGSP_BIC_HP, as mentioned previously. During this work collaboration between the GEANT4 development team and the University of Huddersfield, led by Dr. C. Bungau, created and implemented the first data-driven model for low energy proton interactions, QGSP_BIC_PHP. The initial section of this work, detailed in this chapter, will introduce and discuss the benchmarking simulations and results obtained using these three models for neutron production from light targets and isotope production in heavy targets.

3. BNCT

3.1 Initial GEANT4 Benchmarking Process

As with standard GEANT4 benchmarking procedures, my simulations have used a geometry based on experimental arrangements found in the literature and results have been compared to the corresponding experimental data. Expanding on previous collaborative work between members of our group and those at the University of Birmingham, the Birmingham target design was used for the experimental verification of these simulations, in the hope that, if reliable, the results could be used to undertake further optimisation of the target assembly.

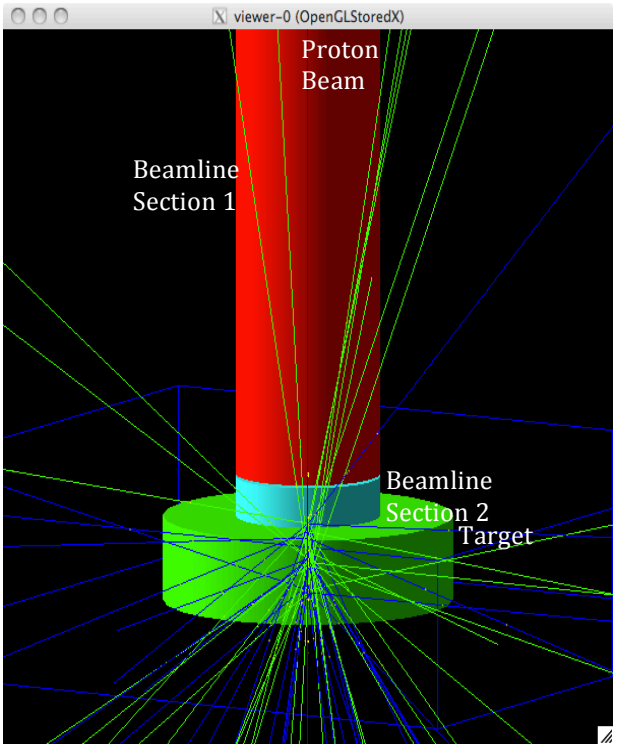

Figure 21. Visualisation of the target (green disc), beampipe(red and aqua cylinder) and particle trajectories(blue and green lines)

For the purposes of benchmarking neutron yields only a simple geometry consisting of the target in a near vacuum system was modelled as depicted in fig.21. The initial simulations carried out were of a 0.7mm thick lithium disc (diameter = 40mm) bombarded by a beam of 10^9 protons. Due to runtime constraints 10^9 is the largest number of particles it is practical to use. However, this number is sufficient to provide reliable results that can be extrapolated to

assess the effects of higher beam currents. The simulations were carried out over a range of proton energies just above threshold (E_{th} = 1.9MeV)[13] , i.e. for 2MeV < E_p < 4MeV in various step sizes from 0.1 - 0.3MeV for a data-driven model QGSP_BIC_PHP and two theoretical models; the binary cascade(QGSP_BIC_HP) and the Bertini cascade (QGSP_BERT_HP).

Following on from the lithium simulations further studies were undertaken using a target of the same dimensions comprised of beryllium, and the same batch of simulations for each of the three models were run in order to make a suitable comparison between the targets and the code's capability.

3.2 Results

The raw results of these simulations are obtained as a count of neutrons from the target i.e. when the simulated neutron crosses the boundary between the target volume and the world it is counted to the output file as illustrated in fig.22.

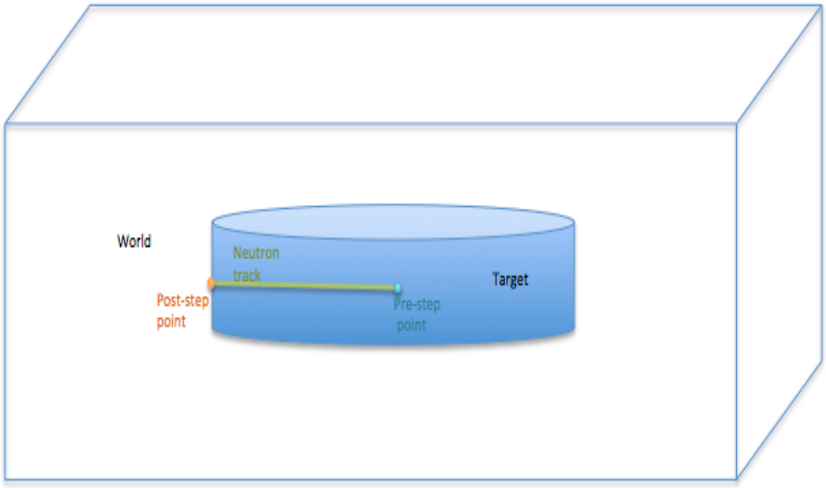

Figure 22. Pictorial representation of the step used to acquire the neutron count

These count rates can then be turned into either cross-sections or yields in a format that best relates to the published experimental data. In the case of the neutron production data the experimental data was displayed in terms of neutrons per coulomb of incident protons.

3.2.1 Uncertainties

For the data obtained from all the following simulations in this thesis using GEANT4 the uncertainty can be expressed using standard Poisson statistics appropriate to random counting processes via the relationship[61]

$$\Delta N = \sqrt{N} \tag{13}$$

where N in this context is the neutron count. In the graphical representation of the data error bars are shown where it is possible to do so. Only in the cases where the error bars are so small as to be negligible or such that even at the smallest point size they are too small to be visible have they been omitted.

3.2.2 Experimental Results

Experimental results from the literature, including those obtained by the group at Birmingham(fig.23), for both a lithium and a beryllium disc target are used for the benchmarking comparison and can be seen below in figs.23&24.

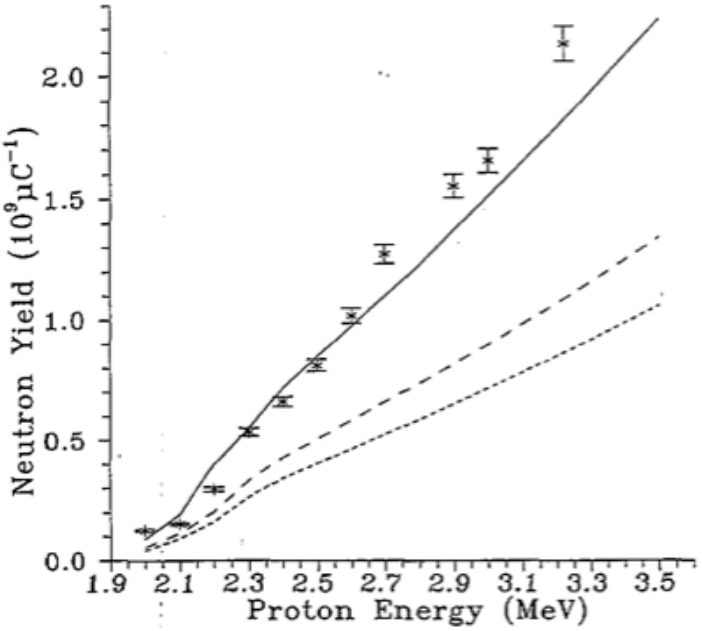

Figure 23. MCNP (solid line)[26] and Experimental (*)[© 1977 IEEE[62]] neutron yields from a thick Li target. Reproduced with relevant permission. Both dashed lines correspond to Li compound targets, which are not of interest in this study.

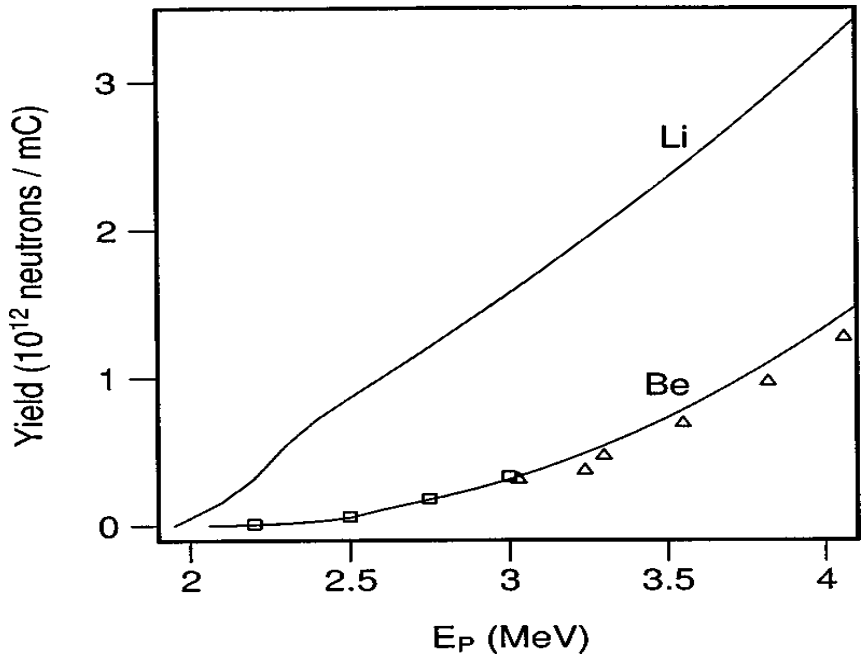

Figure 24. [23]Calculated neutron yields (lines) for Li [63] and Be[64] targets and experimental yields for Be (squares[62] and triangles[65]). Every effort has been made to contact the relevant permission holder to reproduce this image.

3.2.3 QGSP_BERT_HP

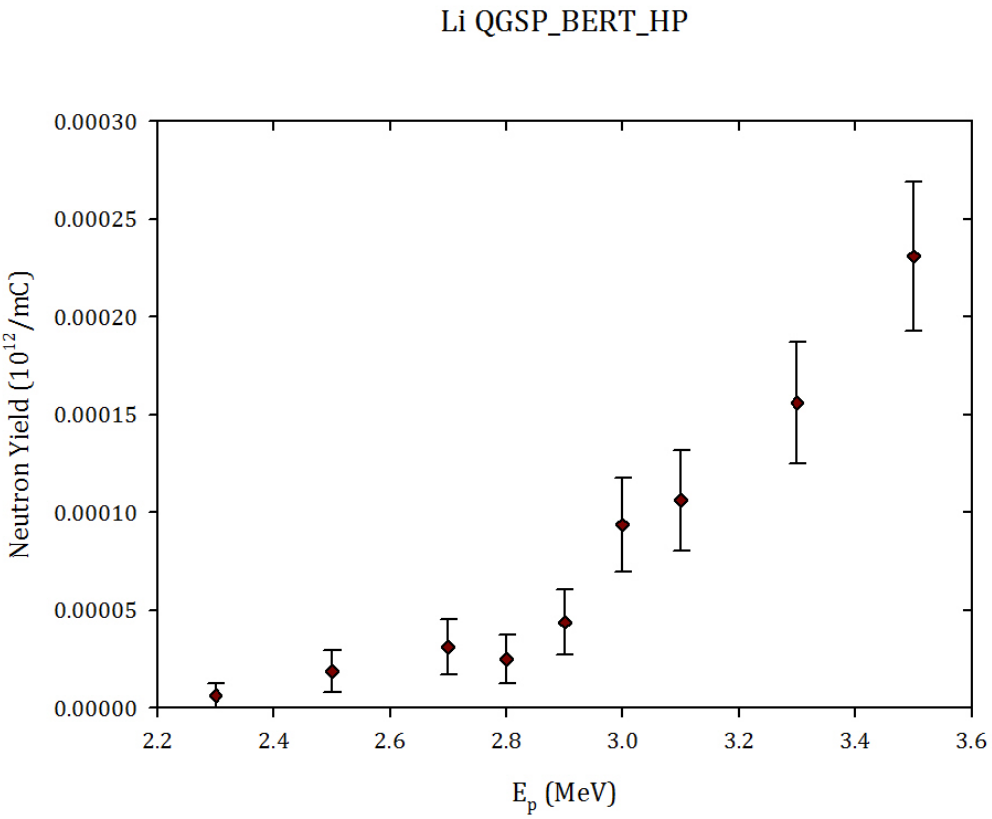

Figure 25. Neutron yield vs incident proton energy using GEANT4.9.5.p01 QGSP_BERT_HP

The simulation results that differ most from the experimental results during this benchmarking phase are those obtained from applying the Bertini cascade to the lithium target, which are shown in fig.25. There are serious discrepancies in both the value and the trend of the neutron yields obtained with this model (figs.25&26) compared to both sets of experimental results, fig.23&24. The neutron counts from the lithium and beryllium target are four and three orders of magnitude less than the experimental results respectively.

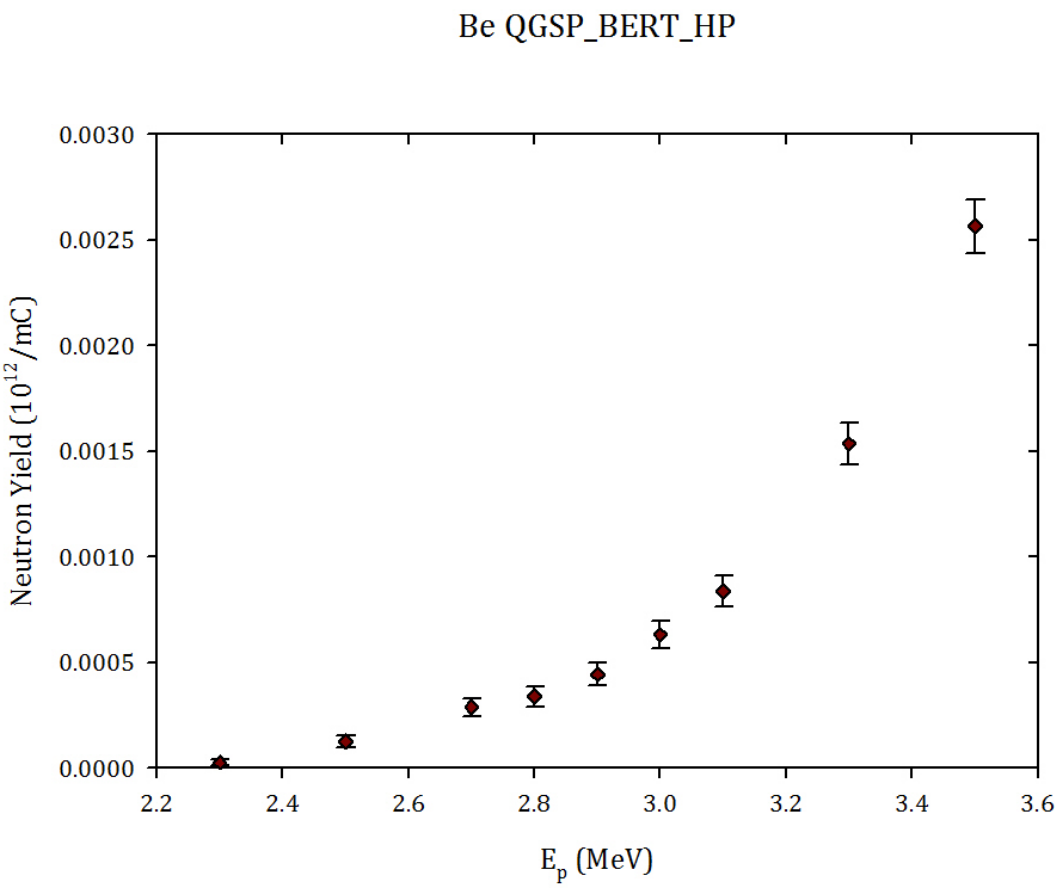

Figure 26. Neutron yield vs incident proton energy using GEANT4.9.5.p01 QGSP_BERT_HP

3.2.4 QGSP_BIC_HP

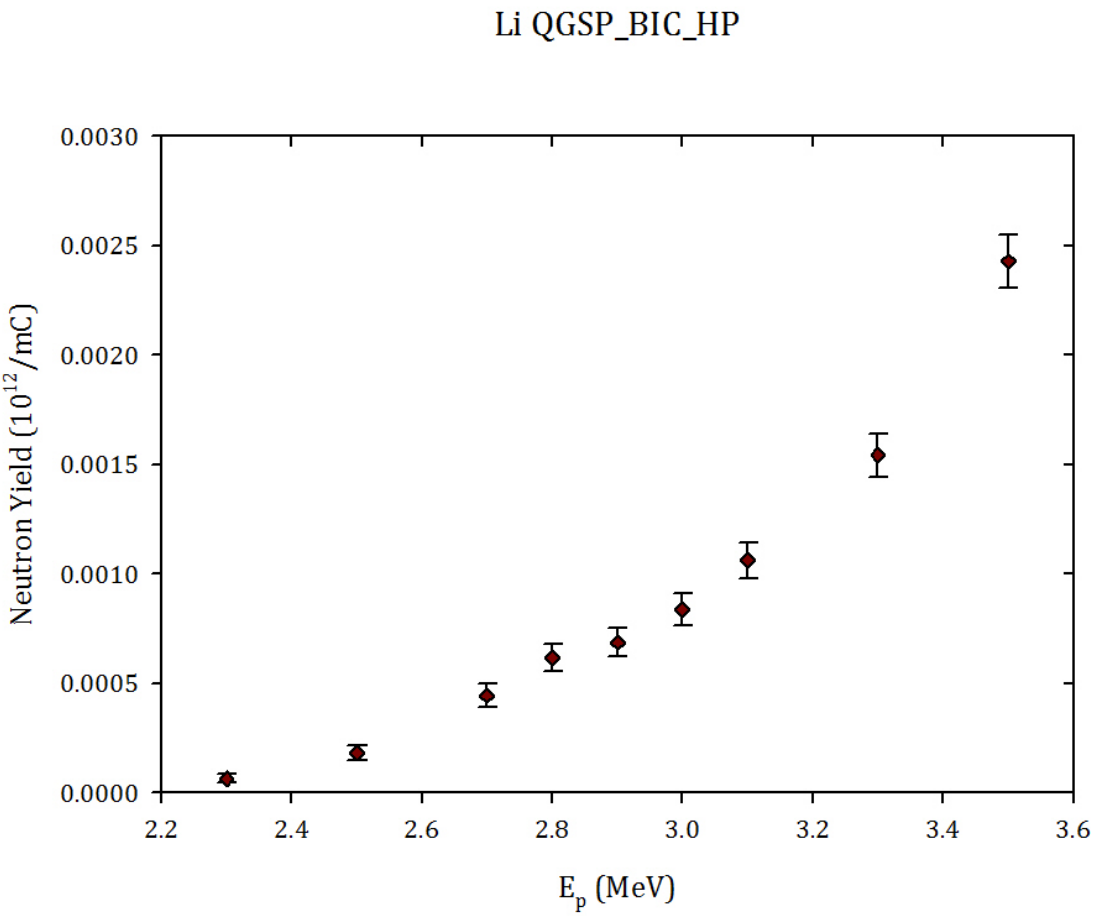

Figure 27. Neutron yield vs incident proton energy using GEANT4.9.5.p01 QGSP_BIC_HP

The results obtained for the lithium target using the binary cascade, shown in fig.27, show some noticeable differences to those of the Bertini cascade presented in fig.25. The binary results, are similar in shape to that of Bertini. The value of the neutron count rate obtained with the binary cascade is an order of magnitude greater than that of Bertini, and therefore three orders of magnitude less than the experimental results. For the beryllium target, comparing figs. 26 & 28 there is little difference between the Bertini and Binary models. Both trend and value still show significant discrepancies in comparison to the experimental results given in figs. 23 & 24. With the binary cascade the neutron count is three orders of magnitude lower than would be expected and of a steeper trend than seen from the experimental results.

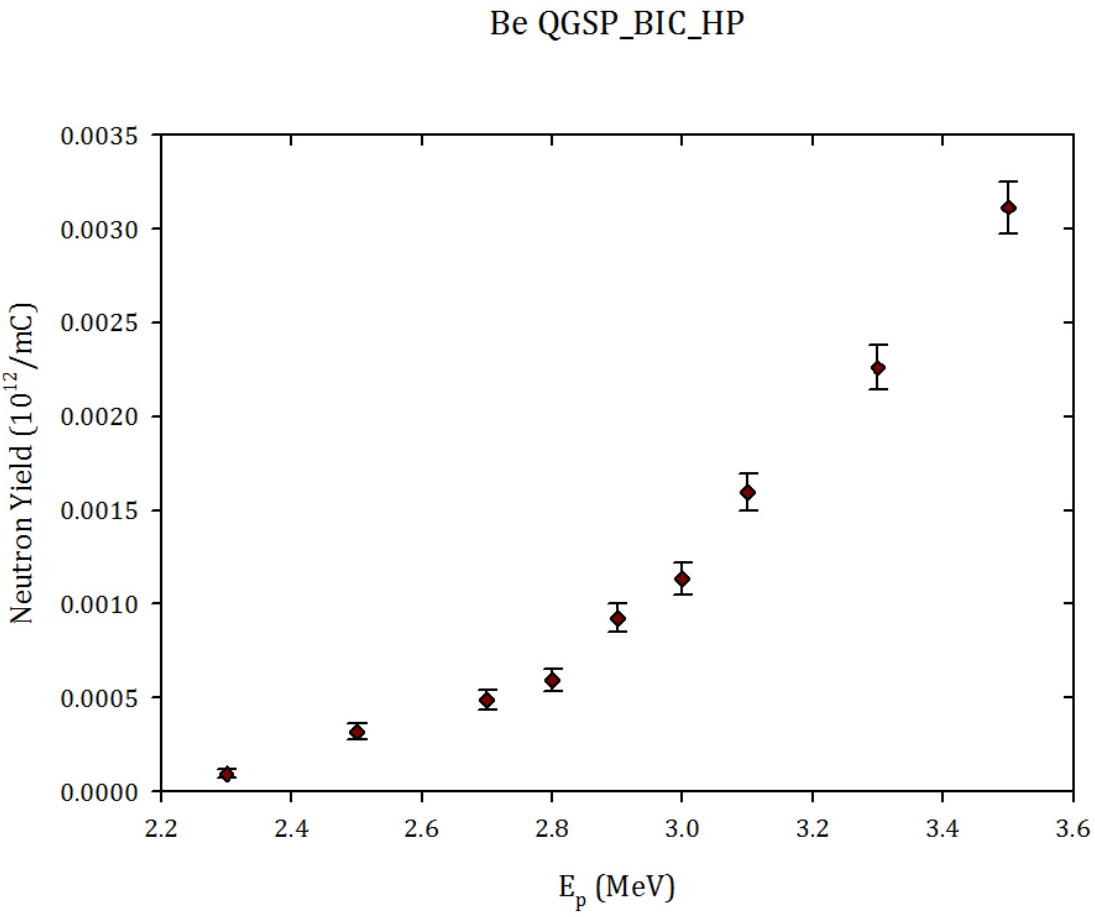

Figure 28. Neutron yield vs incident proton energy using GEANT4.9.5.p01 QGSP_BIC_HP

These two models were chosen for this benchmarking as the most promising of the current models available in GEANT4 libraries as they have already been well validated and implemented for the interaction of higher energy (E_p > 100 MeV) protons. However the results obtained from this initial benchmarking phase of the project clearly shows major discrepancies indicating that there are shortcomings in these models. From the results presented in this and the previous sections (3.2.3 & 3.2.4) it can be seen that both models breakdown at the lower limits of proton energy and low target Z numbers. The results and findings of this benchmarking work has been presented at IPAC'12, the conference proceedings paper can be seen in appendix B.

As a direct consequence of these results we began to work with the GEANT4 developers in order to develop and trial a new data-driven model for low energy proton interactions, QGSP_BIC_PHP. This model uses the accepted experimental

cross-sections contained within the data libraries to calculate the reactions and their outcomes during the simulation.

3.2.5 QGSP_BIC_PHP

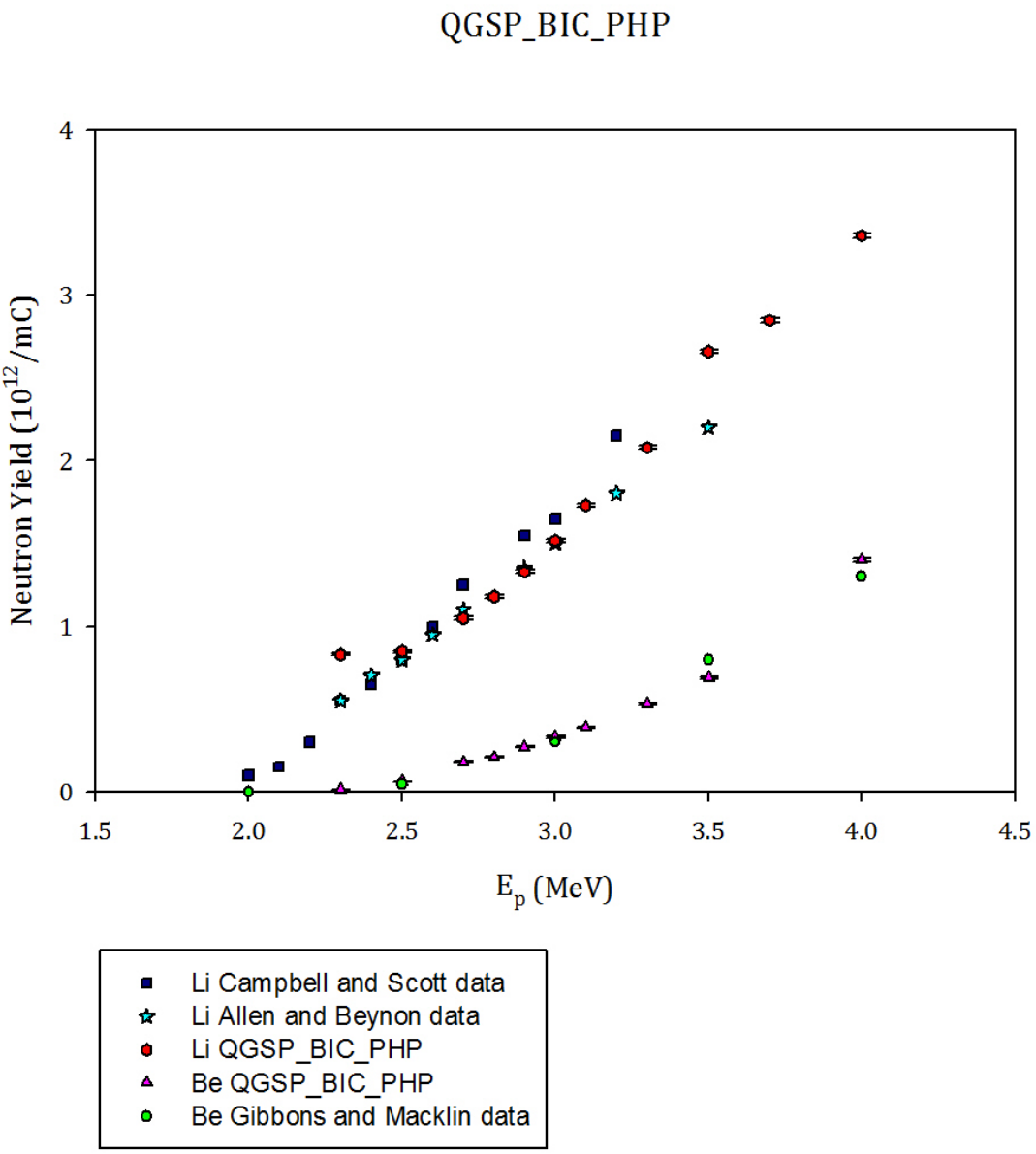

Figure 29. Experimental results Li[23]and Be(yields calculated from experimental cross-section data from[64]) overlaid with simulation results for both Li and Be targets using GEANT4.5.9.p01 QGCP_BIC_PHP. Data obtained and reproduced in accordance with EXFOR guidelines

The results obtained with the data-driven model QGSP_BIC_PHP can be seen in fig.29, overlaid with the digitised version of the experimental results shown earlier in fig.23 for Li and Be neutron yields calculated from the experimental

cross-sections obtained from the EXFOR libraries (which match the line shown in fig.24). This illustrates the improvements that can be made to simulation work when a data-driven model is used. There is a much better agreement shown between the sets of data presented in fig.29 for both target materials than that seen form the results obtained with the two theoretical models, figs. 25-28. These improvements gained with the new model and the initial benchmarking was presented at IPAC'13, the conference proceedings paper can be seen in appendix C.

3.3 Further Simulation Studies: Effect of Target Thickness

After reliable results for the neutron yield from light element targets at low proton energies had been obtained the next step was to take this model forward to develop the Birmingham BNCT target design.

The first question to be addressed is the effect of target thickness on neutron production. When designing a target, especially a fixed solid target, the thickness of the target is generally considered the most important of the dimensions. Taking the example of a disc target, the diameter has little effect on the production rates as long as it is larger than the diameter of the beam spot. Physics states that after the point where a target becomes thick (greater than the stopping distance of the incident particles within the target material) the neutron count from the target will reach a plateau. It is also possible to make the target too thick such that the target material absorbs some of the neutrons and the count rate drops[67].

3.3.1 Simulations

For the rest of this section of work the energy of the proton beam was kept constant at 2.8MeV, as is currently used at the Birmingham facility, and, as for the same reasons as before, a beam of 10^9 protons was used. All other aspects of the simulation were also kept constant apart from the target thickness, which was varied in steps of 0.05mm and 0.1mm between $0.05\text{mm} < t < 0.8\text{mm}$. The

neutron count rate obtained from the simulations was converted into suitable units for comparison as before.

3.3.2 Results

The results of these simulations (neutron yield vs target thickness) can be seen in fig.30. These GEANT4 simulations provide information on the useful range of protons in lithium. The neutron yield becomes constant at a target thickness that corresponds to the distance travelled when the energy of the incident protons falls below the threshold energy of the reaction of interest. Due to the low threshold for the ^{7}Li(p,n) reaction this distance should be close to the stopping distance for protons in lithium. From fig.30 the useful range of the incident protons can be seen to be between 0.15mm and 0.2mm

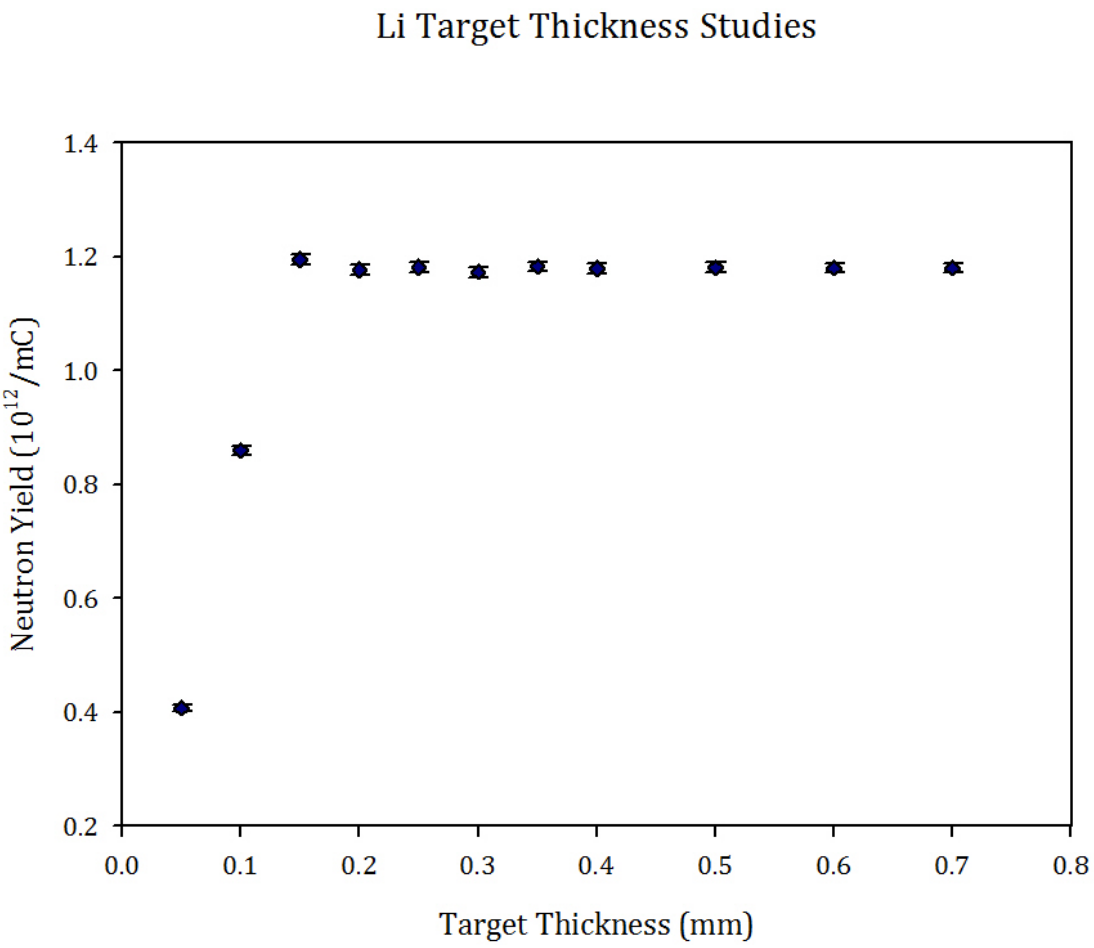

Figure 30. Neutron yield obtained from a lithium target of various thicknesses

The following calculation[68] can be used to approximate the stopping distance to be 0.18mm.

$$R_m = 3.2\times10^{-4}\frac{\sqrt{M}}{\rho}R_{air} \tag{14}$$

R_m = range in target material

M = atomic mass of target material

ρ = density of target material

R_{air} = range of incident particles in air

$$R_{air}(m) = \left(\frac{E_p}{9.3}\right)^{1.8} \tag{15}$$

E_p = incident particle energy

For protons in lithium

$$R_m = 3.2\times10^{-4}\frac{\sqrt{7}}{0.534}\left(\frac{2.8}{9.3}\right)^{1.8}\times10^2 = 0.0182cm = 0.18mm \tag{16}$$

The stopping distance of 0.18mm coincides with the useful range obtained by the simulations. With a stopping distance much less than the target thickness used the 0.7mm target used by the Birmingham group is considered to be a thick target, although not so thick as to become detrimental to the neutron yield. It can also be seen that given the difficulties of practically implementing such a target, as discussed in chapter1, that there would be no real advantages to using a thinner target and a thicker target would only increase the difficulties in making sure the target was adequately cooled.

3.4 Further Simulation Studies: Angular Distribution of Neutrons From The Target

The second part of this work is a study of the effect of geometry orientation and the angular distribution of the neutrons as they leave the target. The current geometry of the facility provides an outgoing neutron beam at 90° to the incident proton beam. This set up was primarily dictated by the placement of the existing Dynamitron, to be used as the incident particle source, in such a way as to provide a vertically downward beam onto the target. This set up did, however,

enable the use of a flat horizontal target so that the beam could hit the surface of the target straight on and the cooling system could be housed behind the target within the copper backing. While there are some practical advantages to this set up, is this the most efficient set up to obtain the required neutron flux for therapy? It would be expected from classical kinematics that although neutrons should leave the target in all directions, the highest flux rate would occur through the bottom surface of the target in a straight through trajectory. However, if the solid angle differential is taken into account the highest flux occurs in the 20° - 40° region[69].

3.4.1 Simulations

In this case the specific parameters used by the Birmingham group were implemented, with a single run of 10^9 protons of energy 2.8MeV incident on a 0.7mm thick ^{7}Li target. This time however the geometry also included a set of 39 detectors surrounding the target each spanning a 10° segment. A visualisation of the detectors in one quadrant (90°-180°)of the set up is shown in fig.31.

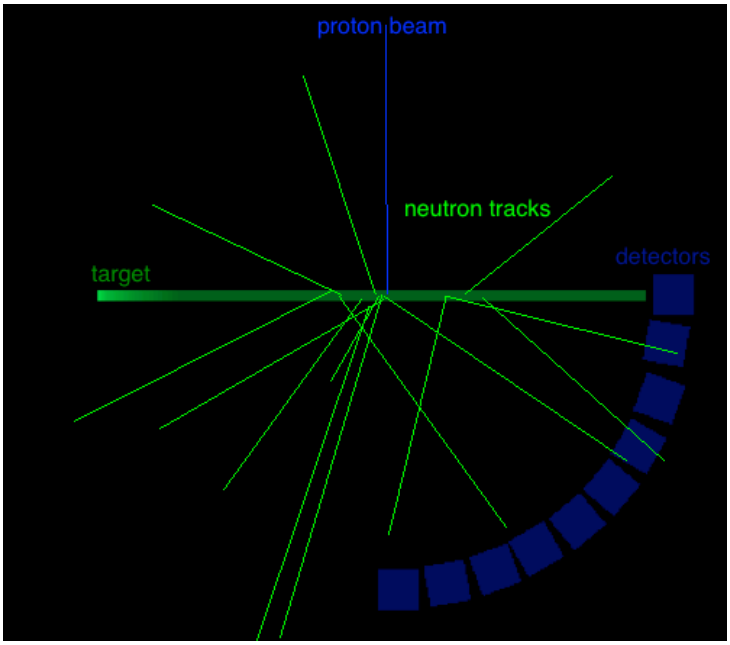

Figure 31. A representation of the detector (blue blocks) geometry used to measure the angular distribution in the segment of 90°-180° in 10° steps

3.4.2 Results

The Neutron count rate from each of these detectors has been plotted in fig.32 showing a symmetric pattern around the 0° point. It can also be seen that while there is no drop in flux at 0° within the 20° - 40° region the peak flux is reached and plateaus over the 0° region. From these results the most useful flux can be obtained through the bottom surface of the target and are lost into the cooling system. Water was chosen for the cooling system due to its low neutron activation under these fluxes. This geometry orientation is therefore certainly worthy of consideration when a new hospital-based facility can be built without constraints imposed by the pre-installed equipment.

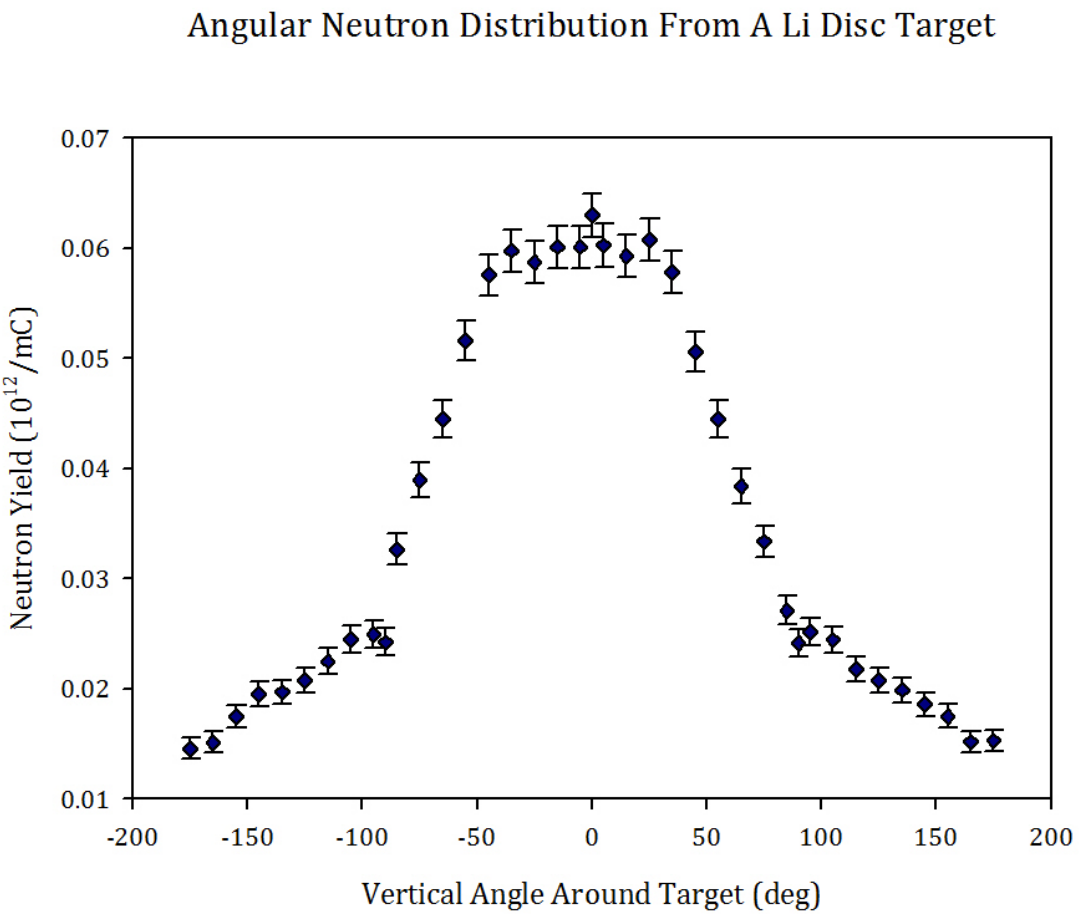

Figure 32. Plot of angular distribution of neutrons from a Li disc target

3.4 Conclusions

From the current studies deficiencies in the capabilities of GEANT4 have been identified and addressed, although under rather limited parameters and criteria. At the start of this work there had been almost no previous work using GEANT4 for the interactions of low energy protons with light element targets despite the reliable comprehensive theoretical models available for the interactions of high-energy (> 100MeV) protons. The physical processes contained within the Bertini and binary cascade models made them the most suitable of the currently available models to try in this work, benchmarking GEANT4 for interactions of low energy protons and low Z targets. Unfortunately I have found that at these limits the cascade models break down and cannot accurately reproduce experimental results. In light of these findings a new data-driven model has been developed and incorporated into GEANT4. From the limited simulations that have been presented here it can be concluded that for the case of low energy protons and light element targets this new model is able to accurately reproduce experimental results of these reactions.

It was hoped to also carry out some study into the energy spectrum of the neutrons produced for further design considerations. However, as the new data-driven model is based on the binary cascade it is more suited to provide more accurate yield counts. The initial studies carried out with the PHP model, while giving the correct distribution shape, showed a shift in energy of each neutron by approximately +5MeV. This is due to the fact that the binary cascade does not include the energy conservation laws that are applied in the Bertini model as described earlier in chapter2. In order to carry out a proper study into energy distribution these additional conditions would need to be applied or a new data-driven model based on the Bertini cascade developed.

4. GEANT4 BENCHMARKING FOR MEDICAL ISOTOPE PRODUCTION

4.1 Introduction

In this section I shall continue the benchmarking processes discussed in the previous chapter but now the focus is upon the capability of GEANT4 to reproduce the results of isotope production in heavier element targets. In particular, several currently used cyclotron-produced medical isotopes, such as ^{64}Cu, ^{89}Zr, and ^{123}I, have been used in this more extensive comparison of theoretical and data-driven models in GEANT4. For the purposes of this study only QGSP_BIC_HP(theoretical) and QGSP_BIC_PHP(data-driven) have been used for benchmarking, as the previous results show the binary cascade model to be more suitable than the Bertini model for such reactions. I have focused upon the low threshold energy reactions (p,n) as these represent the most useful radioisotope production mechanisms and therefore the most important processes for benchmarking.

For the rest of the simulations in this work the significant GEANT4 output is the estimation of the amount of specific isotope nuclei produced within the target. To obtain this information the stepping action was used in much the same way as used previously for the neutron count with the pre-step volume defined as the target and the particle defined as the ground state nucleus. Unfortunately at the inception of this project there was no way to define the metastable state of an isotope in GEANT4. This means it was not possible to simulate the direct production of many SPECT isotopes including the popular ^{99m}Tc, and therefore only generator production routes could be studied using GEANT4. However the newest GEANT4 release version 10.0 (6/12/13) now includes the isomers with a half-life of over 1μs produced from hadronic interactions that could be used for further work studying the production of SPECT isotopes.

4.2 COPPER-64

With a half-life of 12.7hours[33] and decaying by both positron and β- emission ^{64}Cu has applications in joint therapy and diagnostic tests[70]. Combined with targeting molecules the ^{64}Cu is administered to the patient for uptake into cancerous cells. The emitted positrons can be used in connection with PET detectors to image the tumour site while the β- radiation acts in much the same way as the alpha radiation from BNCT in damaging the cells.

^{64}Cu is currently produced by medical cyclotron facilities ($E_p \sim 16MeV$), and there are three reactions that can be utilized[70][71]

$$^{64}Ni(p,n)^{64}Cu \quad (17)$$

$$^{68}Zn(p,\alpha n)^{64}Cu \quad (18)$$

$$^{66}Zn(d,\alpha)^{64}Cu \quad (19)$$

The most common and efficient of these production routes, and the one explored here, is the (p,n) reaction, (17). This is a simple reaction that, according to current studies, provides a clean supply of ^{64}Cu from an easy to produce enriched single isotopic target. Excitation functions for this reaction, which can be seen in fig. 33, show a low threshold energy and rapidly rising cross-section, reaching a peak of ~800mb at proton energies of 10MeV. This reaction therefore falls within the constraints set by the current programme.

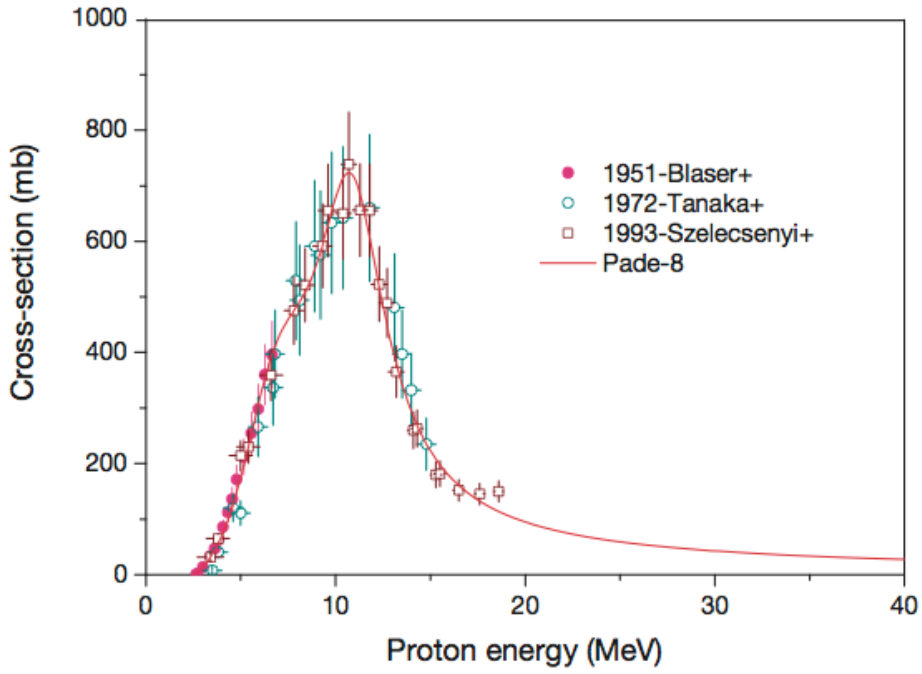

Figure 33. Experimental excitation function for the ^{64}Ni(p,n)^{64}Cu reaction[72]. Image reproduced in accordance to IAEA copyright

4.2.1 Simulations

The target design for this set of simulations was based on the experimental targets used to measure the excitation functions for medium weight nuclei. A thin layer, ~20μm thick, of target material is deposited on a square aluminium backing foil with a side length of 25mm. Simulations comprised 10^9 protons in an energy range of 1 – 10MeV in steps of 0.5MeV for both models.

4.2.2 Results

Experimental cross-sections from the excitation functions of the ^{64}Ni(p,n)^{64}Cu reaction are overlaid with the simulation results from the theoretical and data-driven models in fig.34. The uncertainties in all the simulation results in this chapter were calculated as in section 3.2.1 and carried through the calculations accordingly. Error bars are shown where it is possible to do so, however in some cases they are too small to be visible and it may appear as if they are not present. For errors on experimental data refer back to their original figures.

At the higher end of this energy range, 5.5MeV < E_p < 10MeV, all three sets of results in fig.34 show a reasonable agreement within error. However below 5MeV the theoretical model appears to breakdown, much as was seen in the results for the lighter element targets in the BNCT simulations. The yield values become so low from QGSP_BIC_HP that the estimated cross-section tends to zero. In this same energy range the data-driven model continues to match experimental data and the cross-section tends to zero close to the experimental reaction threshold (E_{th} < 1MeV)[71]. This highlights the deficiencies in the theoretical models at the limits of low energy proton interactions even for heavier target materials.

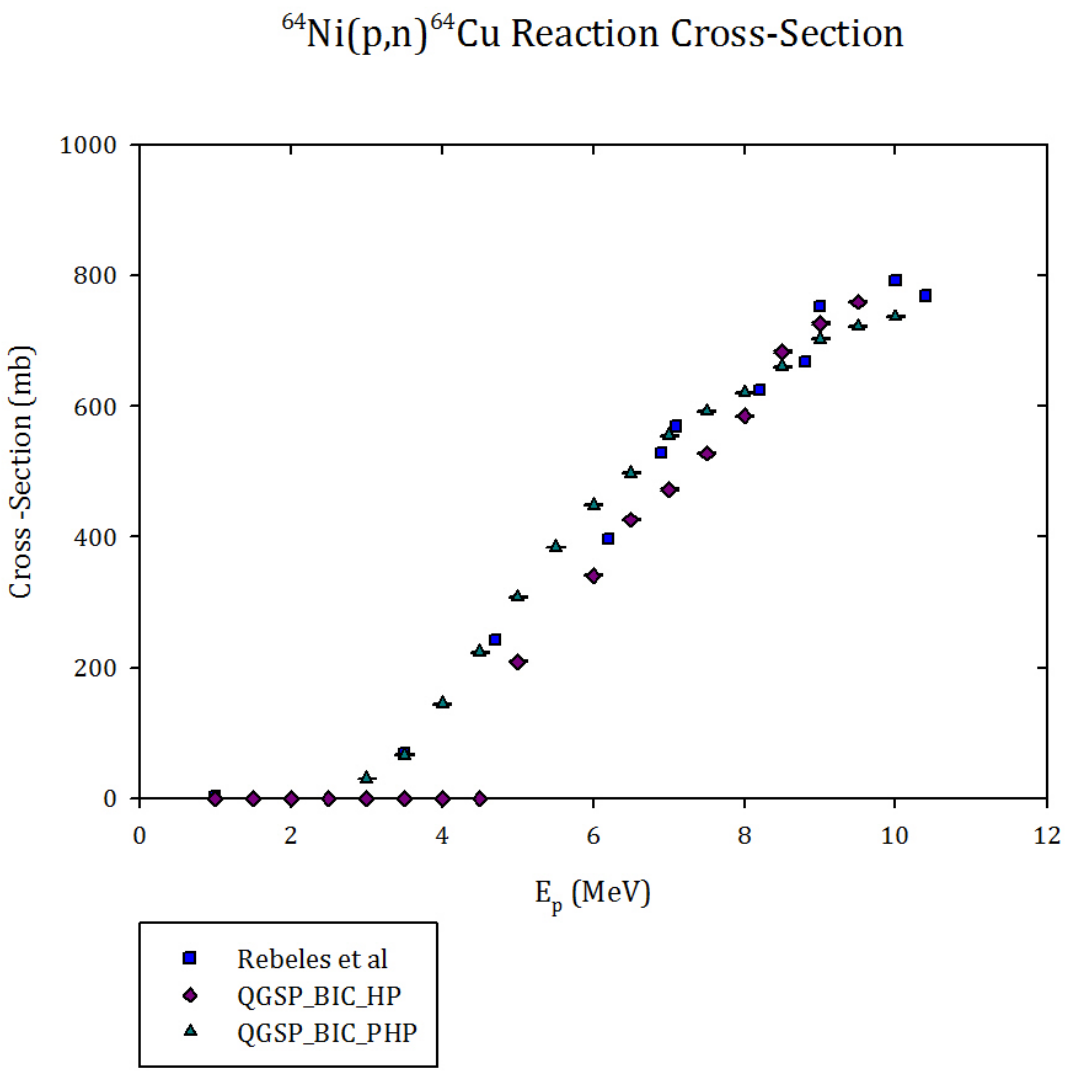

Figure 34. Experimental[73] and simulation results for ^{64}Ni(p,n)^{64}Cu reaction. Data obtained and reproduced in accordance with EXFOR guidelines

4.3 ZIRCONIUM-89

4.3.1 Background

^{89}Zr is a positron emitting isotope with a half-life of ~3.3 days[33][70]. As ^{89}Zr has a considerably longer half-life than many imaging isotopes it is particularly suitable for studying longer biological processes[74]. Its primary application is as an immuno-PET tracer combined with antibodies with a long uptake time to study cancer cells.

Current ^{89}Zr production is carried out using a medical cyclotron via either proton or deuteron reactions in the 10-20MeV range[70]

$$^{89}\mathrm{Y}(\mathrm{d},2\mathrm{n})^{89}\mathrm{Zr} \quad (20)$$

$$^{89}\mathrm{Y}(\mathrm{p},\mathrm{n})^{89}\mathrm{Zr} \quad (21)$$

The (p,n) reaction, (21), is the most common production route for ^{89}Zr and hence this is the focus of this study. As ^{89}Y is the only natural and stable isotope of yttrium a pure target is straightforward and simple to manufacture and correspondingly produces a “clean” final product. The excitation function for this reaction is shown in fig.35 and demonstrates the peak cross-section to be approximately 14MeV. While this is just outside the main energy range of interest the cross-section at 10MeV is still high enough to be of interest here, approximately 300-400mb.

The following simulations use a target with the same geometry as that used for the simulation of ^{64}Cu production described in 4.2.

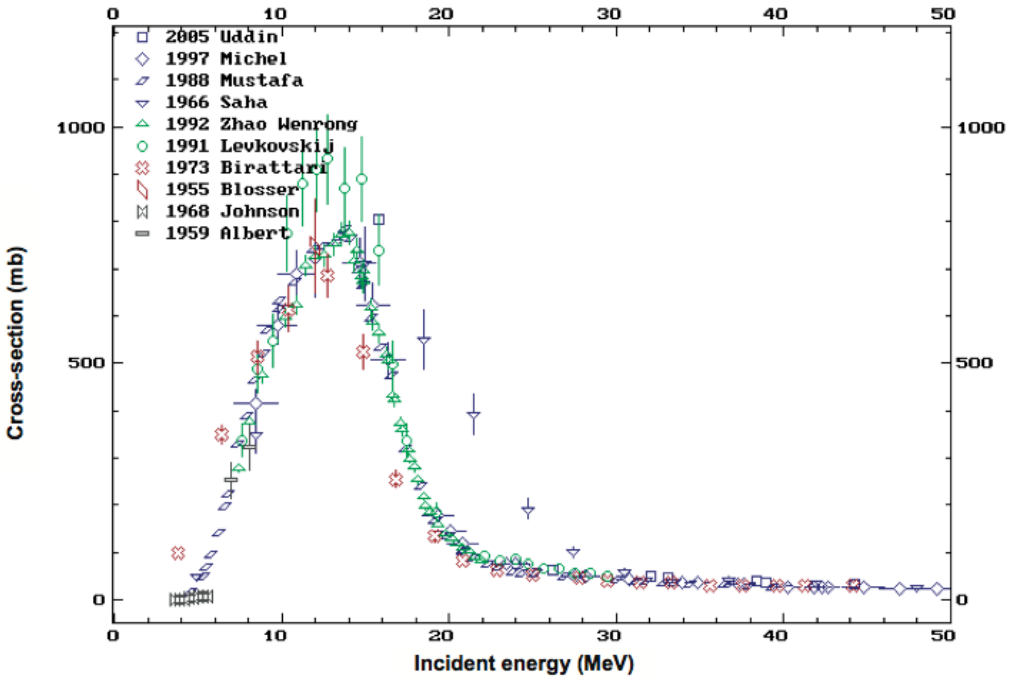

Figure 35. Experimental excitation function of the ^{89}Y(p,n)^{89}Zr reaction[70]. Image reproduced in accordance to IAEA copyright

4.3.2 Results

Experimental cross-sections for the (p,n) reaction were taken from Levkovskij[76], shown in fig.35, for benchmarking comparison with simulation results. This experimental data is only available in the region of E_p > 7MeV. However the high cross-section (of the order 100mb) at this point allowed this to be a suitable reaction for study and the energy range for the comparison was increased to 15MeV from the previous 10MeV.

Some of the experimental data, Levkovskij 1991[76], from fig.35 can be seen overlaid with the simulation results in fig.36. In the higher proton energy region where experimental data is available, as shown in fig.36, there is a reasonable agreement for all three sets of results. Unfortunately no suitable data could be found in the available online libraries for the lower energy region. However fig.36 shows that the theoretical simulation results again start to breakdown with cross-sections falling to zero at a higher energy, ~5.5MeV, than that found in the data-driven model. The cross-sections show that the data-driven model

still produces an isotope yield down to proton energies of ~4MeV, the threshold shown in the excitation functions.

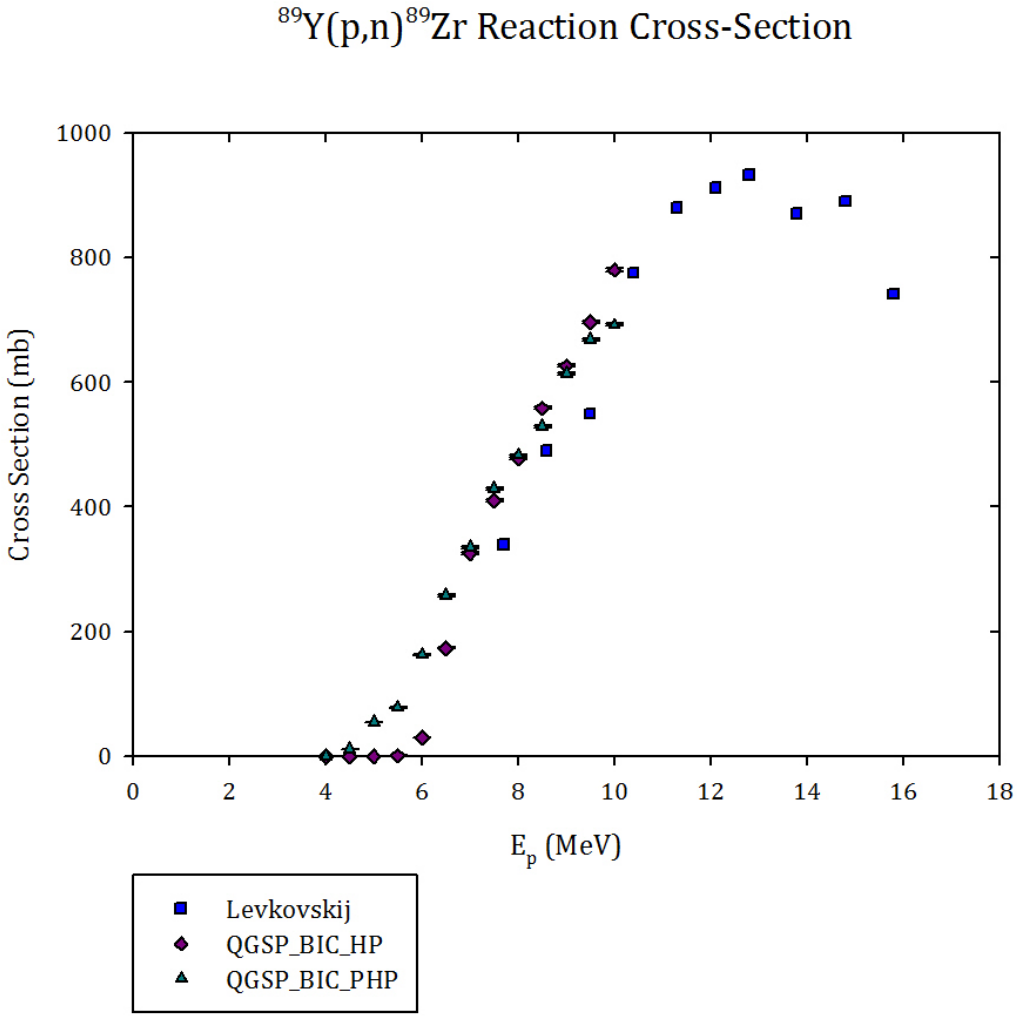

Figure 36. Experimental[76] and simulation results for the $^{89}Y(p,n)^{89}Zr$ excitation function. Data obtained and reproduced in accordance with EXFOR guidelines

4.4 IODINE-123

4.4.1Background

Iodine-123 is the most favoured isotope for studies of the thyroid[77]. ^{123}I is a SPECT isotope that decays via a 159keV gamma with a half-life of 13.2 hours. This half-life makes is suited for use with the 24hour uptake test to check the function of the thyroid[70]. The energy of the emitted gamma is not much higher than that of the most common SPECT isotope ^{99m}Tc, and is suitable for use with

the most common design of gamma camera, i.e. those based upon sodium iodide detectors originally designed for use with ^{99m}Tc[98].

There are several different production routes available for ^{123}I that utilise different incident particles and energies e.g.[70]

Generator Production:

$^{127}I(p,5n)^{123}Xe:^{123}I$ (22)

Direct Production:

$^{122}Te(d,n)^{123}I$ (23)

$^{124}Te(p,2n)^{123}I$ (24)

$^{121}Sb(^{4}He,2n)^{123}I$ (25)

The reaction of interest here is $^{123}Te(p,n)^{123}I$ which fulfils the requirements of this study[78] and which has relatively high cross-sections at lower proton energies <10MeV.

The simulated target geometry used here was once again similar to that used for ^{64}Cu production in 4.2.

4.4.2 Results

Experimental cross-sections from both Takacs[79] and Scholten[80] can be seen in fig.37, overlaid with the theoretical and data-driven simulation results. A different trend in results can be seen as the atomic mass of the target increases, as now both of the simulated data sets over-estimate the experimentally determined cross-section. However, the data-driven model is once again the preferred model for reliable reproduction of experimental results. Within the lower proton energy region, < 6MeV, the data driven model shows some agreement, within error, with the experimental results whereas the theoretical model significantly overestimates the cross-section for the whole energy range.

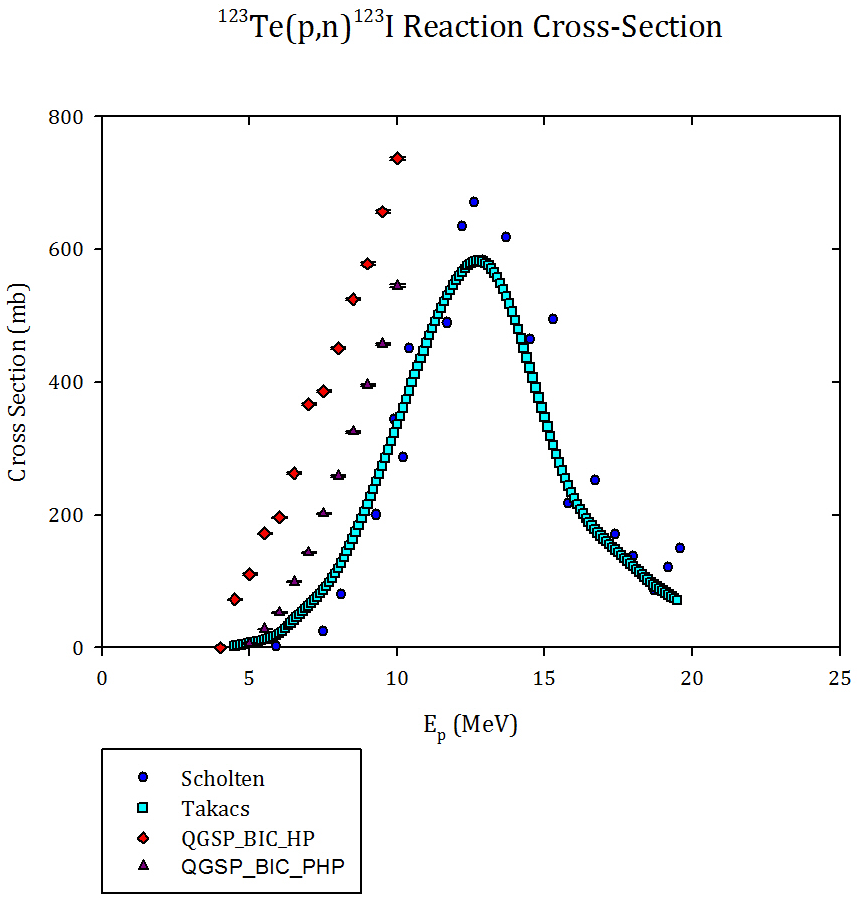

Figure 37. Experimental and simulation results for the reaction $^{123}Te(p,n)^{123}I$ [79][80]. Data obtained and reproduced in accordance with EXFOR guidelines

4.5 Conclusions

This second benchmarking phase has extended the previous study to the effect of target nuclear mass on the reliability of the physics models available in GEANT4. From these results it can be seen that in the limits of the low proton energy region, < 5MeV, the theoretical models in GEANT4 breakdown and can not accurately reproduce experimental cross-sections for isotope production from (p,n) reactions.

Work on a new data-driven model has been beneficial and the first version of this still developing code has shown much improvement in ability to reproduce these reaction cross-sections. The initial benchmarking results presented in this chapter have been presented at IPAC'13, the conference proceedings paper can be seen in appendix C.

5. LOW ENERGY PRODUCTION OF ^{99}MO/^{99m}TC

Technetium, so named as the first non-naturally occurring element, was discovered by Segre and Seaborg in 1938[1][31]. It was produced during some of the first studies into the production of radioactive nuclei by a cyclotron in which a beam of deuterons were incident on a molybdenum-100 target.

With further study it was found that ^{99m}Tc had ideal properties for use as a radio-tracer isotope. ^{99m}Tc's biocompatible half-life of only 6 hours allows for a short clinical stay for the patient and correspondingly much of modern nuclear medicine has been built around the use of ^{99m}Tc. While most gamma cameras are able to detect gamma rays in several energy regions all of the cameras used for medical imaging are now designed specifically to detect the 140keV gammas emitted by ^{99m}Tc.

In addition to these characteristics the main reason for favouring ^{99m}Tc was the availability of reliable production routes. The invention of the generator system, Tucker-BNL(Brookhaven National Laboratory)[29][37], allowed for wider spread use of the shorter lived nuclides such as ^{99m}Tc whose parent is molybenum-99. ^{99}Mo is a by-product of nuclear reactor fuel, extracted in the necessary processing of spent fuel rods, and is therefore relatively cheap and plentiful. . The ready availability of the ^{99}Mo generator in turn established the popularity of ^{99m}Tc.

Unfortunately, the source of reactor-produced ^{99}Mo is no longer quite as secure, and there is now an impending radioisotope crisis, which could potentially rival that experienced in 2010. To mitigate this impending crisis it is therefore useful to re-evaluate the earlier accelerator-based production methods in order to secure supplies of ^{99m}Tc.

There are several reaction chains that can be utilised for an accelerator based method for either direct or generator production.

Direct	Generator
$^{98}Mo(p,\gamma)^{99m}Tc$ (26)	$^{98}Mo(n,\gamma)^{99}Mo$ (28)
$^{100}Mo(p,p2n)^{99m}Tc$ (27)	$^{100}Mo(\gamma,n)^{99}Mo$ (29)
	$^{100}Mo(p,pn)^{99}Mo$ (30)

In some cases it is advantageous to continue with the existing regional supply chain where the radioisotope generator system is mass produced at a separate facility and transported to the medical facility where the daughter isotope is extracted as needed. This is suitable for medical facilities that are, for the case of the $^{99}Mo/^{99m}Tc$ system, within a few hours transportation from the production site as this allows for a continued reliable supply without the expense of any new or added infrastructure. Therefore some groups are reviewing accelerator-based methods of ^{99}Mo production.

The Canadian government has led the way in the development of alternative ^{99m}Tc supplies by commissioning two projects to develop methods for accelerator-based production as described below

5.1 Canadian Light Source: The Electron Approach

The first ^{99m}Tc production study was undertaken by the Canadian Light Source (CLS)[47]. The CLS project demonstrated a practical method of producing the ^{99m}Tc generator ^{99}Mo from reaction (31).

$$^{100}Mo(\gamma,n)^{99}Mo \quad (31)$$

The photons used in this reaction are produced via Bremsstrahlung from a high energy,~35MeV, electron linac. The resulting hard X-ray photons then impact a ^{100}Mo disc target. The interactions in the target result in the production of ^{99}Mo, which is separated from the target and manufactured into a generator system

similar to the ^{99}Mo obtained from processing reactor fuel. The production chain of both the X-rays and the final product ^{99m}Tc is demonstrated in fig.38.

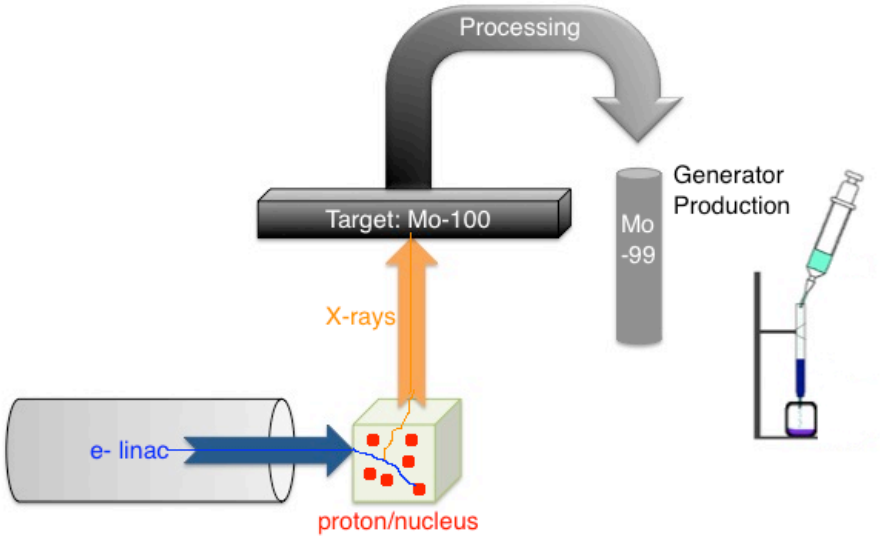

Figure 38. Production chain of ^{99m}Tc from an electron linac system utilising the reaction ^{100}Mo(γ,n)^{99}Mo[47]

This is currently a relatively unexplored approach to isotope production, possibly because the cross-sections for photon induced reactions are typically lower than the more common (p,n) reaction and there are fewer reaction routes possible. However this last point could also become an advantage, if there are fewer reactions possible then fewer contaminants can be produced in the target. The use of a highly enriched, >95%, single isotopic ^{100}Mo target can easily be manufactured and the use of such a target also reduces the level of undesirable by-products created within the target during the irradiation process.

At this time a proof of principle stage has been successfully completed, although behind schedule.

5.2 TRIUMF: The Proton Approach

The second, and probably more successful, of the projects was undertaken at the TRIUMF facility[32][35]. There, the existing <20MeV medical cyclotron was used to demonstrate the capabilities of proton production routes via the reaction

$$^{100}Mo(p,2n)^{99m}Tc \quad (32)$$

for the direct production of ^{99m}Tc. This reaction has a threshold of ~7MeV and peaks in the region 12-16MeV. Within this energy region it is necessary to consider contaminants. The $^{100}Mo(p,pn)^{99}Mo$ reaction produces two other short lived technetium isotopes, namely ^{100}Tc ($t_{1/2}$ = 15.46s)[33][34] and ^{101}Tc ($t_{1/2}$ = 14 min)[33]. However both of these half-lives are considerably shorter than that of ^{99m}Tc and as such the separation of the required isotope is a relatively simple process providing a clean, medical grade product.

The process has been demonstrated by the TRIUMF group, who have shown that it is possible to produce, and separate, suitable medical grade ^{99m}Tc, which has been quality tested against reactor-produced ^{99m}Tc. TRIUMF has also successfully implemented target production, processing, and recycling routes that they are currently optimizing[32][35].

All of this work was completed more efficiently and on a more realistic timescale for implementation than that of the CLS electron approach, although both approaches are viable methods to be taken forward.

5.3 Low Energy Production of ^{99m}Tc

While the TRIUMF facility has had considerable success with their project, here we assess the potential of producing ^{99m}Tc, either directly or via the ^{99}Mo generator, using protons with an energy of less than 10MeV in order to maintain, and even expand, the supply of ^{99m}Tc to those facilities where the regional generator supply chain is unsuitable.
There are three potential routes that could be explored:

Direct

$^{100}Mo(p,2n)^{99m}Tc$ (33)

$^{98}Mo(p,\gamma)^{99m}Tc$ (34)

Generator

$^{100}Mo(p,pn)^{99}Mo$ (35)

5.3.1 Direct Production

Unfortunately in GEANT4 it is not possible to simulate direct production of ^{99m}Tc as there is no way to define the metastable state in the GEANT4 version available during this project. However recent studies have yielded some experimental data available enabling yields and activities to be estimated from cross-section data for given target specifications for feasible production routes.

Firstly the ^{100}Mo(p,2n) reaction is currently being studied by many groups including that at TRIUMF as mentioned previously. From their work it is possible to see that while the energy threshold for this reaction is low enough to be of use, i.e.~7MeV, the cross-section is approximately 100mb at 10MeV and is dominated by the ^{99}Tc ground state which has a production cross-section of over 300mb at 10MeV. It is therefore questionable if this reaction is suitable for a low energy production method as the practical yield of ^{99m}Tc may well be too low for a commercial system.

The ^{98}Mo(p,γ) reaction is a predominantly low energy reaction, occurring for proton energies less than 5MeV. This range is below the threshold of most reactions that could produce contaminants in the target, ensuring a very clean production route. However (p,γ) reactions typically have low cross-sections, and this particular route is no exception with ^{99m}Tc production cross-sections of the order of 0.1mb. At this rate the yield would be too low even for high incident proton currents (~1mA), to provide a viable commercial source of medical grade ^{99m}Tc.

5.3.2 Generator Production

Possibly the most favoured of the generator production routes observed in the literature of current studies is:

$$^{100}\text{Mo(p,pn)}^{99}\text{Mo} \qquad (36)$$

However there are many sets of experimental excitation function data available, some of which are shown in fig.39, and there seems to be little agreement between them. While the overall trend of the cross-sections appears fairly similar, the initial rate of increase and the maximum cross-section show significant variation between different reports and no standard accepted data set appears to have been agreed.

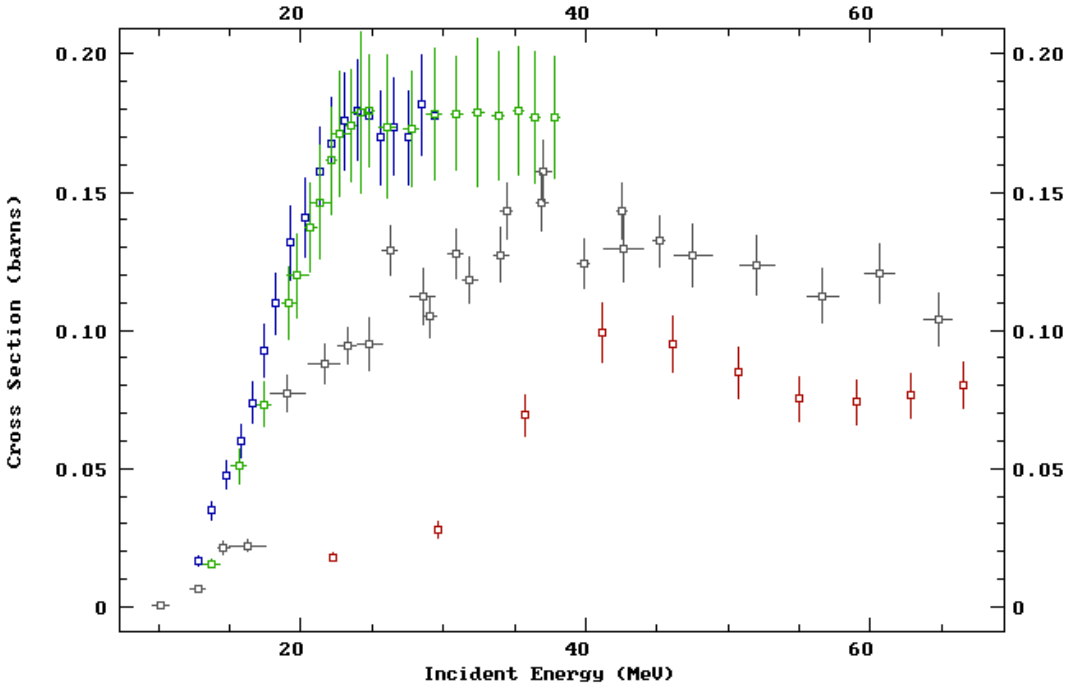

Figure 39. Various experimental cross section data sets for the $^{100}Mo(p,2n)^{99}Mo$ reaction (green-Takacs[81], grey-Scholten[82], blue-Levkovskij[83], red-Uddin[84]). Data obtained and reproduced in accordance with EXFOR guidelines

Even though the threshold energy of this reaction is too high (10MeV< E_{th} <15MeV) to provide a viable production route I considered it worthwhile to carry out a benchmarking study within which the GEANT4 results obtained using data-driven models could be compared with the disparate experimental data sets.

5.4 Further Benchmarking Studies

For this section of the study the target geometries and experimental data were taken from the work of Takacs et al[85] and Scholten et al[86], fig.39. GEANT4 simulations using both the theoretical and data-driven binary cascade models

were run for a simple foil target ~1μm thick with an aluminium backing. Several target compositions were considered; (i) a natural Mo target with yields converted as if for an enriched ^{100}Mo target, (ii) a 97% enriched ^{100}Mo target as described in Scholten[86], and (iii) a 100% enriched ^{100}Mo target.

The results presented in figure 40 are for the 97% enriched target. Due to a lack of data available in ENDF libraries for the reaction of interest the environmental settings used to run these simulations took the required data sets from the TENDL libraries to enable the data-driven model to determine the occurrence of collisions and the final states and products.

The uncertainties in the simulation results in this chapter were calculated as in section 3.2.1 and carried through the calculations accordingly. In fig.40 error bars are shown for points calculated from my simulated data, for errors relating to experimental data refer to the original work, fig39.

Experimental data were selected from Takacs et al[81][85] and Scholten et al[82][86], fig.39, for a comparison to simulated results, which is shown in fig.40. The results obtained by the data-driven model in this section show the effect of differing experimental data sets. The data-driven model shows most agreement with the work of Takacs et al[81][85], which is perhaps not surprising as this is the most recent work and is therefore most likely to be the data available in the libraries. However the theoretical model does show a good agreement with the results of the work of Scholten et al[82][86].

In this case it becomes much more difficult to determine the most reliable results and appropriate model as both models agree with different data sets and there appears not to be an accepted data set. However taking into consideration the previous benchmarking results, it would be reasonable to conclude that the theoretical model is least likely to be accurate and the Takacs[81][85] data to be the most reliable of those presented here, as it is the most recent found in the libraries and therefore most likely to be the data set in the libraries used by GEANT4.

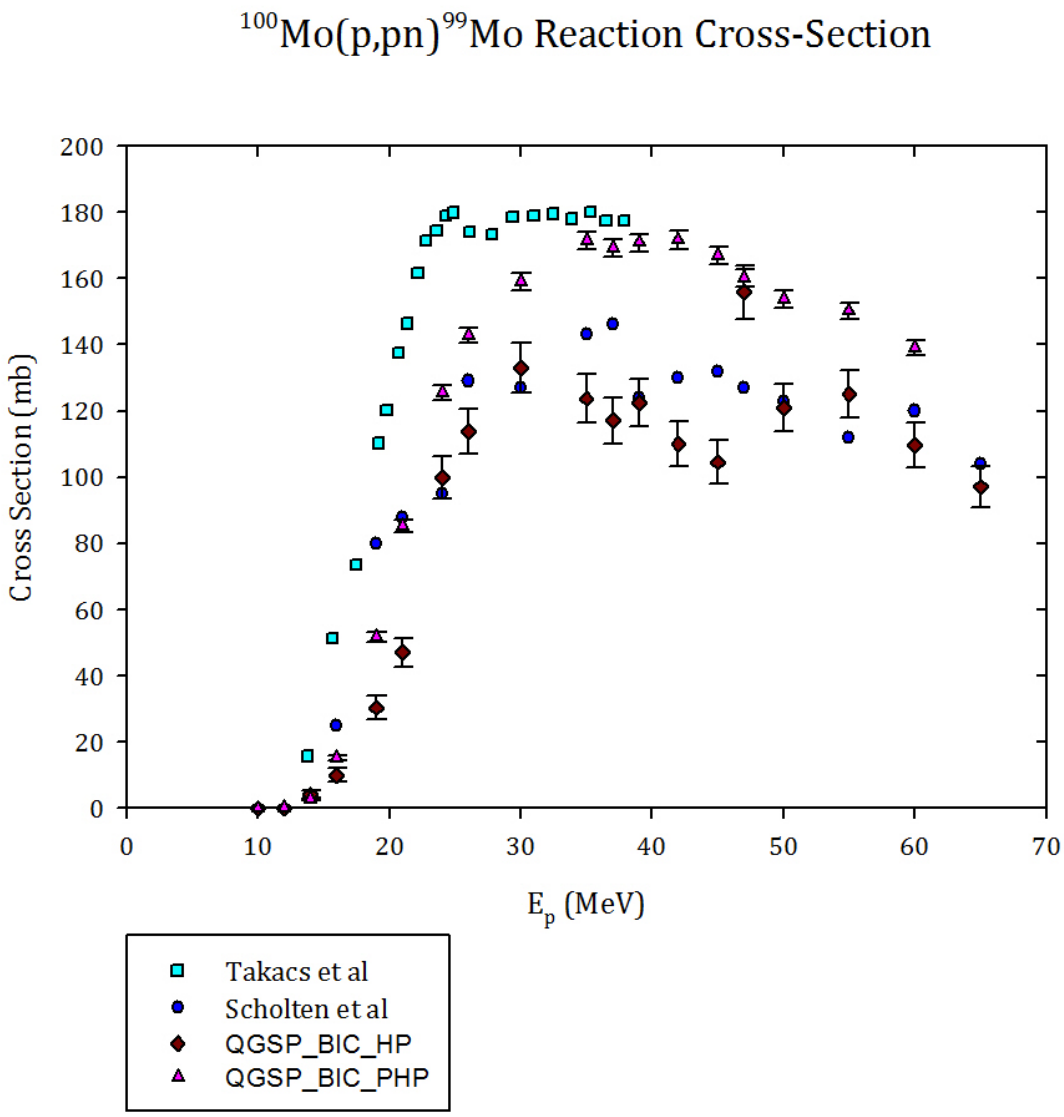

Figure 40. Experimental [81][82] and simulated cross-sections for the reaction $^{100}Mo(p,pn)^{99}Mo$

5.5 Conclusions

This benchmarking case demonstrates the effect and importance of reliable data libraries for use with a data-driven model. Such a model is only as good as the experimental data available within the libraries. Any discrepancies in this data will carry through and be seen in the simulations. However, for the remainder of this work there is sufficient confidence in the results obtained here to continue to use the data-driven model, where data is available, rather than the theoretical model

These simulations have not only provided a useful benchmarking study for the data-driven GEANT4 simulations, they have also demonstrated that in the low energy region (<10MeV) the cross-sections of proton-induced reactions for the production of ^{99m}Tc are too low to provide a suitable quantity for medical applications. It is therefore considered that low energy proton accelerator production of ^{99m}Tc is not a route worth perusing as there are other demonstrably successful routes being explored, such as that at TRIUMF. In light of this result the focus of the present research now moves on to the study of the potential for the low energy proton production of other medical isotopes that could be complimentary to and competitive with ^{99m}Tc SPECT.

Some initial studies into alternative SPECT isotopes was presented at NA-PAC2013, the conference proceedings paper can be seen in appendix D. However due to the complications of modelling metastable isotopes it was decided not to continue with this section of work and to move the study on to the non-metastable positron emitting isotopes used for PET imaging. An extensive list of PET suitable isotopes was compiled by O. Heid of Siemens plc (private communication).

Certain criteria were applied to reduce the number of isotopes on the list for further study. Experimental cross-sections were obtained for the production of each isotope, via (p,n) reactions, from both the online data libraries EXFOR and TENDL (via the code TALYS). Those isotopes with differing data sets from the two libraries were excluded from continued study in this work. Also isotopes with a cross-section of less than 100mb in the range E_p <10MeV were excluded from further study as simulations of reactions with these cross-sections do not produce sufficient yield due to the computing constraints of 10^9 protons per run to enable further study.

Preliminary GEANT4 simulations were carried out for the remainder of the isotopes on the list;

^{38}K, ^{44}Sc, ^{45}Ti, ^{47}V, ^{60}Cu, ^{61}Cu, ^{62}Cu, ^{63}Zn, ^{64}Ga, ^{66}Ga, ^{68}Ga, ^{74,}Br, ^{76}Br, ^{84}Y, ^{86}Y, ^{94}Tc, ^{120}I, ^{122}I

From this list copper and gallium isotopes were selected for further study. The main reason for this is that there are other isotopes of these elements that are already established as therapeutic and diagnostic radioisotopes. As the chemistry for each isotope of the same element should be the same this means that the target production and processing is already in place leading to a smoother introduction of these isotopes into clinical practice than for isotopes of an element that is not already widely used.

With the impending crisis it is imperative that a solution be found and can be implemented as quickly as possible, it is hoped that the isotopes selected would meet least resistance as they are introduced into the commercial market.

6. COPPER ISOTOPES FOR MEDICAL APPLICATIONS

6.1 Background

Copper is one of the most versatile elements and one of the first metals to be exploited by man. Applications range from the everyday tools of the Bronze Age to modern wiring and nuclear medicine. Even within medicine there are a wide range of uses to which various copper isotopes can be applied. Copper is the third most abundant trace metal required by the human body. As such there are well established and understood mechanisms for the behaviour of copper within the body[87]. A more informed approach can be given to targeted drug delivery by knowing where copper is most likely to be taken up and how long these processes take allows for the selection of an isotope with appropriate half-life.

Another advantage to the use of copper isotopes is the simplicity of the chemistry associated with copper, for both target processing and drug labelling. Unlike other transition metals, such as ^{99m}Tc, copper forms three oxidation states, although only two are normally formed. This both simplifies and stabilises the chemistry available. The favoured state for pharmaceutical production is Cu(II) which easily combines to form stable complexes[87].

This work focuses on the radioactive isotopes of copper, those that are currently used such as ^{64}Cu and ^{67}Cu, and potential new isotopes.

6.2 Copper Isotopes for Targeted Radiotherapy

Currently the most common isotopes of copper used in nuclear medicine are ^{64}Cu and ^{67}Cu whose main application is for targeted radiotherapy of cancerous tumours.

^{67}Cu is the longest lived copper isotope with a half-life of 62hours[33][87], it decays via β-decay. It is this decay that makes it most useful for radiotherapy, as the energy deposited into the cells by this radiation is harmful. However ^{67}Cu can

also be used in a combination tracer therapy where SPECT imaging is used during the treatment to monitor distribution of the radioisotope. This is possible as ^{67}Cu decays into both ground and excited states of ^{67}Zn[70]. These excited states then decay via three gammas of energies 91keV, 93keV and 185keV, which are suitable for use with SPECT gamma cameras[70]. The long half-life makes ^{67}Cu suitable for direct production, from either reactor or accelerator systems, and transportation to remote locations that are normally only available to the more popular short-lived isotopes in generator from. This longer half-life is more suited for the study of longer biological processes and allows for long accumulation time in the tumour site.

The other most commonly used copper isotope is ^{64}Cu, also a radiotherapy isotope. ^{64}Cu decays in two ways, partly via β-, useful for radiotherapy, and partly by β+. This second decay mode can be used in conjunction with PET imaging techniques in order to monitor uptake and distribution of the isotope during therapy[70][71]. The half-life of ^{64}Cu is 12.7hours. While not as long as ^{67}Cu this is still a reasonable time to allow for some transportation between production site and hospital for a regional direct production method. Production of ^{64}Cu primarily uses a direct route of an enriched nickel target with a proton beam from a cyclotron as discussed in the benchmarking section[87].

This work focuses on the potential of low energy production routes for current and potential PET isotopes. In this section there are three isotopes of copper to be discussed: ^{62}Cu, ^{61}Cu, and ^{60}Cu.

6.3 Copper Isotopes for Nuclear Imaging: ^{62}Cu

6.3.1 Background

^{62}Cu is a positron emitter with a short half-life of ~ 9.7mins[33]. It is currently used for monitoring of short processes and quick imaging studies. Due to this short half-life ^{62}Cu is useful when rapid repeat testing is required. High quality

PET images of blood flow through the heart and brain have been acquired using ^{62}Cu labelled pharmaceuticals[87-90].

There are two possible cyclotron based production routes available for ^{62}Cu, namely generator or direct production. Due to the short half-life the most common production route used is via a generator system in order to make ^{62}Cu more widely available as a PET imaging isotope. The parent isotope ^{62}Zn has a half-life of 9.24hours, which is sufficient to provide a generator lifetime of up to 3 days. ^{62}Zn is produced from the following reaction

$$^{63}\mathrm{Cu}(\mathrm{p},2\mathrm{n})^{62}\mathrm{Zn} \qquad (37)$$

by a E_p>20MeV cyclotron and natural copper target[90].

The copper can be eluted either by a solution of hydrochloric acid or, for ph sensitive applications, with a neutral glycine solution. Both low and high activity generator systems are available; with a high activity system it is possible to elute approximately 150mCi of ^{62}Cu every 30-40mins[87-90].

A cyclotron of the same energy can be used to produce ^{62}Cu directly from the reaction (38) which has an excitation function as shown in fig.41. There are two very different data sets available for this reaction as depicted in fig.41 and this must be held in mind when considering the simulation results for this reaction.

$$^{62}\mathrm{Ni}(\mathrm{p},\mathrm{n})^{62}\mathrm{Cu} \qquad (38)$$

This cyclotron method takes advantage of the peak to produce sufficient yields. However there is very limited application for this route, as production must occur at the hospital in which the isotope is being used due to the short half-life. This is only possible at large hospital facilities because of the size and expense of the required cyclotron.

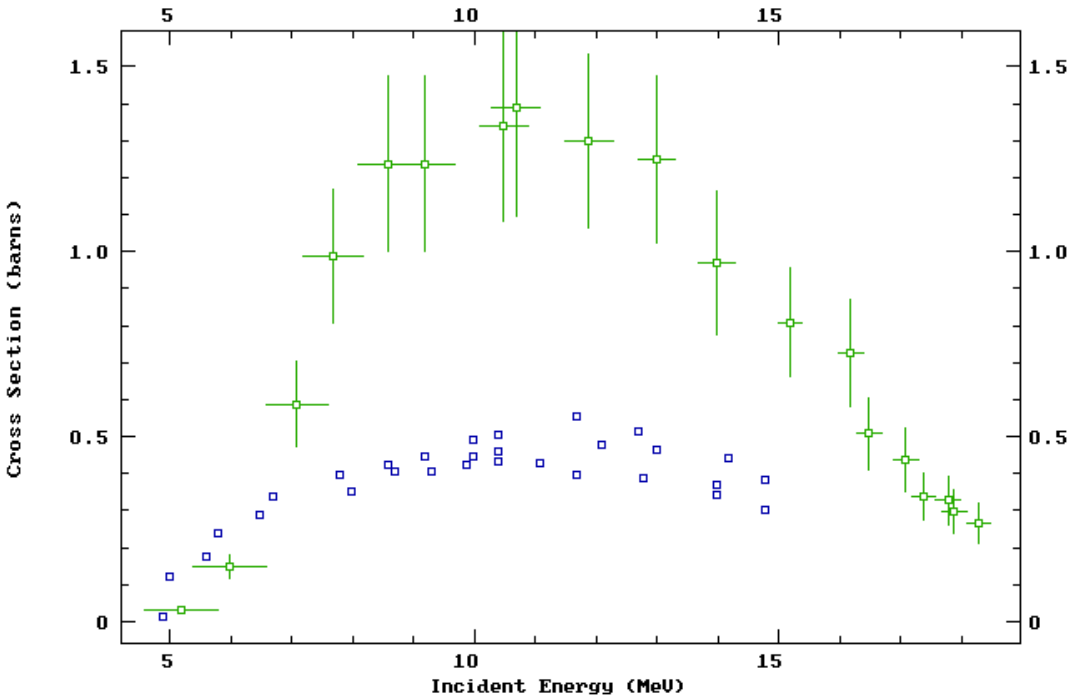

Figure 41. Experimental cross-section data for the reaction $^{62}Ni(p,n)^{62}Cu$ (green-Piel[91], blue-Tanaka[92]). Data obtained and reproduced in accordance with EXFOR guidelines

6.3.2 Low Energy Production

The same reaction can also be utilised at lower energies, E_p <10MeV, both sets of experimental data shown in fig.41 show a sufficiently high value cross-section in the energy region around E_p=10MeV. This has an advantage over the previous route as a smaller accelerator can be used to provide the proton beam in a space that could fit into smaller local hospitals that are currently reliant on generator production. This would provide a more stable supply with the capabilities to produce the isotope on site as needed, in single or multiple dose quantities.

To asses the potential of this method calculations and simulations using the GEANT4 data-driven model QGSP_BIC_PHP have been carried out to determine the yield and activity obtained from a suitable target under various conditions such as target thickness and irradiation times.

6.3.2.1 Target Thickness and Yields

The initial GEANT4 simulations were carried out using a simple disc target of a range of thicknesses, $0.9x10^{-4}$-0.001m, to establish a useful rage of 10MeV protons within the nickel target and a suitable thickness for further work on a practical target design. The simulations were all carried out using a 10^8 particle beam, because of simulation/computing constraints, but the results have been scaled for use of a 1mA proton beam to provide realistic results of what could be expected from the proposed machine. The uncertainties in all the simulation results in this chapter were calculated as in section 3.2.1 and carried through the calculations accordingly. Error bars are shown where it is possible to do so, only in the cases where the error bars are so small as to be negligible or such that even at the smallest point size are too small to be visible have been once again omitted.

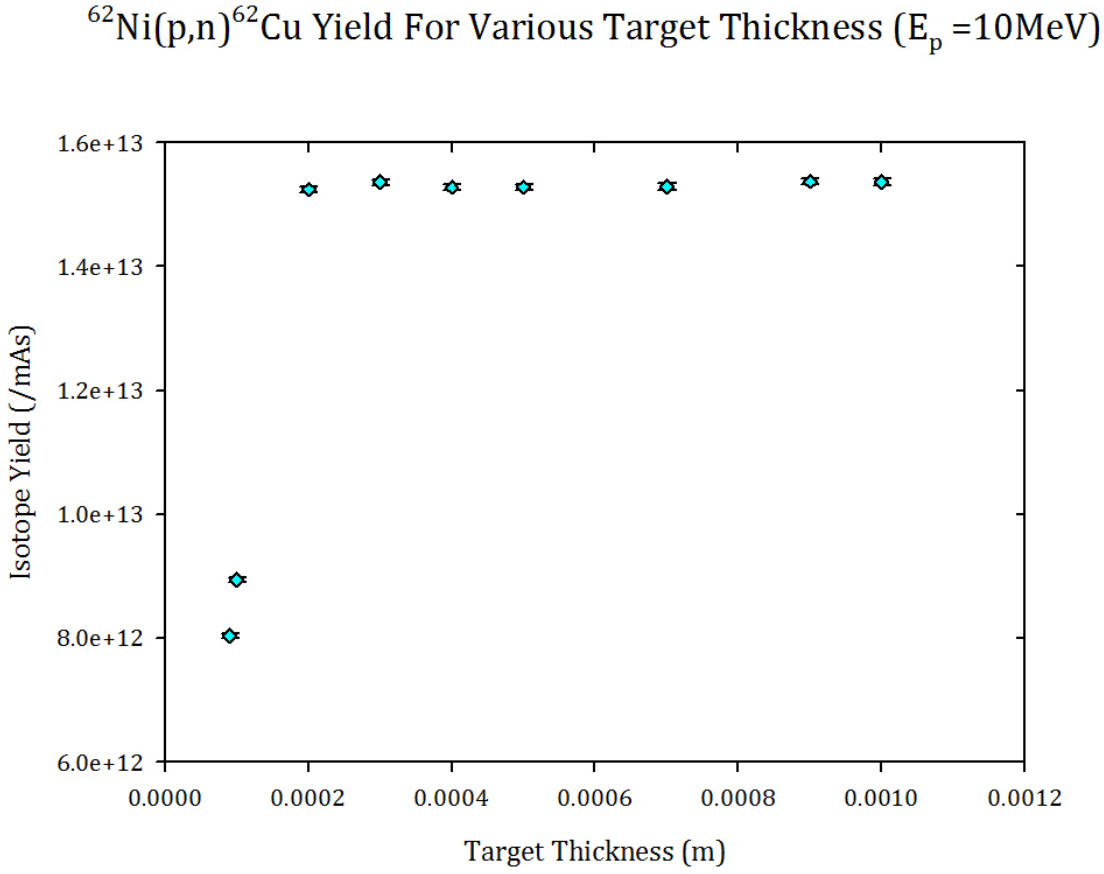

Figure 42. Simulation yields of ^{62}Cu from the reaction ^{62}Ni(p,n)

The results shown in fig.42 give a threshold thickness of approximately 0.003m beyond which the protons have lost so much energy that they are below the energy threshold for the desired reaction and no more isotope nuclei are produced. Stopping distance calculations were also carried out, as in section 3.3.2[68], to determine a suitable thickness of 0.0032m for targets thicker than this there will be no appreciable gain in isotope yields. While not the same these two values are likely to be similar in most cases due to the low threshold energy of the reaction in question.

In terms of the ratio of daughter and parent nuclei, increasing the thickness of the target makes the process less efficient. Therefore, for the most efficient isotope production, a compromise between near stopping distance and target thickness would be ideal. To this end further studies will be carried out using a target of 0.005m, just larger than the stopping distance but more practical to manage.

6.3.2.2 Activity

Calculations into the activity that could be produced from these isotope yields were undertaken. A motivation for this work is the need to produce quickly the required dose of isotope. The irradiation time required to produce sufficient activity for the number of doses that can be used in a reasonable time for a given isotope half-life is therefore an important consideration.

Starting with the isotope yield obtained from the GEANT4 simulations given above for beam parameters of E_p=10MeV and a proton current of 1mA the activity resulting from different irradiation times were calculated. This was done both with and without taking into account the decay of the daughter isotope during the irradiation period.

The following activity equation (39) was used to calculate the total activity and production rate of the daughter isotope during the irradiation period:

$$A = IN\sigma\left(1 - e^{-\lambda t_{rad}}\right) \tag{39}$$

where I is the number of incident protons per target area, N is the total number of nuclei in the target, σ is the cross-section for the reaction in question in cm, $\lambda = 0.693/\text{halflife of the daughter isotope}$, and t_{rad} is the irradiation time[93].

After irradiation the activity is calculated using the standard equation (40):

$$A = N\lambda = \lambda n e^{-\lambda t} \tag{40}$$

where n is equal to the final number of daughter nuclei in the target at the end of irradiation and t is the time from the end of irradiation.

Presented below in figs.43-46 are plots showing the activity of ^{62}Cu produced for various irradiation times, as calculated using the above equations, and the effect of the decay of the daughter isotope during irradiation time.

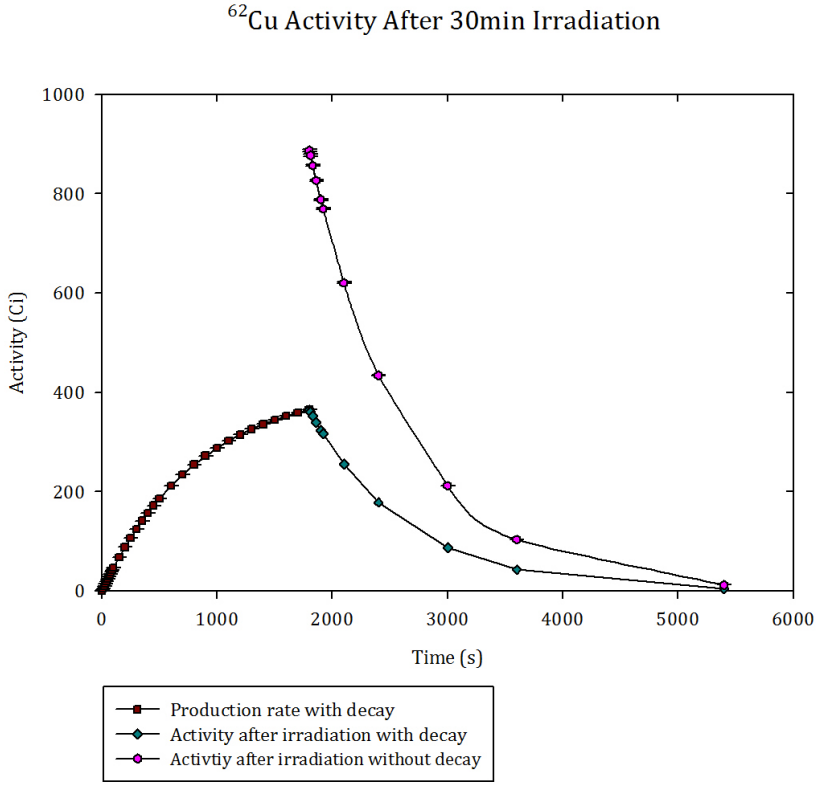

Figure 43. Activity of ^{62}Cu produced after an irradiation time of 30mins with and without accounting for decay during irradiation time

The longest feasible irradiation time for the production of any isotope using this system is 30 min. For ^{62}Cu this is longer than three half-lives and produces more than the required activity. The plot shown in fig.43 also demonstrates how important it is to account for the decay of the daughter when the irradiation time is so much greater than the half-life. The total number of nuclei that would be produced if the isotope did not decay is significantly higher than that when decay is taken into account.

These calculations were repeated for other irradiation times of 15min (fig.44), 10min(fig.45) and 1min(fig.46).

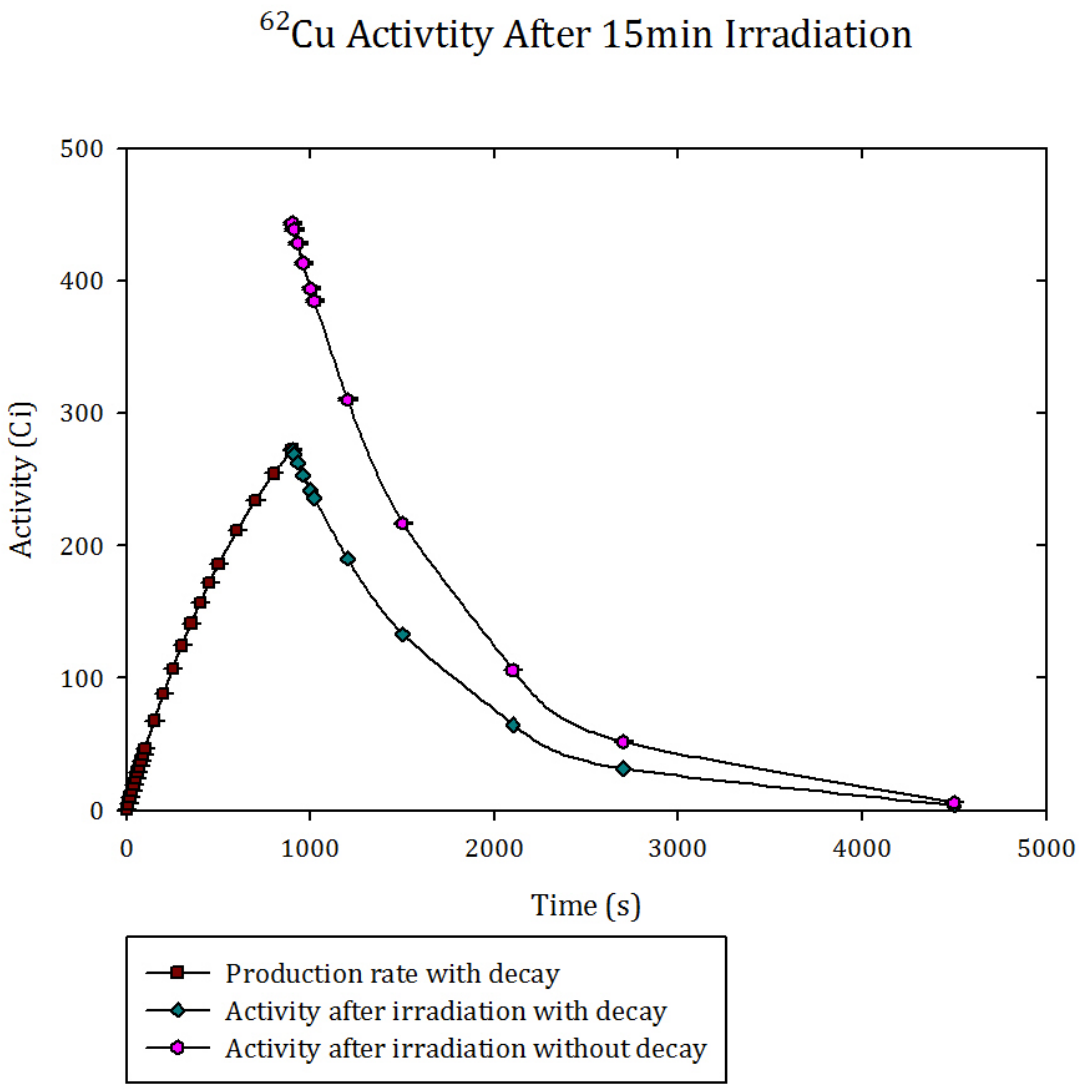

Figure 44. Activity of ^{62}Cu produced after an irradiation time of 15mins with and without accounting for decay during irradiation time

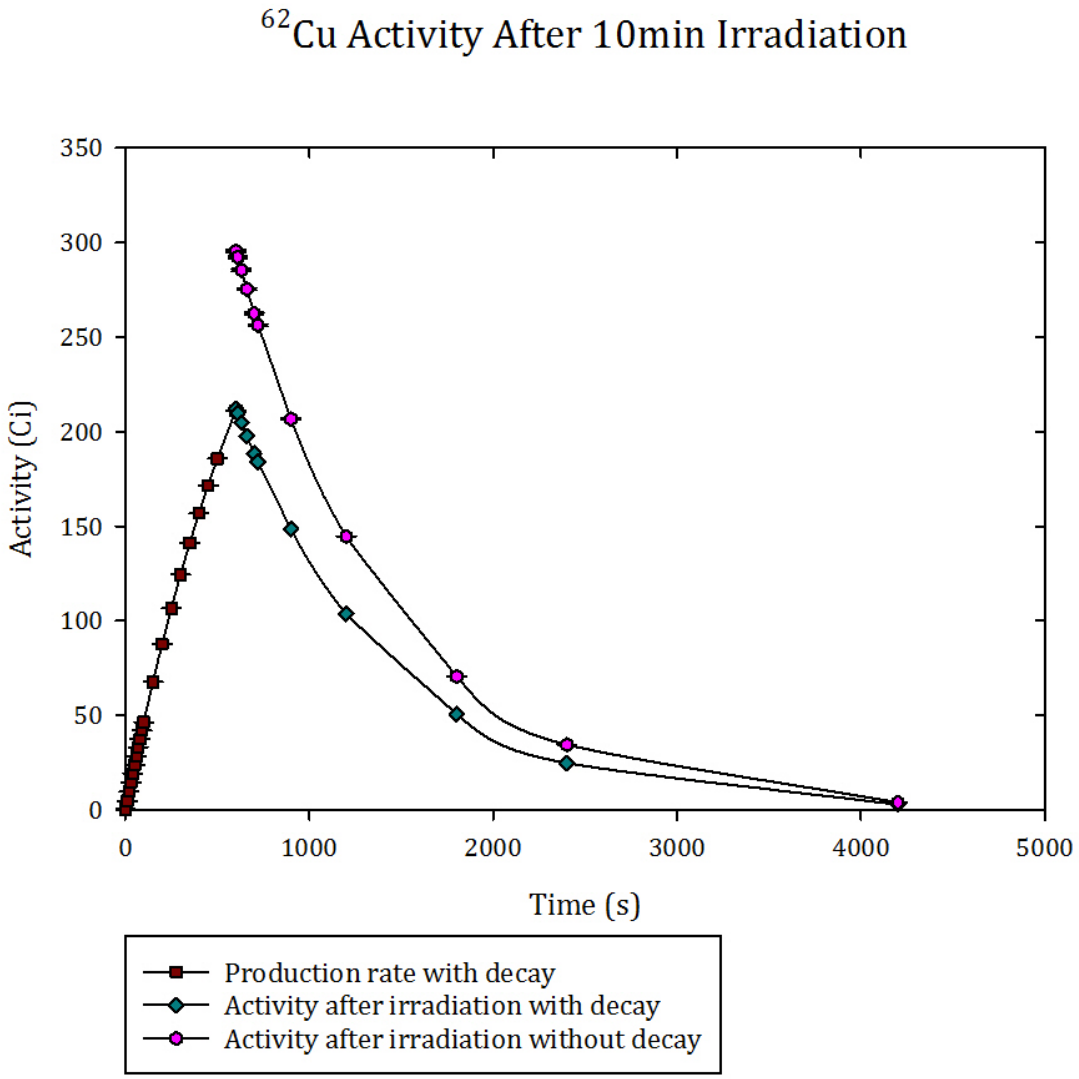

Figure 45. Activity of ^{62}Cu produced after an irradiation time of 10mins with and without accounting for decay during irradiation time

In order to achieve the same activity as that from a single elution from a high activity generator, ~150mCi, an irradiation time of 6.3mins is sufficient for a target thickness of 0.5mm, taking into account the decay during irradiation. This, in principle, should provide a quick on demand method of producing the same medical grade radioisotope as current generator methods. The separation and labelling chemistry for this method should be no different than those already in place for ^{64}Cu and ^{67}Cu. The Cu can be eluted from the target in the same column using either hydrochloric acid or a glycine solution and is then prepared for labelling in exactly the same way as other Cu isotopes.

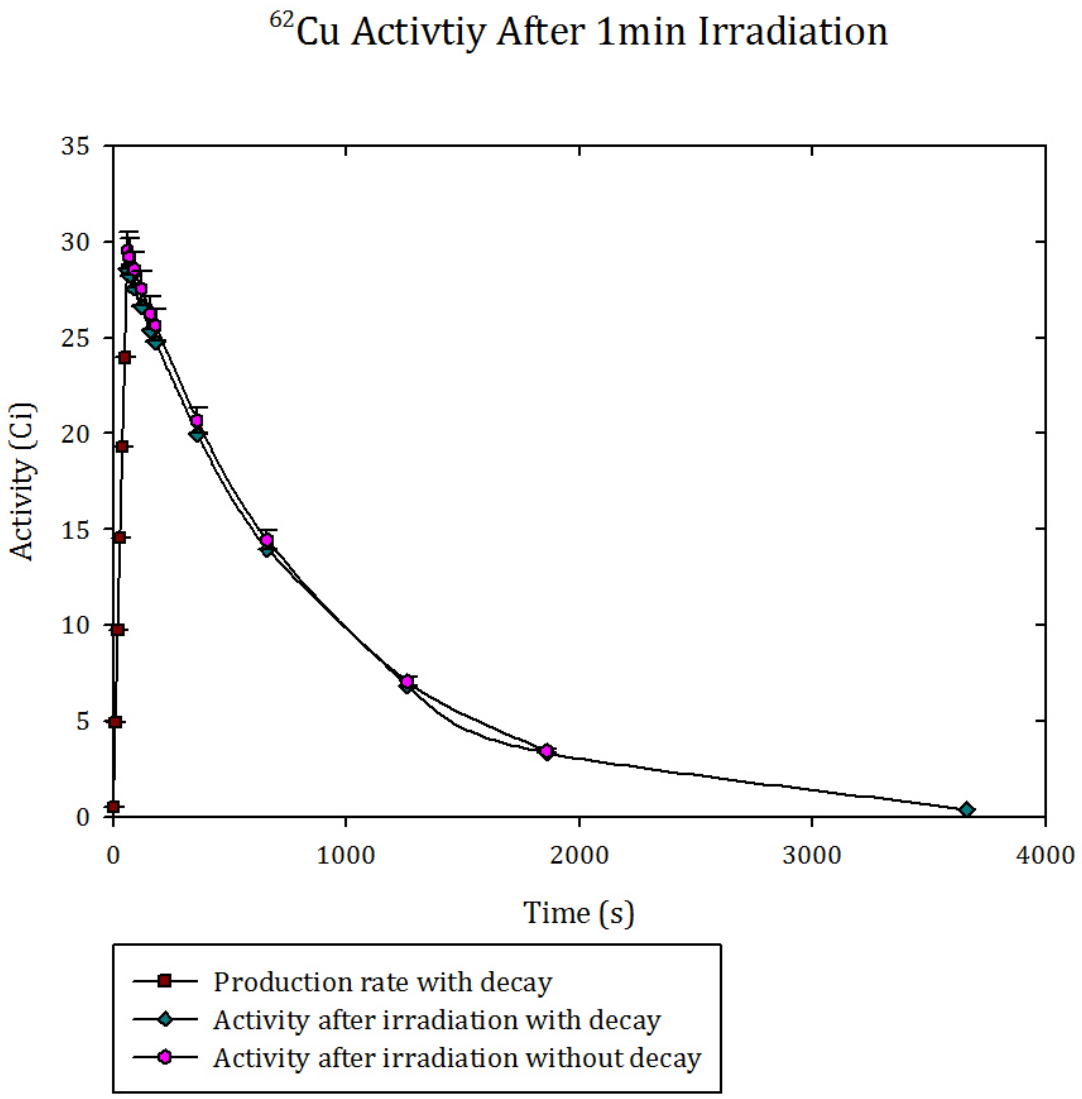

Figure 46. Activity of ^{62}Cu produced after an irradiation time of 1min with and without accounting for decay during irradiation time

The results presented in figures 44-46 further show the significance of the decay of the daughter isotope. It is not until very short times, i.e. fractions of the half-life, that the decay ceases to play a role in the total number of nuclei at the end of irradiation. For isotopes with a short half-life this is an important factor in calculating the yield and activities obtainable from a production system. This should matter less in the production of an isotope with a long half-life compared to irradiation time as is the case for the production of ^{67}Cu.

Calculations were also undertaken to compare the activities obtained with the experimental cross-section taken from the excitation function in fig.41 and the

value obtained from the simulation results. A comparison of these simulated and experimental results is shown in fig.47. As the experimental cross-sections were obtained using a thin target the calculations used the simulated yields from the 0.1mm thin target to provide a comparable cross section.

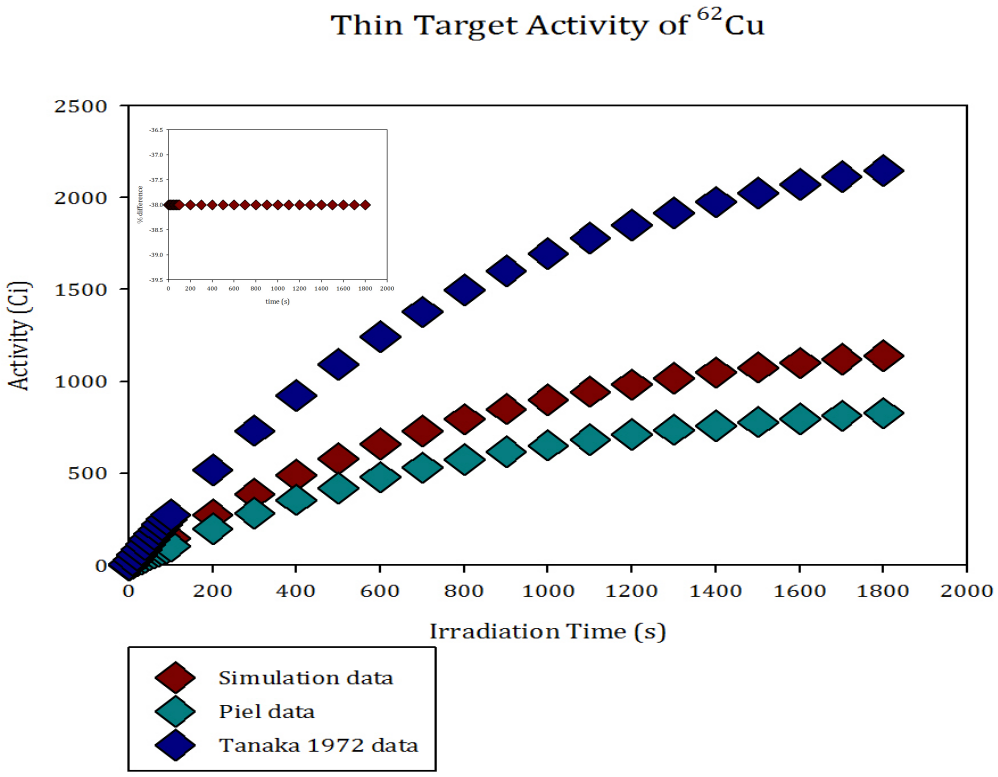

Figure 47. Activity of ^{62}Cu calculated using both experimental and simulated cross sections for a thin target – H. Piel[91] and S.Tanaka[92] [inset- percentage difference simulation/Piel]. Data obtained and reproduced in accordance with EXFOR guidelines

There was again a wide range of data available on the EXFOR library, the data set showing the largest cross-section and the data set showing the smallest cross-section for the reaction were used for comparison to simulated yields, fig.47. A constant systematic error of ~40% can be seen between the lower end experimental (Piel)[91] and simulated activities. The actual uncertainties in the simulated data are again small, such that they cannot be clearly represented here, however the significant contribution lies in the simulated results. From the plot shown in fig.47 it can be seen that in this case the simulation over estimates

the yield for the lower data set, and therefore the cross-section and activity, of ^{62}Cu production when compared with the experimental results.

The difference between data sets is large enough that the simulation data significantly underestimates the Tanaka[92] data set. However, at an irradiation time required to produce a single dose there is much more convergence between the experimental and simulated results.

It also appears, when comparing fig.43 to fig.47, that the activity produced from a thick target is lower than the activity calculated from the experimental cross-section, as would be expected.

6.3.3 Target Processing and Production

Other factors that must be considered in calculating the overall activity produced is the efficiency and time required for the target processing and isotope removal. Due to the low incident proton energy it would be expected that there are few contaminants produced in the target as we are specifically utilising a reaction with one of the lowest threshold energies. This has been confirmed by running simulations with the TALYS code to obtain all isotopes produced within the simulated target for incident proton reactions in the E_p<10MeV range. It appears that only ^{63}Cu and ^{59}Co are produced, in addition to the daughter isotope and excess target nuclei, in the target after irradiation, both of which are stable and have a cross-section of less than a millibarn. The typical method of separation for radiolabeling is elution, this process only separates different elements and not different isotopes. In this case only one other isotope of the same element as the radiotracer is produced, the contamination from ^{63}Cu should be negligible due to low cross-section and its stability. It is therefore a simple procedure to elute out the Cu in a glycine solution as is used with the current generator and higher energy production methods. This infrastructure is already in place and the current technicians are well trained in the process, so that there will be very little disruption to implement this system. The production of the isotopic target

should also be fairly straightforward and already available, or at least possible, as shown by some higher energy, cyclotron based production methods.

6.4 Copper Isotopes for Nuclear Imaging: ^{61}Cu

6.4.1 Potential of ^{61}Cu

^{61}Cu decays partially by electron capture but predominantly by positron emission with a half-life of 3.3hours[33]. This half-life is longer than most current PET isotopes and is therefore useful for studying longer processes. Whilst there is little reported work on ^{61}Cu for medical applications, its use as a suitable PET isotope has been demonstrated[87][94]. The results from these trials have been compared to images taken using ^{64}Cu, as another isotope with only partial β+ decay. As the fraction of β+ decay is larger for ^{61}Cu, more β+ are emitted, the images obtained are of a higher resolution and quality than those of ^{64}Cu[87][94].

6.4.2 Current Production Routes

There are several production routes that can be employed to obtain ^{61}Cu using an accelerator-based system, some of which can be seen below[70]

$$^{nat}\mathrm{Ni}(\alpha,p)^{61}\mathrm{Cu} \quad (41)$$

$$^{60}\mathrm{Ni}(d,n)^{61}\mathrm{Cu} \quad (42)$$

$$^{59}\mathrm{Co}(\alpha,2n)^{61}\mathrm{Cu} \quad (43)$$

These reactions require incident particles of a range of energies from 10MeV for reaction (42) to 45MeV for reaction (43)[70]. However none of these production methods are appropriate to the low energy, proton-induced reactions we are exploring here.

6.4.3 Low Energy Production

One reaction that is appropriate for at lower energy, (9-12MeV) proton irradiation is[70]:

$$^{61}Ni(p,n)^{61}Cu \qquad (44)$$

The experimental excitation function of this reaction can be seen in fig.48.

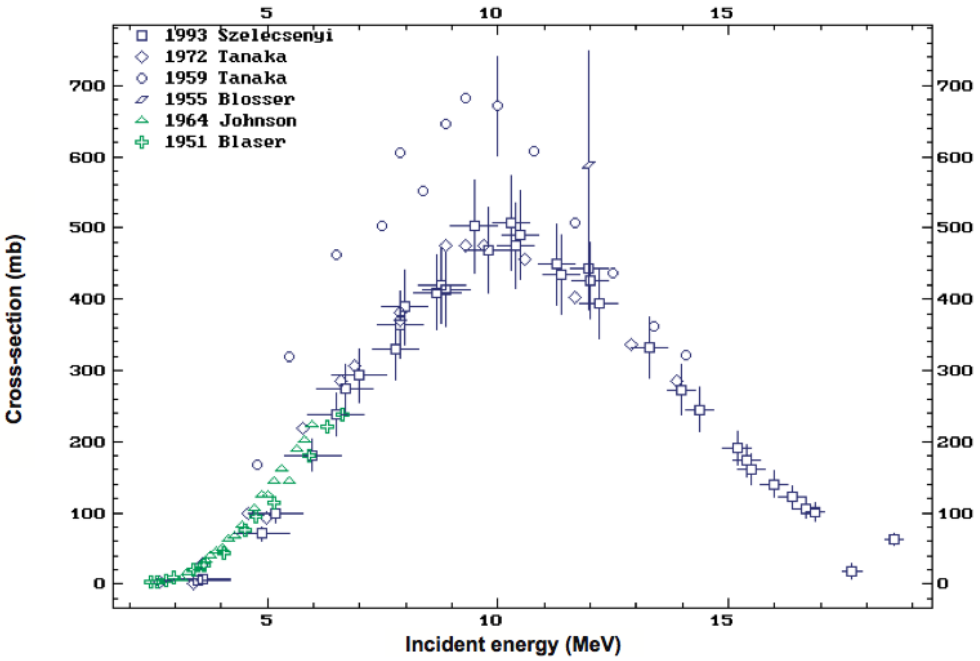

Figure 48. Experimental[95] cross-section data for the reaction $^{61}Ni(p,n)^{61}Cu$. Image reproduced in accordance to IAEA copyright.

Most of the data shown in fig.48 is in good agreement, with only those of Tanaka 1959[95] showing some discrepancy. The peak cross-section for the reaction is ~10MeV with a value of ~500mb. Therefore sufficient yields for medical uses, especially for single dose supply, should be available from a low energy proton production system.

The same set of simulations and calculations were carried out here as for ^{62}Cu, to determine the viability of this production route.

6.4.43.1 Target Thickness and Yields

Initial GEANT4 simulations using QGSP_BIC_PHP were carried out for a 100% enriched ^{61}Ni disc target of thicknesses from 0.9x10^{-4}-0.001m.

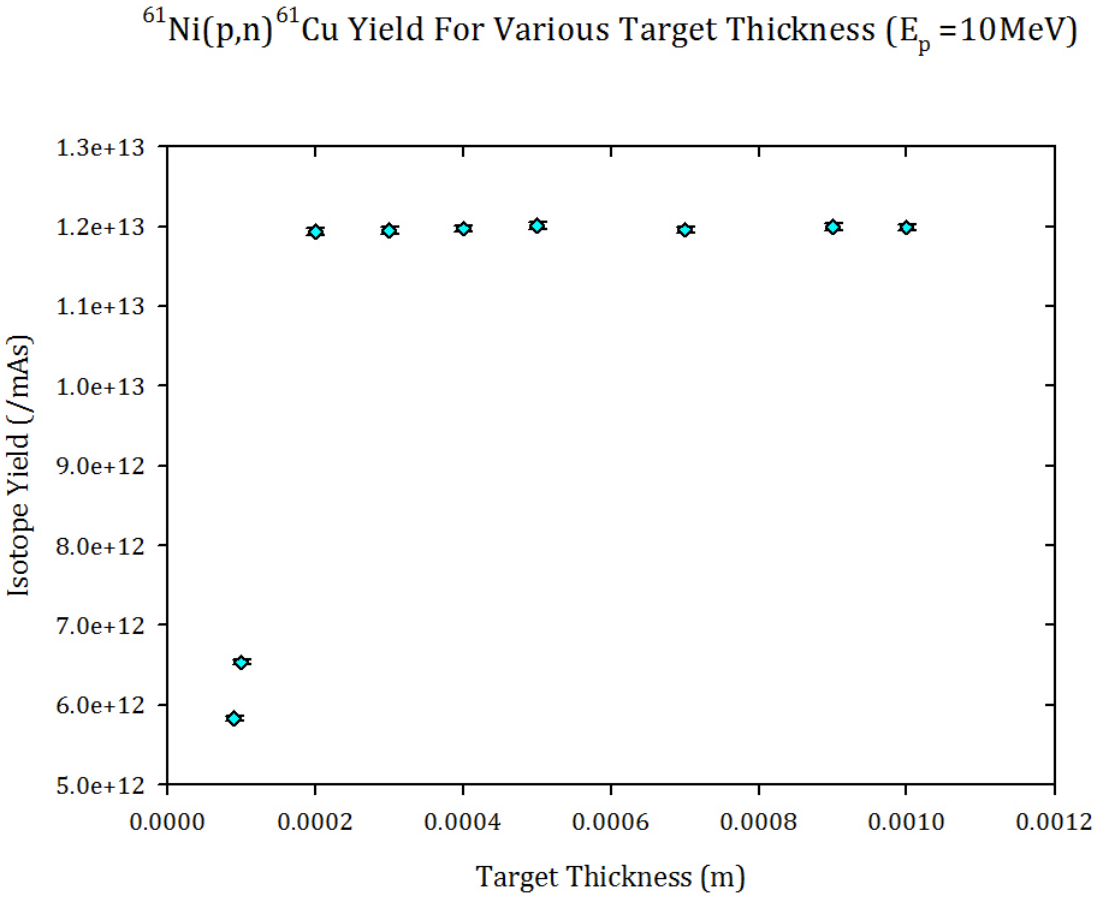

Figure 49. Simulation yields of the reaction ^{61}Ni(p,n)^{61}Cu

From the simulated yields presented in fig.49 the useful range for 10MeV protons in this target could be determined as ~0.2x10^{-3}m. The stopping distance for 10MeV protons within this target was calculated, using the approximation in section 3.3.2[68], to be 0.34x10^{-3}m.

The thickness used for further studies of the production of this isotope will, again, be 0.0005m, which is a reasonable compromise for a practical working target and the most efficient isotope production.

6.4.3.2 Activity

The activity of ^{61}Cu that can be obtained using this target for various irradiation times was calculated, as in section 6.3.2.2[93], and can be seen below in figs. 50 & 51.

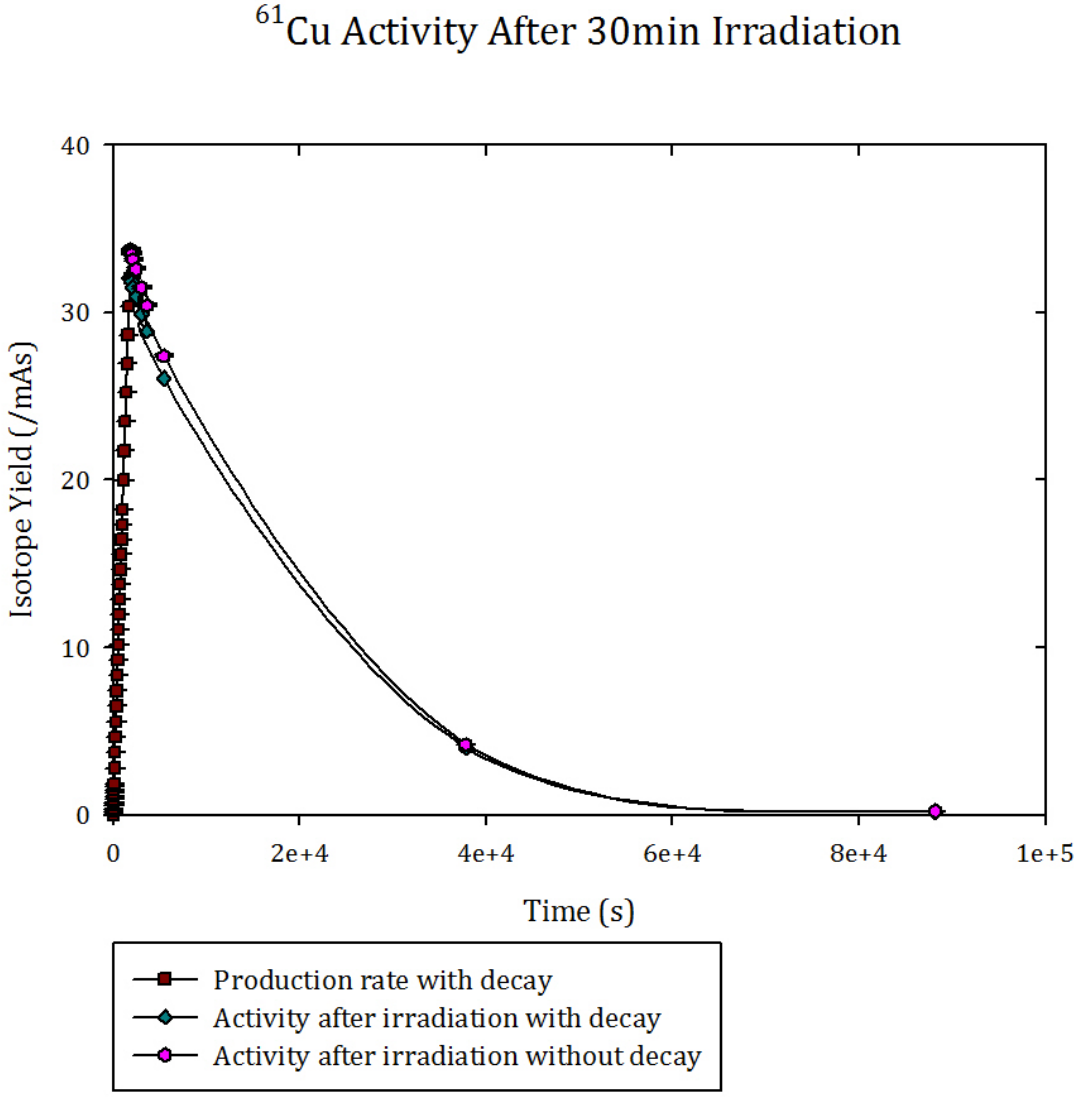

Figure 50. Activity of ^{61}Cu produced after an irradiation time of 30mins with and without accounting for decay during irradiation time

The activity from an irradiation time of 30mins has been calculated both with and without taking into account the decay during irradiation. The results in fig.50 show that 30min irradiation time is a small enough fraction of the half-life that there is little affect from the decay during this time on the overall activity produced. A significantly smaller activity is produced during this time than that

seen for shorter half-life isotopes such as ^{62}Cu. However this should still be sufficient for a single dose, of the order 10mCi, on demand production facility.

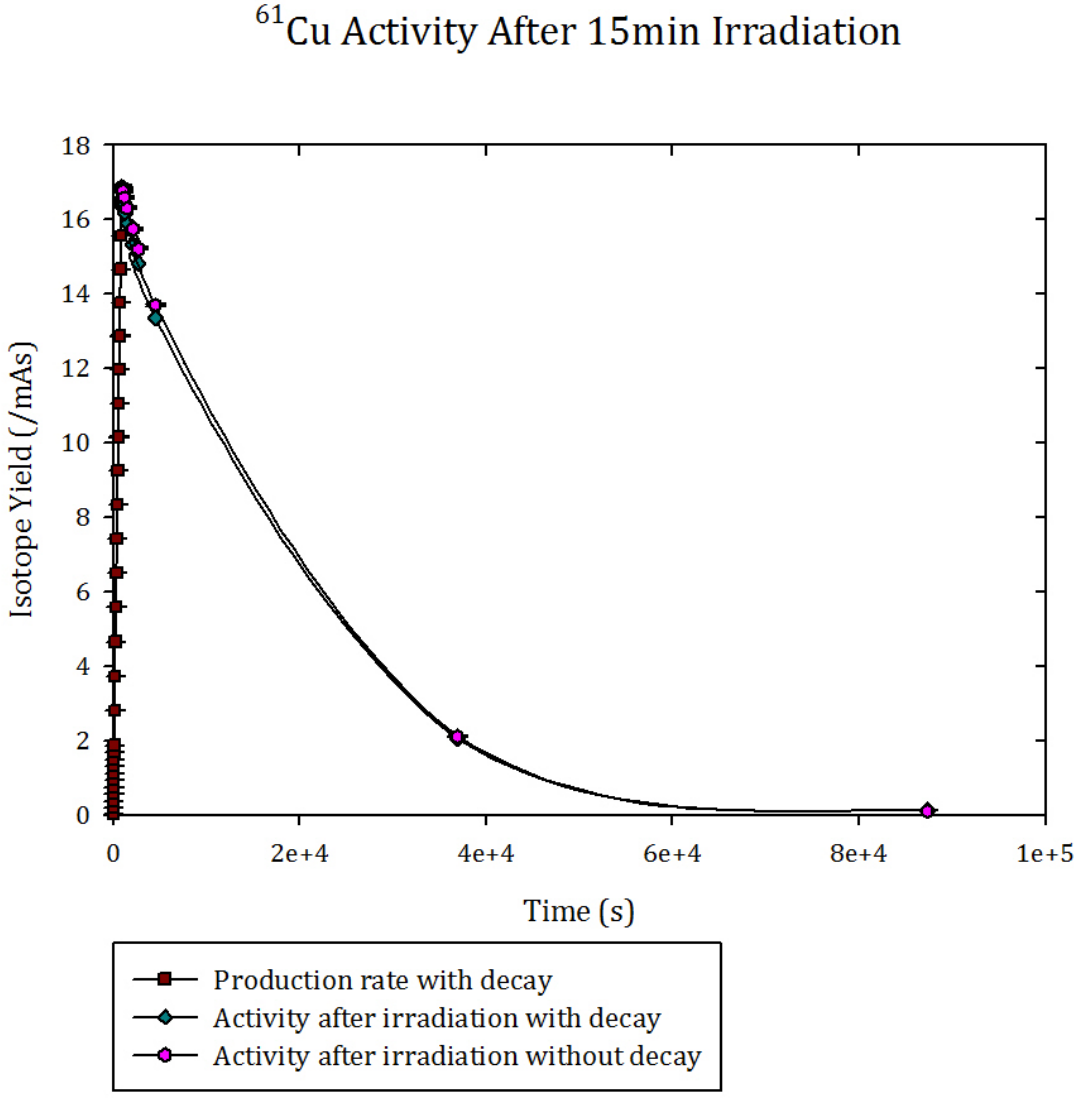

Figure 51. Activity of ^{61}Cu produced after an irradiation time of 15mins with and without accounting for decay during irradiation time

A 15min irradiation time is also sufficient to obtain a single dose quantity of ^{61}Cu, as demonstrated by the plot presented in fig.51.

A comparison has also been made between the activities calculated using the experimental cross-sections, from fig.48, and those of the thin (t=0.1mm) simulated target, the results of these calculations are presented in fig52.

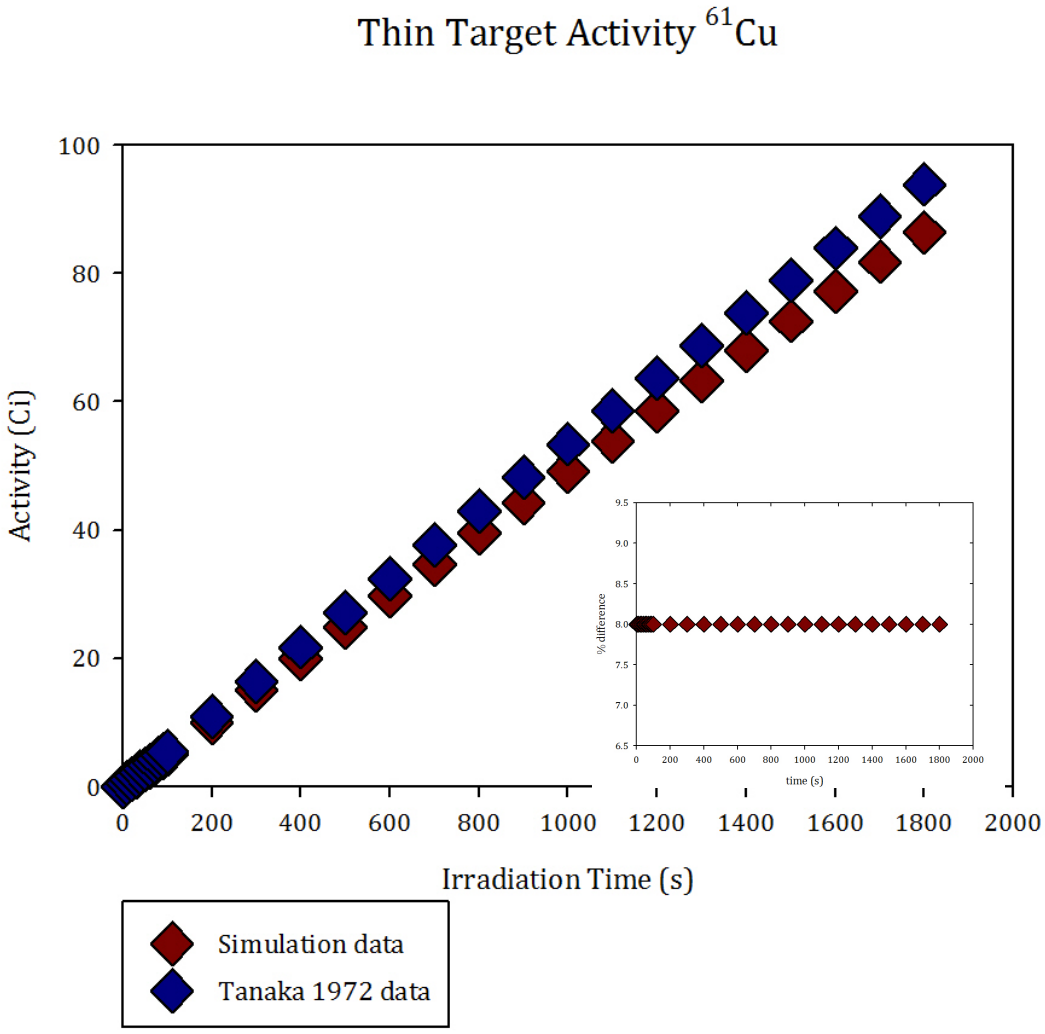

Figure 52. Activity of ^{61}Cu calculated using both experimental[95] and simulated cross sections for a thin target [inset- percentage difference simulation/experimental]

In this case there is much closer agreement between the activities derived from the simulated and experimental cross-sections, a constant percentage difference of only 8% can be seen between the experimental and simulated activities in the fig52 inset. The actual uncertainties in the simulated data are again small, such that they cannot be clearly represented here, however the significant contribution lies in the simulated results. The irradiation time is also small enough in comparison to the half-life of the isotope that there is still an agreement, within error, between the simulated and experimental expected activities.

6.4.4 Target Processing and Production

TALYS studies and EXFOR data suggests that again there are few contaminants produced within the target, ^{62}Cu and ^{58}Co(ground and metastable states), each with low cross-sections of the order of milibarns or less. Unlike the contaminants produced with ^{62}Cu both of these isotopes are radioactive. The half-life of the metastable and ground states of ^{58}Co are 9hours and 70days respectively. It is much easier to separate products when the difference in half-lives are larger. In this case the contaminant half-lives are longer than that of ^{61}Cu by enough that the processing and removal of the Cu by glycine elution should not be any more difficult than it is for ^{62}Cu. The half-life and cross-section of the ^{62}Cu isotope produced during irradiation is also small enough that it is not a significant consideration, much of the ^{62}Cu should have decayed during processing and a negligible fraction would be present at the time of use.

The production of the isotopic target is a process that is already available and which can be utilised.

6.5 Copper Isotopes for Nuclear Imaging:^{60}Cu

6.5.1 Potential Uses

^{60}Cu is a positron emitting isotope with a half-life of 23.7mins[33]. A typical PET isotope half-life, ^{60}Cu shows to be suitable for many of the same applications as ^{62}Cu, such as imaging of blood flow and the heart, but with a more flexible time schedule. Although there is little published in the literature on the medical applications of ^{60}Cu, that which can be found demonstrates ^{60}Cu to be a suitable PET imaging isotope comparable in performance to ^{62}Cu[87][88][94]. Indeed the short half-life of ^{62}Cu(9.7mins) makes this isotope difficult to process, label and administer the pharmaceuticals in a time such that a suitable dose reaches the required area of the body to produce the highest quality image. In comparison the longer half-life of ^{60}Cu allows for a longer time during processing and

delivery of the drug, while also short enough to not require long post procedure hospital stays.

6.5.2 Current Production

Production methods of ^{60}Cu employed in previous tests utilised the reaction

$$^{60}\text{Ni(p,n)}^{60}\text{Cu} \qquad (45)$$

from either an enriched ^{60}Ni or ^{Nat}Ni target with a 14MeV proton cyclotron accelerator.

The experimental excitation function for this reaction(45) presented in fig.53, shows a peak in the production cross-section at ~14MeV with a value of ~400mb. This peak is utilised in existing production methods in order to obtain the highest yields of ^{60}Cu.

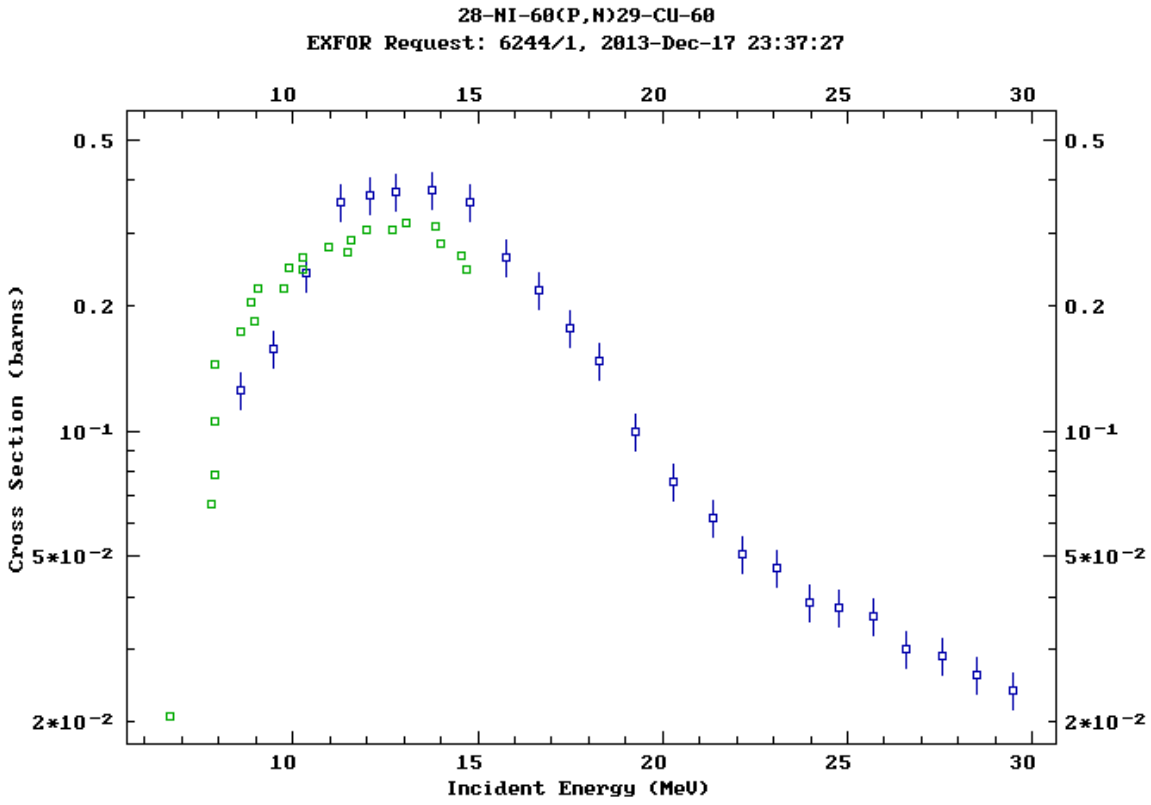

Figure 53. Experimental cross-section data (Levkowskij[96]-blue squares with error bars, Tanaka[97]-green squares) for the reaction ^{60}Ni(p,n)^{60}Cu. Data obtained and reproduced in accordance with EXFOR guidelines

6.5.3 Low Energy Production

While fig.53 shows the maximum cross-section is outside the energy range of interest to this work the cross-section at 10MeV is still relatively high, with a value of approximately 200mb. This suggests that the yields that can potentially be obtained from an enriched ^{60}Ni target at 10MeV should be adequate for at least single dose on demand isotope production.

6.5.3.1 Target Thicknesses and Yields

GEANT4 simulations using QGSP_BIC_PHP were carried out to asses the ^{60}Cu yield obtainable from a 100% enriched ^{60}Ni disc target utilising the (p,n) reaction at E_p=10MeV for a range of target thicknesses, the results of which can be seen in fig.54.

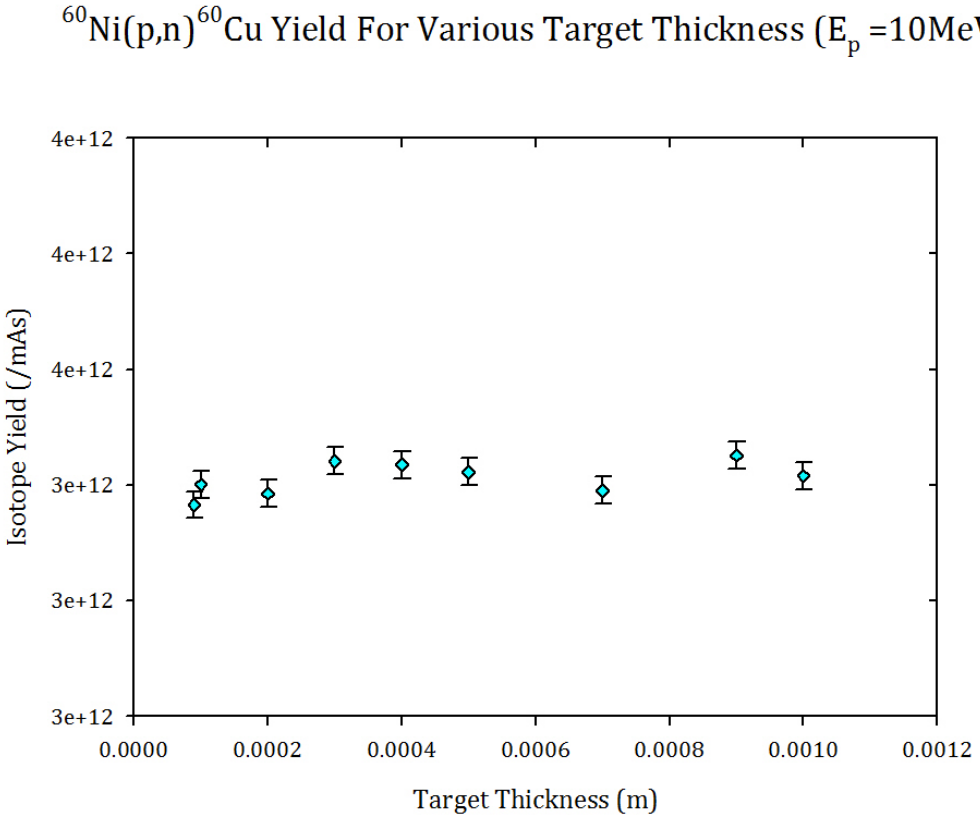

Figure 54. Simulation yields from the reaction ^{60}Ni(p,n)^{60}Cu

The range of 10MeV protons in ^{60}Ni has been calculated as $0.34x10^{-3}$m as per the calculations in section 3.3.2. This is significantly longer than the apparent useful range of protons in this target as GEANT4 results show in fig.54.

There is little difference in the simulated isotope yields from target thicknesses in the range $0.9x10^{-4}$-0.001m, shown in fig.54, suggesting that the thickness at which the proton energy drops below the threshold for this reaction is smaller than those used here.

It appears that any target thickness can be considered as a "thick target". For the same practical reasons as discussed in 6.3.2.1, a target thickness of 0.0005m will be used in the following simulations.

6.5.3.2 Activity

The activity of ^{60}Cu that can be obtained from a 0.0005m target of ^{60}Ni for various irradiation times was calculated from the simulated yields, as in section 6.3.2.2[93], and can be seen below in figs.55-57. Firstly activity was calculated for an irradiation time of 30mins(fig.55). This is longer than the half-life of the daughter isotope of interest and so the activity was calculated both with and without taking into account the decay of ^{60}Cu during the irradiation period to see if the decay during irradiation reduced the yield as much as when the irradiation time is shorter than the half-life of the daughter isotope.

It appears that single dose production would be available from a 30min, fig.55, irradiation time with a processing and administration time of over an hour before the activity becomes too low to be useful.

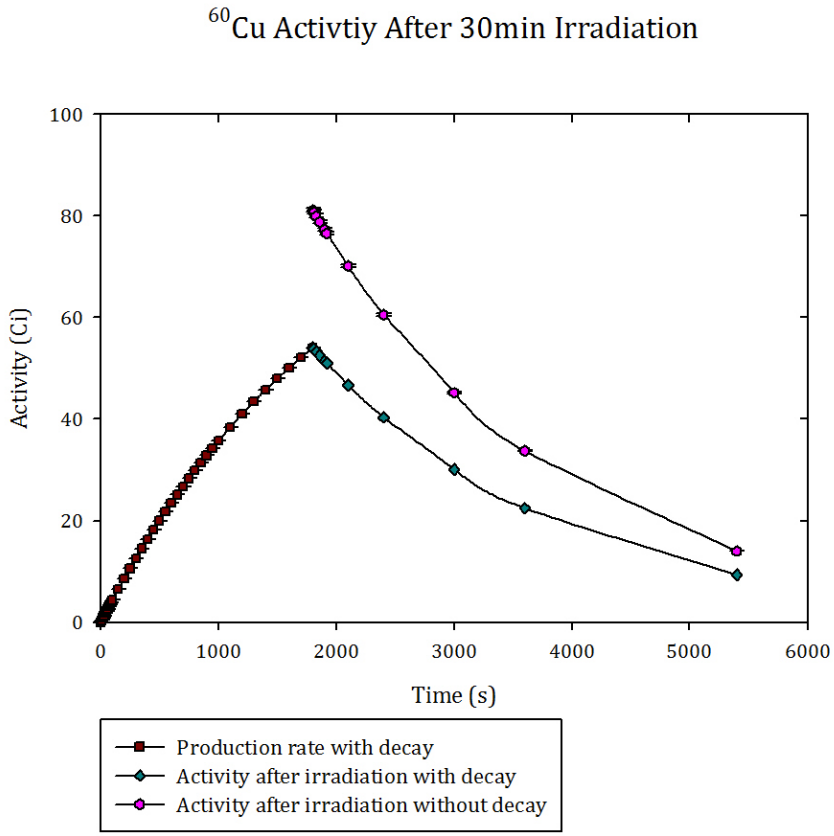

Figure 55. Activity of ^{60}Cu produced after an irradiation time of 30mins with and without accounting for decay during irradiation time

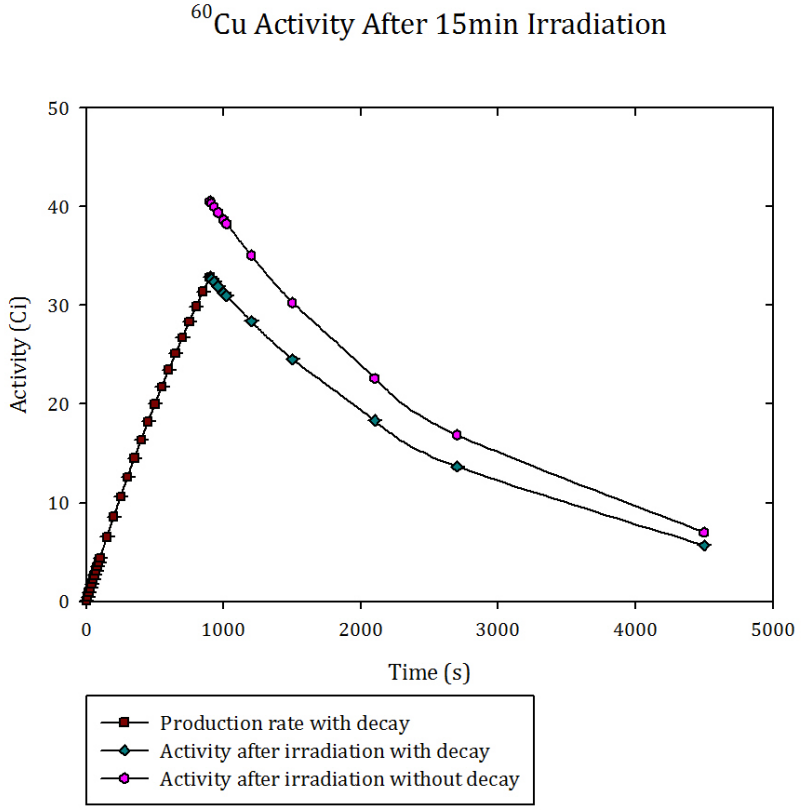

Figure 56. Activity of ^{60}Cu produced after an irradiation time of 15mins with and without accounting for decay during irradiation time

It can be seen that even a 15min(fig.56) or 10min(fig.57), irradiation time can produce sufficient activity for a low single dose.

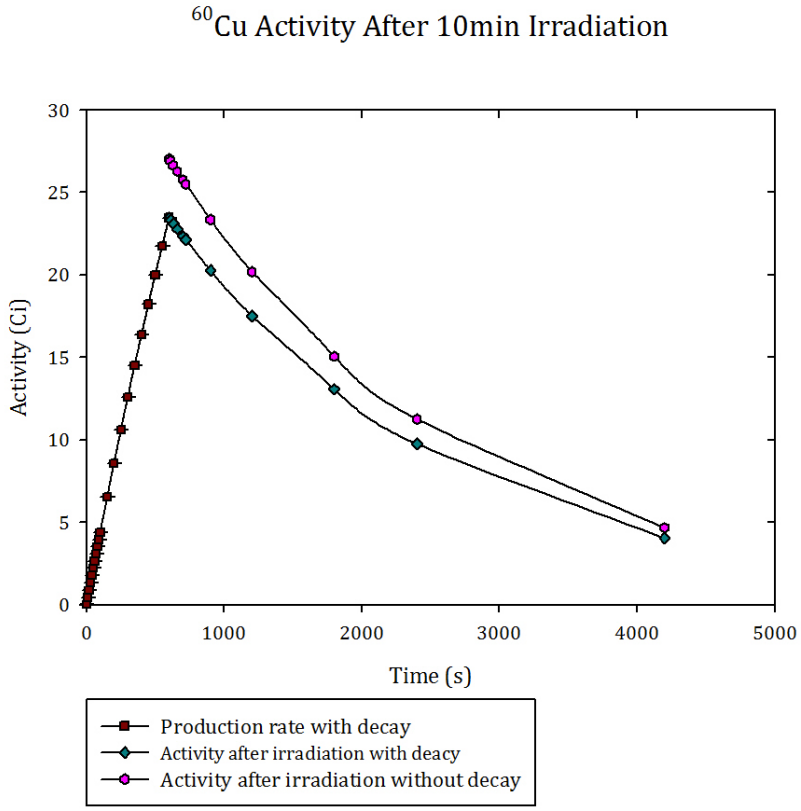

Figure 57. Activity of ^{60}Cu produced after an irradiation time of 10mins with and without accounting for decay during irradiation time

A practical irradiation time for the production of ^{60}Cu is approximately equal to its half-life. Because of this the decay of ^{60}Cu during irradiation is enough to result in a significant reduction in the yield of ^{60}Cu at the end of irradiation and hence in the resultant activity compared to the values if this decay is not taken into account.

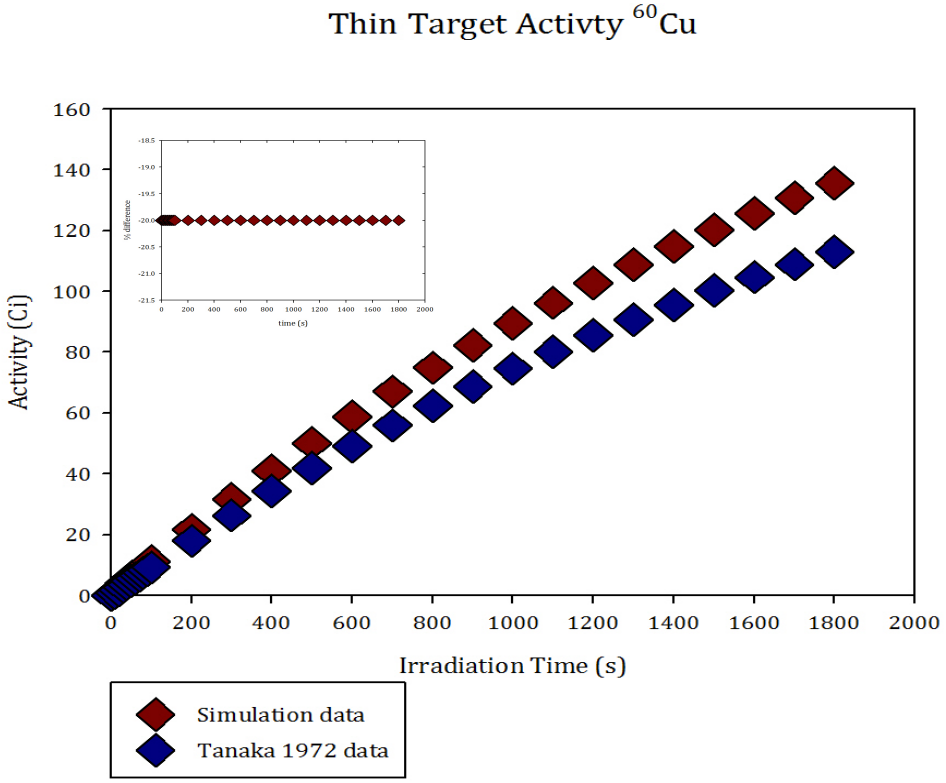

Figure 58. Activity of ^{60}Cu calculated using both experimental[97] and simulated cross sections for a thin target[inset- percentage difference simulation/experimental]

The activities calculated using both experimental cross-sections, taken from fig.53, and cross-sections calculated using simulated thin (t=0.0001m) target yields were compared and can be seen in fig.58. In this case the simulation results slightly over estimate the activities available from a 30min irradiation. Again as expected the thick target simulation activates are significantly less than those for both the simulated and experimental thin target values. A constant percentage difference of only 20% can be seen between the experimental and simulated activities. The actual uncertainties in the simulated data are again small, such that they cannot be clearly represented here, however the significant contribution lies in the simulated results.

6.5.4 Target Processing and Production

The contaminants in this target are much the same as for the other nickel targets in that there are some small contributions from ^{61}Cu and ^{57}Co, each with a production cross-section of milibarns or less according to TALYS and EXFOR

libraries. Both of these isotopes have significantly longer half-lives than the required isotope. It is possible to elute the Cu with a glycine solution and separate the elements so that there is no final contamination due to the Co. The half-life of ^{62}Cu is much longer than that of ^{62}Cu therefore other isotopic separation techniques, which are currently in use, maybe required to remove this contamination before use so that the patient does not see a longer lasting effect from a dose of ^{61}Cu.

6.6 Conclusions

This study has demonstrated the viability of low energy proton induced reactions as a production method for several copper isotopes for use in medical imaging. Calculations using both experimental and simulated data have shown that ^{60}Cu, ^{61}Cu, and ^{62}Cu can all be produced in reasonable quantities with activities larger than the typical dose of approximately 10mCi from a low energy high current proton accelerator system. A summary of the activity results presented in this chapter can be seen below in table 1. Activity of ^{60}Cu for a 30min irradiation is shown in fig. 55 and the value of activity after a 15min irradiation is taken from fig.56. The activities of ^{61}Cu are taken from fig.50 for a 30min irradiation and fig.51 for a 15min irradiation. Referring back to fig.43 shows the activity of ^{62}Cu obtainable from a 30min irradiation and fig.44 that of a 15min irradiation. Such a system should be small enough to replace many of the on site generator systems currently in use for a local on-demand production, thereby providing a more convenient and flexible supply.

Isotope	Half-life (mins)	Decay energy (MeV)	Activity (Ci) 30min irrad.	Activity (Ci) 15min irrad.
Cu-60	23.7	6.12	54.0	32.8
Cu-61	198	2.24	32.0	16.4
Cu-62	9.7	3.94	364.0	272.0

Table1. A summary of the PET isotopes and their production studied in this chapter [33]

An irradiation time of 30mins is seen to be sufficient to produce adequate activity for each of the suggested isotopes. Any longer irradiation would be impractical for the type of production system we hope to achieve, and would reduce the advantages of on-demand production. Large cross-sections and shorter half-lives allows for a shorter irradiation time as both increase the resultant activity. However, shorter half-lives also mean that more of the daughter isotope will be lost than for those isotopes with a longer half-life. Therefore a quicker and more efficient means of target processing, isotope removal and drug labelling and delivery is required so as not to waste the induced activity and ensure that an optimal dose is delivered to the patient.

In principle most of the necessary processing procedures are already in place or should be readily adaptable from previous trials of isotopes produced by higher energy proton cyclotron irradiation methods, drug trials and experiences with the use of other isotopes of the same element, for which the isotopic separation and drug delivery should not be significantly different.

7. GALLIUM ISOTOPES FOR MEDICAL APPLICATIONS

7.1 Background

Gallium is a group 3 metal with only two stable isotopes and is not naturally occurring in its elemental form. The main applications of gallium are in the electronics industry and in medicine[98]. While there is no known biological use of gallium the behaviour of this element within the body is similar to that of iron, which allows for its use in studying several biological processes. It is most useful as a salt, typically used in the form gallium citrate[70][98]. In this form it can be bound to many important biological proteins and ligands designed for targeted uptake in specific cell types.

Therefore, a suitable positron or photon emitting isotope of gallium can be applied as tracers to image and monitor a range of tumour types including Hodgkin's and non-Hodgkin's lymphomas, leukaemia, and malignant melanoma[70][98]. There are currently three isotopes of gallium used in nuclear medicine the SEPCT isotope ^{67}Ga and PET isotopes ^{68}Ga and ^{66}Ga.

7.2 Current SPECT Isotope: ^{67}Ga

7.2.1 Background

^{67}Ga decays via three gammas of energies: 93.3keV, 184.6keV and 300.2keV[70] with a half-life of 3.3days[33]. This is a very long half-life in comparison to other SPECT isotopes. In current nuclear medicine it has become important to have a high patient turn around therefore there is a tendency to select SPECT isotopes with shorter half-lives to enable the patients to be discharged soon after the procedure without them retaining too much activity in their system. Using isotopes with long half-lives require a longer hospitalisation time for the patient waiting for the majority of activity to leave the body. However a longer half-life can be useful for imaging those tumours with slow take up where isotope accumulation occurs over several days. Such a long half-life also increases the

availability of ^{67}Ga over other shorter lived isotopes in more remote locations and removes the need for generator production[70][98].

7.2.2 Current Production Routes

There are two useful proton induced reactions for the cyclotron production of ^{67}Ga[70]:

$$^{68}\text{Zn(p,2n)}^{67}\text{Ga} \quad (46)$$

$$^{67}\text{Zn(p,n)}^{67}\text{Ga} \quad (47)$$

The (p,2n) reaction (46) is currently the most favoured production route using a standard 20MeV medical cyclotron. Naturally occurring zinc contains 19% ^{68}Zn, enabling fabrication of either an enriched ^{68}Zn target, or the potential to use a natural zinc target, although natural targets can increase isotopic contamination.

Reaction (46) has an excitation function given in fig.59 which shows a peak cross-section of approximately 800mb at 20MeV and a reaction threshold above 10MeV making this reaction unsuitable for our studies.

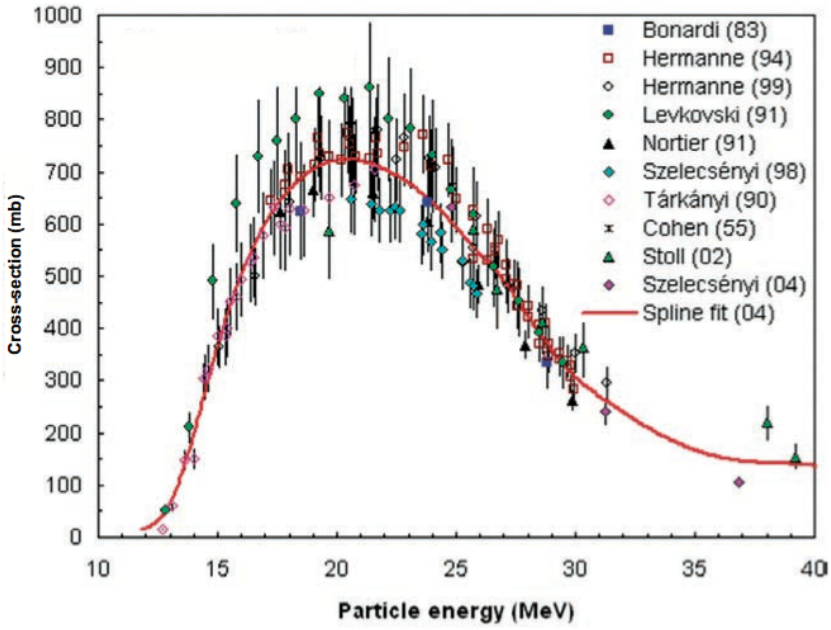

Figure 59. Experimental[99] cross-section data for the reaction ^{68}Zn(p,2n)^{67}Ga Image reproduced in accordance to IAEA copyright.

7.2.3 Low Energy Production

However low energy production is possible with the (p,n) reaction (47), the excitation function of which can be seen in fig.60. With a peak cross-section of 600mb at 10MeV this reaction would be of some interest for this work, although the difficulties of producing the enriched ^{67}Zn target make it less favourable.

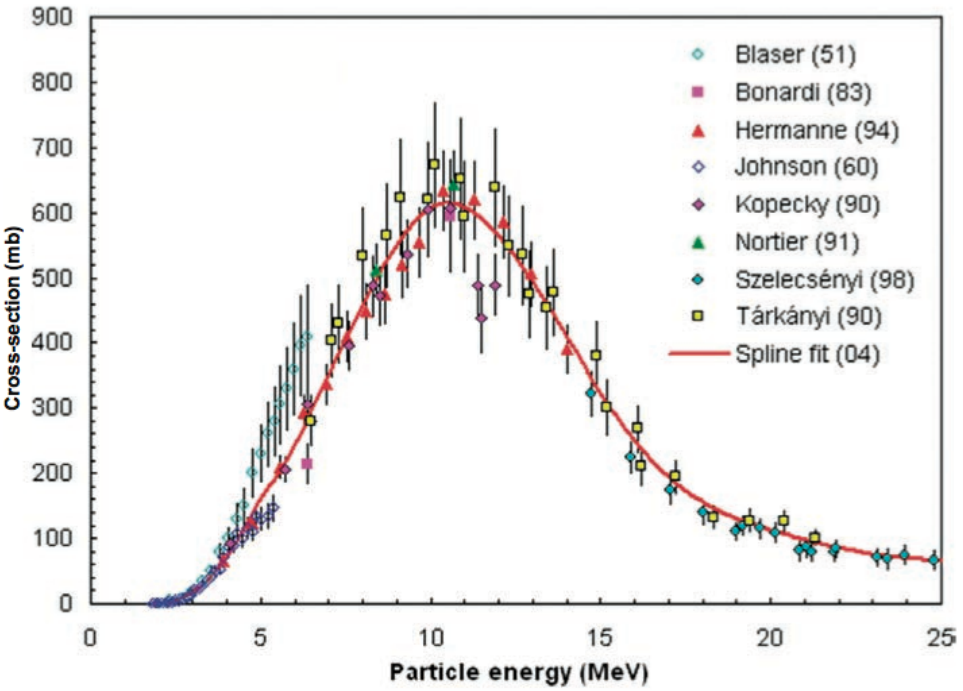

Figure 60. Experimental[100] cross-section data for the reaction ^{67}Zn(p,n)^{67}Ga. Image reproduced in accordance to IAEA copyright.

7.3 PET Isotopes: ^{68}Ga

7.3.1 Applications

Gallium-68 is a positron-emitting radioisotope with a half-life of 68mins[33]. The complexes that can be formed with ^{68}Ga show many advantages over the most common PET radiopharmaceuticals such as ^{18}F-FDG, due to the interaction characteristics of gallium. Gallium labelled drugs have larger accumulation rates for slow growing tumours and produce better quality images for tumours in locations with high background uptake of ^{18}F-FDG by the surrounding healthy tissue, such as in the brain. Many of the pharmaceutical compounds developed

for use with ^{68}Ga have a quick blood clearance that, together with the short half-life, allows for multiple repeat scans to be carried out during the same session[98][101][102].

7.3.2 Current Production Routes

Current production of medical ^{68}Ga uses a generator system. Due to the short half-life this make ^{68}Ga more accessible in remote locations where directly produced short-lived isotope such as ^{18}F are not available. The parent isotope of ^{68}Ga is ^{68}Ge, which has a half-life of 270 days. This gives a useful generator lifetime of up to a year. ^{68}Ge is normally produced using high-energy spallation facilities utilising some of the following reactions (48) & (49) and their excitation functions are shown in figs. 61 & 62[103]:

$$^{nat}Zn(a,x)^{68}Ge \qquad (48)$$

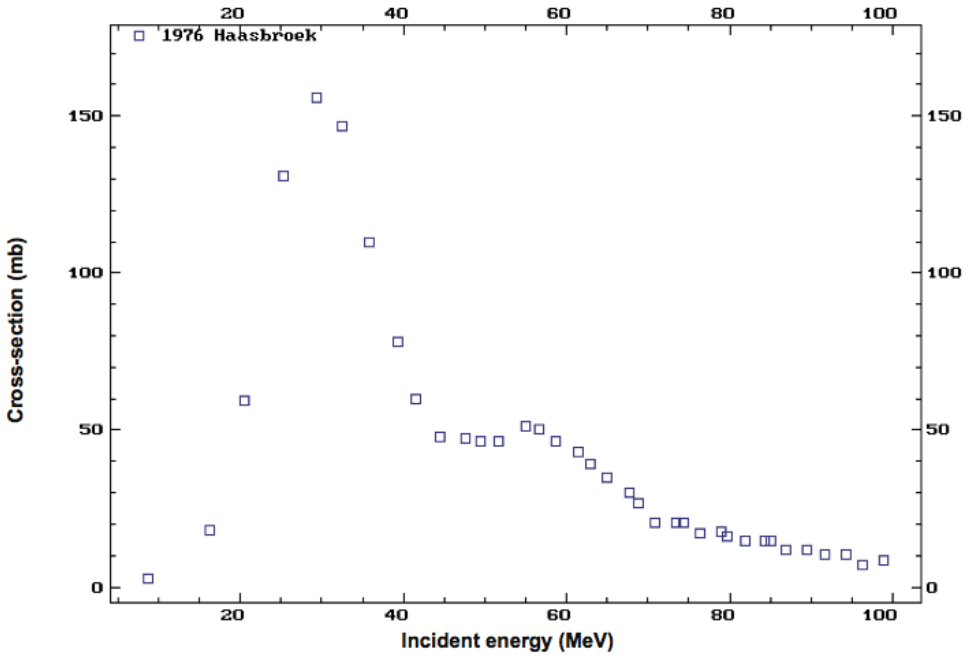

Figure 61. Experimental[103] cross-section data for the reaction ^{nat}Zn(a,x)^{68}Ge. Image reproduced in accordance to IAEA copyright.

$^{nat}Ga(p,x)^{68}Ge$ (49)

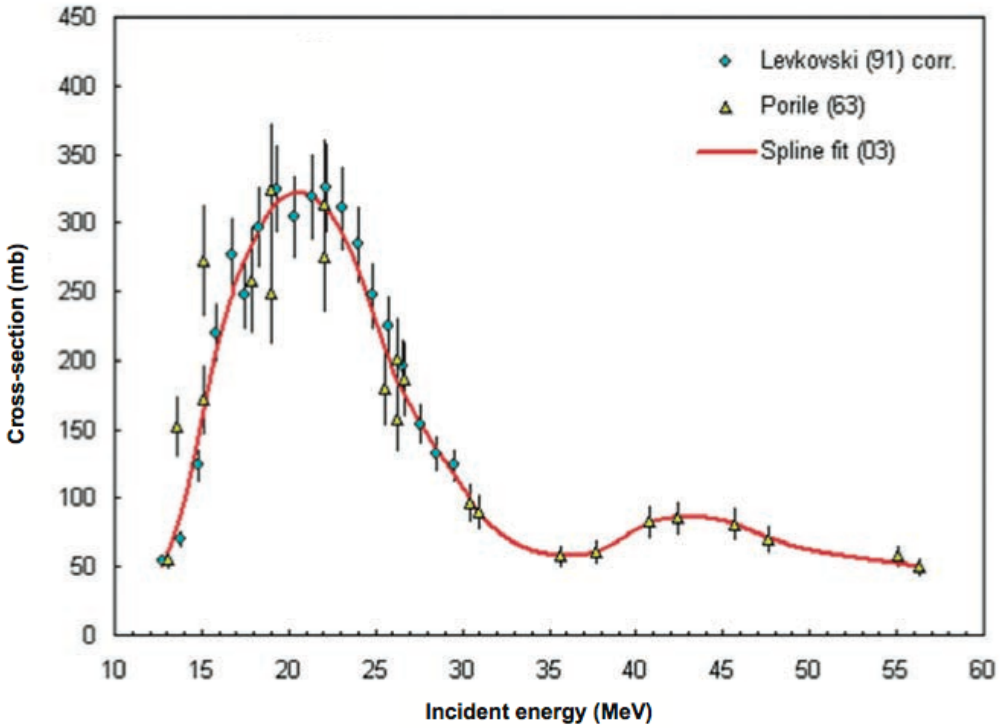

Figure 62. Experimental[103] cross-section data for the reaction $^{nat}Ga(p,x)^{68}Ge$. Image reproduced in accordance to IAEA copyright.

The original generator systems were inefficient and difficult to process. The daughter isotope would form complexes that require breaking down following elution before the solution can be mixed with the ligands for labelling. This requires a long processing time, compared to the half-life, making it an inefficient procedure and consequently there has been little advancement of ^{68}Ga procedures until the last decade when developments in production simplified and sped up the processing of ^{68}Ga from the generator to provide a cleaner product more efficiently.

7.3.3 Low Energy Production

The developments to improve the production of ^{68}Ga, especially associated with efficient target processing, have lead to low energy proton accelerator based production routes for localised on demand supply.

Direct production of ^{68}Ga is possible utilising reaction (50) and its excitation function which is shown in fig.63:

$$^{68}\text{Zn(p,n)}^{68}\text{Ga} \qquad (50)$$

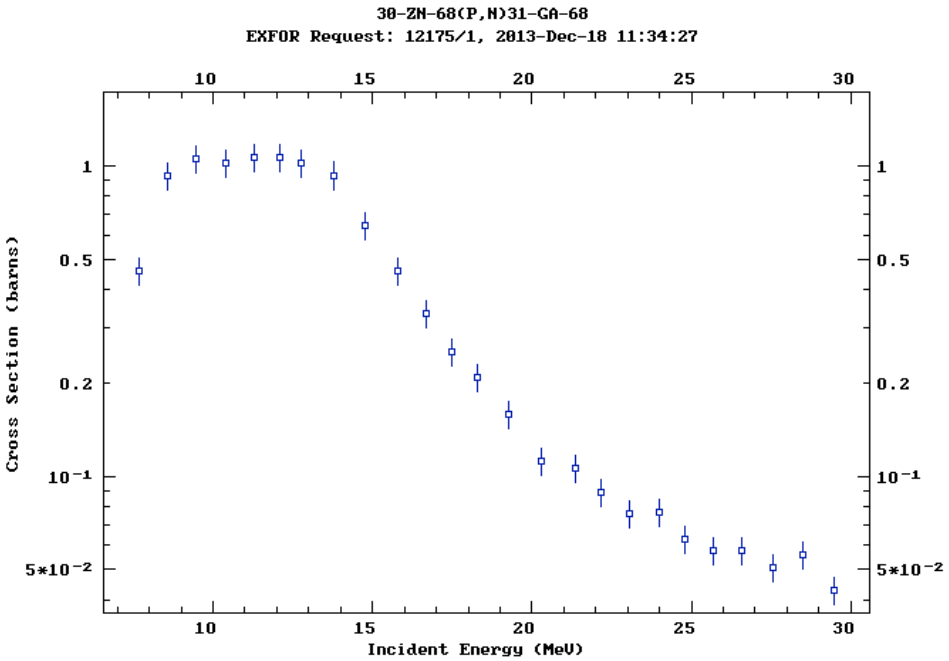

Figure 63. Experimental[104] cross-section data for the reaction ^{68}Zn(p,n)^{68}Ga. Data obtained and reproduced in accordance with EXFOR guidelines

As previously mentioned there are already suitable manufacturing procedures in place for the production of an enriched ^{68}Zn target, which could be used with a low energy proton beam. The production cross-section of ^{68}Ga for this reaction at the energy range of interest (E_p<10MeV) is where the cross-section reaches its peak with a value of ~1b (fig.63).

7.3.3.1 Target Thickness and Yields

The first question to be addressed is what is a suitable target thickness. A thick target, just greater than the stopping thickness or useful proton range provides the best compromise between efficient isotope production (isotopes produced per target nuclei available for conversion) and a thick pellet target, which is easier for handling and processing.

Initial GEANT4 simulations using the QGSP_BIC_PHP model were carried out for 10^8 protons with an energy of 10MeV, scaled for a realistic beam current of 1mA bombarding an enriched ^{68}Zn target over a range of thicknesses. The uncertainties in all the simulation results in this chapter were calculated as in section 3.2.1 and carried through the calculations accordingly. Error bars are shown where it is possible to do so, only in the cases where the error bars are so small as to be negligible or such that even at the smallest point size are too small to be visible have again been omitted

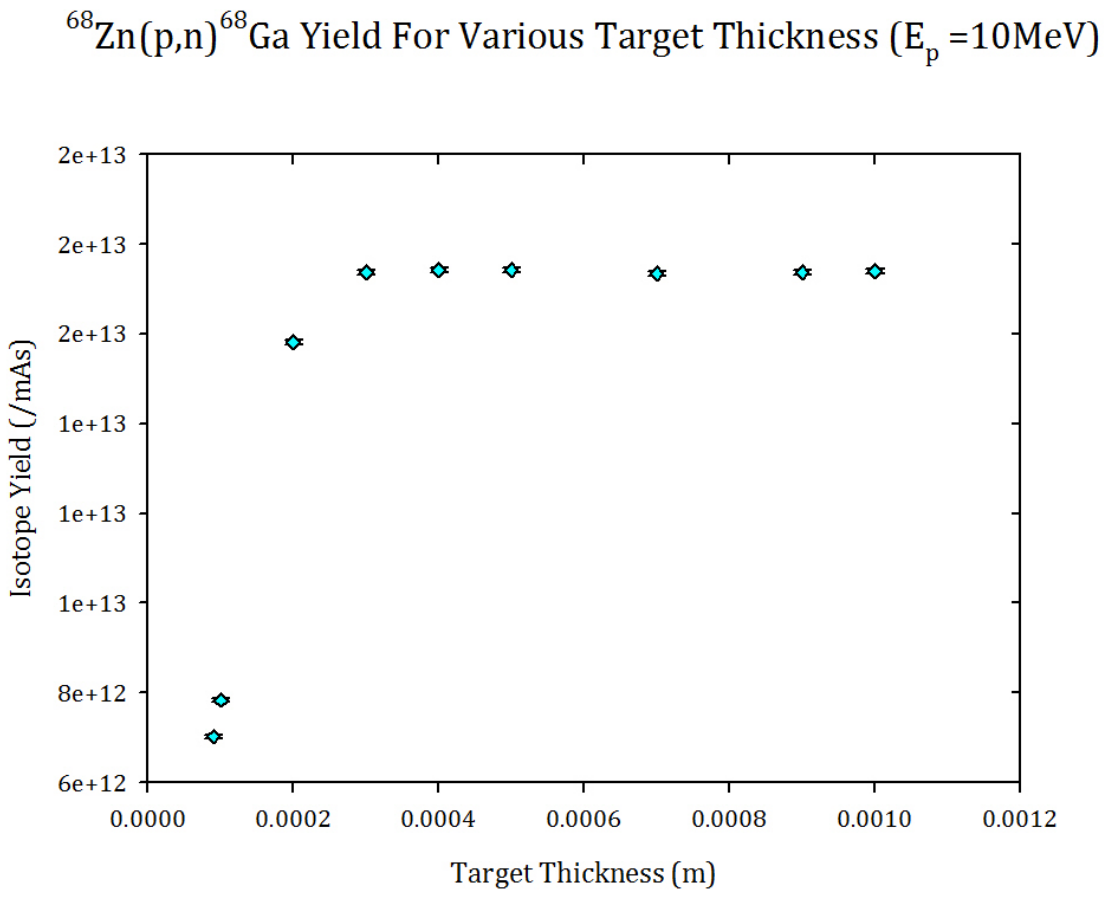

Figure 64. Simulation yields of ^{68}Ga from the reaction ^{68}Zn(p,n)

From the results presented in figure 64 it is possible to determine the useful range of 10MeV incident protons on to a ^{68}Zn target to be ~0.0003m. Using the equation (14) from section 3.3.2[68] it is also possible to calculate the stopping distance of the incident protons in this target to be 0.45mm.

To explore the viability of this production method a target thickness of 0.0005m has been chosen as a suitable compromise between optimum production rates and practical target implementation.

7.3.3.2 Activity

The next stage is to calculate the potential activity that can be produced from this target under different irradiation times for a 1mA, 10MeV proton beam. Once again, this activity has been calculated in two ways to demonstrate the effect of decay of the daughter isotope during irradiation, as described previously in section 6.3.2.2[93].

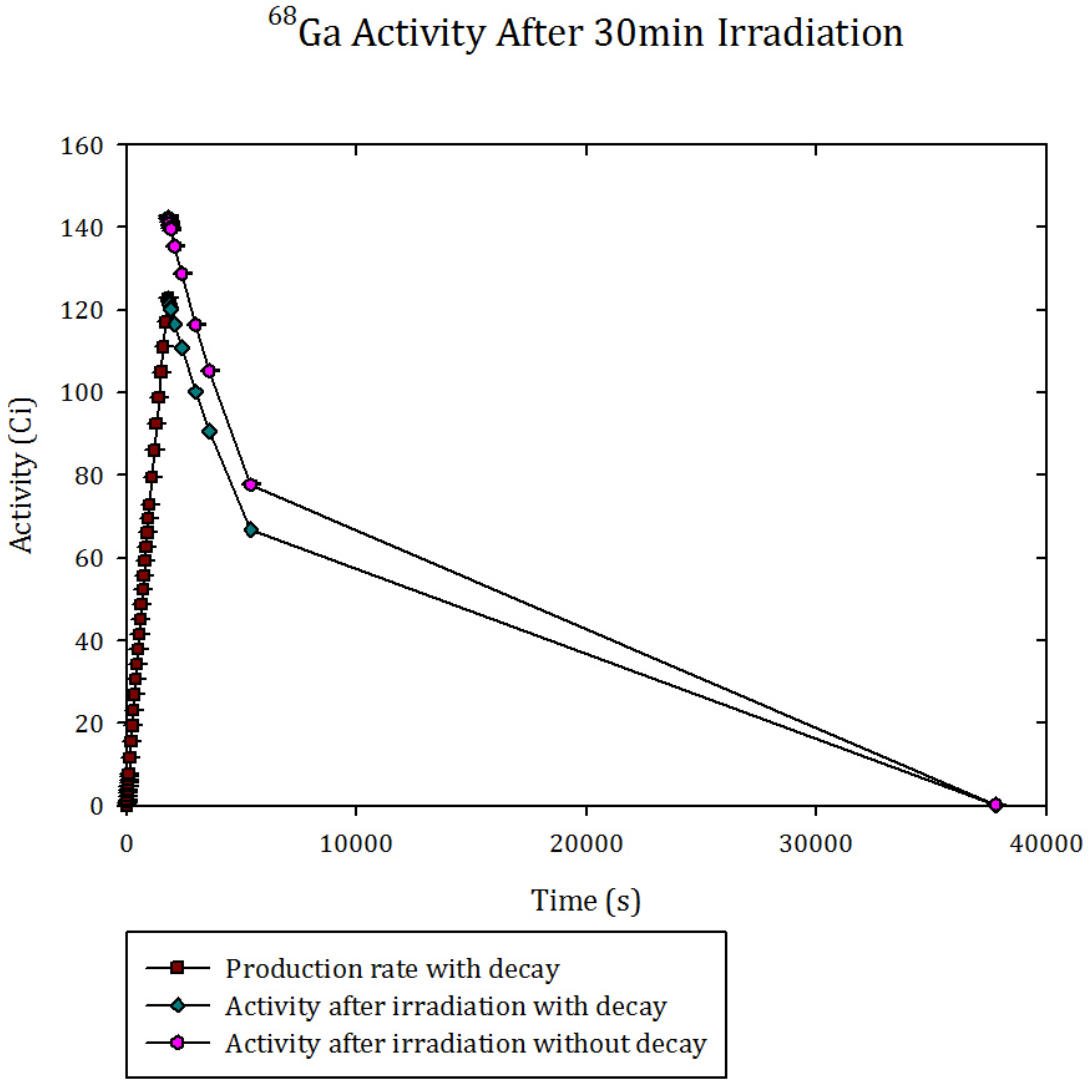

Figure 65. Activity of ^{68}Ga produced after an irradiation time of 30mins with and without accounting for decay during irradiation time

A 30min irradiation time is approximately the time for half of one half-life and, as can be seen from fig.65, shows that this is still a large enough fraction that the decay of the ^{68}Ga during the irradiation time makes a difference to the final activity produced from irradiation. This is also seen to be a long enough time to produce multiple doses of ^{68}Ga, where a typical dose administered to a patient is of the order <10mCi.

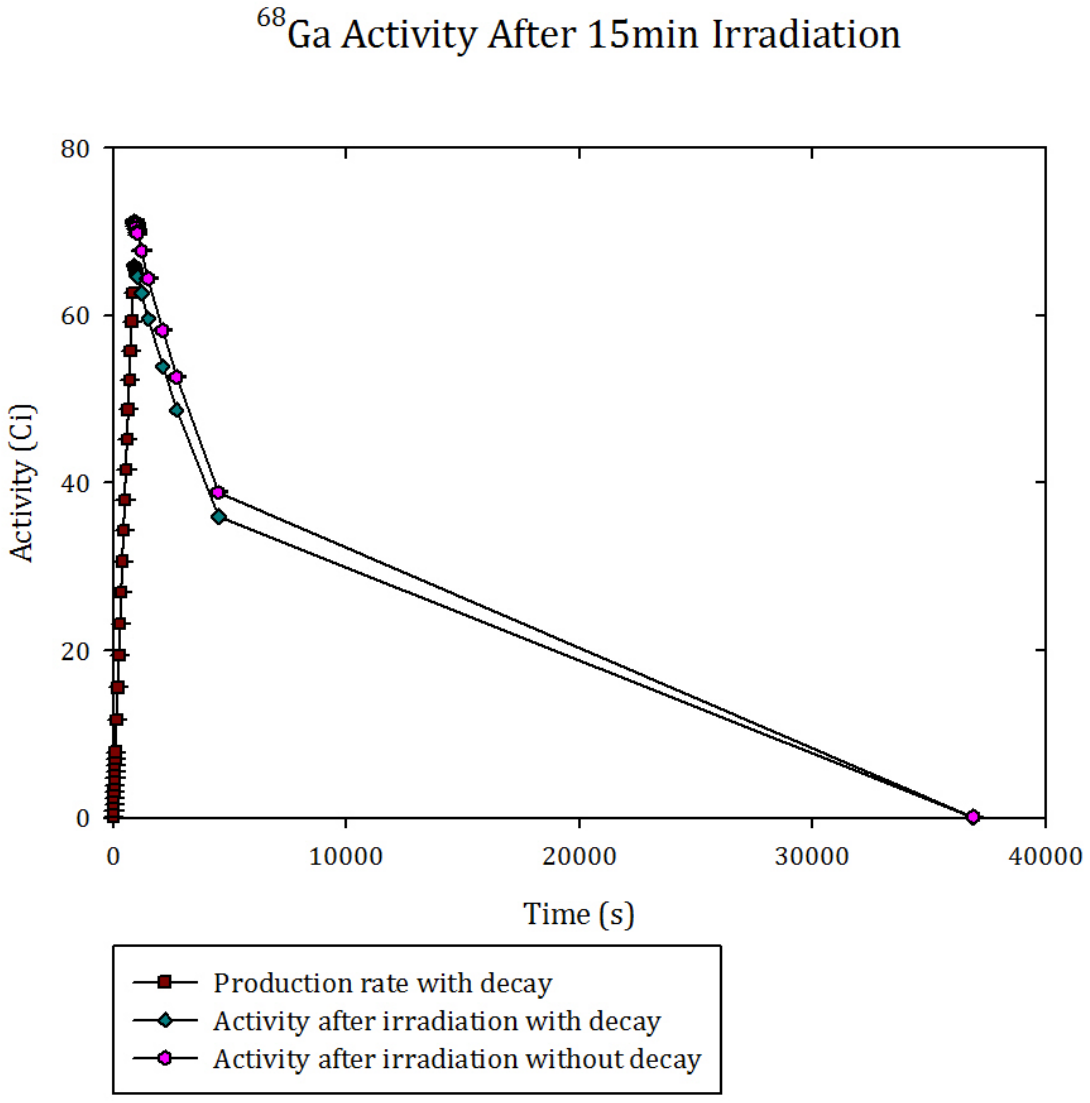

Figure 66. Activity of ^{68}Ga produced after an irradiation time of 15mins with and without accounting for decay during irradiation time

As the irradiation time of 15min is approximately a quarter of the daughter isotope's half-life there is still some discrepancy seen between the two methods of calculating the activity from and after irradiation if the decay of the daughter isotope during irradiation is not considered as shown in fig.66.

The activity shown in fig.66 for a 15min irradiation is still enough for several doses of gallium to be produced and also allow for processing losses, as activity after irradiation does not drop to below a dose quantity until more than 2hours after irradiation ends.

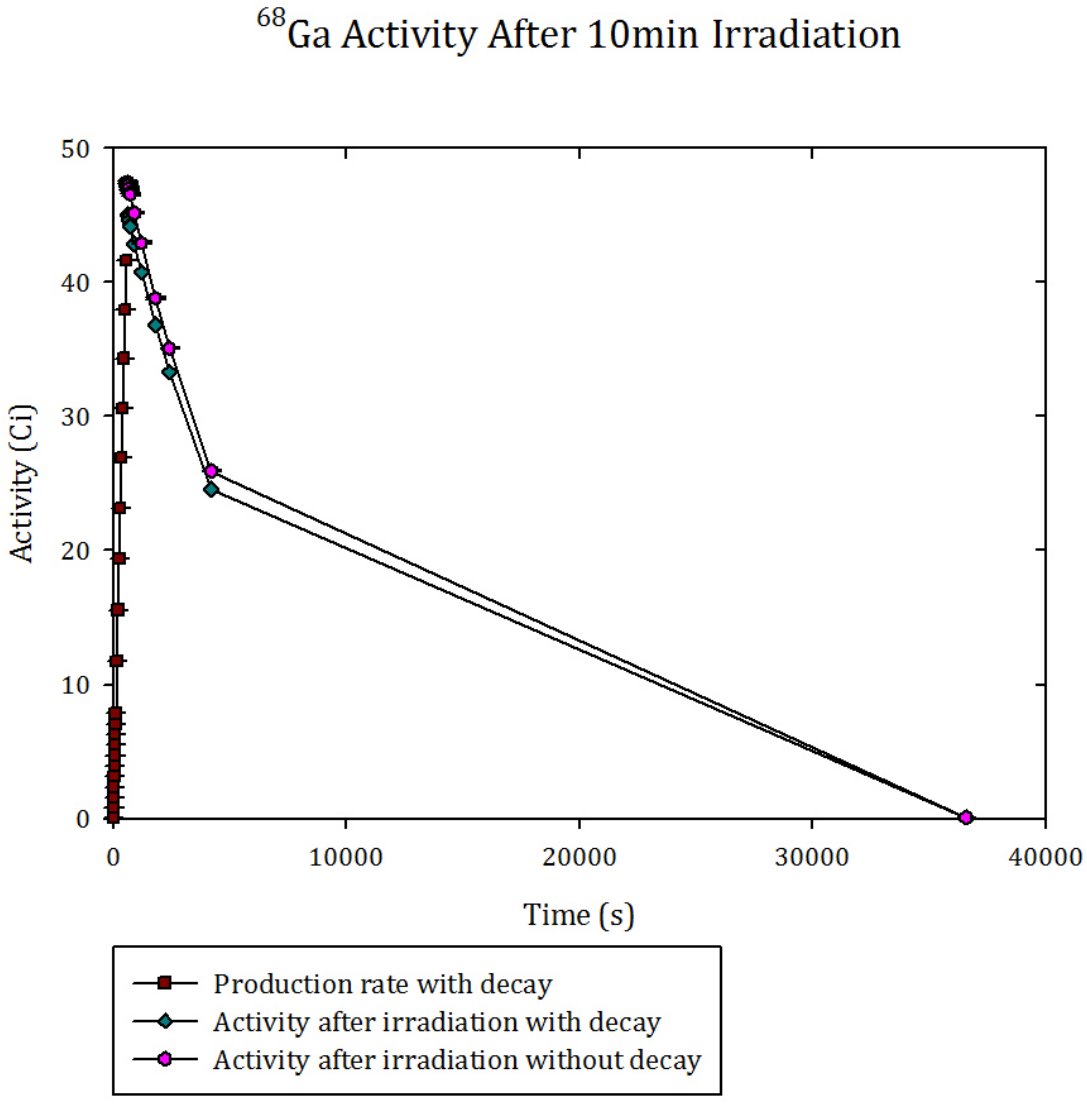

Figure 67. Activity of ^{68}Ga produced after an irradiation time of 10mins with and without accounting for decay during irradiation time

From the results shown in fig. 67 it appears that a 10min irradiation time to produce an isotope with a 68min half-life is a small enough fraction, i.e. ~1/7th, that the decay during irradiation is an almost negligible negative contribution to the overall activity produced during this time.

10 minutes irradiation is therefore sufficient to produce at least a single dose of ^{68}Ga from a thick target. However to mitigate for the activity lost during processing of the isotope a 10 minute irradiation may not produce sufficient isotope to provide multiple doses.

The experimental, taken from fig.63, and simulated cross-sections of a thin (t=0.0001m) target were also used to calculate the activity produced during a 30min irradiation for a validation comparison as shown in fig.68.

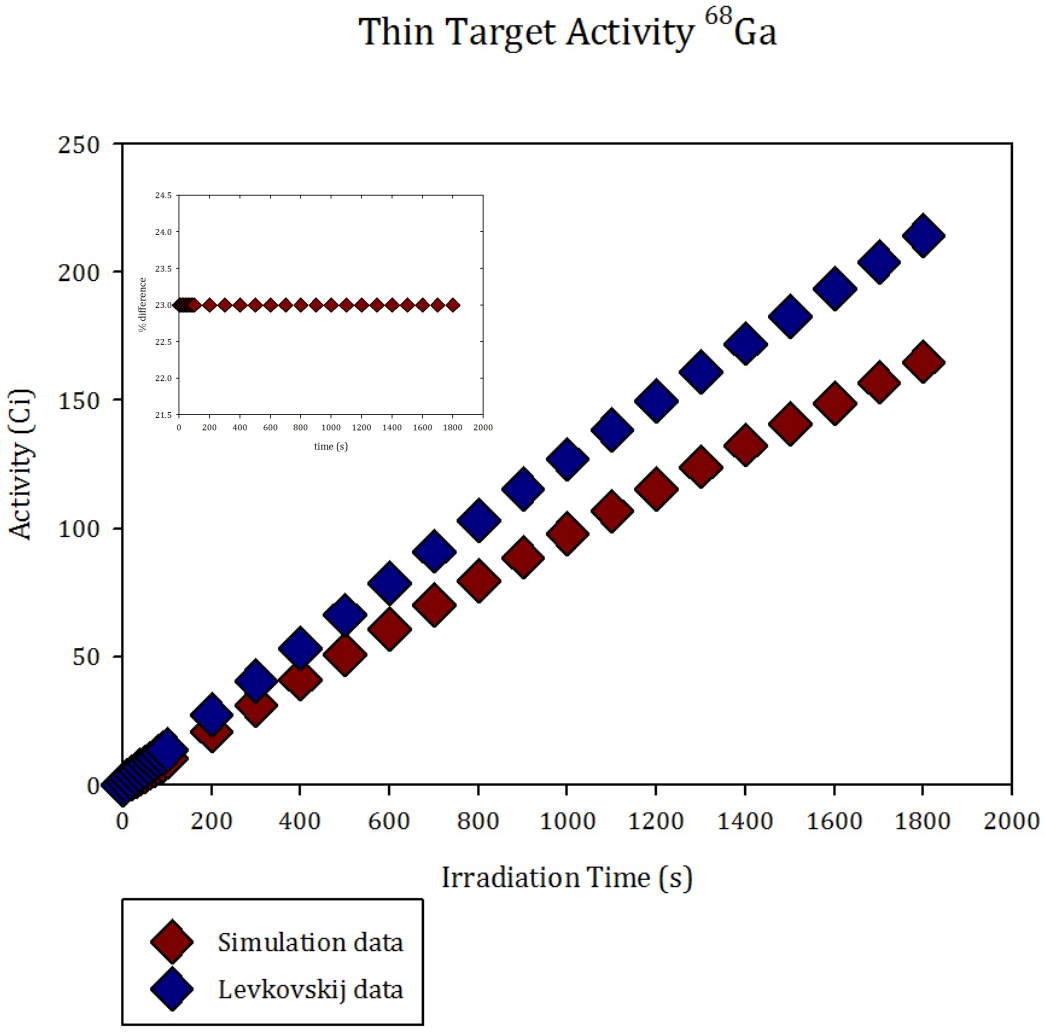

Figure 68. Activity of ^{68}Ga calculated using both experimental[104] and simulated cross sections for a thin target [inset- percentage difference simulation/experimental]. Data obtained and reproduced in accordance with EXFOR guidelines

Fig.68 shows that the simulated results underestimate the activity that is calculated using the experimental thin target cross-section: both activities for a

thin target over estimate that calculated for a thick target, as would be expected. A constant percentage difference of only 23% can be seen between the experimental and simulated activities. The actual uncertainties in the simulated data are again small, such that they cannot be clearly represented here, however the significant contribution lies in the simulated results.

7.3.4 Target Processing and Production

The easiest target in terms of manufacturing processes is that of a natural composition. As was mentioned earlier the natural composition of zinc is such that there is sufficiently high percentage of the required ^{68}Zn for the desired reaction that a natural target could be adequate to produce enough activity for medical applications. The previously presented simulations and calculations of the ^{68}Zn target were also carried out for a natural zinc target and the activity of ^{68}Ga from a 30min irradiation can be seen in fig.69.

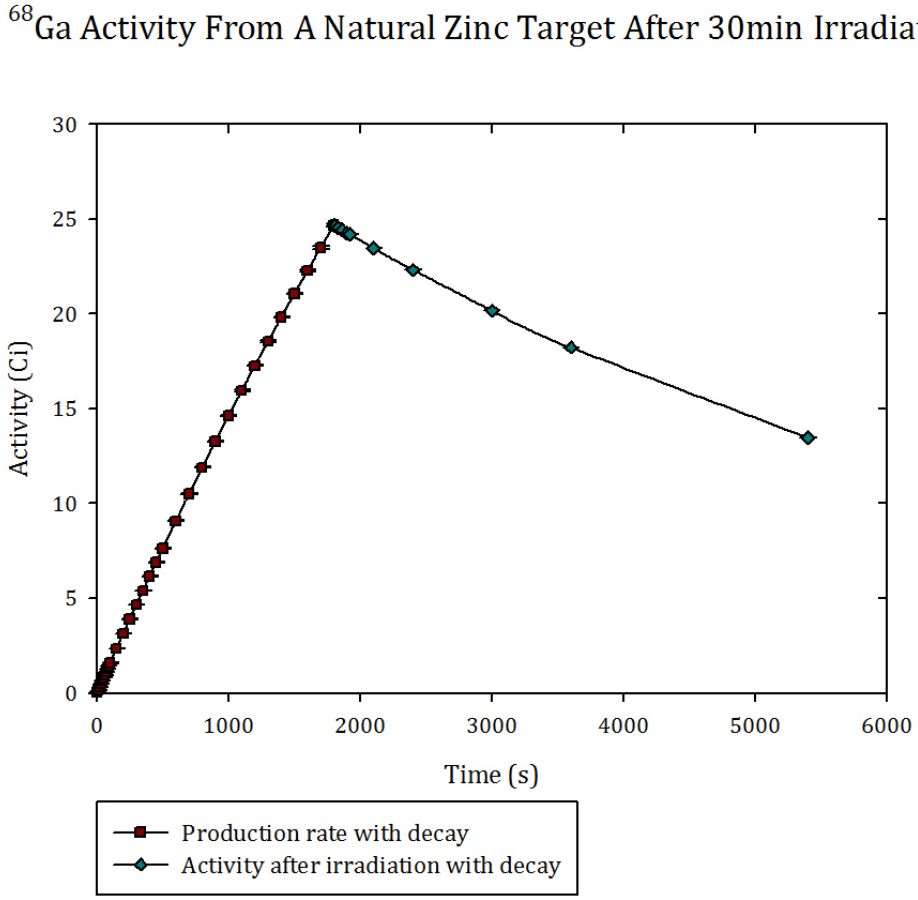

Figure 69. Activity of ^{68}Ga produced after an irradiation time of 30mins with and without accounting for decay during irradiation time using a natural zinc target

Fig.69 shows there is sufficient activity produced using a natural target for on-demand single dose production. However, due to the isotopic composition of the target many more contamination nuclei are produced simultaneously. This makes post-irradiation target processing and isotope separation more difficult and time consuming and reduces the efficiency of the production process and quantity of activity available to be administered to the patient.

It is therefore concluded that an enriched target would be more beneficial to the production process, supplying a larger activity and reducing the processing time between isotope production and administration to the patient. Although more processing would be required in the target production stage this is already a well-established procedure and is not too costly in terms of the advantages gained by fewer contamination nuclei and easier isotope separation. According to TALYS and EXFOR libraries only two contamination isotopes are produced with the enriched (p,n) reaction (50); ^{65}Cu and ^{69}Ga both of which are stable and have production cross-sections of less than 1mb, so as can be considered negligible.

7.4 PET Isotopes: ^{66}Ga

7.4.1 Background

^{66}Ga is a positron-emitting isotope with a half-life of 9.5hours[33]. Although this isotope is currently unused, development and testing is being carried out into the potential of ^{66}Ga as a PET isotope. Its half-life suggests that ^{66}Ga may be suitable for use as an imaging isotope for some cancerous cell types with medium to slow isotope uptake[105].

7.4.2 Production Routes

^{66}Ga used in testing is currently produced from a relatively low energy (~15MeV) cyclotron using reaction (51)[70]:

$^{66}Zn(p,n)^{66}Ga$ (51)

with both natural and isotopically enriched Zn targets.

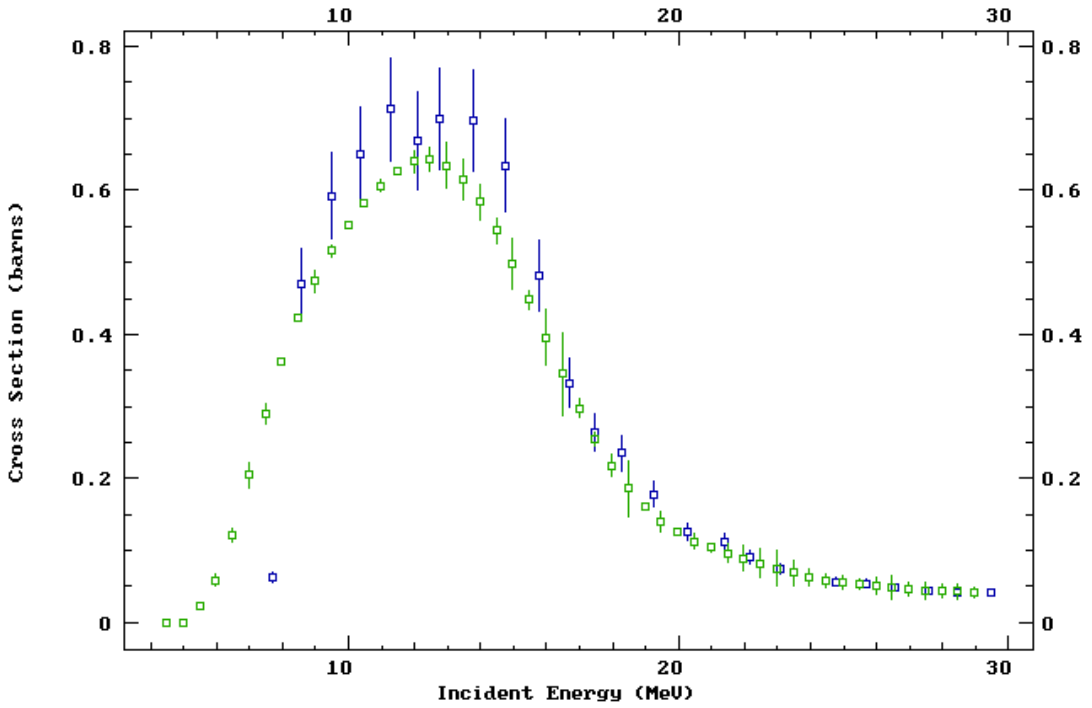

Figure 70. Experimental cross-section data (Levkovskij[106]-blue, Szelecsenyi[107]-green) for the reaction $^{66}Zn(p,n)^{66}Ga$. Data obtained and reproduced in accordance with EXFOR guidelines

The excitation function of reaction (51) seen in fig.70 shows a peak of approximately 600mb at 14-15MeV. However at 10MeV the cross-section is still sufficiently high, i.e. 300mb, that adequate yields could be achieved for at least a single dose on-demand production.

7.4.2.1 Target Thickness and Yields

To asses the potential of this production route, GEANT4 simulations with the QGSP_BIC_PHP model were carried out to determine the yield of ^{66}Ga produced from a 100% enriched ^{66}Zn target with the beam parameters E = 10MeV and I = 1mA.

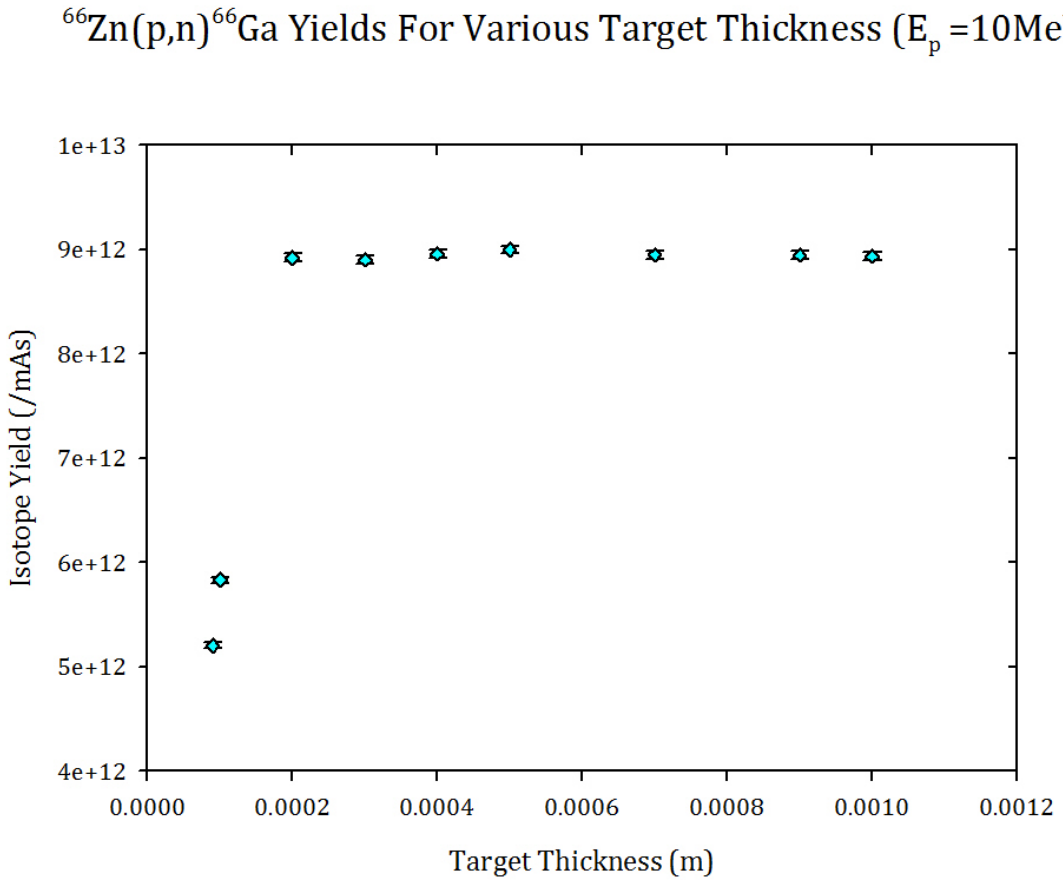

Figure 71. Simulation yields of ^{66}Ga from the reaction ^{66}Zn(p,n)^{66}Ga

From the yields obtained, which are presented in fig.71, the useful range for 10MeV protons in this target could be determined as 0.0002-0.0003m. The stopping distance for 10MeV protons within this target was calculated, using the approximation in section 3.3.2[68], to be 0.00041m.

The thickness used for further studies of the production of this isotope will, again, be 0.0005m, which is a reasonable compromise for a practical working target and the most efficient isotope production.

7.4.2.2 Activity

As ^{66}Ga has a long half-life any irradiation time short enough for this study is going to be a small fraction of the half-life and so the decay of the daughter isotope during the irradiation time is going to have a negligible effect on the total activity produced at the end of irradiation.

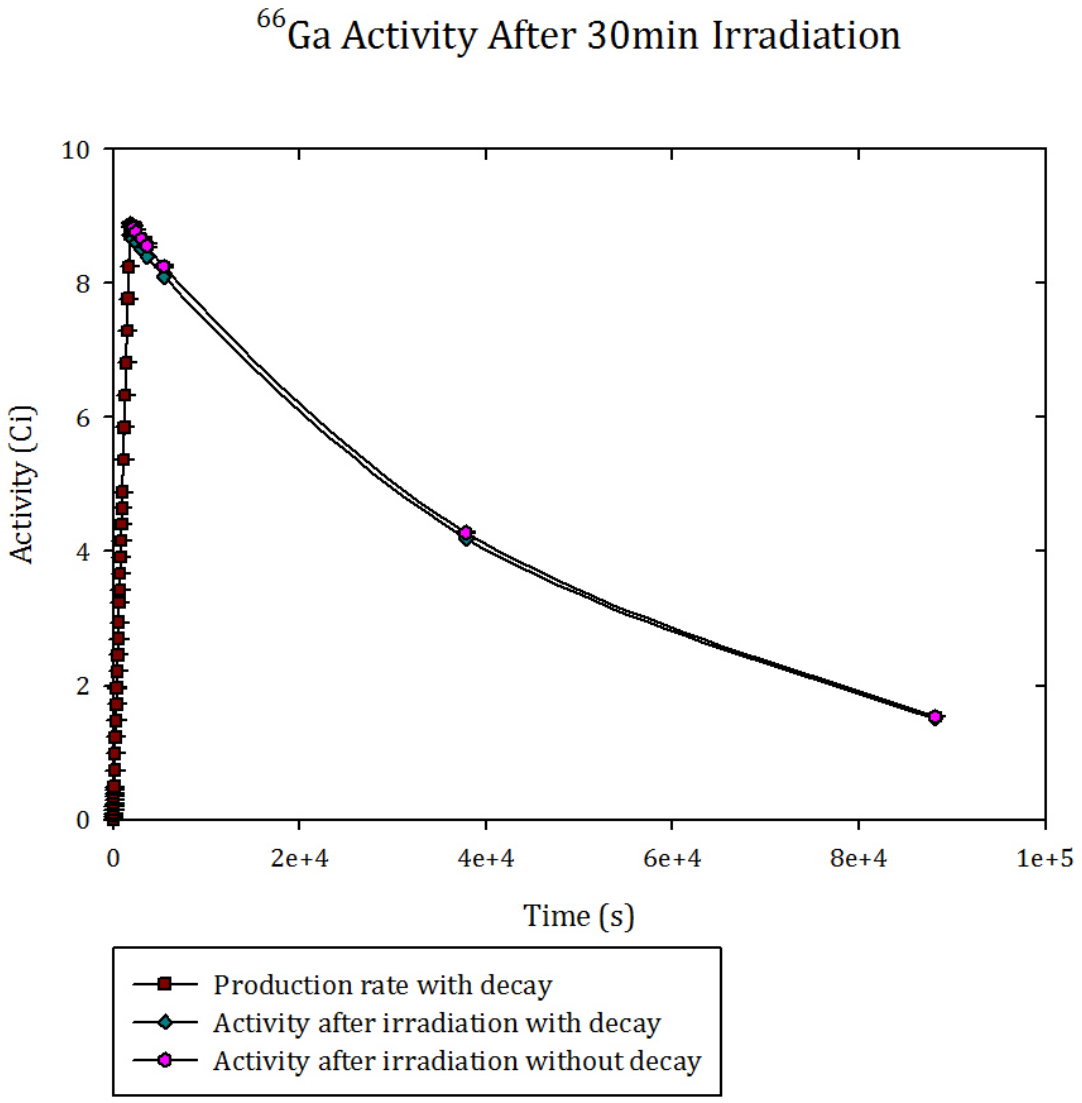

Figure 72. Activity of ^{66}Ga produced after an irradiation time of 30mins with and without accounting for decay during irradiation time

Fig.72 shows that the activity obtained from a 30min irradiation period, ~9Ci, is sufficient to produce a single dose, typically <10mCi, of ^{66}Ga for medical use. The long half-life also allows for a reasonable processing and administration time of ~1hour, before the activity drops to a value too low to provide the image quality required.

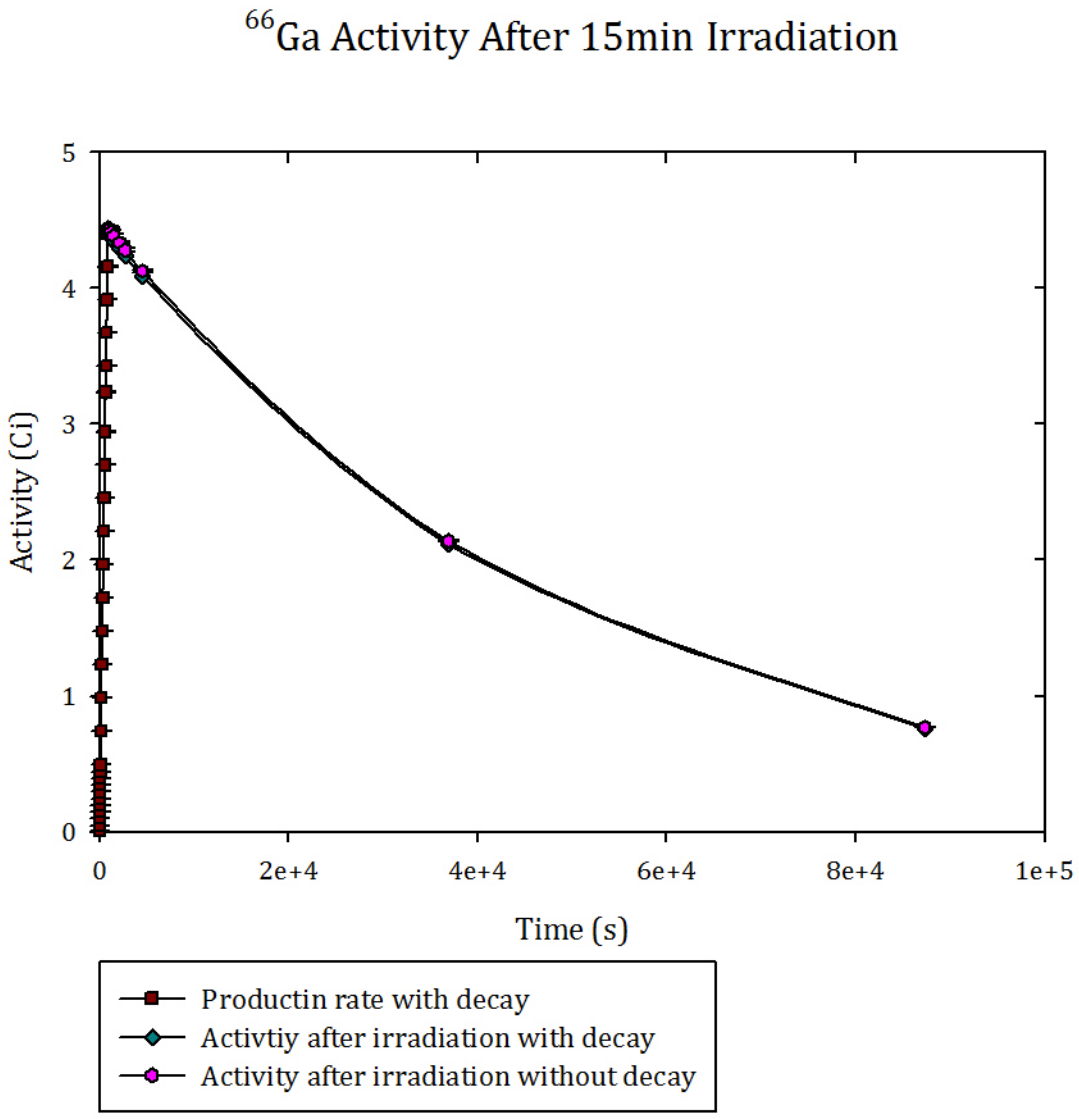

Figure 73. Activity of ^{66}Ga produced after an irradiation time of 15mins with and without accounting for decay during irradiation time

Referring to fig.73 it can be seen that potentially insufficient activity is produced during irradiation periods shorter than 30mins, depending on the efficiency of the radiolabeling process. Consequently this route is not a viable production method for a single dose quantity of ^{66}Ga.

Calculations were also undertaken to compare the activities obtained from a thin (t=0.1mm) target for both simulated and experimental data, fig.70.

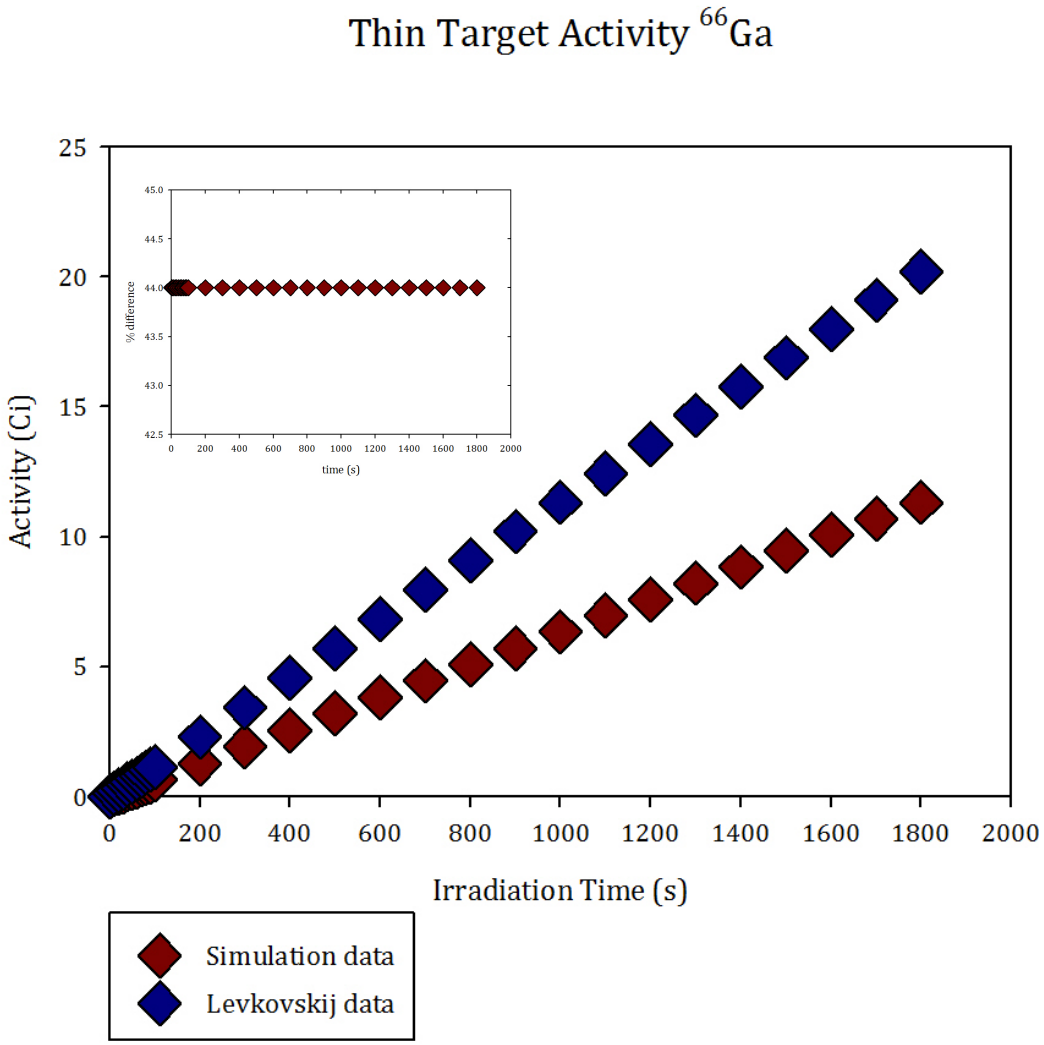

Figure 74. Activity of ^{66}Ga calculated using both experimental[106] and simulated cross sections for a thin target [inset- percentage difference simulation/experimental]. Data obtained and reproduced in accordance with EXFOR guidelines

The simulated results shown in fig.74 underestimate the activity that is calculated using the experimental thin target cross-section, both activities for a thin target over estimate that calculated for a thick target, as would be expected. A constant percentage difference of only 23% can be seen between the experimental and simulated activities as shown in the fig.74 inset. The actual uncertainties in the simulated data are again small, such that they cannot be clearly represented here, however the significant contribution lies in the simulated results.

7.4.3 Target Processing and Production

Because of the low isotopic concentration of ^{66}Zn in naturally occurring zinc the production of an enriched target of this isotope is more challenging than is case for a ^{68}Zn target. However, it is still feasible as demonstrated in previous studies of higher energy (~15MeV) production of ^{66}Ga in medical testing. From the TALYS and EXFOR libraries it seems that a particular advantage of a single isotopic target is that there are no contaminants produced that could make the separation of the resulting isotope from the target difficult.

7.5 Conclusions

This study was undertaken to assess the viability of using a low energy proton accelerator system as a source of gallium isotopes for medical imaging. Calculations using both experimental and simulated data have shown that, using an enriched target, ^{68}Ga and ^{66}Ga can be produced in sufficient multiple dose quantities by a 30min irradiation time in a low energy proton accelerator system. A summary of the activity results presented in this chapter can be seen below in table 2. The activities of ^{66}Ga for a 30min and 15min irradiation time can be seen in figs.72 and 73 respectively. For ^{68}Ga the activity obtainable from a 30min irradiation time is taken from fig.65 and that from a 15min irradiation time is taken from fig.66. Whilst the induced activity of ^{66}Ga is significantly lower than any of the other isotopes explored in this and the previous chapter it is still sufficient to provide multiple doses. Moreover the long half-life allows for longer processing time with proportionally reduced loss of activity before administration to the patient.

Isotope	Half-life (mins)	Decay energy (MeV)	Activity (Ci) 30min irrad.	Activity (Ci) 15min irrad.
Ga-66	570	5.18	8.72	4.4
Ga-68	68	2.92	122.5	66.0

Table2. A summary of the PET isotopes and their production studied in this chapter [33]

These levels of activity also mean shorter irradiation times can be used, increasing the advantage of an on-demand supply and reducing the time between start of production and final administration to the patient.
Whilst results from a natural composition target have been shown here to produce suitable activity of the required daughter isotope there are other complications that arise form the increased contamination products that make this method less favorable, although possible.

As both of these isotopes are in use, or at least at the trial stage, the target processing is already an established procedure and can easily be adopted. Isotope production via this system should be within the capabilities of the current technicians that use generator production systems.

8. CONCLUSIONS

The aim of this work was to investigate the potential medical applications of a low energy (<10MeV) proton accelerator as a source of other particles including low energy neutrons and radioisotope nuclei. The methods implemented in this work utilized the prominent particle interaction simulation code GEANT4 to study proton beam-target interactions. A literature search showed that little work had been done using GEANT4 in the low proton energy range we were interested in studying. Initial benchmarking studies highlighted several failings in the physical models currently available in the GEANT4 libraries. When compared to suitable experimental data these models were seen to breakdown within the limits of low incident proton energy and low target Z number. Low threshold high cross-section (p,n) reactions were studied for light (Li and Be) targets and heavier (including Ni, Mo and Te) targets. Using the accepted Bertini and Binary cascade models GEANT4 was unable to accurately reproduce yield and cross-section results for these reactions.

These results prompted the development of a new data-driven model for low energy proton reactions. Unlike those currently available the new model uses experimental cross-sections from the data libraries ENDF and TENDL in order to calculate collisions, secondary particle production and final states. Both libraries are available for access online and can be downloaded with the GEANT4 installation. The results obtained with the new model showed an improved agreement with the experimental results over those obtained from the theoretical models. In fact the results obtained with this benchmarking phase of the data-driven model, while limited to a very specific selection of materials and reactions, gives confidence in the use of this model for further studies and continued development to lead to the general release of low energy data-driven model.

While the sweeping statement can be made that the data-driven model provides accurate modelling of these reactions, and is a significant improvement over the theoretical models, there are some nuances of the model which must be kept in

mind when analysing the results. Two such examples highlighted in this work are the effect of experimental data sets and the effect of target mass. An effect which is also seen in the theoretical models is that for light mass targets the simulated results generally underestimate the experimental data and over estimate for higher mass targets. This is due to the statistics in calculating the probability of an interaction; the more nucleons there are the higher the probability of an interaction. This effect is less pronounced in the results from the data-driven model than for the theoretical model.

The effect of experimental data is a much greater concern. This was first highlighted in the molybdenum benchmarking exercise where the data library that had previously been used did not contain the relevant data for the reaction of interest and returned null results. We therefore had to change environmental settings of the simulations to use data from the other available library. However the experimental data that was obtained from the online libraries contained a wide range of data for this reaction with no clear accepted data set. A comparison of the simulated results with several selected data sets from this library demonstrated just how dependent the simulated results are on the experimental data that are used by the model. The data-driven results agreed more closely with the most recent set of experimental results as these are the most likely to be those contained in the library, however when there is such a large range of data available this does not mean that these are the most correct data. This could have a huge impact on the simulated results for reactions where the data are not very well known or have large discrepancies. In these cases, particularly for heavier element targets, it may be preferable to use the current theoretical or semi-empirical models, where cross-sections can be extrapolated from the available data.

The examples explored here represent only a preliminary version of the data-driven model and very limited test cases. Much more work still needs, and is being, done to improve and test this model, a task that falls to the GEANT4 development team and the collaboration working on this model. Hopefully it will not be too long before a version of QGSP_BIC_PHP is available for general release.

There were several motivating factors behind the initial benchmarking of GEANT4. Firstly there was little in the literature on the use of GEANT4 for proton interactions at the low energies of interest in this study and so a benchmarking to assess the capabilities of the current models available was logical first step before the bulk of new study was carried out. A suitable test case came about through the collaboration with the Birmingham University Medical Physics Group, which has an experimental test facility to study neutron production from near threshold (E_p<3MeV) ^{7}Li(p,n) reactions for use in neutron capture therapy. Previous simulation study of this target has been carried out using MCNPX in previous PhD projects[13][14], which provides other simulation results and experimental data for benchmarking comparison. It was also intended that, following a successful benchmarking, further simulation studies of this target and any potential design considerations for optimisation of this and future facilities could be carried out using GEANT4 as a part of this project.

It was during this benchmarking phase that the failings in the theoretical models utilised in GEANT4 and mentioned above were realised. This, in turn, was the motivation for the development of the data-driven model. It has therefore proved to be an invaluable benchmarking test case.

Following this benchmarking the study has also highlighted some potential considerations for optimization of the system for when a clinical facility can be designed and implemented. In particular the results presented here indicate that
(i) The setup may not give optimum neutron production and a rearrangement may prove to be beneficial in the efficiency of the system.
(ii) There is a range within which the target thickness is satisfactory and a change in the current target thickness could be reconsidered with a redesign of the system.

Using the data-driven GEANT4 model it has also been demonstrated that it is indeed possible to use low energy proton beams to produce suitable medical quantities of radioisotopes for diagnostic procedures. The simulations carried out considered both thick and thin targets. Both types of target can be used with

a variety of accelerator based systems, so, although we have considered designs specifically for use with new low energy proton accelerators (such as the ONIAC and PIP) the same targets should also be suitable for use with current cyclotrons.

Several different isotopes have been studied here, some of which show more potential than others in terms of both practical application and production rates. One of the main conclusions that can be drawn from this work is that on balance it would not be worth pursuing the use of low energy protons for the production of medical quantities of ^{99}Mo, the generator production route of the most commonly used radioisotope ^{99m}Tc. However not enough work has been done here to say if direct production maybe worth pursuing with either incident protons or other particle beams, such as alpha or deuteron beams. The work being carried out by groups such as those at TRIUMF provides an efficient method of directly producing ^{99m}Tc. Their experimental studies have shown that the most advantageous energy range for ^{99m}Tc production is in the range 16MeV < E_p < 19MeV, significantly higher than the proton energies considered here. However cross-section measurements also show that a lower energy range may still produce suitable quantities for the single dose target market of a low energy system. Unfortunately due to the constraints of the code it was not possible to carry out our own simulations for the direct production of ^{99m}Tc. This could be the subject of further studies in the future with the improved capabilities of the new GEANT4 release.

However I conclude that pursuing generator production with a low energy system is not a worthwhile endeavour. Firstly, the motivation for the design and development of a compact system is to secure a replacement for the generator systems for short-lived isotopes. Secondly the obtainable yields are too small to be a viable source of the quantities required for medical procedures.

In light of these findings it was determined that the best course of action for this work would be to study suitable complementary or replacement radioisotopes. Due to the constraints of the GEANT4 code it was not possible to study the direct

production of SPECT isotopes as many, if not all of interest, are metastable isotopes. The focus was therefore placed on positron emitting PET isotopes.

Due to the commercial nature of this study, and the urgency of finding a solution to the impending radioisotope crisis it was decided to narrow the scope of the project to isotopes of those elements that already have well-established radioisotopes in clinical use. This allows for a quicker transition from this study phase into clinical use as the chemistry of isotopes of the same element is the same and so most of the target production and processing should already be available as well-established procedures. However some experimental verification of this simulation study is needed.

All of the isotopes that were finally chosen (^{60}Cu, ^{61}Cu, ^{62}Cu, ^{66}Ga, and ^{68}Ga) have at least been through initial trials to determine their clinical potential. All isotope studies showed that a suitable level of activity could be produced for single dose production by low energy proton irradiation. However the actual activity of the isotope obtained from such systems is dependent on the efficiency of the processing and isotope extraction process, which can and must be determined by experimental study if this work is to be progressed to a clinical trial phase. A summary of the PET isotopes studied in this section and the activities obtained for short irradiation times, previously presented in tables 1 and 2 are reproduced here in table 3.

Isotope	Half-life (mins)	Decay energy (MeV)	Activity (Ci) 30min irrad.	Activity (Ci) 15min irrad.
Cu-60	23.7	6.12	54.0	32.8
Cu-61	198	2.24	32.0	16.4
Cu-62	9.7	3.94	364.0	272.0
Ga-66	570	5.18	8.72	4.4
Ga-68	68	2.92	122.5	66.0

Table3. A summary of the PET isotopes and their production studied in this work [33]

Throughout this work choices have been made to “create a path of least resistance” to enabling a rapid clinical deployment of radioisotopes that will enable a greater availability of lifesaving diagnostic procedures. It has been demonstrated that the manufacture of these isotopes can be carried out using compact low energy/power accelerators. Large expensive machines are not necessary for wide scale distribution and implementation of some of the most important radioisotopes.

References

1. Physics and Medicine: a historical perspective, S.F. Keevil, The Lancet, Vol.379(9825), pg1517-1524 (2012)

2. The contribution of medical physics to nuclear medicine: a physicians perspective, P.J. Ell, EJNHMI Physics, Vol.1(3) (2014)

3. Meandering in medical physics: a personal account of hospital physics, J.E. Roberts, IOP Publishing ltd, ISBN:0-7503-0494-4 (1999)

4. Radiation physics for medical physicists (2nd edition), E.B. Podgorsak, Springer, ISBN: 978-3-642-00875-7 (2010)

5. Back to the future: the history and development of the clinical linear accelerator, D.I. Thwaites and J.B. Tuohy, Phys. Med. Biol., Vol51(13), pg R343-R362 (2006)

6. Proton beam therapy: W.P. Levin, British Journal of Cancer, Vol93(8), pg849-854 (2005)

7. New stratigies in radiation therapy: exploiting the full potential of protons, R. Mohan et al, Clinical Cancer Research, Vol.19(23), pg6338-6343 (2013)

8. Personal communication P. Beasley

9. Personal communication R. Barlow

10. Biological effects and therapeutic possibilities of neutrons, G. Locher, The American Journal of Roentgenology and Radiation Vol.36(1), pg1-13 (1936)

11. Possible existence of a neutron, J. Chadwick, PRSL A, Vol.136(830), pg692-708 (1932)

12. S.J. Friesenhahn et al: Data file EXFOR 10303.006 dated 2010-10-27, compare Conf. on Nucl. Cross-Sect. and Techn., Washington, Vol.1, pg232 (1075). EXFOR data retrieved from IAEA Nuclear Data Section, Vienna.

13. Development of a high-power neutron producing lithium target for boron neutron capture therapy, A. Brown, University of Birmingham, (2000)

14. Neutron activated boron therapy for cancer treatment, R. Lingotpavanathar, Masters thesis, university of Surrey (2010)

15. The requirements and development of neutron beams for neutron capture therapy of brain cancer, R.L. Moss et al, Journal of Neuro-Oncology Vol.33(1-2), pg 27-40 (1997)

16. Early history of development of boron neutron capture therapy of tumours, W. H. Sweet, Journal of Neuro-Oncology Vol.33(1-2), pg19-26 (1997)

17. On the optimal energy of epithermal neutron beams for BNCT, E. Bisceglie et al, Phys. Med. Biol. Vol.45(1), pg49-58 (2000)

18. Boron neutron capture therapy: clinical brain tumour studies, Y. Nakagawa and H. Hatanaka, Journal of Neuro-Oncology Vol.33(1-2), pg105-115 (1997)

19. Clinical review of the Japanese experience with boron neutron capture therapy and a proposed strategy using epithermal neutron beams, Y. Nakagawa et al, Journal of Neuro-Oncology Vol.62(1-2), pg87-99 (2003)

20. Developments in accelerator based boron neutron capture therapy, S. Green, Radiat. Phys. Chem. Vol.51(4-6), pg561-569 (1998)

21. What is the best proton energy for accelerator-based BNCT using the ^{7}Li(p,n)^{7}Be reaction, D. A. Allen and T. D. Beynon, Med. Phys. Vol.27(5), pg1113-1118 (2000)

22. Accelerator-based epithermal neutron sources for boron neutron capture therapy of brain tumours, T. E. Blue and J. C. Yanch, Journal of Neuro-Oncology Vol.62(1-2), pg19-31 (2003)

23. A practical target system for accelerator-based BNCT which may effectively double the dose rate, G. Randers-Pehrson and D. J. Brenner, Med. Phys. Vol.25(6), pg894-896 (1998)

24. Thick beryllium target as an epithermal neutron source for neutron capture therapy, C.-K. Wang and B. R. Moore, Med. Phys., Vol.21(10), ph1613-1618(1994)

25. Measurement of the thick target ^{9}Be(p,n) neutron energy Spectra, W. B. Howard et al, Nuclear Science and Engineering, Vol.138(2), pg145-160 (2001)

26. A design study for an accelerator-based epithermal neutron beam for BNCT, D. A. Allen and T. D. Beynon, Phys. Med. Biol. Vol.40(5), pg807-821 (1995)

27. In-Phantom characterisation studies at the Birmingham accelerator-generated epithermal neutron source (BAGINS) BNCT facility, C.N.

Culbertson et alApplied Radiation and Isotopes Vol.61(5), pg733-738 (2004)

28. Manual of Nuclear Medicine Imaging, C. C. Kuni and R. P. duCret, Thieme Medical Publishers, ISBN: 0-86577-568-0 (1997)

29. Cyclotron Produced Radionuclides: Principles and Practice, IAEA Technical Reports Series No.465, ISBN: 978-92-0-100208-2 (2008)

30. The Production of High Speed Light Ions Without the Use of High Voltages, E. O. Lawrence and M. S. Livingston, Physical Review, Vol.40, pg19-35 (1932)

31. Nuclear Isomerism in Element 43, G. T. Seaborg and E. Segre, Phys. Rev. Vol.55, pg808-814 (1939)

32. Cyclotron production of technetium radioisotopes, T. Morley et al, J. Nucl. Med., Vol.52(1), pg291 (2011)

33. Handbook of Chemistry and Physics, 55th Edition, CRC Press , ISBN: 087819-454-1(1974-1975)

34. Technetium-99m in production and use, J. Vucina et al, Nuclear Technology & Radiation Protection, Vol.24(1), pg68-73 (2009)

35. Cyclotron production of technetium radioisotopes, P. Schaffer et al, J. Nucl. Med., Vol.51(2), pg1468 (2010)

36. Cyclotron production of Technetium-99m: A collaborative program for the production of Tc-99m using Canada's existing medical cyclotron infrastructure, S. Zeisler, Workshop on Accelerator-Driven Production of Medical Isotopes, Daresbury Laboratory, U.K. (2011)
https://eventbooking.stfc.ac.uk/uploads/accelerator_driven_production_of_medical_isotopes/zeislercylotron-production-of-99mtccockroft.pdf

37. Production of Long Lived Parent Radionuclides for Generators: ^{68}Ge, ^{82}Sr, ^{90}Sr and ^{188}W, IAEA Radioisotopes and Radiopharmaceuticals Series No.2, (2010)

38. A Sr^{87m} Generator for Medical Applications, J.F. Allen and J. J. Pinajian, International Journal of Applied Radiation and Isotopes Vol.16(5), pg319-325 (1965)

39. Introductory Nuclear Physics, K. S. Hrane, John Wiley & Sons, ISBN: 978-0-471-80553 (1988)

40. PET vs SPECT: Strengths, Limitations and Chanllenges, A. Rahmim and H. Zaidi, Nuclear Medicine Communications Vol.29(3). pg193-207 (2008)

41. Scintillation camera with multichannel collimators, H. Anger, J. Nucl. Med., Vol.5(7), pg515-531 (1964)

42. Event – Driven Motion Compensation in Positron Emission Tomography: Development of a Clinically Applicable Method, J. Langer, University of Technology Dresden (2008)

43. High-Yield, Low-Pressure [^{18}O] Water Targets of Titanium and Niobium for F-18 Production on MC-17 Cyclotrons, M. S. Berridge et al, Applied Radiation and Isotopes Vol.57(3), pg303-308 (2002)

44. Production of [^{18}F} Fluoride with a High-Pressure Disposable [^{18}O} Water Target, C. E. Gonzalez Lepera and B. Dembowski, Appl. Radiat. Isot. Vol.48(5), pg613-617 (1997)

45. The Medical Isotope Shortage: Cause, Effects and Options, M. Zakzouk, The Library of Parliament Research Publications, Canada, Background paper no. PRB09-04E (2009)

46. Accelerating Production of Medical Isotopes, T. Ruth, Nature (essay),Vol.457, pg536-537 (2009)

47. Producing Medical Isotopes using X-rays, M.S. de Jong, Proceedings of IPAC2012, New Orleans, THXA01 (2012)

48. Production of ^{99m}Tc on a Medical Cyclotron: A Feasibility Study, J. E. Beaver and H. B. Hupf, Journal of Nuclear Medicine Vol.12(11), pg739-741 (1971)

49. GEANT4 – A Simulation Toolkit, S. Agostinelli et al, Nuclear Instruments & Methods in Physics Research Section A: Accelerators, Spectrometers, Detectors and Associated Equipment, Vol.506(3), pg250-303 (2003)

50. GEANT4 Developments and Applications, J. Allison et al, IEEE Transactions on Nuclear Science Vol.53(1), pg270-278 (2006)

51. GEANT4 Monte Carlo Simulations of the International Space Station Radiation Environment, T. Ersmark, Doctoral Thesis, Sweden, ISBN: 91-7178-398-9 (2006)

52. Overview of GEANT4 Applications in Medical Physics, L. Archambault et al, IEEE Nuclear Science Symposium Conference Record, Vol.3, pg1743-1745 (2003)

53. Range Uncertainties in Proton Therapy and the Role of Monte Carlo Simulations, H. Paganetti, Physics in Medicine and Biology Vol.57(11), pgR99-117 (2012)

54. GEANT4 User's Guide for Application Developers, version GEANT4 9.3, GEANT4 Collaboration (2009)
http://geant4.web.cern.ch/geant4/UserDocumentation/UsersGuides/ForApplicationDeveloper/BackupVersions/V9.3/fo/BookForAppliDev.pdf

55. Transition Between Hadronic Models in GEANT4, A. Ribbon et al, IEEE Nuclear Science Symposium Conference Record, pg526-529 (2009)

56. GEANT4 Physics reference manual, version GEANT4 9.4, GEANT4 Collaboration (2010)
http://geant4.web.cern.ch/geant4/UserDocumentation/UsersGuides/PhysicsReferenceManual/BackupVersions/V9.4/fo/PhysicsReferenceManual.pdf

57. Bertini Intra-Nuclear Cascade Implimentation in GEANT4, A. Heikkinen, N. Stepanov and J.P. Wellisch, Computing in High Energy and Nuclear Physics, California, MOMT008 (2003)

58. Recent Developments In Pre-Equilibrium and De-Excitation Models in GEANT4, J.M. Quesada et al, Joint International Conference Supercomputing in Nuclear Applications and Monte Carlo 2010, Progress in nuclear science and technology, Vol.2, pg936 (2011)

59. The Binary Cascade: Nucleon nuclear reactions, Eur. Phys. J. A. Vol.21(3), pg407-417 (2004)

60. GEANT4 and its Validation, K. Amako et al, Nuclear Physics B – Proceedings Supplements, Proceedings on the 9th topical seminar on innovative particle and radiation detectors, Vol.150, pg44-49 (2006)

61. Private Communication with R. Barlow (2012)

62. Absolute Neutron Yield Measurements for Protons on Li, Cu, Co and Be from Threshold to 3MeV, J. Campbell and M.C. Scott, Proceedings of the 4th Conference on the Scientific and Industrial Applications of Small Accelerators (IEEE), New York (1977)

63. Neutron Production Cross Sections and Energies for the Reactions ^{7}Li(p,n)^{7}Be and ^{7}Li(p,n)^{7}Be*, H. Liskien and A. Paulsen, Atomic Data and Nuclear Data Tables Vol.15(1), pg57-84 (1975)

64. Total Neutron Yields from Light Elements Under Proton and Alpha Bombardment, J.H. Gibbons and R.L. Macklin, Phys. Rev. Vol.114(2), pg572-575 (1959)

65. Thick Target Neutron Yields of Lithium and Beryllium Targets Bombarded with Protons and Deuterons, K. Porges et al, Argonne National Laboratory Report ANL – 7910:361-362, 1972

66. J.H. Gibbons and R.L. Macklin: Data file EXFOR T0010.009 dated 1999-10-11 compare physical review, vol.114, pg571 (1959)

67. Private Communication, R. Barlow (2011)

68. Measurement and detection of radiation (2nd edition), N. Tsoulfanidis, Taylor and Francis, ISBN: 1-56032-317-5 (1995)

69. Thick Target Neutron Yields for the ^{7}Li(p,n)^{7}Be Reaction Near Threshold, C.L. Lee and X.-L. Zhou, Nucl. Instr. And Meth. In Phys. Res. B Vol.152, pg1-11 (1999)

70. Cyclotron Produced Radionuclides: Physical Characteristics and Production Methods, IAEA Technical Reports Series No.468 (2009)

71. Copper-64 Radiopharmaceuticals for PET Imaging of Cancer: Advances in Preclinical and Clinical Research, C.S. Anderson and R. Ferdeni, Cancer Biotherapy and radiopharmaceuticals, Vol.24(4), pg379-393 (2009)

72. Cyclotron produced radionuclides: physical characteristics and production methods, technical reports series no. 468, ©IAEA 2009, pg94

73. R. A. Rebels et al: Data file EXFOR D4207.002 dated 2009-03-25 compare Nucl. Instrum. Methods in Physics Res., Sect.B, Vol.267, pg457 (2009). EXFOR data retrieved from IAEA Nuclear Data Section, Vienna

74. ^{89}Zr Immuno-PET: comprehensive procedures for the production of ^{89}Zr-labeled monoclonal antibodies, I. Verel et al, J. Nucl. Med., Vol.44(8), pg1271-1281 (2003)

75. Cyclotron produced radionuclides: physical characteristics and production methods, technical reports series no. 468, ©IAEA 2009, pg263

76. V.N. Levkovskij: Data file EXFOR A0510.185 dated 2011-07-26 compare Levkovskij, Act. Cs. By Protons and Alphas, Moscow (1999). EXFOR data retrieved from IAEA Nuclear Data Section, Vienna.

77. Use of Iodine-123 as a Diagnostic Tracer for Neck and Whole Body Scanning in Patients With Well-Differentiated Thyroid Cancer. R. Berbano et al, Endocrine Practice, Vol.4(1), pg11-16 (1998)

78. Production of Iodine-123 for Medical Applications, H.B. Hupf, J.S. Eldridge and J.E. Beaver, The International Journal of Applied Radiation and Isotopes Vol.19(4) pg345-346 (1968)

79. S. Takacs et al: Data file EXFOR D4147.007 dated 2010-06-15 compare Nucl. Instrum. Methods in Physics Res., Sect. B, Vol.240, pg790 (2005) EXFOR data retrieved from IAEA Nuclear Data Section, Vienna.

80. B. Scholten et al: Data file EXFOR A0473.002 dated 2009-09-21 compare Applied Radiation and Isotopes, Vol.40, pg127 (1989) EXFOR data retrieved from IAEA Nuclear Data Section, Vienna.

81. S. Takacs et al: Data file EXFOR D4115.002 dated 2004-05-06 compare Journal of Radioanalytical and Nuclear Chemistry, Vol.257, pg195 (2005) EXFOR data retrieved from IAEA Nuclear Data Section, Vienna.

82. B. Scholten et al: Data file EXFOR O0737.002 dated 2000-04-27 compare Applied Radiation and Isotopes, Vol.51, pg69 (1999). EXFOR data retrieved from IAEA Nuclear Data Section, Vienna.

83. V.N. Levkovskij: Data file EXFOR A0510.205 dated 2011-07-26 compare Levkovsij, Act. Cs. By Protons and Alphas, Moscow (1991). EXFOR data retrieved from IAEA Nuclear Data Section, Vienna.

84. M.S. Uddin et al: Data file EXFOR E1894.007 dated 2007-05-14 compare Applied Radiation and Isotopes, Vol.60, pg911 (2004). EXFOR data retrieved from IAEA Nuclear Data Section, Vienna.

85. Evaluation of Proton Induced Reactions on ^{100}Mo: New Cross-Sections for Production of ^{99m}Tc and ^{99}Mo, S. Takacs et al, Journal of Radioanalytical and Nuclear Chemistry Vol.257(1), pg195-201 (2003)

86. Excitation Functions for the Cyclotron Production of ^{99m}Tc and ^{99}Mo, B. Scholton et al, Applied Radiation and Isotopes Vol.51(1), pg69-80 (1999)

87. Copper Radionuclides and Pharmaceuticals in Nuclear Medicine, P.J. Blower, J.S. Lewis and J.Z. Weit, Nuclear Medicine and Biology Vol.23(8), pg957-980 (1996)

88. A Comparison of PET Imaging Characteristics of Various Copper Radioisotopes, H.A. Williams et al, European Journal of Nuclear Medicine and Medical Imaging, Vol.32(12), pg1473-1480 (2005)

89. A New Zinc-62/Copper-62 Generator as a Copper-62 Source for PET Radiopharmaceuticals, Y. Fujibayashi et al, J. Nucl. Med. Vol.30(11), pg1838-1842 (1989)

90. Radiopharmaceuticals for Positron Emission Tomography-Methodological Aspects, G. Stochlin, Springer, ISBN: 978-94-015-8204-9 (1993)

91. H. Piel et al: Data file EXFOR D0056.002 dated 2003-11-11 compare Radiochimica Acta, Vol.57, pg1 (1992). EXFOR data retrieved from IAEA Nuclear Data Section, Vienna.

92. S. Tanaka et al: Data file EXFOR B0020.019 dated 2001-12-20 compare Journal of Inorganic and Nuclear Chemistry, Vol.34, pg2414 (1972). EXFOR data retrieved from IAEA Nuclear Data Section, Vienna.

93. Private communication R. Cywinski

94. High Purity Production and Potential Applications of Copper-60 and Copper-61, D.W. McCarthy et al, Nuclear Medicine and Biology Vol.26(4), pg351-358 (1999)

95. Cyclotron produced radionuclides: physical characteristics and production methods, technical reports series no. 468, ©IAEA 2009, pg91

96. V.N. Levkovskij: Data file EXFOR A0510.001 dated 2011-07-26 compare Levkovskij, Act. Cs. By Protons and Alphas, Moscow (1991). EXFOR data retrieved from IAEA Nuclear Data Section, Vienna.

97. S. Tanaka et al: Data file EXFOR B0020.016 dated 2001-12-20 compare Journal of Inorganic and Nuclear Chemistry, Vo.34, pg2414 (1972). EXFOR data retrieved from IAEA Nuclear Data Section, Vienna.

98. Medical Applications and Toxicities of Gallium Compounds, C.R. Chitambar, International Journal of Environmental Research and Public Health, Vol.7(5), pg2337-2361 (2010)

99. Cyclotron produced radionuclides: physical characteristics and production methods, technical reports series no. 468, ©IAEA 2009, pg119

100. Cyclotron produced radionuclides: physical characteristics and production methods, technical reports series no. 468, ©IAEA 2009, pg118

101. Clinical Applications of Gallium-68, S.R. Banerjee and M.G. Pomper, Applied Radiation and Isotopes Vol.76, pg2-13 (2013)

102. Gallium-68 PET: A New Frontier in Receptor Cancer Imaging, A. Al-Nahhas et al, Anti Cancer Research Vol.27(6B), pg4087-4094 (2007)

103. Cyclotron produced radionuclides: physical characteristics and production methods, technical reports series no. 468, ©IAEA 2009, pg124

104. V.N. Levkovskij: Data file EXFOR A0510.093 dated 2011-07-26 compare Levkivskij, Act. Cs. By Protons and Alphas, Moscow (1991). EXFOR data retrieved from IAEA Nuclear Data Section, Vienna.

105. Production and Purification of Gallium-66 for Preparation of Tumour Targeting Radiopharmaceuticals, M.R. Lewis et al, Nucl. Med. Biol., Vol.29(6), pg701-706 (2002)

106. V.N. Levkovskij: Data file EXFOR A0510.087 dated 2011-07-26 compare Levkovskij, Act. Cs. By Protons and Alphas, Moscow (1991). EXFOR data retrieved from IAEA Nuclear Data Section, Vienna.

107. F. Szelecsenyi et al: Data file EXFOR C0506.008 dated 1998-09-28 compare Applied Radiation and Isotopes, Vol.49, pg1005 (1998). EXFOR data retrieved from IAEA Nuclear Data Section, Vienna

Appendix A: BNCT Full Geometry Code

```
//BNCT.cc


#include "BNCTDetectorConstruction.hh"
#include "BNCTPhysicsList.hh"
#include "BNCTPrimaryGeneratorAction.hh"
#include "BNCTSteppingAction.hh"

#include "G4RunManager.hh"
#include "G4UImanager.hh"
#include "QGSP_BERT.hh"

#ifdef G4VIS_USE
#include "G4VisExecutive.hh"
#endif

#ifdef G4UI_USE
#include "G4UIExecutive.hh"
#endif

int main(int argc, char** argv)
{

//consturct default run manager
  G4RunManager* runManager = new G4RunManager;

//set mandatory initialisation classes

  G4VUserDetectorConstruction* detector = new
BNCTDetectorConstruction;
  runManager->SetUserInitialization(detector);

  G4VUserPhysicsList* physics = new BNCTPhysicsList;
//modified physics list
  runManager->SetUserInitialization(physics);

    //runManager->SetUserInitialization(new QGSP_BERT);
//standard phyiscs model (Bertini) from the libraries

//set mandatory user action class
  G4VUserPrimaryGeneratorAction* gen_action = new
BNCTPrimaryGeneratorAction;
  runManager->SetUserAction(gen_action);

//set optional user action class
  G4UserSteppingAction* step_act = new BNCTSteppingAction;
  runManager->SetUserAction(step_act);

//initialise G4 kernal

  runManager->Initialize();
```

```
#ifdef G4VIS_USE
  G4VisManager* visManager = new G4VisExecutive;
  visManager->Initialize();
#endif


  G4UImanager* UI = G4UImanager::GetUIpointer();

  if (argc!=1) //batch mode
    {  G4String command = "/control/execute ";
      G4String fileName = argv[1];
      UI->ApplyCommand(command+fileName);
    }
   else //interactive mode
    {
#ifdef G4UI_USE
      G4UIExecutive * ui = new G4UIExecutive(argc,argv);
#ifdef G4VIS_USE
      UI->ApplyCommand("/control/execute vis.mac");
#endif
      ui->SessionStart();
      delete ui;
#endif

#ifdef G4VIS_USE
      delete visManager;
#endif
    }


  delete runManager;

  return 0;
}
```

```
//BNCTDetectorConstruction.hh

#ifndef BNCTDetectorConstruction_h
#define BNCTDetectorConstruction_h 1

#include "globals.hh"
#include "G4VUserDetectorConstruction.hh"

class G4Box;
class G4Tubs;
class G4Sphere;
class G4LogicalVolume;
class G4VPhysicalVolume;
class G4Material;


class BNCTDetectorConstruction : public
G4VUserDetectorConstruction
{
public:
  BNCTDetectorConstruction();
  ~BNCTDetectorConstruction();

public:

  G4VPhysicalVolume* Construct();

private:
//world
  G4Box* solidWorld; //pointer to solid World
  G4LogicalVolume* logicWorld; //pointer to logical World
  G4VPhysicalVolume* physiWorld; //pointer to physical World

//reflector
  G4Box* solidReflector;
  G4LogicalVolume* logicReflector;
  G4VPhysicalVolume* physiReflector;

//moderator
  G4Box* solidModerator;
  G4LogicalVolume* logicModerator;
  G4VPhysicalVolume* physiModerator;

 //target
  G4LogicalVolume* logicTarget;
  G4VPhysicalVolume* physiTarget;

//substrate
  G4LogicalVolume* logicSub;
  G4VPhysicalVolume* physiSub;

//coolant bowl
  G4LogicalVolume* logicCoolant;
  G4VPhysicalVolume* physiCoolant;
```

```
//left shield
  G4Box* solidShieldL;
  G4LogicalVolume* logicShieldL;
  G4VPhysicalVolume* physiShieldL;

//rigth shield
  G4Box* solidShieldR;
  G4LogicalVolume* logicShieldR;
  G4VPhysicalVolume* physiShieldR;

//top front shield
  G4Box* solidFrontTop;
  G4LogicalVolume* logicFrontTop;
  G4VPhysicalVolume* physiFrontTop;

//bottom front shield
  G4Box* solidFrontBot;
  G4LogicalVolume* logicFrontBot;
  G4VPhysicalVolume* physiFrontBot;

//beamline in reflector
  G4LogicalVolume* logicBeamLineR;
  G4VPhysicalVolume* physiBeamLineR;

//beamline in moderator
  G4LogicalVolume* logicBeamLineM;
  G4VPhysicalVolume* physiBeamLineM;

//coolant in moderator
  G4LogicalVolume* logicCoolLineB;
  G4VPhysicalVolume* physiCoolLineB;

//coolant in refelctor
  G4LogicalVolume* logicCoolLineC;
  G4VPhysicalVolume* physiCoolLineC;



};
#endif
```

```
//BNCTPhysicsList.hh
//modified physics list from example N01

#ifndef BNCTPhysicsList_h
#define BNCTPhysicsList_h 1
#include "G4ProtonInelasticCrossSection.hh"

#include "G4VUserPhysicsList.hh"
#include "globals.hh"



class BNCTPhysicsList: public G4VUserPhysicsList
{
public:
  BNCTPhysicsList();
  ~BNCTPhysicsList();
  //  virtual ~BNCTPhysicsList();


public:
  virtual void SetCuts();


protected:
  // Construct particle and physics
  virtual void ConstructParticle();
  virtual void ConstructProcess();

  // these methods Construct physics processes and register
them
  virtual void ConstructGeneral();
  virtual void ConstructEM();
  virtual void ConstructHad();
  //  virtual void ConstructOp();


  /*
  // these methods Construct all particles in each category
  virtual void ConstructAllBosons();
  virtual void ConstructAllLeptons();
  virtual void ConstructAllMesons();
  virtual void ConstructAllBaryons();
  virtual void ConstructAllIons();
  virtual void ConstructAllShortLiveds();
  */

  virtual void AddTransportation();

private:
  G4int VerboseLevel;
  G4int OpVerbLevel;
   G4ProtonInelasticCrossSection protonCrossSection;
```

```
  G4double cutForGamma;
  G4double cutForElectron;
  G4double cutForPositron;
  G4double cutForProton;
  G4double cutForAlpha;
  G4double cutForGenericIon;

  // these methods Construct particles
  void ConstructMyBosons();
  void ConstructMyLeptons();
  void ConstructMyHadrons();
  void ConstructMyShortLiveds();

};

#endif
```

```
//BNCTPrimaryGeneratorAction.hh

#ifndef BNCTPrimaryGeneratorAction_h
#define BNCTPrimaryGeneratorAction_h 1

#include "G4VUserPrimaryGeneratorAction.hh"


class G4ParticleGun;
class G4Event;

class BNCTPrimaryGeneratorAction : public
G4VUserPrimaryGeneratorAction
{
  public:
    BNCTPrimaryGeneratorAction();
   ~BNCTPrimaryGeneratorAction();

  public:
    void GeneratePrimaries(G4Event* anEvent);

  private:
    G4ParticleGun* particleGun;

};



#endif
```

```
//BNCTSteppingAction.hh

#ifndef BNCTSteppingAction_H
#define BNCTSteppingAction_H 1

#include "globals.hh"
#include "G4UserSteppingAction.hh"

#include <iostream>
#include <fstream>

class BNCTSteppingAction : public G4UserSteppingAction
{
  public:
    BNCTSteppingAction();
    virtual ~BNCTSteppingAction();

    virtual void UserSteppingAction(const G4Step*);

private:
  std::ofstream file;
};

#endif
```

```
//BNCTDetectorConstruction.cc

#include "BNCTDetectorConstruction.hh"

#include "G4Material.hh"
#include "G4Box.hh"
#include "G4Tubs.hh"
#include "G4Sphere.hh"
#include "G4LogicalVolume.hh"
#include "G4PVPlacement.hh"
#include "G4PVParameterised.hh"
#include "globals.hh"

#include "G4UserLimits.hh"

#include "G4VisAttributes.hh"
#include "G4Colour.hh"

#include "G4ios.hh"

BNCTDetectorConstruction::BNCTDetectorConstruction()
  : solidWorld(0), logicWorld(0), physiWorld(0),
    solidReflector(0), logicReflector(0), physiReflector(0),
    solidModerator(0), logicModerator(0), physiModerator(0),
    logicTarget(0), physiTarget(0),
    logicSub(0), physiSub(0),
    logicCoolant(0), physiCoolant(0),
    solidShieldL(0), logicShieldL(0), physiShieldL(0),
    solidShieldR(0), logicShieldR(0), physiShieldR(0),
    solidFrontTop(0), logicFrontTop(0), physiFrontTop(0),
    solidFrontBot(0), logicFrontBot(0), physiFrontBot(0),
    logicBeamLineR(0), physiBeamLineR(0),
    logicBeamLineM(0), physiBeamLineM(0),
    logicCoolLineB(0), physiCoolLineB(0),
    logicCoolLineC(0), physiCoolLineC(0)
{}
  BNCTDetectorConstruction::~BNCTDetectorConstruction()
{}

//material construction

G4VPhysicalVolume*  BNCTDetectorConstruction::Construct()
{
G4double a,z;
G4double density;
 G4int nel;
  G4int natoms;

//Air
G4Element* N = new G4Element("Nitrogen","N",z= 7., a=
14.01*g/mole);
G4Element* O = new G4Element("Oxygen","O",z=8., a=
16.00*g/mole);
G4Material* Air = new G4Material("Air", density= 0.0*mg/cm3,
```

```
nel=2);
Air->AddElement(N, 70*perCent);
Air->AddElement(O, 30*perCent);

//D2O
 G4Element* D = new
G4Element("Deuterium","D",z=1,a=2.014*g/mole);
 G4Material* D2O = new G4Material("D2O",density=1.107*g/cm3,
nel=2);
   D2O->AddElement(O, natoms=1);
 D2O->AddElement(D, natoms=2);


//Li
 G4Element* Li = new G4Element("lithium","Li", z=3., a=
6.94*g/mole );
//Al
 G4Element* Al = new G4Element("aluminium","Al", z=13., a=
26.98*g/mole);
//F
 G4Element* F = new G4Element("flourine","F", z=9.,
a=19.0*g/mole);
//fluental
G4Material* fluental = new G4Material("fluental",
density=3.0*g/cm3,nel=3);
fluental->AddElement(Al, 43.2*perCent);
fluental->AddElement(F, 55.9*perCent);
fluental->AddElement(Li, 0.9*perCent);

//LiPolythylene

//graphite
 G4Material* Graphite = new G4Material("Graphite", z= 6., a=
12.02*g/mole, density=1.80*g/cm3);

 //Lithium
G4Material* Lithium = new G4Material("Lithium", z= 3., a=
6.94*g/mole, density=0.534*g/cm3);

 //Copper
  G4Material* Cu = new G4Material("Cu",
z=29,a=63.546*g/mole,density=8.94*g/cm3);

 //Lead
 G4Material* Pb = new G4Material("Pb", z=82,a=
207.2*g/mole,density= 11.34*g/cm3);


G4cout << G4endl << "The materials defined are : " << G4endl
<< G4endl;
G4cout << *(G4Material::GetMaterialTable()) << G4endl;

//geometry
```

```
G4double worldLength=1*m;

//target
G4double innerRadOfT = 0.*m;
G4double outerRadOfT = 0.02*m;
G4double hightOfT = 0.00035*m;
G4double startAngOfT = 0.*deg;
G4double spanningOfT = 360.*deg;

//substrate
G4double innerRadOfSub = 0.*m;
G4double outerRadOfSub = 0.03*m;
G4double startPhiOfSub = 0.*deg;
G4double spanningPhiOfSub = 180.*deg;
G4double startThetaOfSub = 0.*deg;
G4double spanningThetaOfSub = 180.*deg;

//coolant
G4double innerRadOfCl = 0.*m;
G4double outerRadOfCl = 0.02*m;
G4double startPhiOfCl = 0.*deg;
G4double spanningPhiOfCl = 180.*deg;
G4double startThetaOfCl = 0.*deg;
G4double spanningThetaOfCl = 180.*deg;

//beamline in reflector
G4double innerRadOfBLR = 0.*m;
G4double outerRadOfBLR = 0.03*m;
G4double hightOfBLR = 0.1*m;
G4double startAngOfBLR = 0.*deg;
 G4double spanningOfBLR = 360.*deg;

//beamline in moderator
G4double innerRadOfBLM = 0.*m;
G4double outerRadOfBLM = 0.03*m;
G4double hightOfBLM = 0.044825*m;
G4double startAngOfBLM = 0.*deg;
G4double spanningOfBLM = 360.*deg;

//coolant in moderator
G4double innerRadOfCLB = 0.*m;
G4double outerRadOfCLB = 0.02*m;
G4double hightOfCLB = 0.029825*m;
G4double startAngOfCLB = 0.*deg;
G4double spanningOfCLB = 360.*deg;

//coolant in reflector
G4double innerRadOfCLC = 0.*m;
G4double outerRadOfCLC = 0.02*m;
G4double hightOfCLC = 0.1*m;
G4double startAngOfCLC = 0.*deg;
G4double spanningOfCLC = 360.*deg;
```

```
//world
solidWorld = new G4Box("world", //name
                       worldLength,worldLength,worldLength
//dimensions
                       ); //solid

logicWorld = new G4LogicalVolume(solidWorld, //solid
                                 Air, //material
                                 "World", //name
                                 0, //magnetic field
                                 0, //sensitive detector
                                 0 //user limits
                                 ); //logical volume

physiWorld = new G4PVPlacement(0, //no rotation
                               G4ThreeVector(), //position
vector
                               logicWorld, //logical volume
                               "World", //name
                               0, //mother volume
                               false, //no boolean operations
                               0 //copy number
                               );//physical volume

//reflector
solidReflector = new G4Box("reflector", 0.25*m,0.29*m,0.32*m);
logicReflector = new
G4LogicalVolume(solidReflector,Graphite,"Reflector",0,0,0
);
physiReflector = new
G4PVPlacement(0,G4ThreeVector(),logicReflector,"Reflector",log
icWorld,false,0);

//moderator
G4ThreeVector positionMod =  G4ThreeVector(0,0,0.1*m);
//position vector

solidModerator = new G4Box("mod", 0.05*m, 0.09*m, 0.22*m);
logicModerator = new
G4LogicalVolume(solidModerator,fluental,"Mod",0,0,0);
 physiModerator = new G4PVPlacement(0,
positionMod,logicModerator,"Mod",logicReflector,false,0);

//target
  G4RotationMatrix* xRot = new G4RotationMatrix;
 xRot->rotateX(90.*deg); //rotation by 90degrees

G4Tubs* target = new G4Tubs("target",innerRadOfT, outerRadOfT,
hightOfT, startAngOfT, spanningOfT);
logicTarget = new
G4LogicalVolume(target,Lithium,"Target",0,0,0);
 physiTarget = new G4PVPlacement(xRot,G4ThreeVector(0,0,-
0.1*m),logicTarget,"Target",logicModerator,false,0);
```

```
//substrate
 G4RotationMatrix* xSRot = new G4RotationMatrix;
xSRot->rotateX(180.*deg);

G4ThreeVector positionSub = G4ThreeVector(0,-0.00035*m,-
0.1*m);

G4Sphere* substrate = new G4Sphere("substrate", innerRadOfSub,
outerRadOfSub, startPhiOfSub, spanningPhiOfSub,
startThetaOfSub, spanningThetaOfSub);
logicSub = new G4LogicalVolume(substrate,Cu,"Sub",0,0,0);
physiSub = new G4PVPlacement(xSRot,positionSub,
logicSub,"Sub",logicModerator,false,0);

//coolant bowl
G4ThreeVector positionCool = G4ThreeVector(0,0.01*m,0);

G4Sphere* coolant = new G4Sphere("coolant", innerRadOfCl,
outerRadOfCl, startPhiOfCl, spanningPhiOfCl, startThetaOfCl,
spanningThetaOfCl);
logicCoolant = new
G4LogicalVolume(coolant,D2O,"Coolant",0,0,0);
physiCoolant = new G4PVPlacement(0,positionCool,
logicCoolant,"Coolant",logicSub,false,0);

//left lead shield
 G4ThreeVector positionSL =  G4ThreeVector(0,0,-0.15*m);

solidShieldL = new G4Box("shieldL", 0.03*m, 0.035*m, 0.01*m);
logicShieldL = new
G4LogicalVolume(solidShieldL,Pb,"ShieldL",0,0,0);
 physiShieldL = new G4PVPlacement(0,
positionSL,logicShieldL,"ShieldL",logicModerator,false,0);

//right lead shield
G4ThreeVector positionSR =  G4ThreeVector(0,0,-0.05*m);

solidShieldR = new G4Box("shieldR", 0.03*m, 0.035*m, 0.01*m);
logicShieldR = new
G4LogicalVolume(solidShieldR,Pb,"ShieldR",0,0,0);
 physiShieldR = new G4PVPlacement(0,
positionSR,logicShieldR,"ShieldR",logicModerator,false,0);

//Front top shield
G4ThreeVector positionFT =  G4ThreeVector(0,0.19*m,0.345*m);

solidFrontTop = new G4Box("frontTop", 0.25*m, 0.1*m, 0.025*m);
logicFrontTop = new
G4LogicalVolume(solidFrontTop,Pb,"FrontTop",0,0,0);
physiFrontTop = new G4PVPlacement(0,
positionFT,logicFrontTop,"FrontTop",logicWorld,false,0);

//Front bottom shield
G4ThreeVector positionFB = G4ThreeVector(0,-0.19*m,0.345*m);
```

```
solidFrontBot = new G4Box("frontBot", 0.25*m, 0.1*m, 0.025*m);
logicFrontBot = new
G4LogicalVolume(solidFrontBot,Pb,"FrontTop",0,0,0);
physiFrontBot = new
G4PVPlacement(0,positionFB,logicFrontBot,"FrontBot",logicWorld
,false,0);

//Beamline in reflector
G4RotationMatrix* xRotBLR = new G4RotationMatrix;
 xRotBLR->rotateX(90.*deg);

G4ThreeVector positionBLR = G4ThreeVector(0,0.19*m,0);

G4Tubs* beamLineR = new
G4Tubs("beamLineR",innerRadOfBLR,outerRadOfBLR,hightOfBLR,star
tAngOfBLR,spanningOfBLR);
logicBeamLineR = new
G4LogicalVolume(beamLineR,Air,"BeamLineR",0,0,0);
 physiBeamLineR = new
G4PVPlacement(xRotBLR,positionBLR,logicBeamLineR,"BeamLineR",l
ogicReflector,false,0);


//BeamLine in moderator
 G4RotationMatrix* xRotBLM = new G4RotationMatrix;
 xRotBLM->rotateX(90.*deg);

G4ThreeVector positionBLM = G4ThreeVector(0,0.045175*m,-
0.1*m);

G4Tubs* beamLineM = new
G4Tubs("beamLineM",innerRadOfBLM,outerRadOfBLM,hightOfBLM,star
tAngOfBLM,spanningOfBLM);
logicBeamLineM = new
G4LogicalVolume(beamLineM,Air,"BeamLineM",0,0,0);
physiBeamLineM = new
G4PVPlacement(xRotBLM,positionBLM,logicBeamLineM,"BeamLineM",l
ogicModerator,false,0);

//Coolant line in Moderator
G4RotationMatrix* xRotCLB = new G4RotationMatrix;
 xRotCLB->rotateX(90.*deg);

G4ThreeVector positionCLB = G4ThreeVector(0,-0.060175*m,-
0.1*m);

G4Tubs* coolLineB = new
G4Tubs("CoolLineB",innerRadOfCLB,outerRadOfCLB,hightOfCLB,star
tAngOfCLB,spanningOfCLB);
logicCoolLineB = new
G4LogicalVolume(coolLineB,D2O,"CoolLineB",0,0,0);
physiCoolLineB = new
G4PVPlacement(xRotCLB,positionCLB,logicCoolLineB,"CoolLineB",l
```

```
ogicModerator,false,0);

//Coolant line in reflector
G4RotationMatrix* xRotCLC = new G4RotationMatrix;
 xRotCLC->rotateX(90.*deg);

G4ThreeVector positionCLC = G4ThreeVector(0,-0.19*m,0);

G4Tubs* coolLineC = new
G4Tubs("CoolLineC",innerRadOfCLC,outerRadOfCLC,hightOfCLC,star
tAngOfCLC,spanningOfCLC);
logicCoolLineC = new
G4LogicalVolume(coolLineC,D2O,"CoolLineC",0,0,0);
physiCoolLineC = new
G4PVPlacement(xRotCLC,positionCLC,logicCoolLineC,"CoolLineC",l
ogicReflector,false,0);



//visulaisation

//world
  logicWorld->SetVisAttributes(G4VisAttributes::Invisible);
//set invisible

//reflector
 G4VisAttributes* simpleBoxref= new
G4VisAttributes(G4Colour(1.0,0.0,0.0)); //colour
  simpleBoxref->SetVisibility(true); //visiblity
  logicReflector->SetVisAttributes(simpleBoxref); // object

//moderator
  G4VisAttributes* simpleBoxMod= new
G4VisAttributes(G4Colour(0.0,0.0,1.0));
  simpleBoxMod->SetVisibility(true);
  logicModerator->SetVisAttributes(simpleBoxMod);

//target
  G4VisAttributes* simpleBoxTarget= new
G4VisAttributes(G4Colour(0.0,1.0,0.0));
  simpleBoxTarget->SetVisibility(true);
  logicTarget->SetVisAttributes(simpleBoxTarget);

//substrate
G4VisAttributes* simpleBoxSub= new
G4VisAttributes(G4Colour(1.0,0.0,1.0));
  simpleBoxSub->SetVisibility(true);
  logicSub->SetVisAttributes(simpleBoxSub);

//coolant bowl
G4VisAttributes* simpleBoxCool= new
G4VisAttributes(G4Colour(1.0,0.0,0.0));
  simpleBoxCool->SetVisibility(true);
  logicCoolant->SetVisAttributes(simpleBoxCool);
```

```
//coolant line in moderator
G4VisAttributes* simpleBoxCLB= new
G4VisAttributes(G4Colour(1.0,0.0,0.0));
  simpleBoxCLB->SetVisibility(true);
  logicCoolLineB->SetVisAttributes(simpleBoxCLB);

//coolant line in reflector
G4VisAttributes* simpleBoxCLC= new
G4VisAttributes(G4Colour(1.0,0.0,0.0));
  simpleBoxCLC->SetVisibility(true);
  logicCoolLineC->SetVisAttributes(simpleBoxCLC);

//left shield
G4VisAttributes* simpleBoxShL= new
G4VisAttributes(G4Colour(1.0,1.0,0.0));
  simpleBoxShL->SetVisibility(true);
  logicShieldL->SetVisAttributes(simpleBoxShL);

//right shield
G4VisAttributes* simpleBoxShR= new
G4VisAttributes(G4Colour(1.0,1.0,0.0));
  simpleBoxShR->SetVisibility(true);
  logicShieldR->SetVisAttributes(simpleBoxShR);

//top front sheild
G4VisAttributes* simpleBoxFT= new
G4VisAttributes(G4Colour(0.0,0.0,1.0));
  simpleBoxFT->SetVisibility(true);
  logicFrontTop->SetVisAttributes(simpleBoxFT);

//bottom front shield
G4VisAttributes* simpleBoxFB= new
G4VisAttributes(G4Colour(0.0,0.0,1.0));
  simpleBoxFB->SetVisibility(true);
  logicFrontBot->SetVisAttributes(simpleBoxFB);

//beamline in reflector
G4VisAttributes* simpleBoxBLR= new
G4VisAttributes(G4Colour(0.0,1.0,0.0));
  simpleBoxBLR->SetVisibility(true);
  logicBeamLineR->SetVisAttributes(simpleBoxBLR);

//beamline in moderator
G4VisAttributes* simpleBoxBLM= new
G4VisAttributes(G4Colour(0.0,1.0,0.0));
  simpleBoxBLM->SetVisibility(true);
  logicBeamLineM->SetVisAttributes(simpleBoxBLM);



return physiWorld;
}
```

```
//BNCTPhysicsList.cc
//modified physics list from example N01 removing unnecessary
optical processes

// --------------------------------------------------------------
---
//   GEANT 4 - Underground Dark Matter Detector Advanced
Example
//
//      For information related to this code contact: Alex
Howard
//      e-mail: alexander.howard@cern.ch
// --------------------------------------------------------------
---
// Comments
//
//                   Underground Advanced
//                by A. Howard and H. Araujo
//                     (27th November 2001)
//
// PhysicsList program
//
// Modified:
//
// 14-02-03 Fix bugs in msc and hIon instanciation + cut per
region
//
// 05-02-05 AH - changes to G4Decay - added is not short lived
protection
//          and redefined particles to allow non-static
creation
//          i.e. changed construction to G4MesonConstructor,
G4BaryonConstructor
//
// 23-10-09 LP - migrated EM physics from the LowEnergy
processes (not supported) to
//          the new G4Livermore model implementation. Results
unchanged.
//
// --------------------------------------------------------------
---

#include "BNCTPhysicsList.hh"

#include "globals.hh"
#include "G4ProcessManager.hh"
#include "G4ProcessVector.hh"

#include "G4ParticleDefinition.hh"
#include "G4ParticleWithCuts.hh"
#include "G4ParticleTypes.hh"
#include "G4ParticleTable.hh"

#include "G4ios.hh"
```

```
#include <iomanip>

#include "G4UserLimits.hh"
#include "G4BinaryCascade.hh"


// Constructor
////////////////////////////////////////////////////////////
BNCTPhysicsList::BNCTPhysicsList() : G4VUserPhysicsList()
{

  defaultCutValue     = 1.*mm; //
  cutForGamma         = defaultCutValue;
  cutForElectron      = 1.*mm;
  cutForPositron      = defaultCutValue;

  VerboseLevel = 1;
  OpVerbLevel = 0;

  SetVerboseLevel(VerboseLevel);
}


// Destructor
////////////////////////////////////////////////////////////
BNCTPhysicsList::~BNCTPhysicsList()
{;}


// Construct Particles
////////////////////////////////////////////////////
void BNCTPhysicsList::ConstructParticle()
{

  // In this method, static member functions should be called
  // for all particles which you want to use.
  // This ensures that objects of these particle types will be
  // created in the program.

  ConstructMyBosons();
  ConstructMyLeptons();
  ConstructMyHadrons();
  ConstructMyShortLiveds();

}


// construct
Bosons:////////////////////////////////////////////////////
void BNCTPhysicsList::ConstructMyBosons()
{
  // pseudo-particles
  G4Geantino::GeantinoDefinition();
  G4ChargedGeantino::ChargedGeantinoDefinition();
```

```
  // gamma
  G4Gamma::GammaDefinition();

  //OpticalPhotons
  //  G4OpticalPhoton::OpticalPhotonDefinition();

}


// construct
Leptons:////////////////////////////////////////////////////
void BNCTPhysicsList::ConstructMyLeptons()
{
  // leptons
  G4Electron::ElectronDefinition();
  G4Positron::PositronDefinition();
  G4MuonPlus::MuonPlusDefinition();
  G4MuonMinus::MuonMinusDefinition();

  G4NeutrinoE::NeutrinoEDefinition();
  G4AntiNeutrinoE::AntiNeutrinoEDefinition();
  G4NeutrinoMu::NeutrinoMuDefinition();
  G4AntiNeutrinoMu::AntiNeutrinoMuDefinition();
}


#include "G4MesonConstructor.hh"
#include "G4BaryonConstructor.hh"
#include "G4IonConstructor.hh"

// construct
Hadrons:////////////////////////////////////////////////////
void BNCTPhysicsList::ConstructMyHadrons()
{
 //  mesons
  G4MesonConstructor mConstructor;
  mConstructor.ConstructParticle();

 //  baryons
  G4BaryonConstructor bConstructor;
  bConstructor.ConstructParticle();

 //  ions
  G4IonConstructor iConstructor;
  iConstructor.ConstructParticle();

}


// construct
Shortliveds:////////////////////////////////////////////////
///
void BNCTPhysicsList::ConstructMyShortLiveds()
```

```
{
  // ShortLiveds
  ;
}



// Construct Processes
////////////////////////////////////////////////////
void BNCTPhysicsList::ConstructProcess()
{

  AddTransportation();

  ConstructEM();

  // ConstructOp();

  ConstructHad();

  ConstructGeneral();

}


// Transportation
////////////////////////////////////////////////////////
//#include "DMXMaxTimeCuts.hh"
//#include "DMXMinEkineCuts.hh"
#include "G4StepLimiter.hh"

void BNCTPhysicsList::AddTransportation() {

  G4VUserPhysicsList::AddTransportation();

  theParticleIterator->reset();
  while( (*theParticleIterator)() ){
    G4ParticleDefinition* particle = theParticleIterator-
>value();
    G4ProcessManager* pmanager = particle-
>GetProcessManager();
    G4String particleName = particle->GetParticleName();
    /*
    // time cuts for ONLY neutrons:
    if(particleName == "neutron")
      pmanager->AddDiscreteProcess(new DMXMaxTimeCuts());
    // Energy cuts to kill charged (embedded in method)
particles:
    pmanager->AddDiscreteProcess(new DMXMinEkineCuts());
    */
    // Step limit applied to all particles:
    pmanager->AddProcess(new G4StepLimiter,       -1,-1,1);
```

```
  }
}


// Electromagnetic Processes
//////////////////////////////////////////////
// all charged particles

// gamma
#include "G4PhotoElectricEffect.hh"
#include "G4LivermorePhotoElectricModel.hh"

#include "G4ComptonScattering.hh"
#include "G4LivermoreComptonModel.hh"

#include "G4GammaConversion.hh"
#include "G4LivermoreGammaConversionModel.hh"

#include "G4RayleighScattering.hh"
#include "G4LivermoreRayleighModel.hh"


// e-
#include "G4eMultipleScattering.hh"

#include "G4eIonisation.hh"
#include "G4LivermoreIonisationModel.hh"

#include "G4eBremsstrahlung.hh"
#include "G4LivermoreBremsstrahlungModel.hh"


// e+
#include "G4eIonisation.hh"
#include "G4eBremsstrahlung.hh"
#include "G4eplusAnnihilation.hh"


// alpha and GenericIon and deuterons, triton, He3:
#include "G4EnergyLossTables.hh"

//muon:
#include "G4MuIonisation.hh"
#include "G4MuBremsstrahlung.hh"
#include "G4MuPairProduction.hh"
#include "G4MuonMinusCaptureAtRest.hh"

//OTHERS:
#include "G4hIonisation.hh"
#include "G4hMultipleScattering.hh"
#include "G4hBremsstrahlung.hh"
#include "G4ionIonisation.hh"
#include "G4IonParametrisedLossModel.hh"
```

```
//em process options to allow msc step-limitation to be
switched off
#include "G4EmProcessOptions.hh"

void BNCTPhysicsList::ConstructEM() {

  //set a finer grid of the physic tables in order to improve
precision
  //former LowEnergy models have 200 bins up to 100 GeV
  G4EmProcessOptions opt;
  opt.SetMaxEnergy(100*GeV);
  opt.SetDEDXBinning(200);
  opt.SetLambdaBinning(200);

  theParticleIterator->reset();
  while( (*theParticleIterator)() ){
    G4ParticleDefinition* particle = theParticleIterator-
>value();
    G4ProcessManager* pmanager = particle-
>GetProcessManager();
    G4String particleName = particle->GetParticleName();
    G4String particleType = particle->GetParticleType();
    G4double charge = particle->GetPDGCharge();

    if (particleName == "gamma")
      {
    //gamma
    G4RayleighScattering* theRayleigh = new
G4RayleighScattering();
    theRayleigh->SetModel(new G4LivermoreRayleighModel());
//not strictly necessary
    pmanager->AddDiscreteProcess(theRayleigh);

    G4PhotoElectricEffect* thePhotoElectricEffect = new
G4PhotoElectricEffect();
    thePhotoElectricEffect->SetModel(new
G4LivermorePhotoElectricModel());
    pmanager->AddDiscreteProcess(thePhotoElectricEffect);

    G4ComptonScattering* theComptonScattering = new
G4ComptonScattering();
    theComptonScattering->SetModel(new
G4LivermoreComptonModel());
    pmanager->AddDiscreteProcess(theComptonScattering);

    G4GammaConversion* theGammaConversion = new
G4GammaConversion();
    theGammaConversion->SetModel(new
G4LivermoreGammaConversionModel());
    pmanager->AddDiscreteProcess(theGammaConversion);

      }
    else if (particleName == "e-")
      {
```

```
    //electron
    // process ordering: AddProcess(name, at rest, along step,
post step)
    // Multiple scattering
    G4eMultipleScattering* msc = new G4eMultipleScattering();
    msc->SetStepLimitType(fUseDistanceToBoundary);
    pmanager->AddProcess(msc,-1, 1, 1);

    // Ionisation
    G4eIonisation* eIonisation = new G4eIonisation();
    eIonisation->SetEmModel(new G4LivermoreIonisationModel());
    eIonisation->SetStepFunction(0.2, 100*um); //improved
precision in tracking
    pmanager->AddProcess(eIonisation,-1, 2, 2);

    // Bremsstrahlung
    G4eBremsstrahlung* eBremsstrahlung = new
G4eBremsstrahlung();
    eBremsstrahlung->SetEmModel(new
G4LivermoreBremsstrahlungModel());
    pmanager->AddProcess(eBremsstrahlung, -1,-3, 3);
      }
    else if (particleName == "e+")
      {
    //positron
    G4eMultipleScattering* msc = new G4eMultipleScattering();
    msc->SetStepLimitType(fUseDistanceToBoundary);
    pmanager->AddProcess(msc,-1, 1, 1);

    // Ionisation
    G4eIonisation* eIonisation = new G4eIonisation();
    eIonisation->SetStepFunction(0.2, 100*um); //
    pmanager->AddProcess(eIonisation,                -1, 2,
2);

    //Bremsstrahlung (use default, no low-energy available)
    pmanager->AddProcess(new G4eBremsstrahlung(), -1,-1, 3);

    //Annihilation
    pmanager->AddProcess(new G4eplusAnnihilation(),0,-1, 4);
      }
    else if( particleName == "mu+" ||
         particleName == "mu-"    )
      {
    //muon
    pmanager->AddProcess(new G4eMultipleScattering,
-1, 1, 1);
    pmanager->AddProcess(new G4MuIonisation(),          -1, 2,
2);
    pmanager->AddProcess(new G4MuBremsstrahlung(),      -1,-1,
3);
    pmanager->AddProcess(new G4MuPairProduction(),      -1,-1,
4);
    if( particleName == "mu-" )
```

```
      pmanager->AddProcess(new G4MuonMinusCaptureAtRest(), 0,-
1,-1);
      }
    else if (particleName == "proton" ||
        particleName == "pi+" ||
        particleName == "pi-")
      {
    //multiple scattering
    pmanager->AddProcess(new G4hMultipleScattering, -1, 1, 1);

    //ionisation
    G4hIonisation* hIonisation = new G4hIonisation();
    hIonisation->SetStepFunction(0.2, 50*um);
    pmanager->AddProcess(hIonisation,                    -1,
2, 2);

    //bremmstrahlung
    pmanager->AddProcess(new G4hBremsstrahlung,     -1,-3, 3);
      }
    else if(particleName == "alpha"      ||
        particleName == "deuteron"   ||
        particleName == "triton"     ||
        particleName == "He3")
      {
    //multiple scattering
    pmanager->AddProcess(new G4hMultipleScattering,-1,1,1);

    //ionisation
    G4ionIonisation* ionIoni = new G4ionIonisation();
    ionIoni->SetStepFunction(0.1, 20*um);
    pmanager->AddProcess(ionIoni,                   -1, 2, 2);
      }
    else if (particleName == "GenericIon")
      {
    // OBJECT may be dynamically created as either a
GenericIon or nucleus
    // G4Nucleus exists and therefore has particle type
nucleus
    // genericIon:

    //multiple scattering
    pmanager->AddProcess(new G4hMultipleScattering,-1,1,1);

    //ionisation
    G4ionIonisation* ionIoni = new G4ionIonisation();
    ionIoni->SetEmModel(new G4IonParametrisedLossModel());
    ionIoni->SetStepFunction(0.1, 20*um);
    pmanager->AddProcess(ionIoni,                   -1, 2, 2);
      }

    else if ((!particle->IsShortLived()) &&
        (charge != 0.0) &&
        (particle->GetParticleName() != "chargedgeantino"))
      {
```

```
    //all others charged particles except geantino
        G4hMultipleScattering* aMultipleScattering = new
G4hMultipleScattering();
        G4hIonisation* ahadronIon = new G4hIonisation();

    //multiple scattering
    pmanager->AddProcess(aMultipleScattering,-1,1,1);

    //ionisation
    pmanager->AddProcess(ahadronIon,      -1,2,2);
      }

  }

  // turn off msc step-limitation - especially as electron cut
1nm
  opt.SetMscStepLimitation(fMinimal);

}

/*
// Optical Processes
////////////////////////////////////////////////////
#include "G4Scintillation.hh"
#include "G4OpAbsorption.hh"
//#include "G4OpRayleigh.hh"
#include "G4OpBoundaryProcess.hh"

void BNCTPhysicsList::ConstructOp()
{
  // default scintillation process
  G4Scintillation* theScintProcessDef = new
G4Scintillation("Scintillation");
  // theScintProcessDef->DumpPhysicsTable();
  theScintProcessDef->SetTrackSecondariesFirst(true);
  theScintProcessDef->SetScintillationYieldFactor(1.0); //
  theScintProcessDef->SetScintillationExcitationRatio(0.0); //
  theScintProcessDef->SetVerboseLevel(OpVerbLevel);

  // scintillation process for alpha:
  G4Scintillation* theScintProcessAlpha = new
G4Scintillation("Scintillation");
  // theScintProcessNuc->DumpPhysicsTable();
  theScintProcessAlpha->SetTrackSecondariesFirst(true);
  theScintProcessAlpha->SetScintillationYieldFactor(1.1);
  theScintProcessAlpha->SetScintillationExcitationRatio(1.0);
  theScintProcessAlpha->SetVerboseLevel(OpVerbLevel);

  // scintillation process for heavy nuclei
  G4Scintillation* theScintProcessNuc = new
G4Scintillation("Scintillation");
  // theScintProcessNuc->DumpPhysicsTable();
  theScintProcessNuc->SetTrackSecondariesFirst(true);
  theScintProcessNuc->SetScintillationYieldFactor(0.2);
```

```
  theScintProcessNuc->SetScintillationExcitationRatio(1.0);
  theScintProcessNuc->SetVerboseLevel(OpVerbLevel);

  // optical processes
  G4OpAbsorption* theAbsorptionProcess = new G4OpAbsorption();
  //  G4OpRayleigh* theRayleighScatteringProcess = new
G4OpRayleigh();
  G4OpBoundaryProcess* theBoundaryProcess = new
G4OpBoundaryProcess();
  //  theAbsorptionProcess->DumpPhysicsTable();
  //  theRayleighScatteringProcess->DumpPhysicsTable();
  theAbsorptionProcess->SetVerboseLevel(OpVerbLevel);
  // theRayleighScatteringProcess-
>SetVerboseLevel(OpVerbLevel);
  theBoundaryProcess->SetVerboseLevel(OpVerbLevel);
  G4OpticalSurfaceModel themodel = unified;
  theBoundaryProcess->SetModel(themodel);

  theParticleIterator->reset();
  while( (*theParticleIterator)() )
    {
      G4ParticleDefinition* particle = theParticleIterator-
>value();
      G4ProcessManager* pmanager = particle-
>GetProcessManager();
      G4String particleName = particle->GetParticleName();
      if (theScintProcessDef->IsApplicable(*particle)) {
    //      if(particle->GetPDGMass() > 5.0*GeV)
    if(particle->GetParticleName() == "GenericIon") {
      pmanager->AddProcess(theScintProcessNuc); //
AtRestDiscrete
      pmanager-
>SetProcessOrderingToLast(theScintProcessNuc,idxAtRest);
      pmanager-
>SetProcessOrderingToLast(theScintProcessNuc,idxPostStep);
    }
    else if(particle->GetParticleName() == "alpha") {
      pmanager->AddProcess(theScintProcessAlpha);
      pmanager-
>SetProcessOrderingToLast(theScintProcessAlpha,idxAtRest);
      pmanager-
>SetProcessOrderingToLast(theScintProcessAlpha,idxPostStep);
    }
    else {
      pmanager->AddProcess(theScintProcessDef);
      pmanager-
>SetProcessOrderingToLast(theScintProcessDef,idxAtRest);
      pmanager-
>SetProcessOrderingToLast(theScintProcessDef,idxPostStep);
    }
      }

      if (particleName == "opticalphoton") {
    pmanager->AddDiscreteProcess(theAbsorptionProcess);
```

```
    //     pmanager-
>AddDiscreteProcess(theRayleighScatteringProcess);
    pmanager->AddDiscreteProcess(theBoundaryProcess);
      }
    }
}

*/

// Hadronic processes
/////////////////////////////////////////////////////

// Elastic processes:
#include "G4HadronElasticProcess.hh"

// Inelastic processes:
#include "G4PionPlusInelasticProcess.hh"
#include "G4PionMinusInelasticProcess.hh"
#include "G4KaonPlusInelasticProcess.hh"
#include "G4KaonZeroSInelasticProcess.hh"
#include "G4KaonZeroLInelasticProcess.hh"
#include "G4KaonMinusInelasticProcess.hh"
#include "G4ProtonInelasticProcess.hh"
#include "G4AntiProtonInelasticProcess.hh"
#include "G4NeutronInelasticProcess.hh"
#include "G4AntiNeutronInelasticProcess.hh"
#include "G4DeuteronInelasticProcess.hh"
#include "G4TritonInelasticProcess.hh"
#include "G4AlphaInelasticProcess.hh"

// Low-energy Models: < 20GeV
#include "G4LElastic.hh"
#include "G4LEPionPlusInelastic.hh"
#include "G4LEPionMinusInelastic.hh"
#include "G4LEKaonPlusInelastic.hh"
#include "G4LEKaonZeroSInelastic.hh"
#include "G4LEKaonZeroLInelastic.hh"
#include "G4LEKaonMinusInelastic.hh"
#include "G4LEProtonInelastic.hh"
#include "G4LEAntiProtonInelastic.hh"
#include "G4LENeutronInelastic.hh"
#include "G4LEAntiNeutronInelastic.hh"
#include "G4LEDeuteronInelastic.hh"
#include "G4LETritonInelastic.hh"
#include "G4LEAlphaInelastic.hh"
#include "G4HadronCaptureProcess.hh"
// High-energy Models: >20 GeV
#include "G4HEPionPlusInelastic.hh"
#include "G4HEPionMinusInelastic.hh"
#include "G4HEKaonPlusInelastic.hh"
#include "G4HEKaonZeroInelastic.hh"
#include "G4HEKaonZeroInelastic.hh"
#include "G4HEKaonMinusInelastic.hh"
#include "G4HEProtonInelastic.hh"
```

```
#include "G4HEAntiProtonInelastic.hh"
#include "G4HENeutronInelastic.hh"
#include "G4HEAntiNeutronInelastic.hh"


// Neutron high-precision models: <20 MeV
#include "G4NeutronHPElastic.hh"
#include "G4NeutronHPElasticData.hh"
#include "G4NeutronHPCapture.hh"
#include "G4NeutronHPCaptureData.hh"
#include "G4NeutronHPInelastic.hh"
#include "G4NeutronHPInelasticData.hh"
#include "G4LCapture.hh"

// Stopping processes
#include "G4PiMinusAbsorptionAtRest.hh"
#include "G4KaonMinusAbsorptionAtRest.hh"
#include "G4AntiProtonAnnihilationAtRest.hh"
#include "G4AntiNeutronAnnihilationAtRest.hh"


// ConstructHad()
// Makes discrete physics processes for the hadrons, at
present limited
// to those particles with GHEISHA interactions (INTRC > 0).
// The processes are: Elastic scattering and Inelastic
scattering.
// F.W.Jones  09-JUL-1998
void BNCTPhysicsList::ConstructHad()
{
  G4HadronElasticProcess* theElasticProcess = new
G4HadronElasticProcess;
  G4LElastic* theElasticModel = new G4LElastic;
  theElasticProcess->RegisterMe(theElasticModel);

  theParticleIterator->reset();
  while ((*theParticleIterator)())
    {
      G4ParticleDefinition* particle = theParticleIterator-
>value();
      G4ProcessManager* pmanager = particle-
>GetProcessManager();
      G4String particleName = particle->GetParticleName();

      if (particleName == "pi+")
    {
      pmanager->AddDiscreteProcess(theElasticProcess);
      G4PionPlusInelasticProcess* theInelasticProcess =
        new G4PionPlusInelasticProcess("inelastic");
      G4LEPionPlusInelastic* theLEInelasticModel =
        new G4LEPionPlusInelastic;
      theInelasticProcess->RegisterMe(theLEInelasticModel);
      G4HEPionPlusInelastic* theHEInelasticModel =
        new G4HEPionPlusInelastic;
```

```
      theInelasticProcess->RegisterMe(theHEInelasticModel);
      pmanager->AddDiscreteProcess(theInelasticProcess);
    }

      else if (particleName == "pi-")
    {
      pmanager->AddDiscreteProcess(theElasticProcess);
      G4PionMinusInelasticProcess* theInelasticProcess =
        new G4PionMinusInelasticProcess("inelastic");
      G4LEPionMinusInelastic* theLEInelasticModel =
        new G4LEPionMinusInelastic;
      theInelasticProcess->RegisterMe(theLEInelasticModel);
      G4HEPionMinusInelastic* theHEInelasticModel =
        new G4HEPionMinusInelastic;
      theInelasticProcess->RegisterMe(theHEInelasticModel);
      pmanager->AddDiscreteProcess(theInelasticProcess);
      G4String prcNam;
      pmanager->AddRestProcess(new G4PiMinusAbsorptionAtRest,
ordDefault);
    }

      else if (particleName == "kaon+")
    {
      pmanager->AddDiscreteProcess(theElasticProcess);
      G4KaonPlusInelasticProcess* theInelasticProcess =
        new G4KaonPlusInelasticProcess("inelastic");
      G4LEKaonPlusInelastic* theLEInelasticModel =
        new G4LEKaonPlusInelastic;
      theInelasticProcess->RegisterMe(theLEInelasticModel);
      G4HEKaonPlusInelastic* theHEInelasticModel =
        new G4HEKaonPlusInelastic;
      theInelasticProcess->RegisterMe(theHEInelasticModel);
      pmanager->AddDiscreteProcess(theInelasticProcess);
    }

      else if (particleName == "kaon0S")
    {
      pmanager->AddDiscreteProcess(theElasticProcess);
      G4KaonZeroSInelasticProcess* theInelasticProcess =
        new G4KaonZeroSInelasticProcess("inelastic");
      G4LEKaonZeroSInelastic* theLEInelasticModel =
        new G4LEKaonZeroSInelastic;
      theInelasticProcess->RegisterMe(theLEInelasticModel);
      G4HEKaonZeroInelastic* theHEInelasticModel =
        new G4HEKaonZeroInelastic;
      theInelasticProcess->RegisterMe(theHEInelasticModel);
      pmanager->AddDiscreteProcess(theInelasticProcess);
    }

      else if (particleName == "kaon0L")
    {
      pmanager->AddDiscreteProcess(theElasticProcess);
      G4KaonZeroLInelasticProcess* theInelasticProcess =
        new G4KaonZeroLInelasticProcess("inelastic");
```

```
      G4LEKaonZeroLInelastic* theLEInelasticModel =
        new G4LEKaonZeroLInelastic;
      theInelasticProcess->RegisterMe(theLEInelasticModel);
      G4HEKaonZeroInelastic* theHEInelasticModel =
        new G4HEKaonZeroInelastic;
      theInelasticProcess->RegisterMe(theHEInelasticModel);
      pmanager->AddDiscreteProcess(theInelasticProcess);
    }

      else if (particleName == "kaon-")
    {
      pmanager->AddDiscreteProcess(theElasticProcess);
      G4KaonMinusInelasticProcess* theInelasticProcess =
        new G4KaonMinusInelasticProcess("inelastic");
      G4LEKaonMinusInelastic* theLEInelasticModel =
        new G4LEKaonMinusInelastic;
      theInelasticProcess->RegisterMe(theLEInelasticModel);
      G4HEKaonMinusInelastic* theHEInelasticModel =
        new G4HEKaonMinusInelastic;
      theInelasticProcess->RegisterMe(theHEInelasticModel);
      pmanager->AddDiscreteProcess(theInelasticProcess);
      pmanager->AddRestProcess(new
G4KaonMinusAbsorptionAtRest, ordDefault);
    }

      else if (particleName == "proton")
    {
  // Inelastic scattering: Binary model up to  10. GeV
  G4BinaryCascade* binaryModel = new G4BinaryCascade();
  // Energy limit of the Binary model
  G4double binaryHighEnergyLimit = 10. * GeV;
  binaryModel->SetMaxEnergy(binaryHighEnergyLimit);

      pmanager->AddDiscreteProcess(theElasticProcess);
      G4ProtonInelasticProcess* theInelasticProcess =
        new G4ProtonInelasticProcess("inelastic");
          // Activate the cross-sections for proton nuclear
scattering up to 20 GeV
          theInelasticProcess-
>AddDataSet(&protonCrossSection);
          // Set the models
          theInelasticProcess->RegisterMe(binaryModel);
      G4LEProtonInelastic* theLEProtonInelasticModel = new
G4LEProtonInelastic;
  theLEProtonInelasticModel->SetMinEnergy(8.*GeV);
      theInelasticProcess-
>RegisterMe(theLEProtonInelasticModel);
      G4HEProtonInelastic* theHEInelasticModel = new
G4HEProtonInelastic;
      theInelasticProcess->RegisterMe(theHEInelasticModel);
      pmanager->AddDiscreteProcess(theInelasticProcess);
    }

      else if (particleName == "anti_proton")
```

```
    {
      pmanager->AddDiscreteProcess(theElasticProcess);
      G4AntiProtonInelasticProcess* theInelasticProcess =
        new G4AntiProtonInelasticProcess("inelastic");
      G4LEAntiProtonInelastic* theLEInelasticModel =
        new G4LEAntiProtonInelastic;
      theInelasticProcess->RegisterMe(theLEInelasticModel);
      G4HEAntiProtonInelastic* theHEInelasticModel =
        new G4HEAntiProtonInelastic;
      theInelasticProcess->RegisterMe(theHEInelasticModel);
      pmanager->AddDiscreteProcess(theInelasticProcess);
    }

      else if (particleName == "neutron") {
    // elastic scattering
    G4HadronElasticProcess* theNeutronElasticProcess =
      new G4HadronElasticProcess;
    G4LElastic* theElasticModel1 = new G4LElastic;
    G4NeutronHPElastic * theElasticNeutron = new
G4NeutronHPElastic;
    theNeutronElasticProcess->RegisterMe(theElasticModel1);
    theElasticModel1->SetMinEnergy(19*MeV);
    theNeutronElasticProcess->RegisterMe(theElasticNeutron);
    G4NeutronHPElasticData * theNeutronData = new
G4NeutronHPElasticData;
    theNeutronElasticProcess->AddDataSet(theNeutronData);
    pmanager->AddDiscreteProcess(theNeutronElasticProcess);
    // inelastic scattering
    G4NeutronInelasticProcess* theInelasticProcess =
      new G4NeutronInelasticProcess("inelastic");
    G4LENeutronInelastic* theInelasticModel = new
G4LENeutronInelastic;
    theInelasticModel->SetMinEnergy(19*MeV);
    theInelasticProcess->RegisterMe(theInelasticModel);
    G4NeutronHPInelastic * theLENeutronInelasticModel =
      new G4NeutronHPInelastic;
    theInelasticProcess-
>RegisterMe(theLENeutronInelasticModel);
    G4NeutronHPInelasticData * theNeutronData1 =
      new G4NeutronHPInelasticData;
    theInelasticProcess->AddDataSet(theNeutronData1);
    pmanager->AddDiscreteProcess(theInelasticProcess);
    // capture
    G4HadronCaptureProcess* theCaptureProcess =
      new G4HadronCaptureProcess;
    G4LCapture* theCaptureModel = new G4LCapture;
    theCaptureModel->SetMinEnergy(19*MeV);
    theCaptureProcess->RegisterMe(theCaptureModel);
    G4NeutronHPCapture * theLENeutronCaptureModel = new
G4NeutronHPCapture;
    theCaptureProcess->RegisterMe(theLENeutronCaptureModel);
    G4NeutronHPCaptureData * theNeutronData3 = new
G4NeutronHPCaptureData;
    theCaptureProcess->AddDataSet(theNeutronData3);
```

```
    pmanager->AddDiscreteProcess(theCaptureProcess);
    //  G4ProcessManager* pmanager = G4Neutron::Neutron-
>GetProcessManager();
    //  pmanager->AddProcess(new G4UserSpecialCuts(),-1,-1,1);
      }
      else if (particleName == "anti_neutron")
    {
      pmanager->AddDiscreteProcess(theElasticProcess);
      G4AntiNeutronInelasticProcess* theInelasticProcess =
        new G4AntiNeutronInelasticProcess("inelastic");
      G4LEAntiNeutronInelastic* theLEInelasticModel =
        new G4LEAntiNeutronInelastic;
      theInelasticProcess->RegisterMe(theLEInelasticModel);
      G4HEAntiNeutronInelastic* theHEInelasticModel =
        new G4HEAntiNeutronInelastic;
      theInelasticProcess->RegisterMe(theHEInelasticModel);
      pmanager->AddDiscreteProcess(theInelasticProcess);
    }

      else if (particleName == "deuteron")
    {
      pmanager->AddDiscreteProcess(theElasticProcess);
      G4DeuteronInelasticProcess* theInelasticProcess =
        new G4DeuteronInelasticProcess("inelastic");
      G4LEDeuteronInelastic* theLEInelasticModel =
        new G4LEDeuteronInelastic;
      theInelasticProcess->RegisterMe(theLEInelasticModel);
      pmanager->AddDiscreteProcess(theInelasticProcess);
    }

      else if (particleName == "triton")
    {
      pmanager->AddDiscreteProcess(theElasticProcess);
      G4TritonInelasticProcess* theInelasticProcess =
        new G4TritonInelasticProcess("inelastic");
      G4LETritonInelastic* theLEInelasticModel =
        new G4LETritonInelastic;
      theInelasticProcess->RegisterMe(theLEInelasticModel);
      pmanager->AddDiscreteProcess(theInelasticProcess);
    }

      else if (particleName == "alpha")
    {
      pmanager->AddDiscreteProcess(theElasticProcess);
      G4AlphaInelasticProcess* theInelasticProcess =
        new G4AlphaInelasticProcess("inelastic");
      G4LEAlphaInelastic* theLEInelasticModel =
        new G4LEAlphaInelastic;
      theInelasticProcess->RegisterMe(theLEInelasticModel);
      pmanager->AddDiscreteProcess(theInelasticProcess);
    }

    }
}
```

```
// Decays
////////////////////////////////////////////////////////
/////
#include "G4Decay.hh"
#include "G4RadioactiveDecay.hh"
#include "G4IonTable.hh"
#include "G4Ions.hh"

void BNCTPhysicsList::ConstructGeneral() {

  // Add Decay Process
  G4Decay* theDecayProcess = new G4Decay();
  theParticleIterator->reset();
  while( (*theParticleIterator)() )
    {
      G4ParticleDefinition* particle = theParticleIterator-
>value();
      G4ProcessManager* pmanager = particle-
>GetProcessManager();

      if (theDecayProcess->IsApplicable(*particle) &&
!particle->IsShortLived())
    {
      pmanager ->AddProcess(theDecayProcess);
      // set ordering for PostStepDoIt and AtRestDoIt
      pmanager ->SetProcessOrdering(theDecayProcess,
idxPostStep);
      pmanager ->SetProcessOrdering(theDecayProcess,
idxAtRest);
    }
    }

  // Declare radioactive decay to the GenericIon in the
IonTable.
  const G4IonTable *theIonTable =
    G4ParticleTable::GetParticleTable()->GetIonTable();
  G4RadioactiveDecay *theRadioactiveDecay = new
G4RadioactiveDecay();

  for (G4int i=0; i<theIonTable->Entries(); i++)
    {
      G4String particleName = theIonTable->GetParticle(i)-
>GetParticleName();
      G4String particleType = theIonTable->GetParticle(i)-
>GetParticleType();

      if (particleName == "GenericIon")
    {
      G4ProcessManager* pmanager =
        theIonTable->GetParticle(i)->GetProcessManager();
      pmanager->SetVerboseLevel(VerboseLevel);
      pmanager ->AddProcess(theRadioactiveDecay);
```

```
      pmanager ->SetProcessOrdering(theRadioactiveDecay,
idxPostStep);
      pmanager ->SetProcessOrdering(theRadioactiveDecay,
idxAtRest);
    }
    }
}

// Cuts
////////////////////////////////////////////////////////////
///////
void BNCTPhysicsList::SetCuts()
{

  if (verboseLevel >1)
    G4cout << "DMXPhysicsList::SetCuts:";

  if (verboseLevel>0){
    G4cout << "DMXPhysicsList::SetCuts:";
    G4cout << "CutLength : "
       << G4BestUnit(defaultCutValue,"Length") << G4endl;
  }

  //special for low energy physics
  G4double lowlimit=250*eV;
  G4ProductionCutsTable::GetProductionCutsTable()-
>SetEnergyRange(lowlimit,100.*GeV);

  // set cut values for gamma at first and for e- second and
next for e+,
  // because some processes for e+/e- need cut values for
gamma
  SetCutValue(cutForGamma, "gamma");
  SetCutValue(cutForElectron, "e-");
  SetCutValue(cutForPositron, "e+");

  if (verboseLevel>0) DumpCutValuesTable();
}
```

```
//BNCTPrimaryGeneratorAction.cc

#include"BNCTPrimaryGeneratorAction.hh"

#include "G4Event.hh"
#include "G4ParticleGun.hh"
#include "G4ParticleTable.hh"
#include "G4ParticleDefinition.hh"
#include "globals.hh"

BNCTPrimaryGeneratorAction::BNCTPrimaryGeneratorAction()
{
  G4int n_particle = 1;
  particleGun = new G4ParticleGun(n_particle);
//incident particle type
  G4ParticleTable* particleTable =
G4ParticleTable::GetParticleTable();
  G4String particleName;
  particleGun->SetParticleDefinition(particleTable-
>FindParticle(particleName="proton"));
//particle direction
  particleGun->SetParticleMomentumDirection(G4ThreeVector(0.,-
1.,0.));
//particle energy
  particleGun->SetParticleEnergy(2.8*MeV);
//inital position
  particleGun->SetParticlePosition(G4ThreeVector(0,0.29*m,0));
}

BNCTPrimaryGeneratorAction::~BNCTPrimaryGeneratorAction()
{
  delete particleGun;
}

void BNCTPrimaryGeneratorAction::GeneratePrimaries(G4Event*
anEvent)
{
  G4int i = anEvent->GetEventID() % 3;
  G4ThreeVector v(1.0,0.0,0.0);
  switch(i)
    {
    case 0:
      break;
    case 1:
      v.setY(0.1);
      break;
    case 2:
      v.setZ(0.1);
      break;
    }

  particleGun->GeneratePrimaryVertex(anEvent);
}
```

```
//BNCTSteppingAction.cc

#include "BNCTSteppingAction.hh"
#include "G4SteppingManager.hh"
#include "G4Track.hh"
#include "G4Step.hh"
#include "G4StepPoint.hh"
#include "G4TrackStatus.hh"
#include "G4VPhysicalVolume.hh"
#include "G4ParticleDefinition.hh"
#include "G4ParticleTypes.hh"

//create output file
BNCTSteppingAction::BNCTSteppingAction()
{
  file.open("file.txt");
}

BNCTSteppingAction::~BNCTSteppingAction()
{
  file.close();
}

void BNCTSteppingAction::UserSteppingAction(const G4Step *
theStep)
{
  G4Track * theTrack = theStep->GetTrack();


//out put if paticle is a neutron that crosses the target
boundry from target to not target
if(theStep->GetPostStepPoint()->GetPhysicalVolume()) {
  G4StepPoint * thePrePoint = theStep->GetPreStepPoint();
  G4VPhysicalVolume * thePrePV = thePrePoint-
>GetPhysicalVolume();
  G4String thePrePVname = thePrePV->GetName();
  G4StepPoint * thePostPoint = theStep->GetPostStepPoint();
  G4VPhysicalVolume * thePostPV = thePostPoint-
>GetPhysicalVolume();
  G4String thePostPVname = thePostPV->GetName();
  G4ParticleDefinition * particleType = theTrack-
>GetDefinition();

if(thePrePVname=="Target"&&thePostPVname!="Target"&&particleTy
pe==G4Neutron::NeutronDefinition())
{   G4double kinEnergy = theTrack->GetKineticEnergy();
    //output to terminal
 G4cout << "Neutron Energy = "<< kinEnergy <<"MeV" << G4endl;
    //output to file
 file << kinEnergy << G4endl;  } }}
```

Appendix B: IPAC'12 Proceedings

OPTIMISING NEUTRON PRODUCTION FROM COMPACT LOW ENERGY ACCELERATORS

N. Ratcliffe, R. Barlow, A. Bungau, R. Cywinski, T. R. Edgecock
University of Huddersfield, Huddersfield, U.K.

Abstract

There is currently much development in accelerator based methods to provide flexible and reliable neutron generators, in response to a decline in the availability of nuclear reactors. In this paper the focus is on neutron production via a low energy DC proton accelerator (1-10 MeV) and light target system. GEANT4 simulations are being used to study various aspects of target design, beginning with studies into light targets, such as lithium and beryllium, which are already in use. Initially the aim is to replicate these designs and benchmark these simulations with other models and experimental results before investigating how modifications can improve neutron production and tailor experimental geometries to specific applications such as neutron capture therapy and medical isotope production.

INTRODUCTION

There are two main methods of neutron generation: From a particle accelerator induced reaction or a nuclear reactor. Both methods are limited. However with the current views on nuclear technology and its many issues including logistics, flexibility and safety there is a drive towards developing and improving accelerator based sources for neutron production. There are many advantages to using accelerator based sources for neutron production. For example in medical applications an accelerator based source allows for much more flexibility ranging from an ease in logistics, being able to combine a treatment facility with a medical centre, to having more flexibility in selecting the energy range of the neutrons produced.

Many medical applications such as neutron capture therapies use thermal and epithermal neutrons which are best produced using low energy (less than 10 MeV) incident protons colliding with a light (low mass) target. The medical physics team at Birmingham University are implementing such methods of neutron production to develop a Boron Neutron Capture Therapy (BNCT) facility in the UK [1]. By firing a low energy ($\approx$ 3 MeV) proton beam at a thick lithium disc target with a fluental and graphite moderating block they have a working thermal/epithermal neutron source [2] [3].

This working target design has proved to be a good starting point for this work as the Birmingham team have both experimental [2] [3] results and previous model results generated using MCNP [1] with which to compare and benchmark our GEANT4 results, before going on to modify target designs and materials for our own applications. Additionally there seems to have been much discussion in the literature on which element, lithium or beryllium, would make the better target. There are several advantages and disadvantages associated with each element that need to be considered. While lithium has the preferable neutronic properties in terms of the neutron yield obtained under proton bombardment there can be several difficulties in practically implementing such a target due to mechanical and chemical properties, such as low melting point and poor heat conduction etc. In order to overcome these problems a more complex target assembly must be used, for example the Birmingham team have carried out extensive studies in which the lithium is attached to a suitable substrate whilst also providing an adequate cooling system to help combat the large amounts of power that get injected into the target by the proton beam [1]. In comparison a practical beryllium target design could be much simpler, even implemented as a single foil [4]. The price for these much better practical properties is a decrease in the neutronic properties, for example the beryllium neutron yield for an incident proton of 4 MeV is comparable to the lithium neutron yield at around 2.8 MeV [5] [6]. There has also been study of combining layers of these two elements to make a hybrid target to combine the advantages of each element whilst mitigating against the disadvantages of each individual element [7].

In this paper we present the results of simulations for both lithium and beryllium as single element targets for the GEANT4 validation process.

SETUP

The simulated data presented here has been obtained using a 0.7mm thick target disc with a diameter of 40mm in both lithium and beryllium. Simulations were performed with GEANT4 versions 4.9.4.p01 and 4.9.5.p01 using two physics lists, QGSP_BERT and QGSP_BERT_HP, as Bertini models are known to be more reliable at lower energy scales due to incorporated pre-compound models. A point like proton beam is fired in an energy range between 2 and 4 MeV. Results obtained from these simulations give a model count of the number of neutrons that are produced within and exit the target volume. Experimental work has also been done using similar targets and the available results can be used to benchmark our simulations.

RESULTS

For the first part of the validation process the lithium target simulation was used. Results obtained from these

ISBN 978-3-95450-115-1

simulations using GEANT4.9.4.p01 with QGSP_BERT are shown in Fig. 1. These results gave the highest and most reliable neutron yields from the models employed. Experimental results from the Birmingham team can be seen in Fig. 2 [3]. A comparison of these plots shows that the functional form of the simulated data is significantly different from the experimental data. Moreover our results also give a much lower neutron yield (by approximately a factor of 10^4) than the experimental cross sections would suggest.

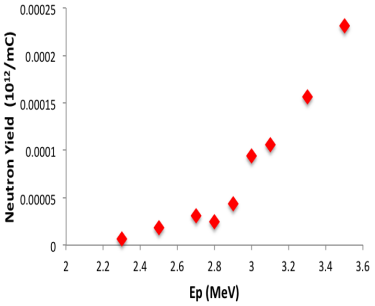

Figure 1: Simulation results of the lithium target using GEANT4.9.4.P01 with the QGSP_BERT model.

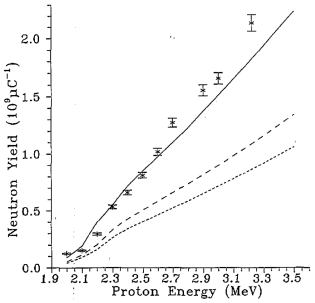

Figure 2: Total neutron yields from a pure thick lithium target (solid line and points). The dashed lines represent lithium compound targets that were also used in experiments by D. A. Allen and T. D. Beynon

In the second part of the validation the lithium disc was replaced by a beryllium disc of similar dimensions. Results obtained from the same Bertini model are shown in Fig. 3 and an experimental comparison can be seen in Fig. 4 [7]. The simulated results follow a similar curve to that shown by the experimental neutron yields from such a target. However the values are significantly lower. For example at 3 MeV the model results give a value of $0.0006^{*}10^{12}$/mC , approximately 500 times lower than the value of $0.3^{*}10^{12}$/mC obtained experimentally at the same proton energy. However results obtained from the Bertini HP model using an updated version of GEANT4 4.9.5.p01 are shown in Fig. 5. These results show a much better correlation with those in Fig. 4, both quantitatively and qualitatively with model and experimental results giving a neutron yield of approximately $1^{*}10^{12}$/mC at 4 MeV.

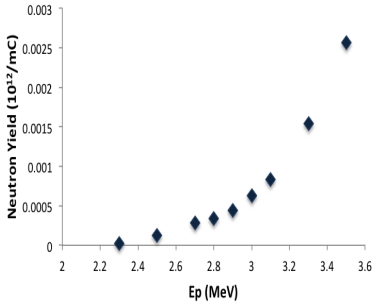

Figure 3: Simulation results of the beryllium target using GEANT4 version 4.9.4.p01 with the QGSP_BERT model.

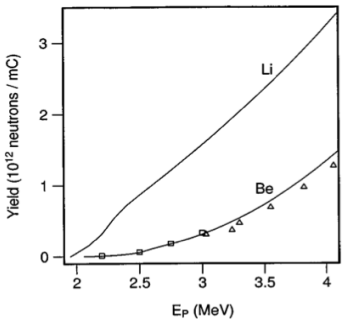

Figure 4: Total experimental neutron yields a for thick lithium target from cross-sections from [9] and a beryllium with data from [10]. Direct neutron yields for a beryllium target are from [8] (squares) and [11] (triangles).

Although the experimental data obtained from beryllium are well modelled, both quantitatively and qualitatively, by the GEANT4.9.5.p01 QGSP_BERT_HP simulations, attempts to use the same modelling procedures for the lithium target gave results which were no better than those obtained with the previous models.

CONCLUSIONS

For beryllium targets at least, both the energy dependence and the magnitude of the neutron yield resulting from the impact of low energy (2-4 MeV) protons are well modelled by the GEANT4.9.5.p01 QGSP_BERT_HP simulations, as can be seen in Fig. 5 where our simulations are compared with the experimentally obtained yields. For

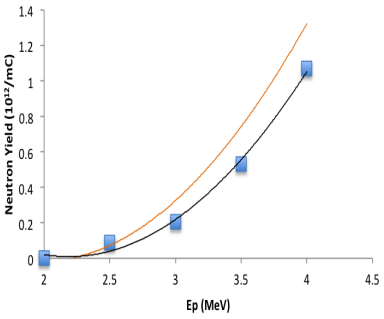

Figure 5: Overlay plot of experimental results (yellow line) for a beryllium target with those obtained using GEANT4.9.5.p01 with the QGSP_BERT_HP model (blue points with dark blue trend line).

lithium targets, however, neither the yield nor its dependence on proton energy are in agreement with experimental data. It is clear that there are significant issues with the physics embodied in GEANT4 at these rather low proton energies. Nevertheless the benchmarking of the GEANT4 simulations against the experimental results from beryllium give us some confidence in moving forward, at least with this target material, to develop more detailed geometrical models with which the production and delivery of thermal and epithermal neutrons for Boron Neutron Capture Therapy can be fully optimised. In so doing it is also important to understand for what materials, and at which energies the simulations begin to break down.

REFERENCES

[1] A. V. Brown, "Development of a High-Powered Neutron Producing Lithium Target for Boron Neutron Capture Therapy," University of Birmingham, August 2000

[2] D. A. Allen and T. D. Beynon, "What is the Best Proton Energy for Accelerator-Based BNCT Using the $^{7}Li(p.n)^{7}Be$ Reaction," Med. Phys. 27 (2000) 1113-1118

[3] D. A. Allen and T. D. Beynon, "A Design Study for an Accelerator-Based Epithermal Neutron Beam for BNCT," Phys. Med. Biol. 240 (1995) 807-821

[4] T. Mitsumoto, K. Fujita, T. Ogasawara, S. Yajima, A. Maruhashi, Y. Sakurai and H. Tanaka, "BNCT System Using 30 MeV H^{-} Cyclotron," Proceedings of Cyclotrons 2010, China

[5] C. Wang and B. R. Moore, "Thick Beryllium Target as an Epithermal Neutron Source for Neutron Capture Therapy," Med. Phys. 21 (1994) 1633-1638

[6] W. B. Howard, J. C. Yanch, S. M. Grimes, T. N. Massey, S. I. Al-Quraishi, D. K. Jacobs and C. E. Brient "Meassurement of the $^{9}Be(p,n)$ Thick Target Spectrum for Use in Accelerator-Based Boron Neutron Capture Therapy," Med. Phys. 23 (1996) 1233-1235

[7] G. Randers-Pehson and D. J. Brenner, "A Practical Target System for Accelerator-Based BNCT Which May Effectively Double the Dose Rate," Med. Phys. 25, June 1998,894-896

[8] J. Campbell and M. C. Scott, "Scientific and Industrial Applications of Small Accelerators," 4th Conf., Denton,TX, 1976

[9] H. Liskien and A. Paulson, "Neutron Production Cross-Sections and Energies for the Reactions $^{7}Li(p,n)^{7}Be$ and $^{7}Li(p,n)^{7}Be$*(431 keV)," At. Data Nucl. Data Tables 15 (1975) 57-84

[10] J. H. Gibbons and R. L. Macklin, "Total Neutron Yields from Light Elements Under Proton and Alpha Bombardment," Phys. Rev. 114 (1959) 571-575

[11] K. Porges, J. L. Snelgrove, R. Gold, A. DeVolpi, R. J. Armani and C. E. Cohn,"Thick Target Neutron Yields of Lithium and Beryllium Targets Bombarded With Protons and Deuterons," Argonne National Laboratory Report ANL -7910, 1972, 361-362

Appendix C: IPAC'13 Proceedings

GEANT4 TARGET SIMULATIONS FOR LOW ENERGY MEDICAL APPLICATIONS

N. Ratcliffe*, R. Barlow, A. Bungau, C. Bungau, R. Cywinski,
University of Huddersfield, Huddersfield, UK

Abstract

The GEANT4 code offers an extensive set of hadronic models for various projectiles and energy ranges. These models include theoretical, parameterized and, for low energy neutrons, data driven models. Theoretical or semi-empirical models sometimes cannot reproduce experimental data at low energies (<100MeV), especially for low Z elements, and therefore recent GEANT4 developments included a new particle_hp package which uses evaluated nuclear databases for proton interactions below 200MeV. These recent developments have been used to study target designs for low energy proton accelerators, as replacements of research reactors, for medical applications. Presented in this paper are results of benchmarking of these new models for a range of targets, from lithium neutron production targets to molybdenum isotope production targets, with experimental data.

INTRODUCTION

Currently the production of medical tracer isotopes for use in imaging techniques such as SPECT (Single Photon Emission Computed Tomography) and PET (Positron Emission Tomography) [1] relies principally upon an aging fleet of nuclear reactors. For example the most common medical isotope ^{99m}Tc, used in over 80% of all radiopharmaceutical procedures, is currently produced, via its generator ^{99}Mo, by nuclear research reactors such as NRU-Canada and HFR-The Netherlands, which together produce over 60% of the worlds ^{99}Mo/^{99m}Tc supply. Both of these reactors are old (>50yrs) and close to decommissioning, but as yet there is no real replacement in place [2] [3]. There is considerable concern that we will soon be facing a similar situation to that of the 2010 isotope crisis, when both reactors were offline simultaneously resulting in a significant decrease in the supply ^{99m}Tc and the postponing or cancelation of many vital radioisotope procedures [1] [2] [3] [4] [5].

We believe that the solution to this impending problem could lie in accelerator-based production methods, of both ^{99m}Tc and possible replacement isotopes. A collaboration with Siemens is focusing on the potential of a compact, low energy proton device for the generation of radioisotopes [6]. A study of optimal target designs for such a system has been undertaken using GEANT4 simulations of low energy (<10MeV) proton induced reactions.

* naomi.ratcliffe@hud.ac.uk

GEANT4

GEANT4 is a well-known, well-used toolkit for the simulation of particle interactions in numerous areas of physics, especially in its origins in high-energy physics. However there has been very little implementation of GEANT4 in simulating the interactions of low energy protons with targets. Moreover, the standard physics models available with the current release of GEANT4 for these types of simulation, such as the QGSP_BIC_HP and QGSP_BERT_HP, are all theoretical [7] [8] [9] [10]. Initial studies of low energy proton interactions with thick (0.7mm) targets comprised of lithium or beryllium have shown that these theoretical models breakdown in the low energy limits. In light of this, a new data driven model, QGSP_BIC_PHP, has been developed to simulate the interactions of protons with energies less than 100MeV with targets. The data for the new model is derived from either the ENDF or TENDL libraries, and is selected by the environmental settings for each simulation.

The initial light element target/neutron production benchmarking was repeated for the new model before a second phase of benchmarking for heavier element targets was undertaken. In this second phase thin foil targets were used for the heavy element targets with proton beams of energy less than 10MeV. In one case the experimental cross sections were so low that a higher energy (<100MeV) proton beam was necessary and hence a thicker pellet type target was used.

This paper presents the results of benchmarking of the new data driven model for a range of targets, including the initial light element targets for neutron production and for several medical radioisotopes produced using accelerator based methods for which reasonable experimental data is available for comparison.

RESULTS

Neutron Production

Initial benchmarking results for both theoretical and data driven models can be seen in fig.1, overlaid with experimental data [11] [12] [13]. It can be seen how the theoretical model completely breaks down for light target low energy proton interactions, significantly underestimating the neutron production from thick lithium and beryllium targets by approximately 3 orders of magnitude. However the data driven model almost perfectly replicates the experimental data for both targets.

ISBN 978-3-95450-122-9

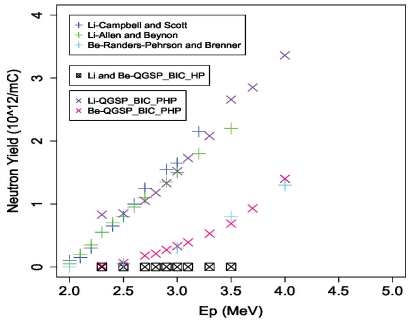

Figure 1: Experimental and data driven simulation results for neuton production targets.

Isotope Production

In the case of radioisotope production a more intensive benchmarking of these models was carried out for these using a range of heavier targets. The simulation and experimental results shown below, Figs.2-5, are for several isotopes currently of interest for medical applications. These isotopes are currently being produced using accelerator-based methods or such production methods are being investigated.

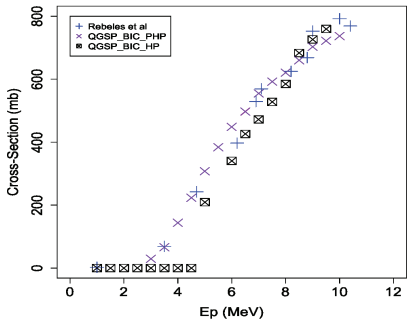

Figure 2: Experimental and simulation results of the ^{64}Ni(p,n)^{64}Cu reaction.

The lightest isotope to be tested is ^{64}Cu, a diagnostic PET isotope used to distinguish malignant tumour tissue [2] [14], which can be produced through the ^{64}Ni(p,n)^{64}Cu reaction. The results are shown in fig.2. It can be seen that while there is good agreement between the experimental [15] [14], theoretical and data driven cross sections at the higher energy range (7-10MeV), the theoretical models start to break down as the energy decreases (<5MeV) at which no isotope production is seen. The data driven model continues to show good agreement with the experimental data down to approximately 3MeV where the cross section becomes too low (<1mb) to obtain simulated production.

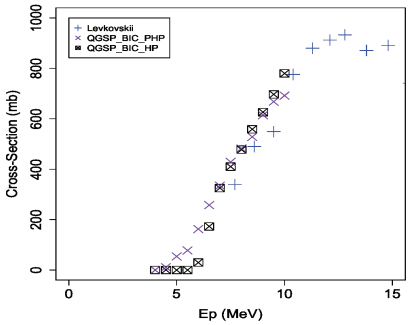

Figure 3: Experimental and simulation results of the ^{89}Y(p,n)^{89}Zr reaction.

Next, the production of ^{89}Zr, a PET diagnostic isotope often used in connection with labelled antibodies [16], from the ^{89}Y(p,n) reaction was simulated. The results can be seen in fig.3. Again, at the higher energies (7-10MeV) there is reasonable agreement between both simulation results and the experimental data [17] [14]. However the theoretical model starts to break down at approximately 6MeV. The data driven model still shows isotope production down to 4MeV for this reaction.

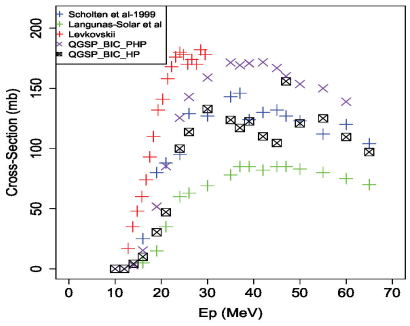

Figure 4: Experimental and simulation results of the ^{100}Mo(p,pn)^{99}Mo reaction.

Possibly the most important test case is the simulation of the production of the ^{99m}Tc generator via the ^{100}Mo(p,pn)^{99}Mo reaction. A range of experimental data is available from the literature [17] [18] [19] and online libraries (such as EXFOR), some examples of which can be seen in fig.4. This example shows how the available data sources can affect the simulation results obtained using the

ISBN 978-3-95450-122-9

data driven model and with such a range of experimental results from which to choose a sensible comparison between experimental and simulated data is not always possible. In such cases the theoretical model may provide more reliable results.

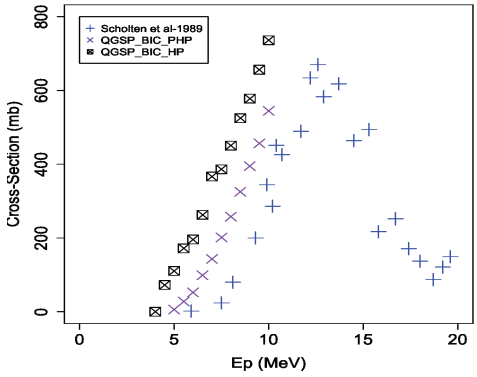

Figure 5: Expermental and simulation results for the ^{123}Te(p,n)^{123}I reaction.

The final test case in this phase was the reaction ^{123}Te(p,n)^{123}I, producing an isotope currently being used for thyroid SPECT imaging [2]. It can be seen from the results in fig.5 that both simulation models over estimate the experimental [20] isotope production cross-sections in the less than 10MeV energy region, the theoretical results more so than the data driven model.

CONCLUSION

In this paper we have introduced a data driven model for the simulation of accelerator driven radioisotope production at low proton energies. The benchmarking results presented are encouraging and indicate that a successful low energy data driven model can indeed be used successfully in GEANT4 to simulate low energy proton interactions. However the test cases presented here are limited and a much more stringent validation process must yet be carried out before this new model can be included in the standard GEANT4 release with confidence.

ACKNOWLEDGMENT

N. Ratcliffe acknowledges the receipt of a joint EPSRC/Siemens CASE studentship.

REFERENCES

[1] M. Zakzouk, *The Medical Isotope Shortage: Cause, Effects and Options*, (Library of Parliament, Canada, 2009).

[2] *Cyclotron Produced Radionuclides: Principles and Practice*, IAEA, Technical Reports Series no.456, 2008.

[3] S. Zeisler, "Cyclotron Production of Technetium-99m," Workshop on Acclerator-driven Production of Medical Isotopes, Daresbury Laboratory, UK, 2011.

[4] *A Review of the Supply of Molybdenum-99, the Impact of Recent Shortages and the Implications for Nuclear Medicine Services in the UK*, Administration of Radioactive Substances Advisory Committee, 2010.

[5] J. Nolen, "Current and Possible New Methods for Acclerator-Based Production of Medical Isotopes," XXV International Linac Conference, 2010.

[6] P. Beasley and O. Heid, "Progress Towards a Novel Compact High Voltage Electrostatic Accelerator," PAC'11 New York, WEP207 (2011).

[7] S. Agostinelli et al, "GEANT4 - a simulation toolkit," Nuclear Instraments and Methods in Physics Reasearch A 506 (2003) 250-303.

[8] A. Ribon et al, "Transition Between Hadronic Models in GEANT4," IEEE Nuclear Science Symposium Conference Record (2009).

[9] A. Heikkinen and N. Stepanov, "Bertini Intra-Nuclear Cascade Implementation in GEANT4," Computing in High Energy and Nuclear Physics (2003).

[10] G. Floger, V.N. Ivanchenko and J.P. Wellisch,"The Binary Cascade," The European Physical Journal A 21 (2004) 407-417.

[11] J. Campbell and M.C. Scott, "Absolute Neutron Yield Measurements for Protons on Li, Cu, Co and Be from Threshold to 3 MeV," Scientific and Industrial Applications of Small Accelerators,1977.

[12] D.A. Allen and T.D. Beynon, "A Design Study for an Accelerator-Based Epithermal Neutron Beam for BNCT," Phys. Med. Biol. 40 (1995) 807-821.

[13] G. Randers-Pehrson and D.J. Brenner "A Practical Target System for Accelerator-Based BNCT Which May Effectively Double the Dose Rate," Med. Phys. 25 (1998).

[14] *Cyclotron Produced Radionuclides: Physical Characteristics and Production Methods*, IAEA, Technical Reports Series no.468, 2009.

[15] R.A. Rebeles et al, "New Measurement and Evaluation of the Excitation Function of ^{64}Ni(p,n) Reaction for the Production of ^{64}Cu," Nuclear Instruments and Methods in Physics Research Section B, 267 (2009) 457-467.

[16] Y. Zang, H. Hong and W. Cai, "PET Tracers Based on Zirconium-89," Curr Radiopharm (2011).

[17] V.N. Levkovskij, "Activation cross section nuclides of average masses (A=40-100)by protons and alpha-particles with average energies (E=10-50 MeV)," Act. Cs. By Protons and Alphas (1991).

[18] B. Scholten et al, "Excitation Functions for the Cyclotron Production of ^{99m}Tc and ^{99}Mo," Applied Radiation and Isotopes 51 (1999) 69-80.

[19] M.C Langunas-Solar et al, "Cyclotron Production of NCA ^{99m}Tc and ^{99}Mo. An Alternative Non-Reactorsupply Source of Instant ^{99m}Tc and ^{99}Mo $\rightarrow$ ^{99m}Tc Generators," Appl. Radiat. Isot. 42 (1991) 643.

[20] B. Scholten et al, "Excitation Functions of Proton Induced Nuclear Reactions on Natural Tellurium and Enriched Te-123 Production of I-123 via the Te-123(p,n)I-123 Process at a Low-Energy Cyclotron," Applied Radiation and Isotopes 40 (1989) 127.

ISBN 978-3-95450-122-9
3719

Appendix D: PAC2013 Proceedings

DEVELOPMENT OF LOW ENERGY ACCELERATOR-BASED PRODUCTION OF MEDICAL ISOTOPES

N. Ratcliffe*, R. Barlow, R. Cywinski, University of Huddersfield, Huddersfield, HD1 3BH, UK
P. Beasley, Siemens AG, Oxford, OX1 2EP, UK

Abstract

Here we present methods for production of new and existing isotopes for SPECT (Single Photon Emission Computed Tomography) and PET (Positron Emission Tomography) imaging using accelerator-based systems. Such isotopes are already widely used in medical diagnostics and research, and there is constant development of new drugs and isotopes. However the main production method for ^{99m}Tc, is currently in research reactors and is at risk due to scheduled and unscheduled shut downs. Therefore, a low cost an alternative accelerator-based system could provide many advantages. Various compact low energy proton machines are being proposed to enable cheap and accessible production: here we present a discussion of potential new SPECT isotopes and simulations of suitable targets for their manufacture.

INTRODUCTION

Currently the production of medical tracer isotopes for use in imaging techniques such as SPECT (Single Photon Emission Computed Tomography) and PET (Positron Emission Tomography) [1] relies principally upon an ageing fleet of nuclear reactors. For example the most common medical isotope ^{99m}Tc, used in over 80% of all radiopharmaceutical procedures, is currently produced, via its generator ^{99}Mo, by nuclear research reactors such as NRU-Canada and HFR-The Netherlands, which together produce over 60% of the worlds ^{99}Mo/^{99m}Tc supply. Both of these reactors are old (>50yrs) and close to decommissioning, and while several projects are looking at other production routes for this isotope, as yet there is no real replacement in place [2, 3]. As these reactors near their decommissioning, currently set at 2014-2016, there is considerable concern that we will soon be facing a similar situation to that of the 2010 isotope crisis, when both reactors were offline simultaneously resulting in a significant decrease in the supply of ^{99m}Tc and the postponing or cancelation of many vital radioisotope procedures [1–5]. Due to ^{99m}Tc monopolising the medical isotope market little work was done developing other isotopes and many potential isotopes fell by the wayside. The aim of this work is to resurrect some of these isotopes as alternatives to ^{99m}Tc as we head into another shortage in the hope of preventing another crisis. There are several short lived SPECT and PET isotopes that have the potential to take some of the workload from ^{99m}Tc.

* naomi.ratcliffe@hud.ac.uk

LOW ENERGY ISOTOPE PRODUCTION

We believe that the solution to this impending problem could lie in accelerator-based production methods, of both ^{99m}Tc and possible replacement isotopes. A collaboration with Siemens is focusing on the potential of a compact, low energy proton device for the generation of radioisotopes [6]. Such a machine could provide many more localised isotope production centres and allow for the use of isotopes with shorter halflives. A study of optimal target designs for such a system has been undertaken using GEANT4 simulations of low energy (<10MeV) proton induced reactions.

^{113M}INDIUM

^{113m}In is a metastable radioactive isotope that decays via a 392 keV γ into stable ^{113}In with a half life of 1.7hours [7]. In 1965 it was first proposed for use as an alternative medical tracer isotope to ^{99m}Tc for SPECT imaging in several applications such as brain and lung scanning. Trials of this isotope showed it to give results comparable to ^{99m}Tc images [7]. ^{113m}In showed several advantages over ^{99m}Tc such in terms of chemical properties. A successful generator production system for In was developed using ^{113}Sn [7, 8].

Generator Production

There are several advantages of a longer lived generator system, such as the Sn/In system. The longer gap between parent half life and daughter half life makes it easier to separate the two nuclei. It also increases the longevity of the system for example the Sn/In(parent half life approximately 118 days) system only needs replacing once every 6 months where as the Mo/Tc(parent half life approximately 3 days) system needs replacing weekly. However due the plentiful and cheap supply of Tc at the time very little serious work was carried forward with this isotope. The simplicity of the generator production system and the advantages available from such a system has prompted the exploration of a low energy method of production for this generator using the reaction:

^{113}In(p,n)^{113}Sn $\rightarrow$ ^{113m}In $\rightarrow$ ^{113}In

Preliminary simulation results from the TALYS data libraries show that such a reaction at 10 MeV gives a production cross section of 570mb. Further GEANT4 simulations have been used to study target designs and feasibility of this reaction using a <10MeV proton beam. In terms of daughter yield the most appropriate target thickness is that of just

ISBN 978-3-95450-138-0

over the stopping distance, which from these simulations is given to be approximately 0.5mm. The generator and daughter activity for this reaction after a 30min irradiation of the target can be seen in Fig. 1.

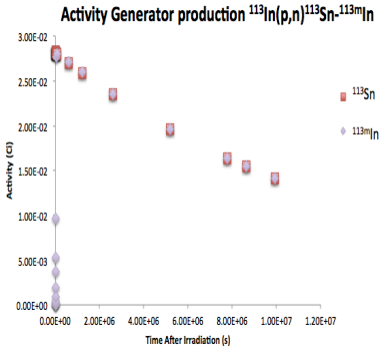

Figure 1: Activity of parent ^{113}Sn and daughter ^{133m}In produced from the generator reaction.

The lifetime of a typical Sn/In generator system is 3-6 months [9]. The activity for this time after irradiation can be seen in Fig. 1. Even after this time this small sample generator is producing an activity of 0.9 mCi which in comparison to a typical single dose of microcuries per gram [10], shows the potential of a low energy accelerator based system for the generator production of ^{113m}In.

Direct Production

Direct production of ^{113m}In appears to be less common due to the short halflife of the isotope and the lack of local facilities in which to produce it. However with the introduction of our proposed system it should be possible to make this a much more feasible production route. Both the TENDL and EXFOR libraries can be seen to agree that a cross section of just over 200mb can be obtained for the following reaction:

^{113}Cd(p,n)^{113m}In

for a proton beam between 9 and 10 MeV. The corresponding activity of In for a 0.5mm thick target after a 30min irradiation can be seen in Fig. 2.

The activity obtained for direct production is significantly larger than that of generator production. Such activity should be enough to service the needs for a local facility as is the proposed purpose of a low energy isotope production system.

^{87M}STRONTIUM

Strontium 87m is a metastable radioactive isotope that decays via a 388keV γ into stable ^{87}Sr with a half life of 2.8hours [11]. Several different strontium isotopes have an application in nuclear medicine as due to the similar

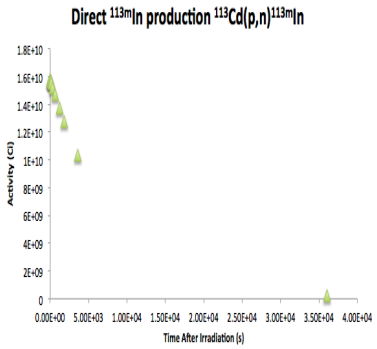

Figure 2: Activity of ^{113}In produced from the direct reaction.

chemistry to calcium it is readily taken up in bone. There are some isotopes such as ^{90}Sr which are undesirable for medial use as replace calcium in the bone and are toxic. Others however such as ^{87m}Sr can be used in both diagnostic and therapeutic techniques for various skeletal diseases [11–14].

Generator Production

^{87m}Sr is produced primarily using the ^{87}Y/^{87m}Sr generator. Literature shows many different possible methods of producing this generator. However these are all at higher energies (>20 MeV). This work is focusing on low energy techniques e.g. reactions such as

^{87}Sr(p,n)^{87}Y $\rightarrow$ ^{87m}Sr $\rightarrow$ ^{87}Sr

According to the TALYS/EXFOR libraries this reaction has a cross section of approximately 600mb at 10 MeV. Further study of target design were carried out using GEANT4 to obtain a suitable target that provides a viable yield for medical applications. The activity obtained from a 0.9mm thick metal target can be seen in Fig. 3.

Activity of the generator route from our simulations is of the order of curies whilst a diagnostic dose is of the order of millicurie. However from previous studied such as [11] it is apparent that this target is impractical and a compound target such as $SrCl_2$ would be more appropriate. This reduces the number of Sr nuclei within the target requiring a thicker compound target to keep the activity sufficient for the 2 week lifespan that is typical of this type of generator system.

Direct Production

It is also proposed that direct production of ^{87m}Sr is possible through the reaction:

^{87}Rb(p,n)^{87m}Sr

which according to the EXFOR libraries has a cross section of approximately 200mb in the energy range <10MeV. The TALYS libraries also gave a cross section of 240mb at

ISBN 978-3-95450-138-0

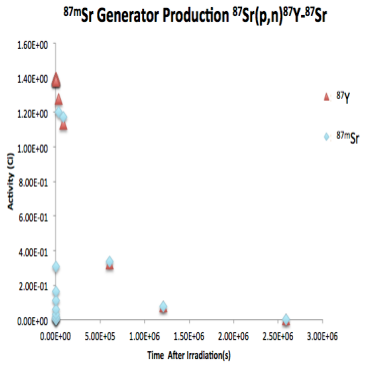

Figure 3: Activity of ^{87m}Sr produced using the ^{87}Y/^{87m}Sr generator.

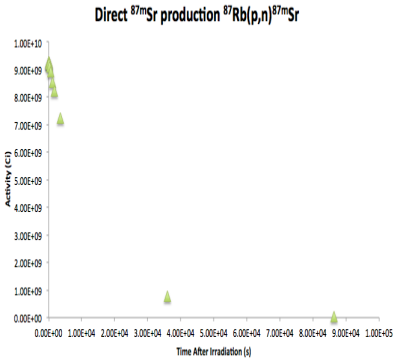

Figure 4: Activity of ^{87m}Sr produced using the direct reaction.

10MeV from which the activity of ^{87m}Sr that is produced after a 30min irradiation of a 0.5mm thick target can be seen in Fig. 4.

Even with such a simple, crude design such a large activity is obtained with this reaction. With more adjustment a suitable target could be configured so as to optimise the activity. An isotope with such a short half life is much more likely to be produced using the direct reaction on demand and so any effort to minimise the production time such as short irradiation time, from these initial results this time could be less than 30mins.

CONCLUSION

This work has shown a first test case of the feasibility and practicality of using a low energy proton accelerator system as a method of producing radioisotopes in quantities suitable for medical applications. This work will go on to optimise the low energy production routes for these isotopes in the hopes of minimising the reduction of SPECT isotopes in the predicated crisis. We will also go on to study the potential of using this system to manufacture potential isotopes to be introduced for both SPECT and PET.

ACKNOWLEDGMENT

N. Ratcliffe acknowledges the receipt of a joint EPSRC/Siemens CASE studentship.

REFERENCES

[1] M. Zakzouk, *The Medical Isotope Shortage: Cause, Effects and Options*, (Library of Parliament, Canada, 2009).

[2] *Cyclotron Produced Radionuclides: Principles and Practice*, IAEA, Technical Reports Series no.456, 2008.

[3] S. Zeisler, "Cyclotron Production of Technetium-99m," Workshop on Acclerator-driven Production of Medical Isotopes, Daresbury Laboratory, UK, 2011.

[4] *A Review of the Supply of Molybdenum-99, the Impact of Recent Shortages and the Implications for Nuclear Medicine Services in the UK*, Administration of Radioactive Substances Advisory Committee, 2010.

[5] J. Nolen, "Current and Possible New Methods for Acclerator-Based Production of Medical Isotopes," XXV International Linac Conference, 2010.

[6] P. Beasley and O. Heid, "Progress Towards a Novel Compact High Voltage Electrostatic Accelerator," PAC'11 New York, WEP207 (2011).

[7] J. Clements et al., "Indium 113m DIETHYLTRIAMINOPENTAXETIC Acid (DTPA): A New Radiopharmacutical For Brain Scanning," 1968.

[8] L. Colombetti et al., "Preparation and Testing of a Sterile Sn113-In113m Generator," 1969.

[9] N. Ramamoorthy et al., "Studies on the Preparation of ^{113}Sn-^{113m}In Generators," Isotopenpraxis Isotopes in Environmental and Health Studies, 2008.

[10] www.iem-inc.com/toolmed1.html

[11] J.F. Allen and J.J. Pinajian, "A ^{87m}Sr Generator for Medical Applications," International Journal of Applied Radiation and Isotopes, 1965.

[12] H.B.S. Kemp et al., "The Role of Fluorine-18 and Strontium-87m Scintigraphy in the Management of Infective Spondylitis," The Journal of Bone and Joint Surgery, 1973.

[13] M. Van Laere et al., "Strontium 87m Scannong of the Sacroiliac Joints in Ankylosing Spondylitis," Annals of the Rheumstic Diseases, 1972.

[14] R.L. Meckelnburg, "Clinical Value of Generator Produced 87-m Strontium," Journal of Nuclear Medicine, 1964.

[15] A.G.M. Janssen et al., "A Rapid and High-Yield Preparation Method for ^{87}/^{87m}Sr Generators Using the ^{88}Sr(p,2n) Reaction," Int. J. Radiat. Appl. Instrum. Part A, Appl. Radiat. Isot., 1986.